AFFDL-TR-73-42
Part II, Volume II

DEVELOPMENT AND EVALUATION OF METHODS OF PLANE STRESS FRACTURE ANALYSIS

Part II. Volume II. Fracture Resistance and Material Property Characterization

D.P. WILHEM
J. H. FITZGERALD

NORTHROP CORPORATION
AIRCRAFT DIVISION

AUGUST 1977

TECHNICAL REPORT AFFDL-TR-73-42, PART II, VOLUME II
Report for Period January 1973 – December 1974

AIR FORCE FLIGHT DYNAMICS LABORATORY
AIR FORCE SYSTEMS COMMAND
WRIGHT-PATTERSON AIR FORCE BASE, OHIO 45433

NOTICE

When Government drawings, specifications, or other data are used for any purpose other than in connection with a definitely related Government procurement operation, the United States Government thereby incurs no responsibility nor any obligation whatsoever; and the fact that the Government may have formulated, furnished, or in any way supplied the said drawings, specifications, or other data, is not to be regarded by implication or otherwise as in any manner licensing the holder or any other person or corporation, or conveying any rights or permission to manufacture, use, or sell any patented invention that may in any way be related thereto.

This report has been reviewed by the Office of Information (OI) and is releasable to the National Technical Information Service (NTIS). At NTIS, it will be available to the general public, including foreign nations.

This technical report has been reviewed and is approved for publication.

George P. Sendeckyj

G.P. SENDECKYJ
Project Engineer

R.M. Bader

ROBERT M. BADER, Chief
Structural Integrity Br
Structural Mechanics Division

FOR THE COMMANDER

HOWARD L. FARMER, Colonel, USAF
Chief, Structural Mechanics Division

Copies of this report should not be returned unless return is required by security considerations, contractual obligations, or notice on a specific document.

AIR FORCE/56780/17 October 1977 — 500

Unclassified

SECURITY CLASSIFICATION OF THIS PAGE *(When Data Entered)*

REPORT DOCUMENTATION PAGE		READ INSTRUCTIONS BEFORE COMPLETING FORM
1. REPORT NUMBER AFFDL-TR-73-42, Part II, Volume II	2. GOVT ACCESSION NO.	3. RECIPIENT'S CATALOG NUMBER
4. TITLE *(and Subtitle)* Development and Evaluation of Methods of Plane Stress Fracture Analysis, Part II, Volume II, Fracture Resistance and Material Property Characterization		5. TYPE OF REPORT & PERIOD COVERED Part II (Phase II) Final Report--January 1973-December 1974.
		6. PERFORMING ORG. REPORT NUMBER NOR 74-309
7. AUTHOR(s) D. P. Wilhem, J. H. FitzGerald		8. CONTRACT OR GRANT NUMBER(s) F33651-72-C-1796
9. PERFORMING ORGANIZATION NAME AND ADDRESS Northrop Corporation, Aircraft Division, 3901 West Broadway, Hawthorne, Calif. 90250		10. PROGRAM ELEMENT, PROJECT, TASK AREA & WORK UNIT NUMBERS Project 486U, Task 0204
11. CONTROLLING OFFICE NAME AND ADDRESS Air Force Flight Dynamics Laboratory, Wright-Patterson Air Force Base, Ohio 45433		12. REPORT DATE August 1977
		13. NUMBER OF PAGES 195
14. MONITORING AGENCY NAME & ADDRESS*(if different from Controlling Office)* SAME		15. SECURITY CLASS. *(of this report)* Unclassified
		15a. DECLASSIFICATION/DOWNGRADING SCHEDULE

16. DISTRIBUTION STATEMENT *(of this Report)*

Approved for Public Release; Distribution Unlimited

17. DISTRIBUTION STATEMENT *(of the abstract entered in Block 20, if different from Report)*

18. SUPPLEMENTARY NOTES

19. KEY WORDS *(Continue on reverse side if necessary and identify by block number)*

Crack growth resistance	2024-T3	Compliance Relationships
K_R Curves	Ti-6Al-4V	Side Grooving
Toughness	Ti-6Al-6V-2Sn	Crack line wedge loaded specimen
7075-T6	9Ni-4Co-.2C	
7075-T73		

20. ABSTRACT *(Continue on reverse side if necessary and identify by block number)*

In this Volume those data required to characterize a materials fracture behavior and necessary to the residual strength prediction method proposed in Volume I are presented for the materials examined in this study. These data were developed from an extensive series of crack growth resistance tests, performed on the relatively new crack line wedge loaded (CLWL) specimen geometry. The following materials were examined in both the LT and TL fracture plane orientations in two thicknesses (approximately 80, total specimens):

DD FORM 1 JAN 73 1473 EDITION OF 1 NOV 65 IS OBSOLETE

Unclassified

SECURITY CLASSIFICATION OF THIS PAGE *(When Data Entered)*

20. ABSTRACT (Continued)

7075-T6, 7075-T73, 2024-T3, Ti-6Al-4V (Beta Mill Annealed), Ti-6Al-6V-2Sn (Mill Annealed). Crack growth resistance data were also obtained for a 9 nickel steel sheet in both crack orientations. Normal and extended range stress-strain data have been recorded for each material. In addition to yield and ultimate strength, material moduli have been obtained by strain gage as well as conventional extensometer for use in the double compliance method for determining crack length and applied load.

FOREWORD

This report was prepared by Northrop Corporation, Aircraft Division, Hawthorne, California, under Air Force Contract F33615-72-C-1796. The project was initiated under Project Number 486U, Task 0204, "Advanced Metallic Structures," Advanced Development Program. The work reported herein was administered under the direction of the Air Force Flight Dynamics Laboratory, Air Force Systems Command, Wright-Patterson Air Force Base, Ohio, by Captain George F. Zielsdorff, (FBR, currently of ASD) and Dr. George Sendeckyj (FBEC).

The research was conducted between January 1973 and December 1974 as a conclusion to Phase II. The first report (AFFDL-TR-73-42, Park I (May 1973), indicated the current state-of-the-art of residual strength prediction and provided the framework and direction to the Phase II research activity. This report was submitted by the authors D. P. Wilhem and J. H. FitzGerald, February 1975, for AFFDL review. The report has been assigned NOR 74-309 for internal control at Northrop Corporation.

The authors wish to acknowledge the assistance of D. E. McCabe and R. H. Heyer of Armco Steel Corporation for providing technical support in design of the crack line wedge loaded specimen test fixture and test procedure. The secretarial assistance of Donna Robards is also acknowledged. The aforementioned program was under the supervision of C. Rosenkranz of the Structures Research and Technology Department.

TABLE OF CONTENTS

TABLE OF CONTENTS (Continued)

LIST OF ILLUSTRATIONS

LIST OF ILLUSTRATIONS (Continued)

LIST OF ILLUSTRATIONS (Continued)

LIST OF ILLUSTRATIONS (Continued)

LIST OF ILLUSTRATIONS (Continued)

LIST OF ILLUSTRATIONS (Continued)

LIST OF ILLUSTRATIONS (Continued)

LIST OF ILLUSTRATIONS (Continued

LIST OF TABLES

I INTRODUCTION

This report describes the research activity conducted during Phase II of a three phase investigation into the development of an improved method of thin section residual strength prediction where conditions of plane stress or mixed mode fracture prevails.

In this volume those data required to characterize a materials fracture behavior and necessary to the method proposed in Volume I are presented for the materials examined in this study. These data were developed from an extensive series of crack growth resistance tests, performed on the relatively new crack line wedge loaded (CLWL) specimen geometry. Since these data were also obtained from material which is well characterized in mechanical properties a good comparative basis was thus available. It was felt advisable to present these data, as obtained, so that those wishing to examine other analysis methods or perhaps their own particular technique would have a common material data source from which to draw. The crack growth resistance data presented herein were obtained essentially following the proposed recommended practice for R-Curve Determination as published by ASTM for information only, dated November 1974.

In Section II the material coding and heat treatment for all materials are presented along with a complete metallurgical history of the titanium 6Aℓ-4V material which was obtained as surplus SST material. In particular, the role of material anisotropty caused by preferred rolling on development of crack growth resistance data from the CLWL specimen geometry in the LT direction is explored.

Mechanical property data for all materials, thicknesses and test directions, including representative load-strain curves are also presented in Section III.

Section IV details the specifics of the CLWL specimen, the development of the calibration data and interpretation of the data. All CLWL data is presented in Section V in the form of deflection traces and as crack growth resistance K_R data in Section VI.

These material property and fracture resistance data form the basis for the residual strength prediction technique developed during Phase II and serve as complimentary information to the failure criterion of the method given in Volume I of this report.

II MATERIAL AND PROCESSING VARIABLES

2.1 MATERIAL AND SPECIMEN CODING

The materials which were tested during Phase II of this program are given in Table I.

TABLE I MATERIALS

ALUMINUMS	TITANIUMS	STEEL
7075-T6	Ti-6Aℓ-4V	9Ni-4Co-.2C
7075-T73	Ti-6Aℓ-6V-2Sn	
2024-T3		

Except for the 9 nickel steel, two thicknesses were tested of each alloy type. Heat treatment of 7075-T6 material to the overaged-T73 condition produced the required difference in toughness conditions from one lot of material. Additional information on heat treatment procedures will be presented in subsequent discussion in this report.

Figure 1 shows the basic specimen coding for all of the crack line wedge loaded (CLWL) specimens. A basic seven letter/numeral code identifies the material and specimen. The AB code (first two identification digits, see Figure 1) identifies the material, the C and D code the sheet or plate thickness and lot number, E the specimen type and FG the fracture plane orientation. The last two digits (XX) indicate the specimen number within a given test series.

2.2 MATERIAL POST PROCESSING

2.2.1 Aluminum

The 7075-T6 and the 2024-T3 alloy of Table I were purchased from the same lots of material. Moreover, some of the 7075-T6 sheet and plate were heat treated to the -T73 condition by overaging, in air to 325°F for 24 hours. No further heat treatment was performed on the aluminum alloys.

2.2.2 Steel

Post processing of the 9 Nickel sheet was not necessary.

2.2.3 Titaniums

The titanium 6Aℓ-6V-2Sn was received in the mill annealed condition and no additional processing was felt necessary. The Ti-6Aℓ-4V sheet and plate were supplied from excess material inventory under SST contract. The heat number for

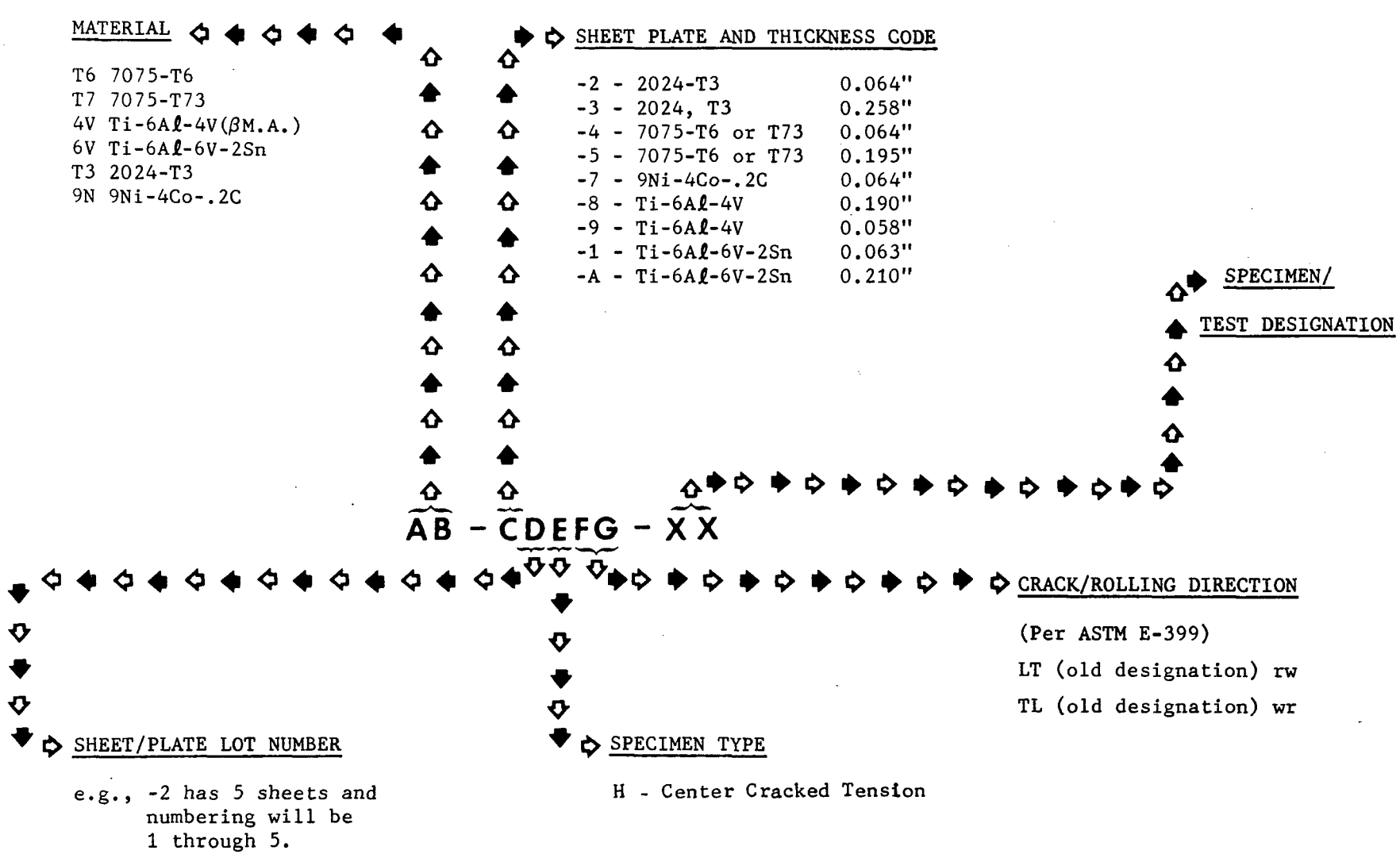

Figure 1. Specimen Numbering Code

the 0.198 inch thick material was K-7621, no heat reference number was available for the sheet material. Both thicknesses of the Ti-6Aℓ-4V material showed large scatter and banding in crack growth resistance data. An investigation was performed to determine the cause of banding and to recommend corrective action.

2.2.4 Ti-6Aℓ-4V Material

The Ti-6Aℓ-4V material (nominally 0.198 and .058 inch thickness) received as excess inventory lots from terminated contract FA-SS-67-3 for this study was metallurgically examined to determine the reason for nonrepeatability of crack growth resistance, K_R data. This material was processed to contractor specification BMS7-174A which we understood was a beta mill annealed condition. Typical micro-structure is shown in Figures 2 and 3 for both thicknesses. From the 100X photo micrographs it is evident that banding conditions are prevalent. The higher magnification indicates that the beta mill annealed condition was never reached and large amounts of primary alpha remain.

In subsequent discussion with SST contractor personnel it was determined that the BMS7-174A specification was a beta-rolled process and that many lots of this material were part of the excess inventory lot. The beta mill annealed condition carries the contractor's BMS7-174B designation.

The mechanical property data for this material in the as received condition are given in Table II.

To determine if the as received titanium could be placed in the beta mill annealed condition a small sample (from specimen 4V-81CTL-005) was heat treated to the following specification supplied by the SST contractor.

- Heat in vacuum to 1900°F.
- Hold at 1900°F for 5 minutes.
- Cool to 1350°F.
- Hold at 1350°F for 2 hours.
- Cool to room temperature (R.T.).

This specification is essentially the BMS7-174B treatment (as called for by the contractor) where the only variance is that the -174B specification calls for a cool to R.T. and reheat to 1350°F.

The results of this treatment are shown in Figure 4 at two magnifications. Comparison with the prior microstructure indicates that the beta mill annealed condition has been achieved with a not unexpected increase in grain growth.

Based on the results of this study approximately one-half of the as received Ti-6Aℓ-4V material was heat treated to the above specification. This beta mill annealed material was subsequently used during this program and no further testing of the beta processed material was attempted.

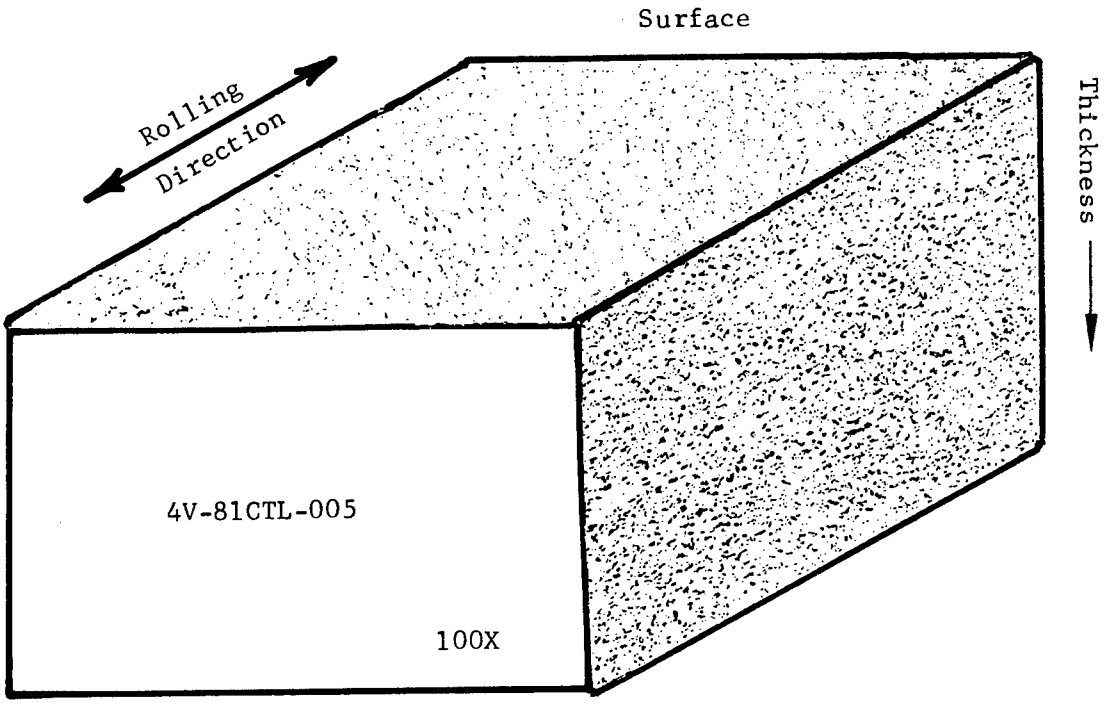

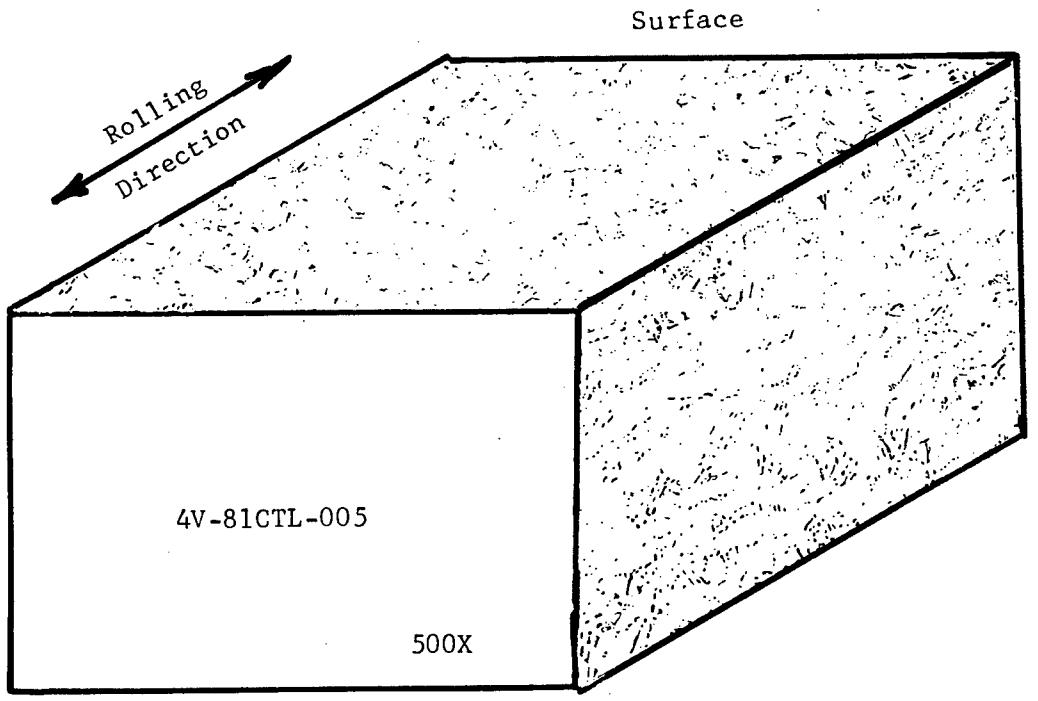

Figure 2. Microstructure of As Received Ti-6Al-4V Material, B = 0.198 Inche

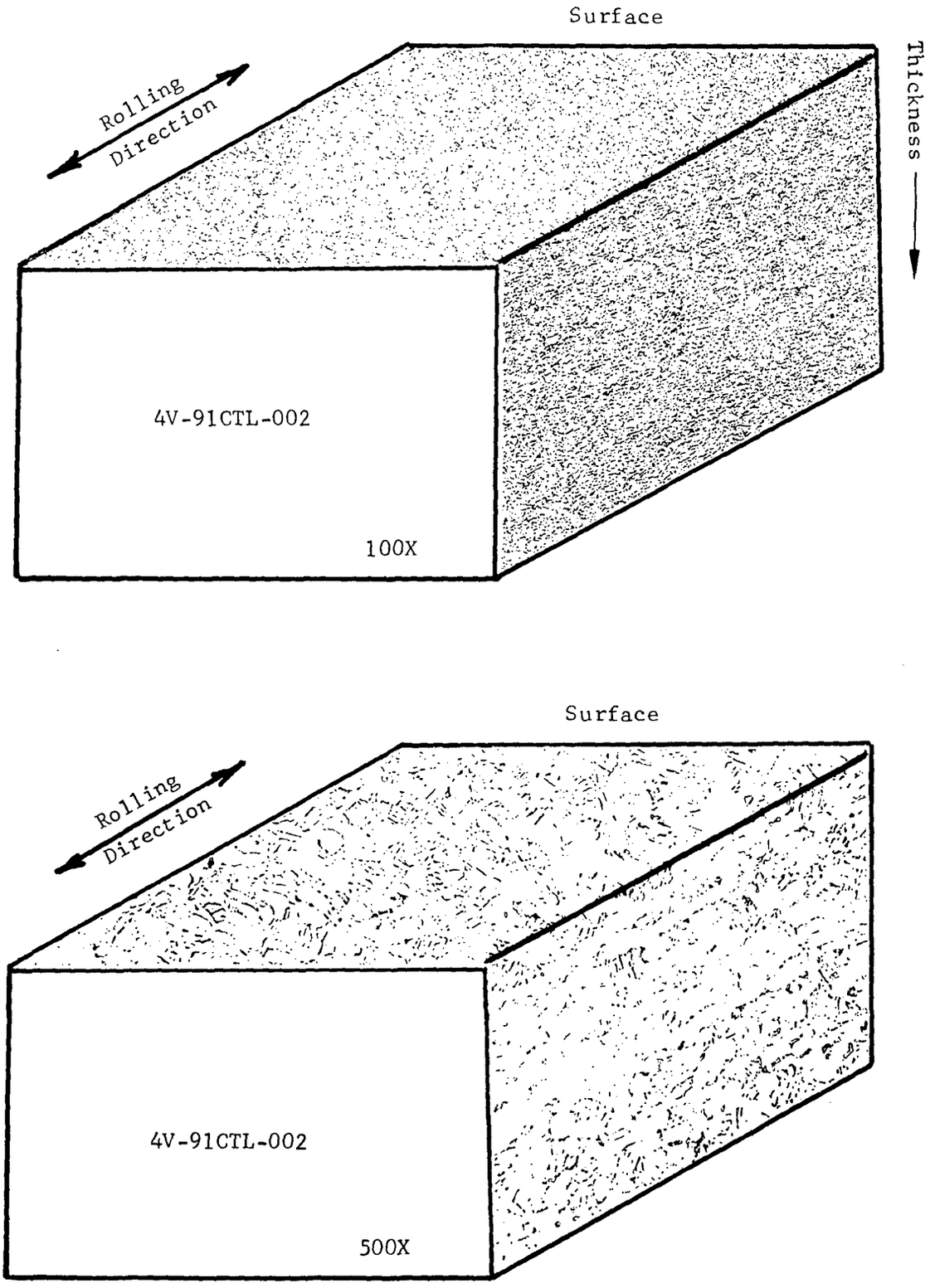

Figure 3. Microstructure of As Received Ti-6Aℓ-4V Material, B = 0.058 Inches

TABLE II MECHANICAL PROPERTY DATA FOR AS RECEIVED BETA ROLLED PROCESS - Ti-6Al-4V

MATERIAL	FROM SHEET/ PLATE NO.	TEST DIREC-TION	THICKNESS (inches)	0.2% OFFSET YIELD, F_{ty} (psi)	ULTIMATE STRENGTH, F_{tu} (psi)	MODULI	
						FROM STRAIN GAGE ($psix10^6$)	FROM EXTEN-SOMETER ($psix10^6$)
Ti-6Al-4V	91	LT	.058	139,300	149,120	16.91	17.54
Ti-6Al-4V	91	LT	.058	138,250	148,770	—	17.03
Ti-6Al-4V	91	TL	.059	136,210	147,930	18.06	16.26
Ti-6Al-4V	91	TL	.059	136,680	147,060	—	16.16
Ti-6Al-4V	81	LT	.197	139,394	149,370	19.29	18.53
Ti-6Al-4V	81	LT	.198	139,086	143,045	—	17.81
Ti-6Al-4V	81	TL	.198	133,158	140,950	16.94	17.11
Ti-6Al-4V	81	TL	.198	128,535	135,350	—	18.14

Before Heat Treatment

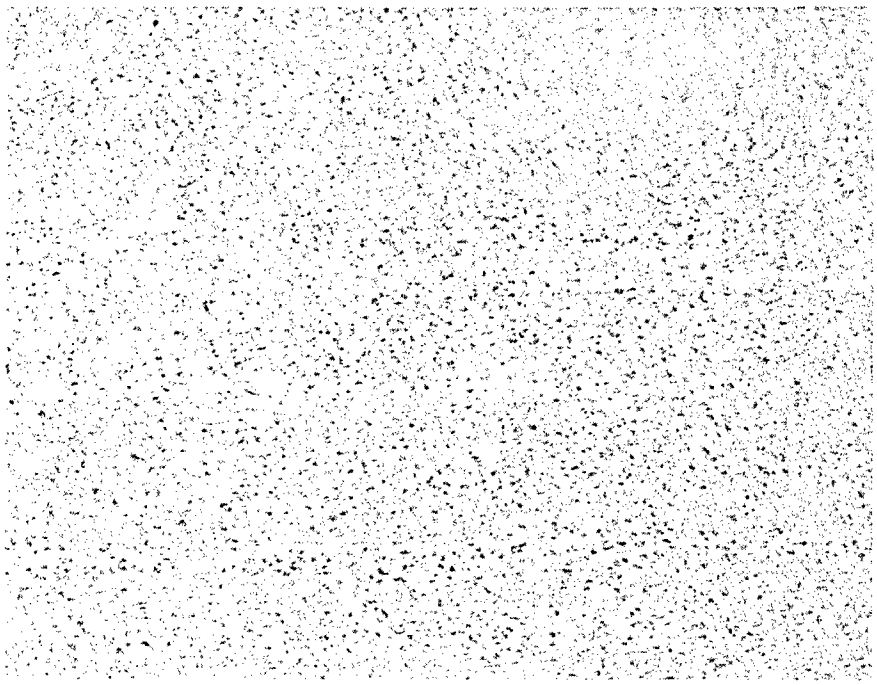

100X

After Heat Treatment

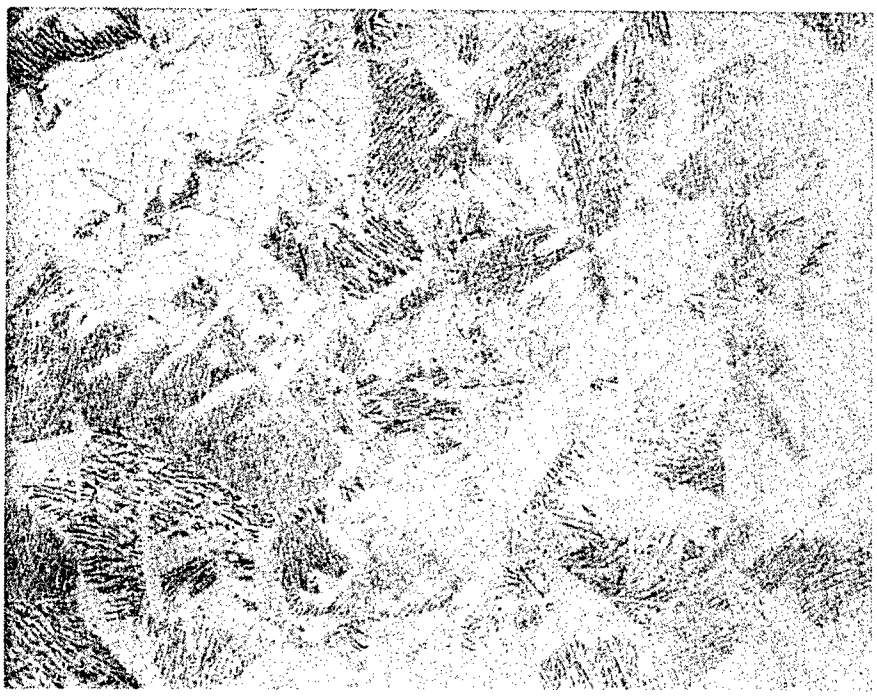

100X

Figure 4. Photomicrographs of Ti-6Aℓ-4V Material, Before and After Beta Mill Annealed Heat Treatment - Longitudinal Direction

Before Heat Treatment

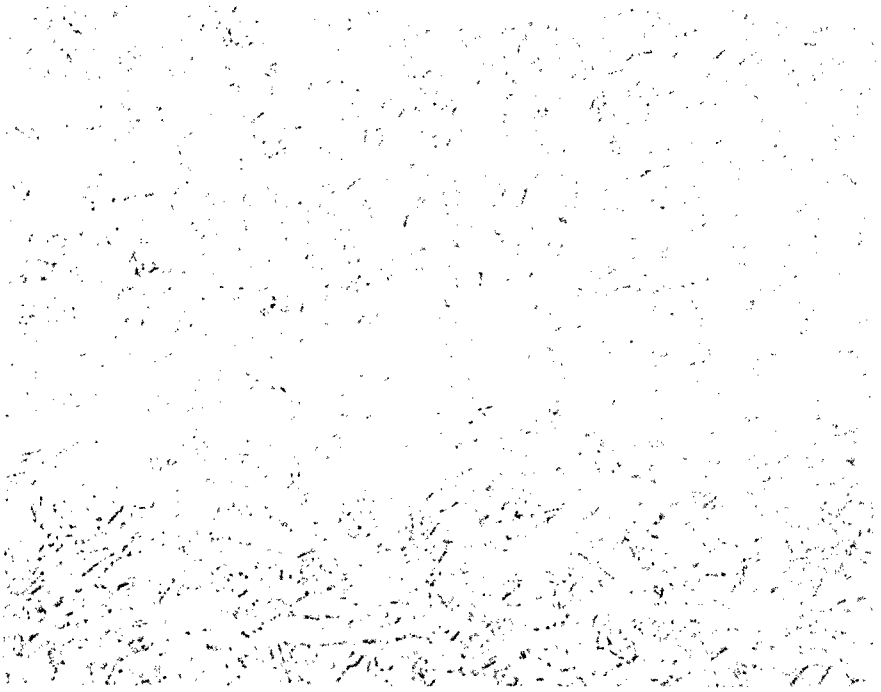

500X

After Heat Treatment

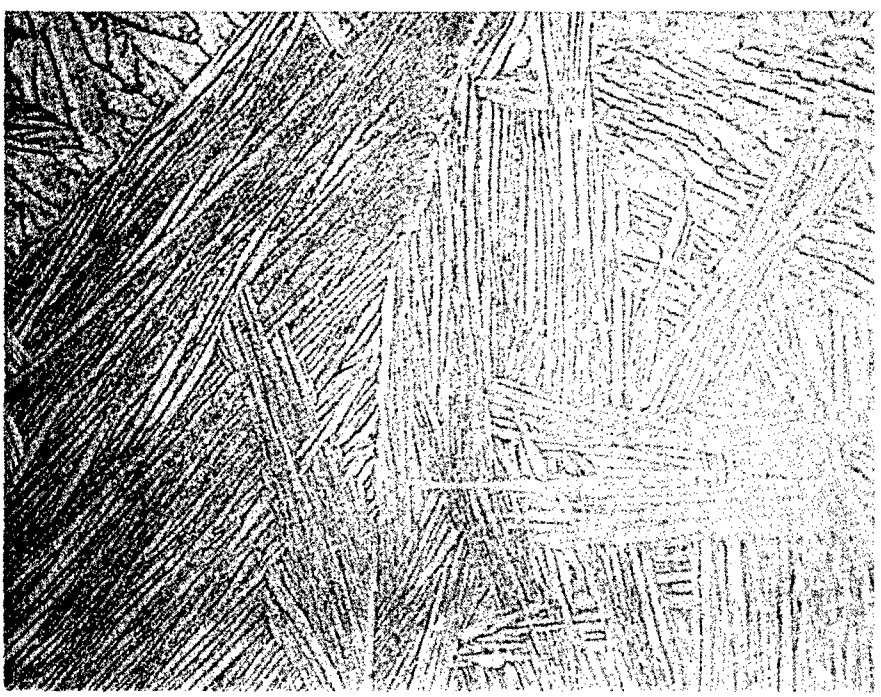

500X

Figure 4. Photomicrographs of Ti-6Aℓ-4V Material, Before and After Beta Mill Annealed Heat Treatment - Longitudinal Direction (Cont'd.)

2.3 INFLUENCE OF PREFERRED ROLLING ON K_R

It became evident early in the generation of crack growth resistance data that testing in the so-called strong (LT) direction could be a problem in some of the materials due to crack deviation out of a plane perpendicular to the loading axis. A separate investigation into means of alleviating this problem by side grooving of the CLWL specimens was attempted. The results of that study are reported in Section IV.

III MECHANICAL PROPERTIES AND LOAD-STRAIN DATA

Mechanical property data were obtained from all material for which crack growth resistance data were obtained. In all cases the tensile coupons were excised from the fractured halves of specified CLWL specimens from two directions--TL and LT (corresponding to fracture plane orientation of ASTM E-399) and were fabricated and tested to ASTM E8-69 (Tension Testing of Metallic Materials).

In addition to the use of a full range SATEC KSM-DH extensometer to record load and strain to fracture, every other specimen was strain gaged to obtain reference Youngs Modulus data. These strain gage determined Moduli were used in all cases in the development of the crack growth resistance data of this report since more scatter was evident in the Modulus data from the extended range extensometer. This scatter is due primarily to the extensometer being an ASTM class B and difficulty in interpretation of the linear slope of the resulting test record.

The mechanical property data for the aluminum material is given in Table III. The mechanical properties of the titanium material are shown in Table IV and those of the 9 nickel steel in Table V.

Data have been separated by test direction (strong LT and weak TL) and thickness by alloy class within each Table.

As supplementary information, typical representative load-strain curves for each thickness and test direction are shown in Figures 5 through 11 for the aluminum alloys; 7075-T6 (Figures 5-6), 7075-T73 (Figures 7-8) and 2024-T3 (Figures 9-11). Figures 12-17 show typical load-strain traces for the titanium alloys tested as part of this study; beta processed Ti-6Al-4V (Figures 12-13), beta mill annealed Ti-6Al-4V (Figures 14-15) and Ti-6Al-6V-2Sn (Figures 16-17) followed by the steel alloy in Figure 18.

The particular tensile coupon from which these traces were obtained can be determined by cross referencing strain to fracture with the tabular data of Tables III-V.

TABLE III MECHANICAL PROPERTY DATA - ALUMINUMS

MATERIAL	FROM SHEET/ PLATE NO.	TEST DIREC-TION	THICKNESS	0.2% OFFSET YIELD, F_{ty}	ULTIMATE STRENGTH, F_{tu}	ELONGA-TION IN 2" G.L.	TOTAL STRAIN TO FRACTURE	MODULI	
								FROM STRAIN GAGE	FROM EXTEN-SOMETER
			(inches)	(psi)	(psi)	(%)	(μinches)	(psix10^6)	(psix10^6)
7075-T6	47	LT	.063	74,367	81,487	13.5	162,530	10.13	9.95
7075-T6	47	LT	.063	74,367	81,487	14.5	146,180	–	9.82
7075-T6	47	TL	.063	71,203	80,696	14.5	165,510	10.01	9.19
7075-T6	47	TL	.063	69,937	81,013	15.5	154,100	–	9.64
7075-T6	54	LT	.195	74,974	80,742	N.A.	147,980	10.30	9.90
7075-T6	54	TL	.195	72,774	83,419	N.A.	132,700	10.27	10.33
7075-T73 (a)	41	LT	.064	61,250	71,875	–	111,190	9.74	10.62
7075-T73 (a)	41	LT	.064	61,912	72,727	–	115,800	–	9.00
7075-T73 (a)	41	TL	.064	62,813	72,813	–	111,900	9.92	9.19
7075-T73 (a)	41	TL	.064	62,382	72,414	–	126,130	–	9.73
7075-T73 (a)	51	LT	.195	67,282	75,897	–	110,360	10.12	10.57
7075-T73 (a)	51	LT	.195	67,626	76,567	–	117,040	–	11.41
7075-T73 (a)	51	TL	.195	67,179	74,359	–	121,680	10.39	11.27
7075-T73 (a)	51	TL	.195	67,318	74,512	–	129,680	–	10.59

(a) Heat treated from same lot as 7075-T6.

TABLE III MECHANICAL PROPERTY DATA - ALUMINUMS (CONTINUED)

MATERIAL	FROM SHEET/ PLATE NO.	TEST DIREC-TION	THICKNESS	0.2% OFFSET YIELD, F_{ty}	ULTIMATE STRENGTH, F_{tu}	ELONGA-TION IN 2" G.L.	TOTAL STRAIN TO FRACTURE	MODULI	
								FROM STRAIN GAGE	FROM EXTEN-SOMETER
			(inches)	(psi)	(psi)	(%)	(μinches)	(psix10^6)	(psix10^6)
2024-T3	21	LT	.064	53,125	74,219	–	197,560	10.61	10.48
2024-T3	21	LT	.064	52,813	74,219	–	199,810	–	10.34
2024-T3	21	TL	.064	44,375	70,313	–	211,360	10.49	11.48
2024-T3	21	TL	.064	45,625	70,625	–	209,980	–	9.41
2024-T351	31	LT	.258	51,116	72,403	–	208,280	10.02	10.19
2024-T351	31	LT	.258	55,233	72,713	–	204,150	–	11.39
2024-T351	31	TL	.258	47,481	71,240	–	220,700	10.59	11.07
2024-T351	31	TL	.258	47,674	70,930	–	209,030	–	10.61
2024-T351 △b	31	LT	.088	53,326	70,642	17.0	170,560	10.37	11.94
2024-T351 △b	31	LT	.082	53,922	70,833	18.5	193,490	10.89	11.14
2024-T351 △b	31	TL	.083	46,489	70,460	19.0	198,640	10.32	11.10
2024-T351 △b	31	TL	.083	47,094	70,823	19.5	198,200	10.34	10.08

△b Chem milled (one side only) from 0.258 inch thick 2024-T351 plate.

TABLE IV MECHANICAL PROPERTY DATA - TITANIUMS

MATERIAL	FROM SHEET/ PLATE NO.	TEST DIREC-TION	THICKNESS	0.2% OFFSET YIELD, F_{ty}	ULTIMATE STRENGTH, F_{tu}	ELONGA-TION IN 2" G.L.	TOTAL STRAIN TO FRACTURE	MODULI	
								FROM STRAIN GAGE	FROM EXTEN-SOMETER
			(inches)	(psi)	(psi)	(%)	(μinches)	(psix10^6)	(psix10^6)
Ti-6Al-4V (c)	91	LT	.058	139,300	149,120	–	119,560	16.91	17.54
Ti-6Al-4V (c)	91	LT	.058	138,250	148,770	–	96,720	–	17.03
Ti-6Al-4V (c)	91	TL	.059	136,210	147,930	–	112,130	18.06	16.26
Ti-6Al-4V (c)	91	TL	.059	136,680	147,060	–	112,180	–	16.16
Ti-6Al-4V (c)	81	LT	.198	139,394	149,370	–	158,020	19.29	18.53
Ti-6Al-4V (c)	81	LT	.197	139,086	143,045	–	161,950	–	17.81
Ti-6Al-4V (c)	81	TL	.198	133,158	140,950	–	143,870	16.94	17.11
Ti-6Al-4V (c)	81	TL	.198	128,535	135,350	–	136,810	–	18.14
Ti-6Al-4V (d)	93	LT	.053	114,015	128,790	12.0	119,520	17.60	17.37
Ti-6Al-4V (d)	93	LT	.054	114,610	129,210	12.0	116,620	–	16.62
Ti-6Al-4V (d)	93	TL	.054	116,604	127,240	8.0	74,520	17.30	16.96
Ti-6Al-4V (d)	93	TL	.053	117,050	128,980	7.5	70,540	–	16.91
Ti-6Al-4V (d)	87	LT	.186	121,720	131,720	11.5	107,920	19.00	19.37
Ti-6Al-4V (d)	87	LT	.187	120,300	130,500	13.0	121,220	–	19.01
Ti-6Al-4V (d)	87	TL	.187	111,230	125,130	12.0	105,060	17.01	16.01
Ti-6Al-4V (d)	87	TL	.187	111,250	125,400	10.0	93,820	–	16.23

(c) As received, surplus SST material in Beta processed condition.

(d) Material as heat treated in vacuum @ 1900±20°F for 5 minutes, cool in vacuum to 1350±15°F; hold for two hours and vacuum cool to 300°F.

TABLE IV MECHANICAL PROPERTY DATA - TITANIUMS (CONTINUED)

MATERIAL	FROM SHEET/ PLATE NO.	TEST DIREC-TION	THICKNESS	0.2% OFFSET YIELD, F_{ty}	ULTIMATE STRENGTH, F_{tu}	ELONGA-TION IN 2" G.L.	TOTAL STRAIN TO FRACTURE	MODULI	
								FROM STRAIN GAGE	FROM EXTEN-SOMETER
			(inches)	(psi)	(psi)	(%)	(μinches)	(psix10^6)	(psix10^6)
Ti-6Al-6V-2Sn (e)	11	LT	.064	159,375	167,190	14.5	158,160	17.08	18.27
Ti-6Al-6V-2Sn (e)	11	LT	.064	159,502	166,360	14.5	151,040	–	17.70
Ti-6Al-6V-2Sn (e)	11	TL	.063	156,804	160,760	13.5	137,200	16.66	17.38
Ti-6Al-6V-2Sn (e)	11	TL	.063	156,329	161,080	13.5	136,300	–	16.22
. . . . .	. . . .	. . . .	. . . . .	. . . . .	. . . . .	. . . . .	. . . . .	. . . . .	. . . . .
Ti-6Al-6V-2Sn (e)	A	LT	.212	156,461	163,860	15.0	152,390	16.84	16.87
Ti-6Al-6V-2Sn (e)	A	LT	.212	155,827	163,350	15.5	156,590	–	16.63
Ti-6Al-6V-2Sn (e)	A	TL	.210	144,402	153,226	13.5	136,780	14.58	14.94
Ti-6Al-6V-2Sn (e)	A	TL	.211	145,024	153,649	13.5	135,910	–	14.92

(e) Mill annealed condition.

TABLE V MECHANICAL PROPERTY DATA - STEEL

MATERIAL	FROM SHEET NO.	TEST DIRECTION	THICKNESS	0.2% OFFSET YIELD, F_{ty}	ULTIMATE STRENGTH, F_{tu}	ELONGATION IN 2" G.L.	TOTAL STRAIN TO FRACTURE	MODULI	
								FROM STRAIN GAGE	FROM EXTENSOMETER
			(inches)	(psi)	(psi)	(%)	(μinches)	(psix10^6)	(psix10^6)
9Ni-4Co-.2C (f)	71	LT	.064	150,000	171,430	—	93,410	28.44	26.77
9Ni-4Co-.2C	71	LT	.064	150,000	171,430	—	93,410	27.40	—
9Ni-4C9-.2C (f)	71	LT	.065	145,570	168,200	—	104,390	29.16	27.30
9Ni-4Co-.2C	71	LT	.065	145,570	168,200	—	104,390	28.56	—
. . . . .	. . .	. . . . .	. . . . .	. . . . .	. . . . .	. . . .	. . . . .	. . . . .	. . . . .
9Ni-4Co-.2C (f)	71	TL	.064	135,510	161,990	—	116,040	25.96	25.53
9Ni-4Co-.2C	71	TL	.064	135,510	161,990	—	116,040	28.32	—
9Ni-4Co-.2C (f)	71	TL	.064	136,640	162,110	—	121,430	26.19	24.84
9Ni-4Co-.2C	71	TL	.064	136,640	162,110	—	121,430	27.05	—

(f) Number 1 Finish. - Back-to-back strain gaged.

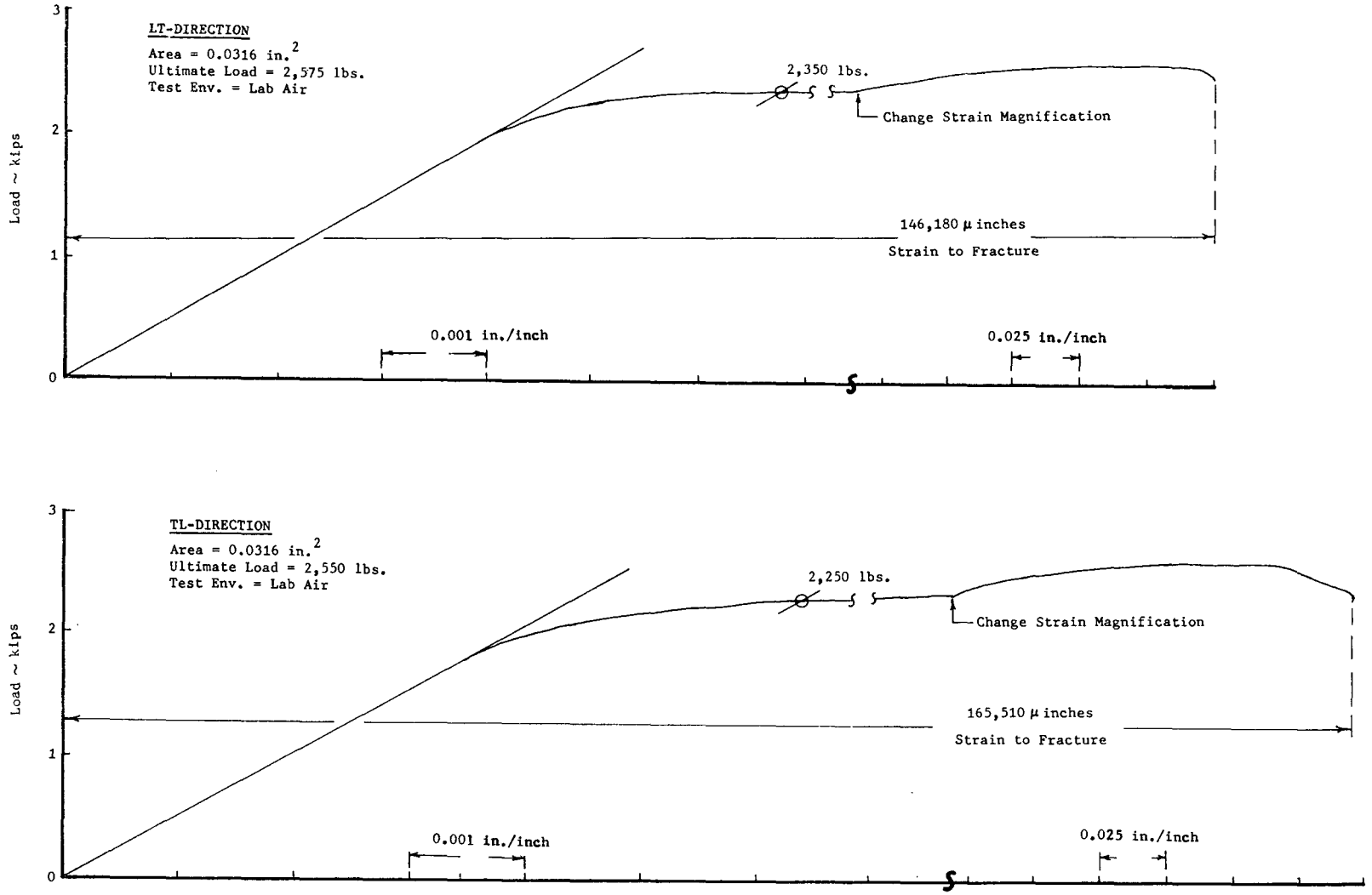

Figure 5. Typical Load-Strain Curves for 0.063 Inch Gage 7075-T6 Sheet

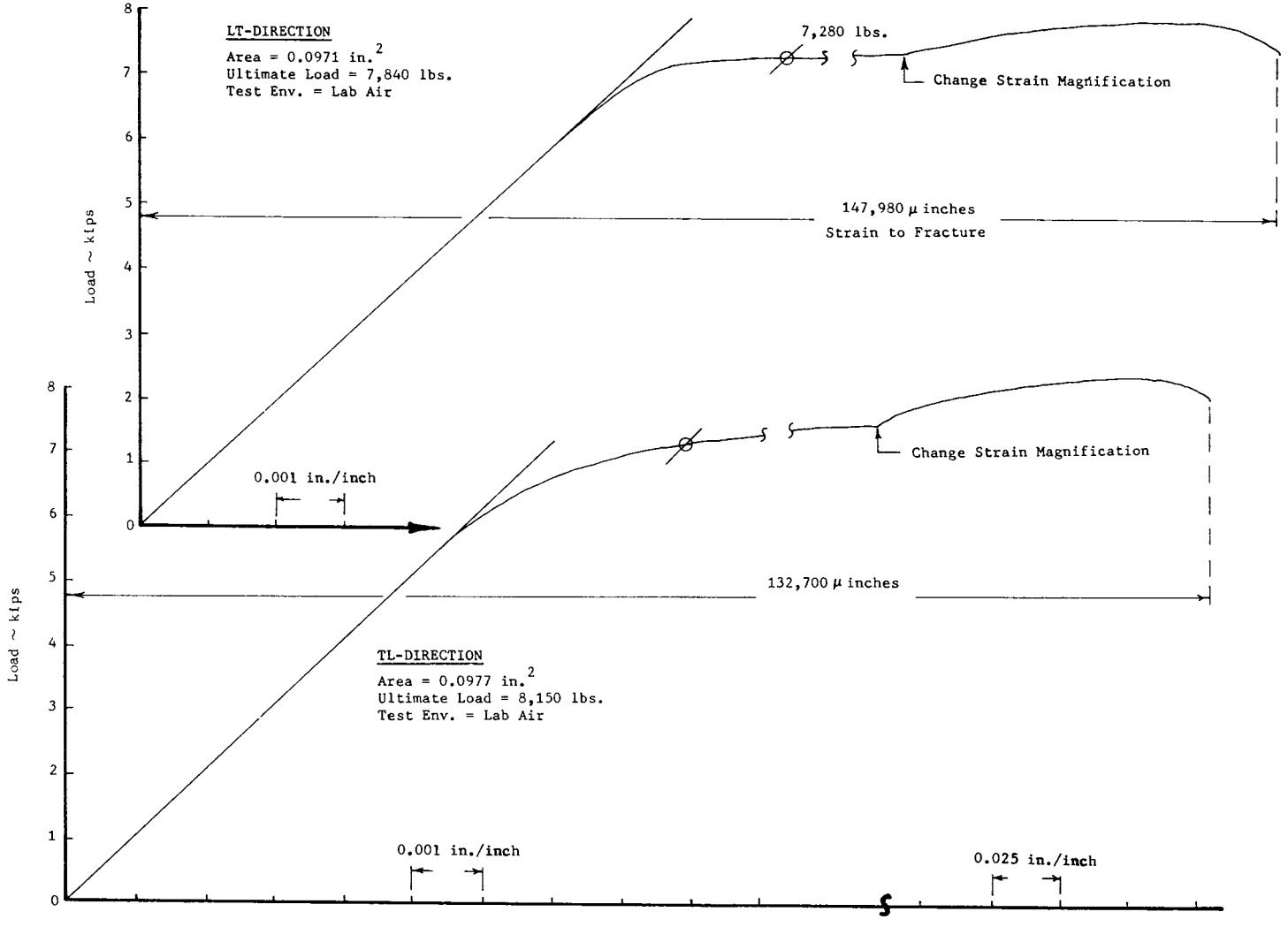

Figure 6. Typical Load-Strain Curves for 0.195 Inch Gage 7075-T6 Plate

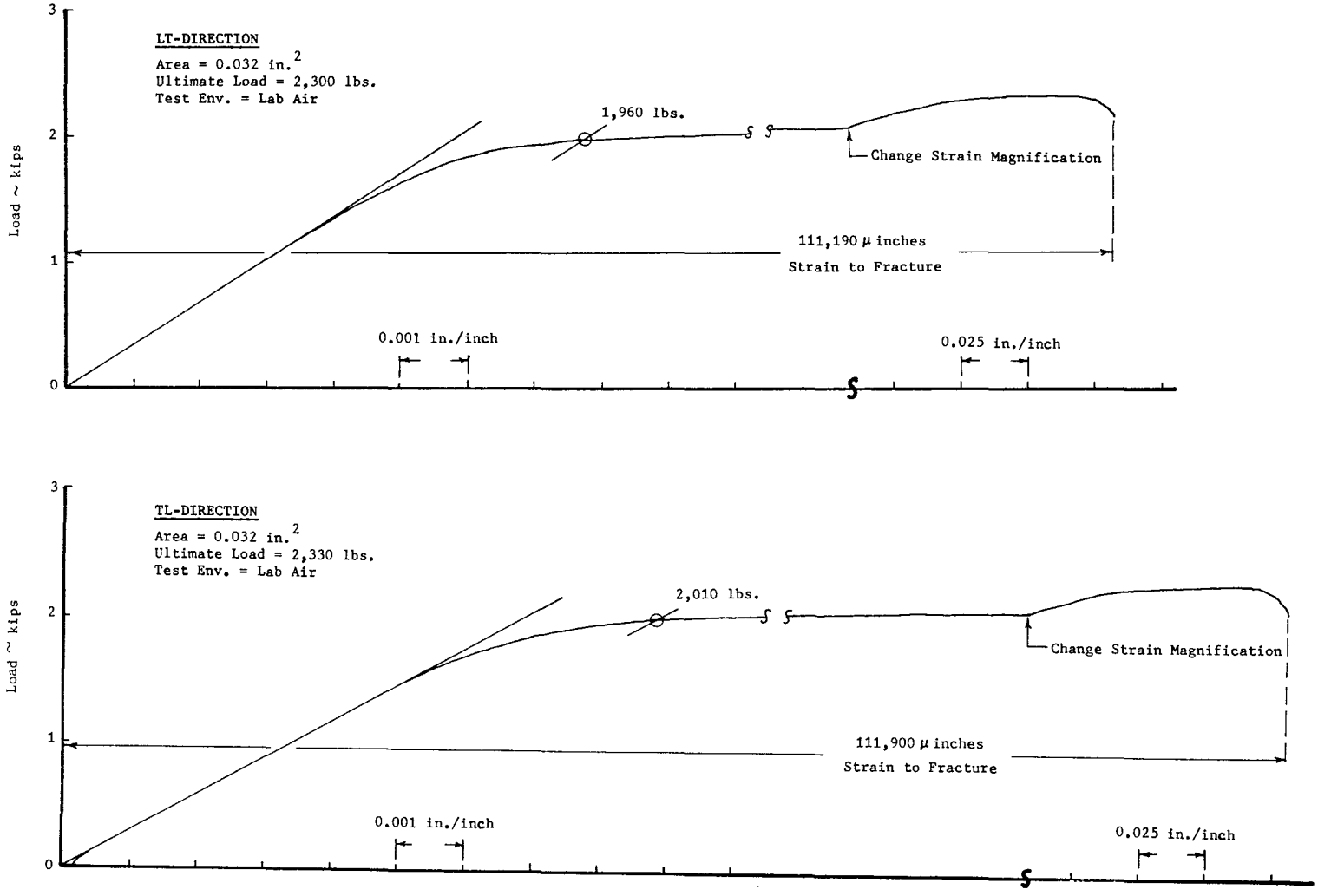

Figure 7. Typical Load-Strain Curves for 0.064 Inch Gage 7075-T73 Sheet

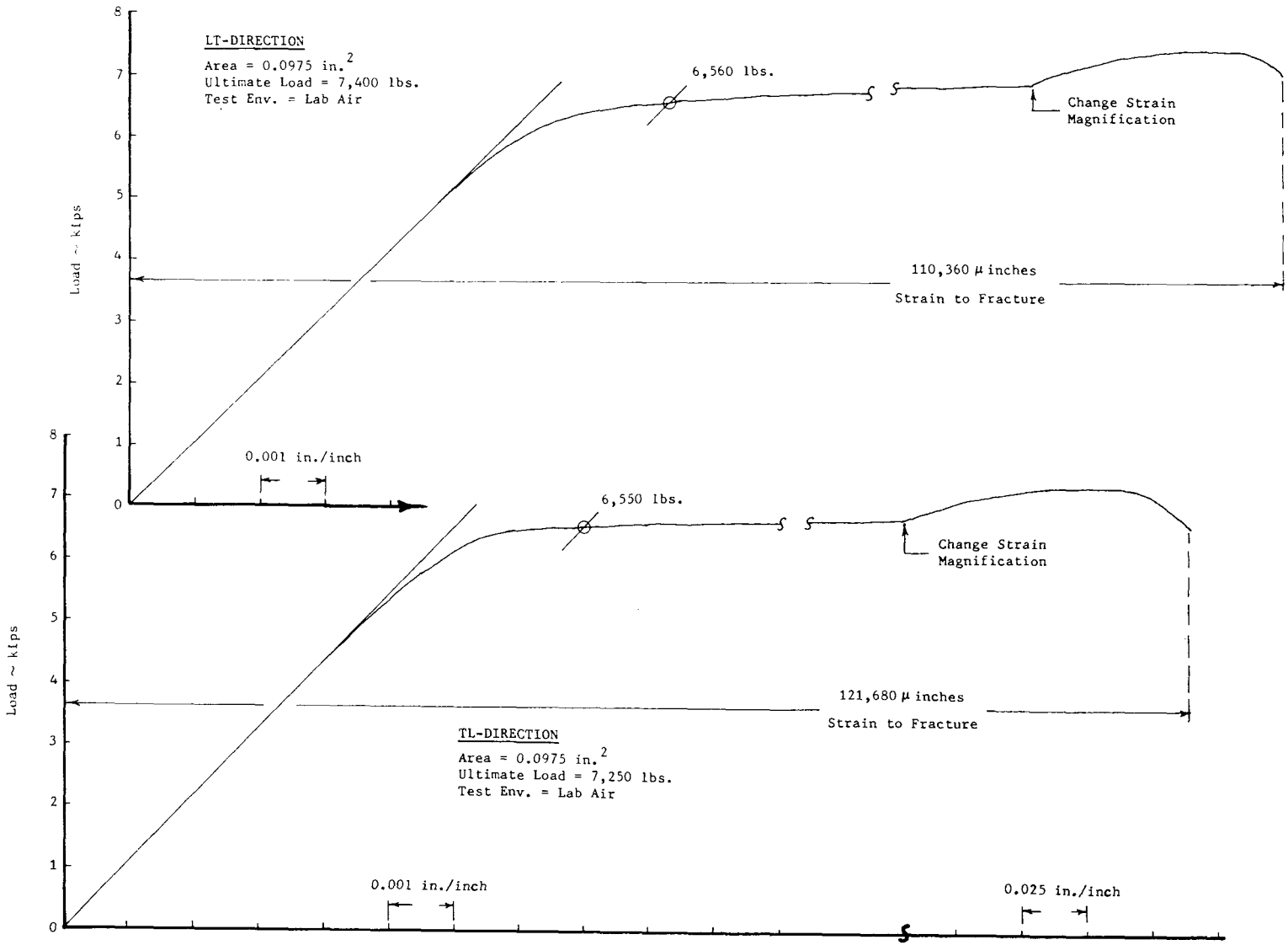

Figure 8. Typical Load-Strain Curves for 0.195 Inch Gage 7075-T73 Plate

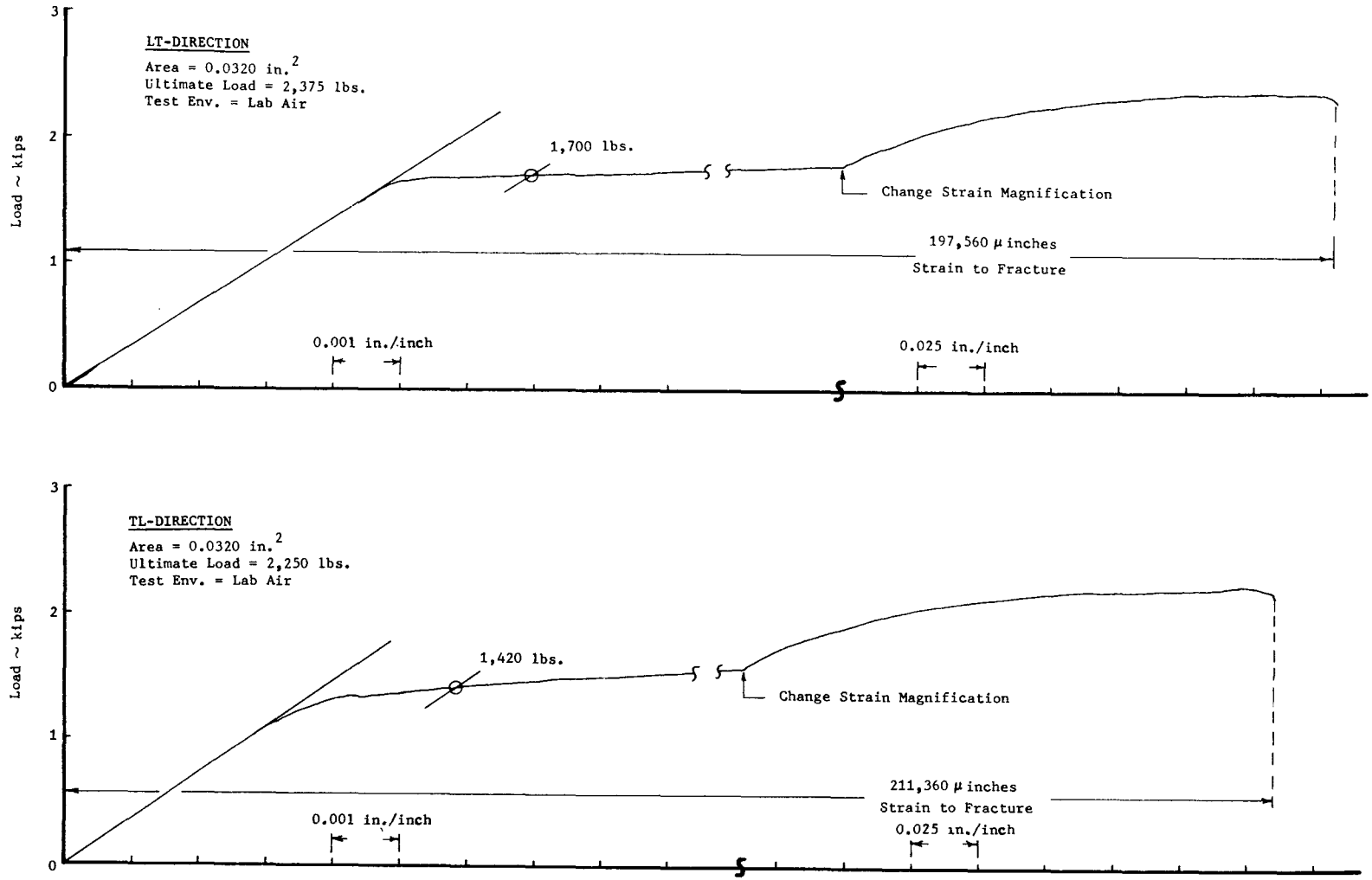

Figure 9. Typical Load-Strain Curves for 0.064 Inch Gage 2024-T3 Sheet

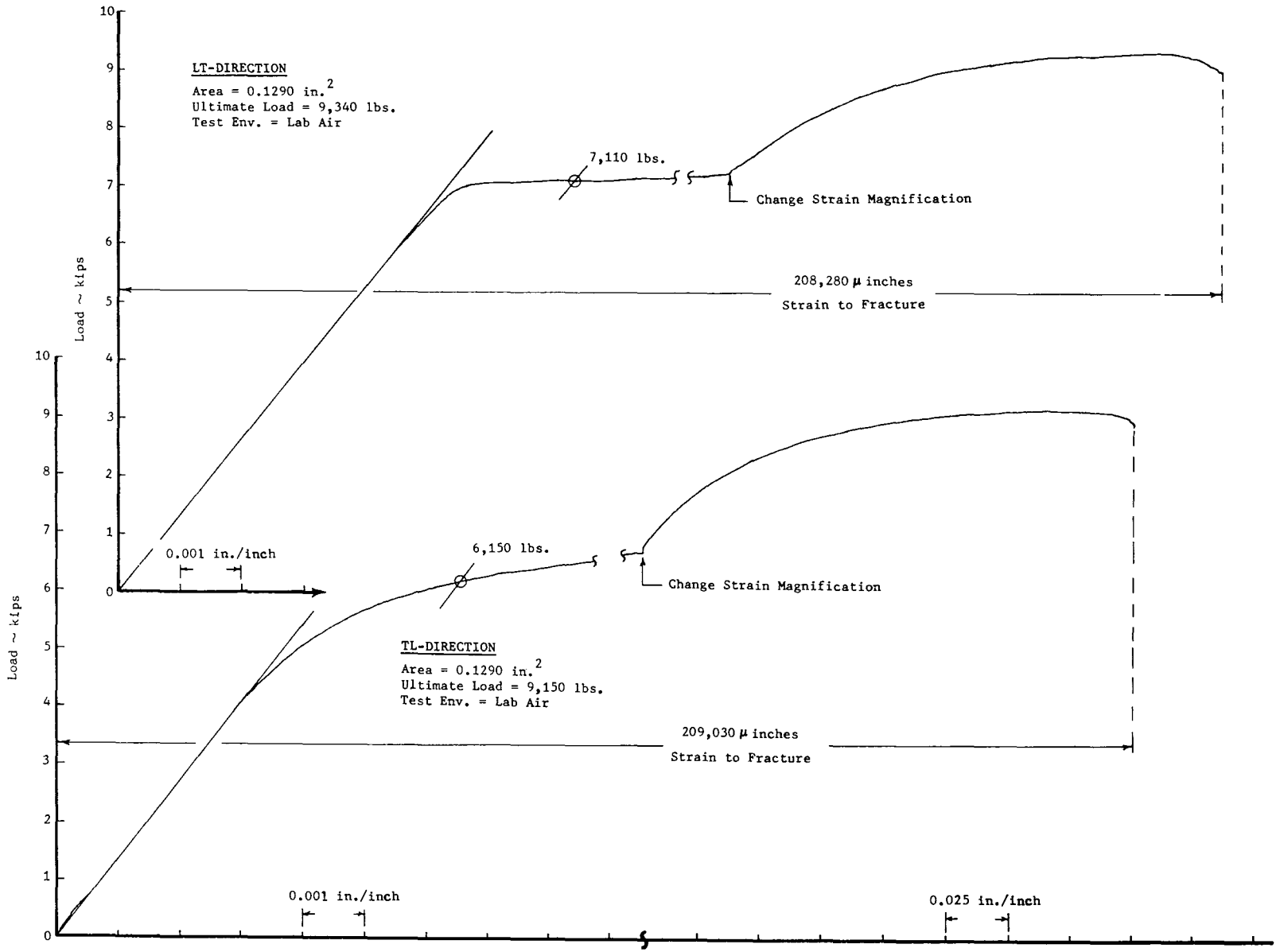

Figure 10. Typical Load-Strain Curves for 0.258 Inch Gage 2024-T3 Plate

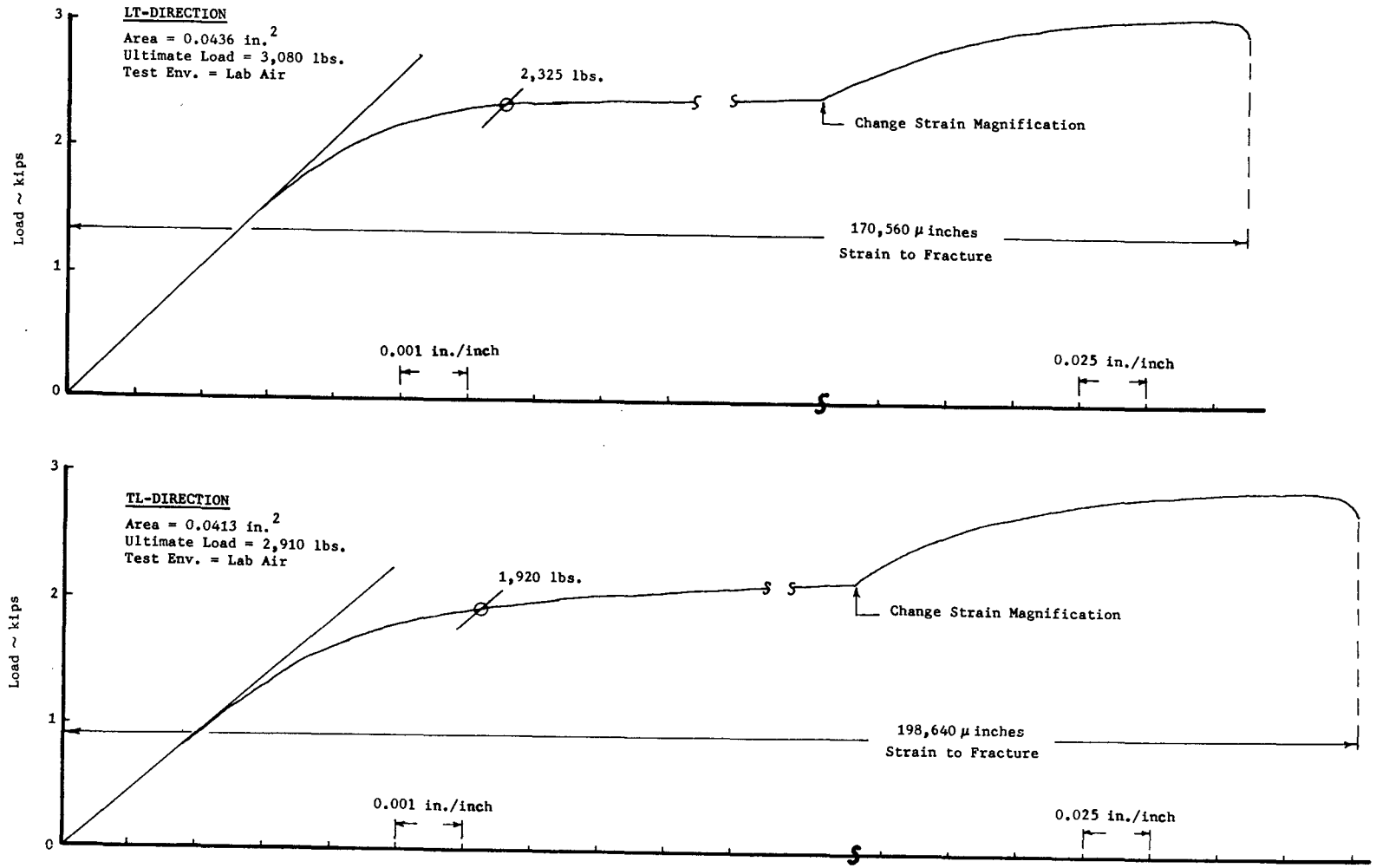

Figure 11. Typical Load-Strain Curves for Chem Milled, 2024-T3 - Nominal Thickness 0.08 Inch

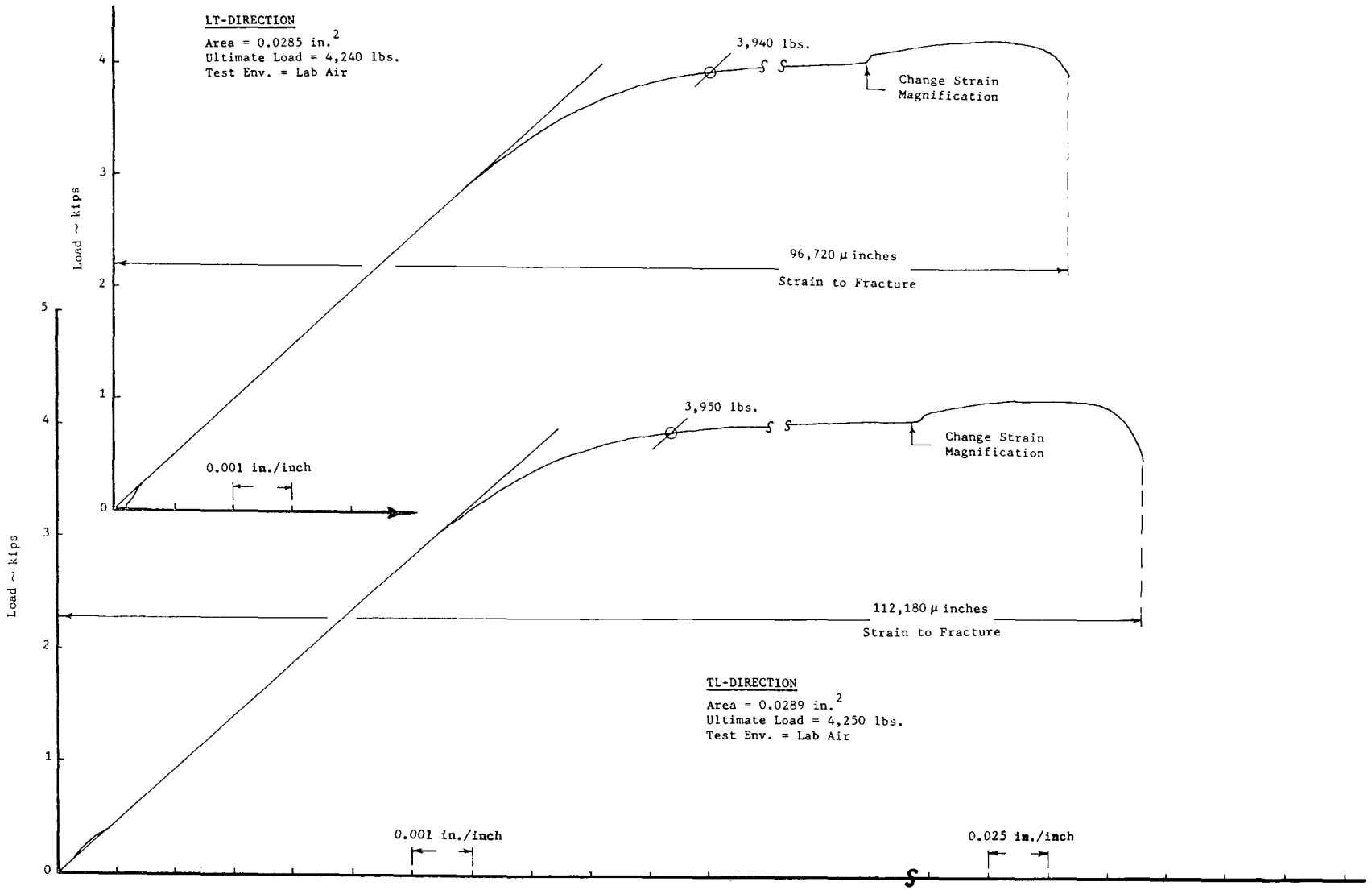

Figure 12. Typical Load-Strain Curves for As Received, 0.58 Inch Gage Beta Processed Ti-6Al 4V Sheet

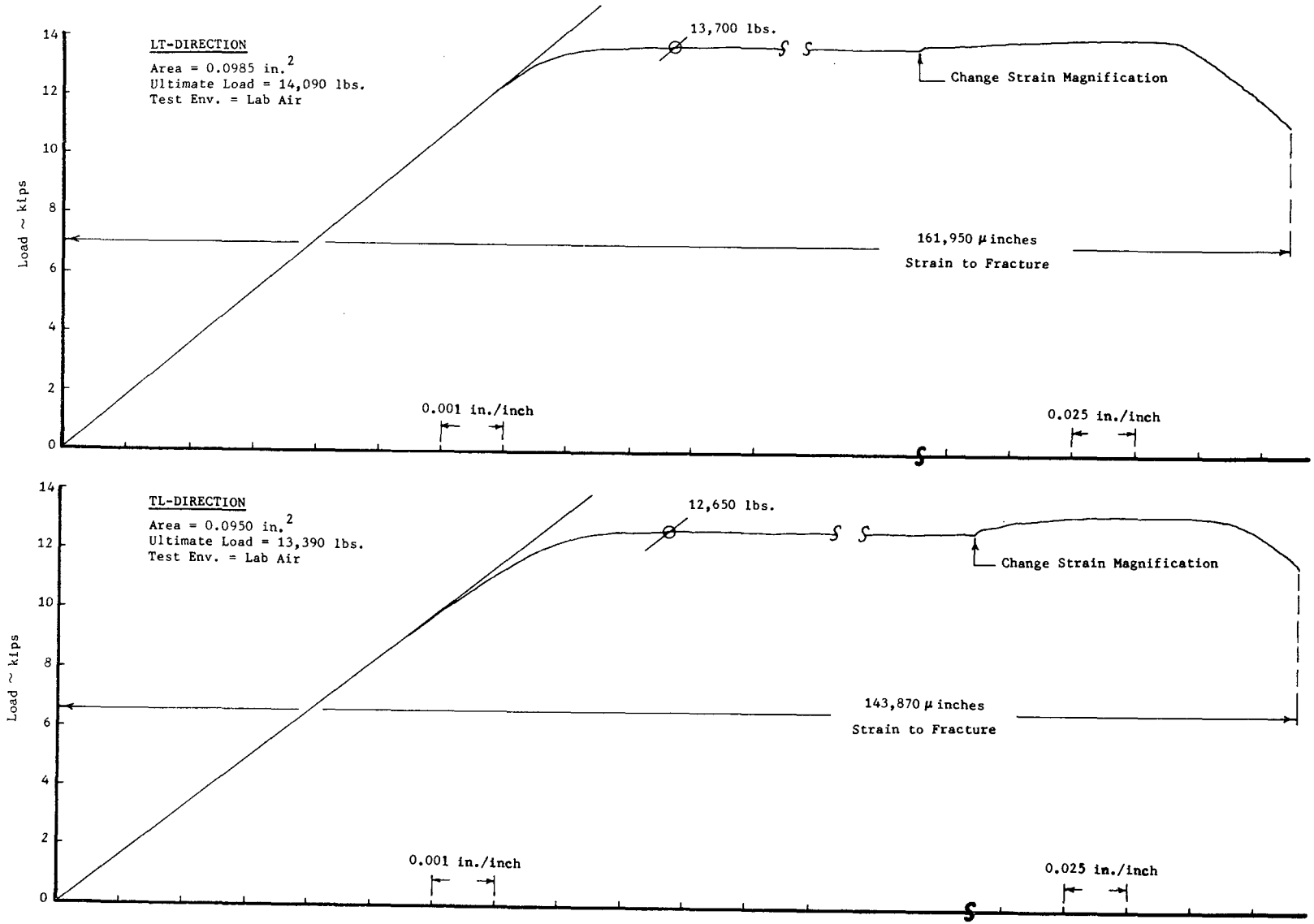

Figure 13. Typical Load-Strain Curves for As Received, 0.198 Inch Gage Beta Processed Ti-6Aℓ-4V Plate

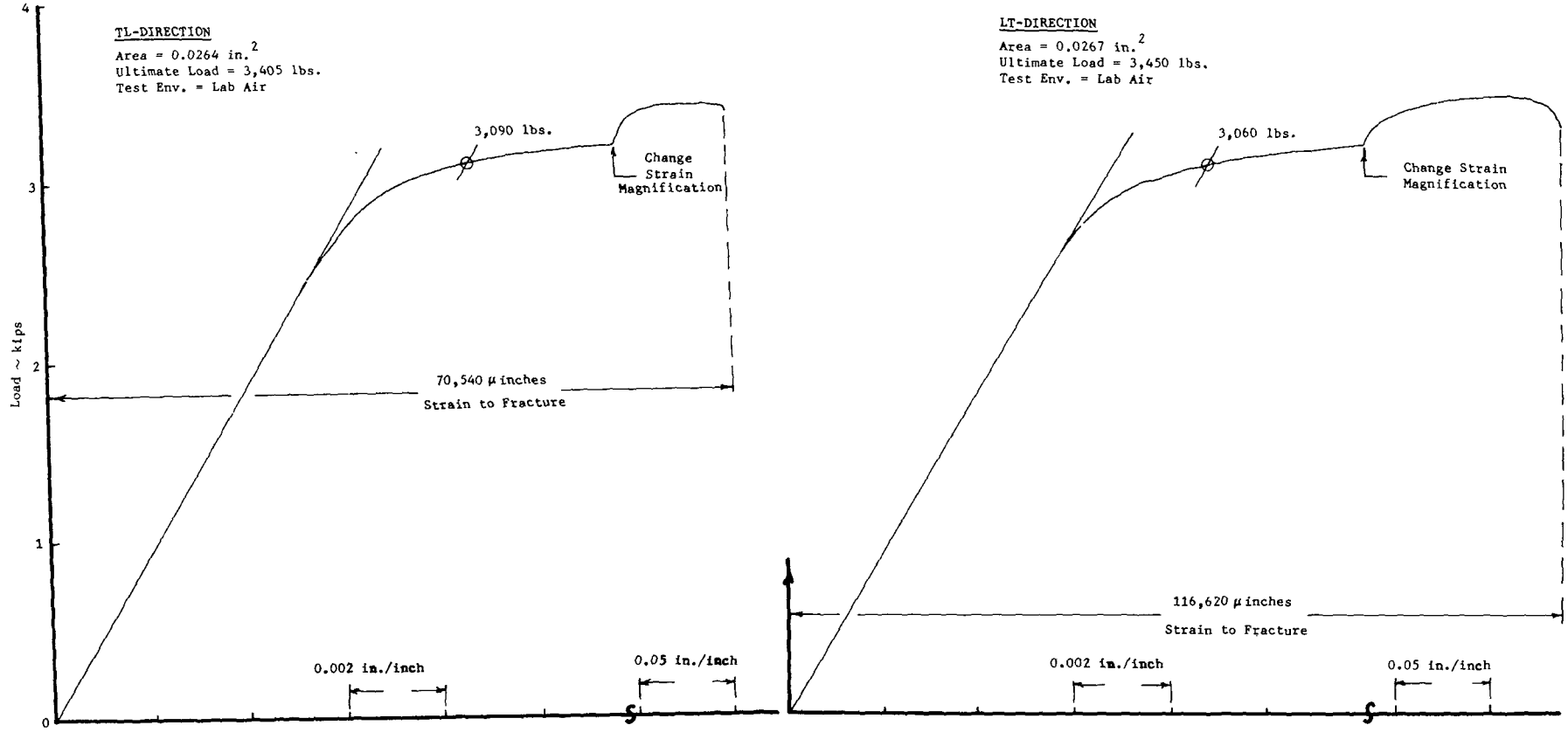

Figure 14. Typical Load-Strain Curves for 0.054 Inch Gage Beta Mill Annealed Ti-6Al-4V sheet

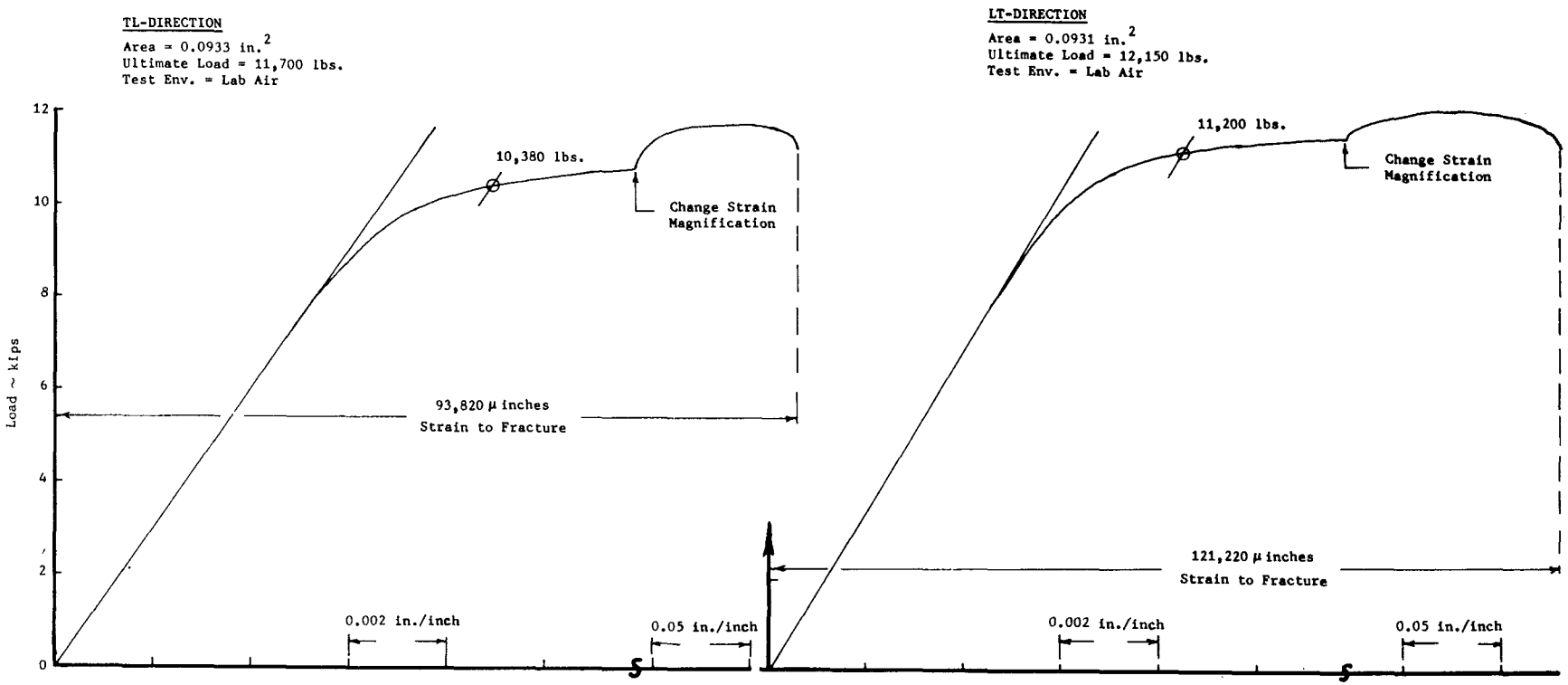

Figure 15. Typical Load-Strain Curves for 0.187 Inch Gage Beta Mill Annealed Ti-6Al-4V Plate

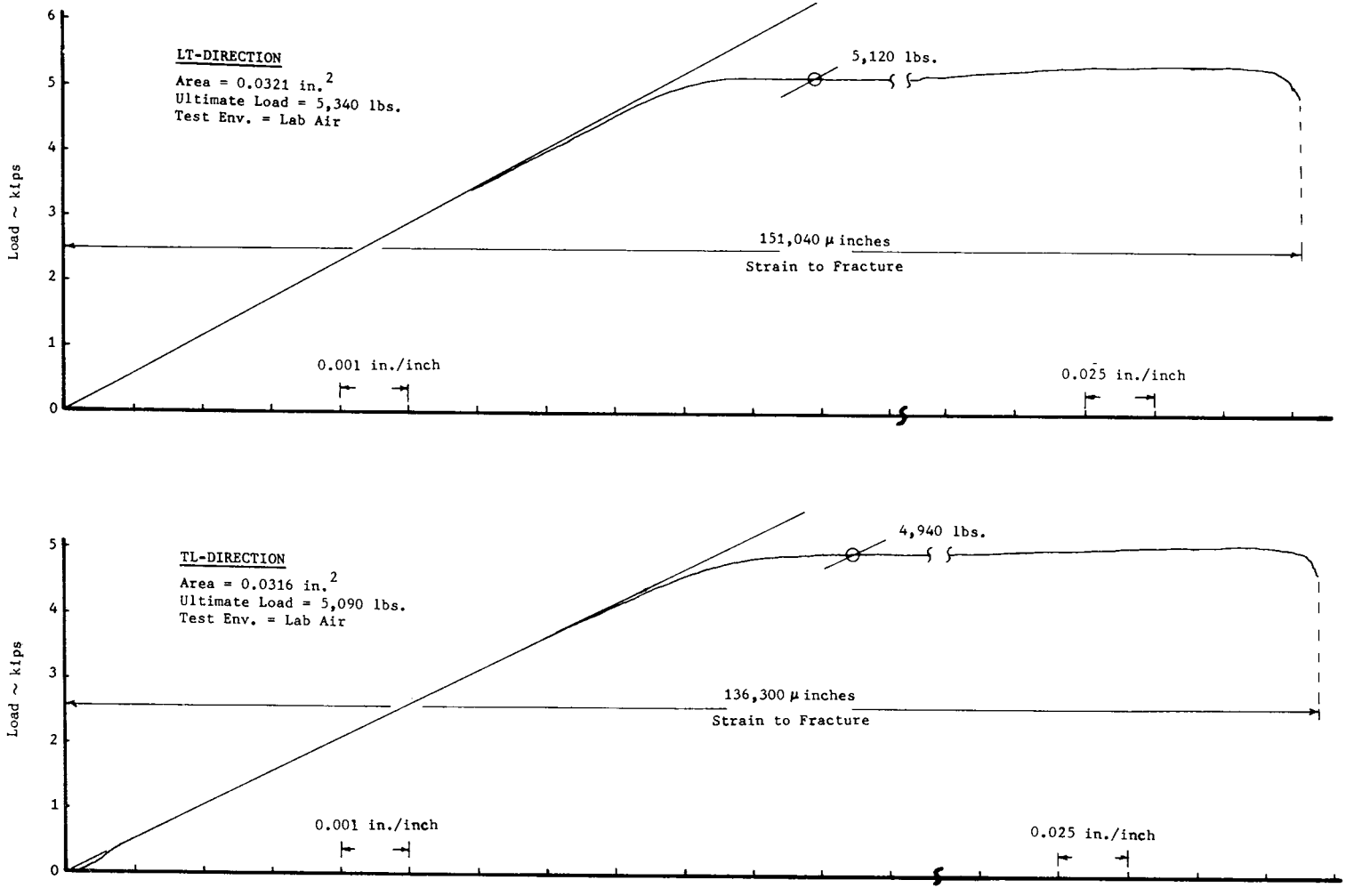

Figure 16. Typical Load-Strain Curves for 0.064 Inch Gage Ti-6Aℓ-6V-2Sn (Annealed) Sheet

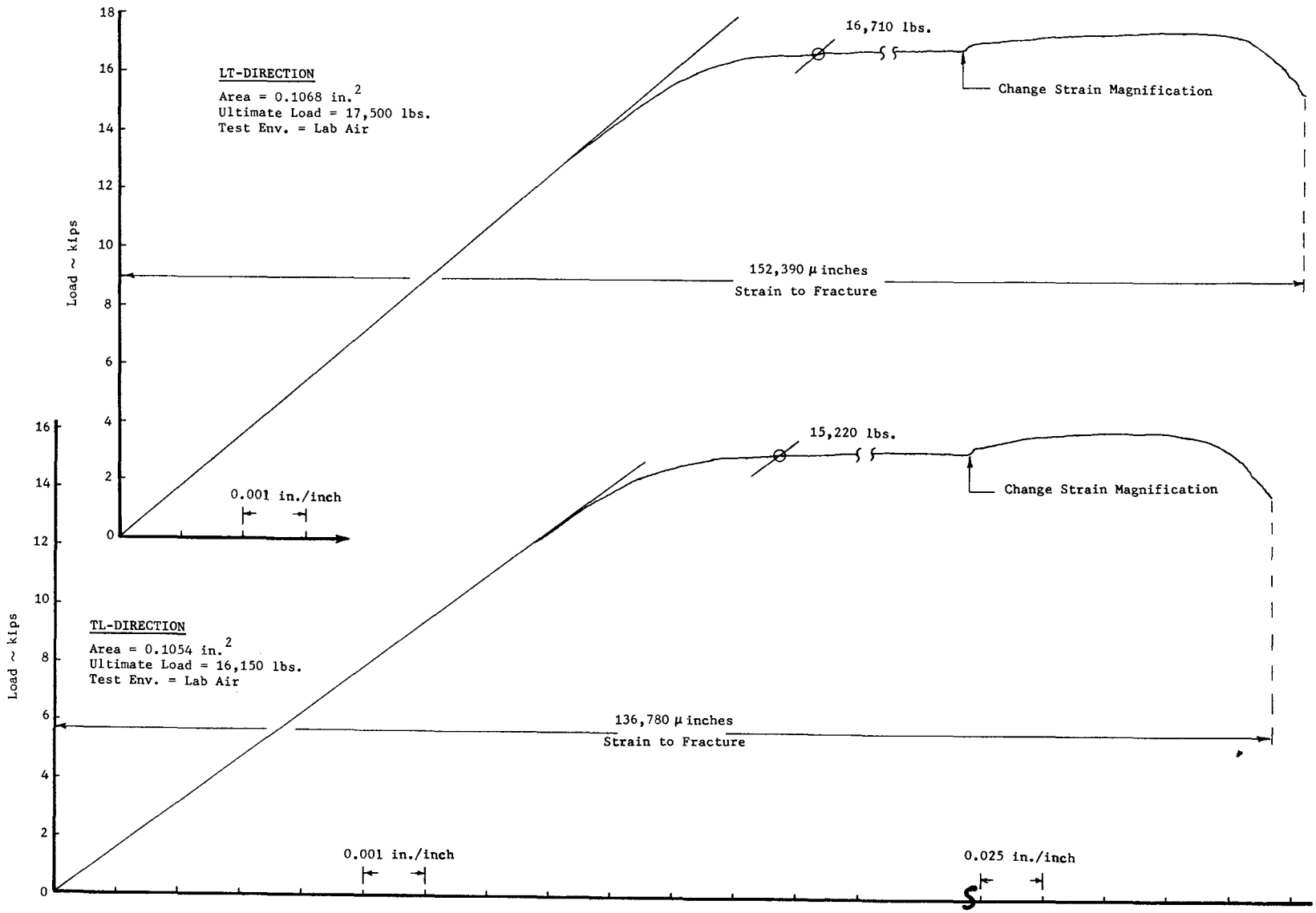

Figure 17. Typical Load-Strain Curves for 0.210 Inch Gage Ti-6Aℓ-6V-2Sn (Annealed) Plate

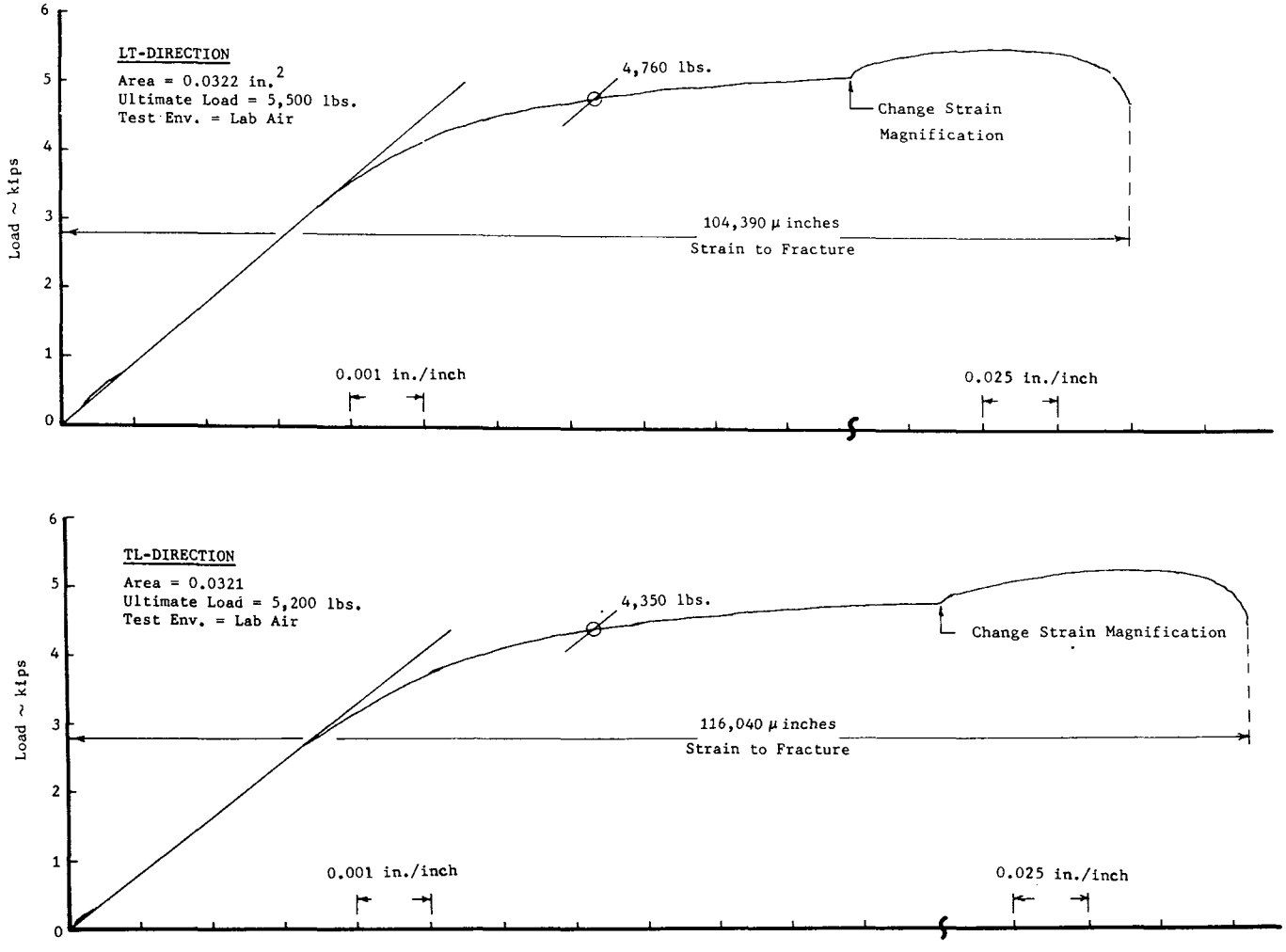

Figure 18. Typical Load-Strain Curves for 0.064 Inch Gage 9Ni-4Co-.2C Steel Sheet

IV CLWL SPECIMEN CALIBRATION AND DATA ANALYSIS PROCEDURE

4.1 THE CRACK LINE WEDGE LOADED (CLWL) SPECIMEN

Figure 19 shows typical dimensions of the CLWL specimen used in this program. The height (H) to width (W) ratio is 0.6. In some cases the specimen width must be reduced to accommodate available material. In all cases the H/W ratio remains the same (0.6) by reducing specimen height. These adjustments are necessary so that the specimen calibration may be used without adjustments for varying H/W. A photo of the CLWL specimen (subsize) is shown in Figure 20.

4.2 DEVELOPMENT OF THE CLWL CALIBRATION CURVES

The procedure used to obtain the calibration curves for the CLWL specimen are essentially the same as those given in Reference 1. However, the interpretation of data, least squares fits and other points peculiar to these data will be described in detail.

An overall view of the calibration set up is shown in Figure 21. The specimen is loaded in tension through half-moon shaped loading devices as shown in Figure 22 (right hand side). In Figure 19 two measurement points, V_1 and V_2 are indicated. These points are located at distances of 0.1576W and 0.303W, respectively from the point of load application, i.e., the centerline of the loading hole. These displacement measurement locations correspond to those given in Reference 2. Two (MTS type) beam clip gages were placed between two round flat head bolts attached to the specimen at the V_1 and V_2 positions. Displacements were recorded for the V_1 and V_2 probe positions on separate charts as a function of load (P) for various crack (slot) lengths.

The calibration specimen was a 1/4 inch thick, clad 2024-T351 material tested with saw slots to simulate the required crack lengths. Two directions of fracture plane orientation were examined, TL and LT to determine if any effect on repeatability of data and test set up could be detected.

Each specimen was loaded in tension (see Figure 22), elastically, with successive saw slot to specimen width ratios, i.e., a/W's. Displacements V_1 vs V_2 as a function of P traces were recorded at each successive a/W's. The slope of these traces was then used to calculate values of $\frac{EV_nB}{P}$ or the required compliance curves for both probe positions. Values of Young's Modulus for this material were determined from four excised tensile coupons from the calibration specimen as described previously in Section III. An average value of 10.338×10^6 psi was used since there was little variation in modulus in the LT and TL direction for this material. Figures 23 and 24 show the compliance data for the V_1 and V_2 probe positions and least squares polynomial fits to those data.

Since the CLWL specimen is loaded in wedge loading and the load, P must be determined from these calibration curves, care was taken that repeatability and

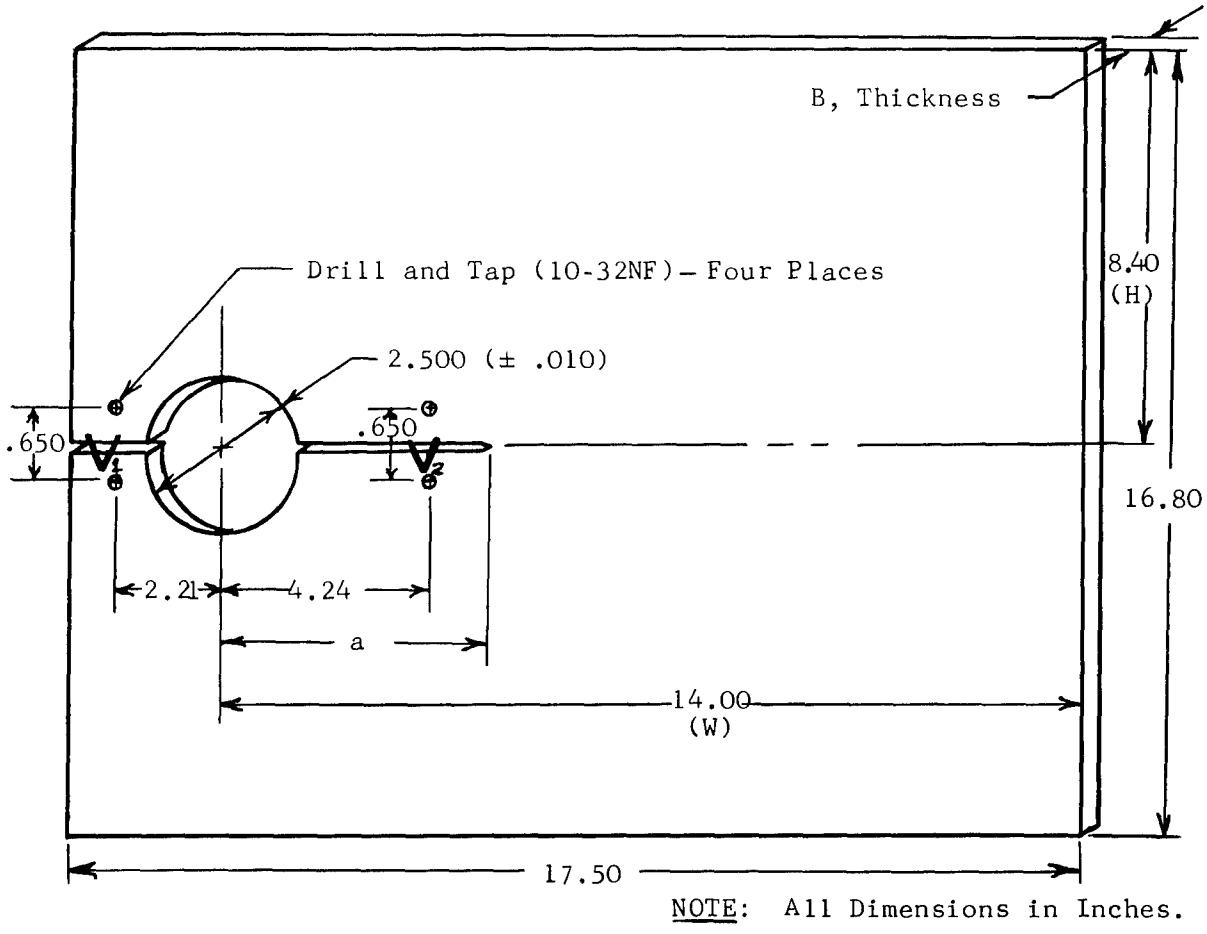

TL - Specimens have rolling direction parallel to slot.

LT - Specimens have rolling direction perpendicular to slot.

Figure 19. Crack Line Wedge Loaded (CLWL), CS Type Specimen (H/W ≈ .6)

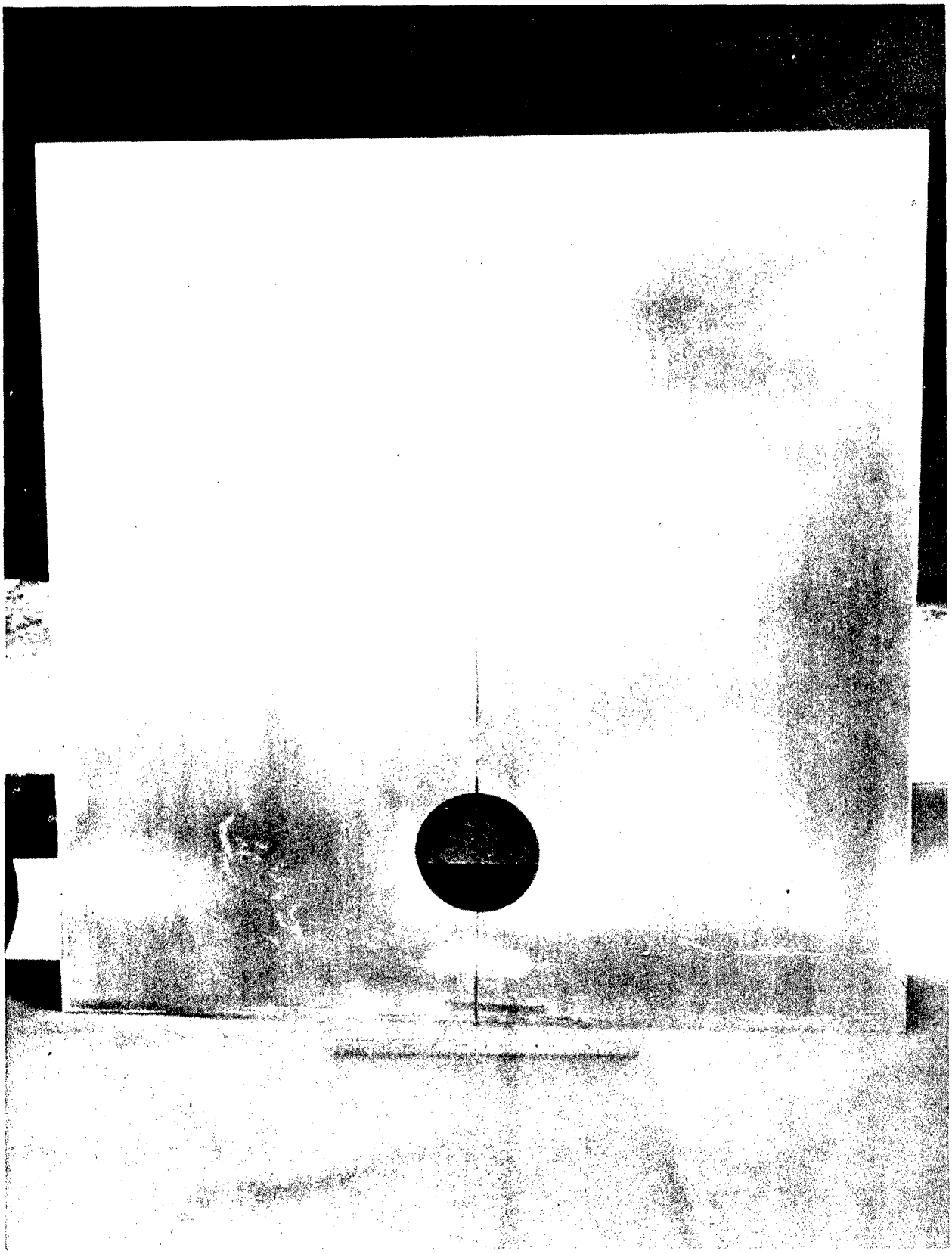

Figure 20. Crack Line Wedge Loaded Specimen (Subsized)

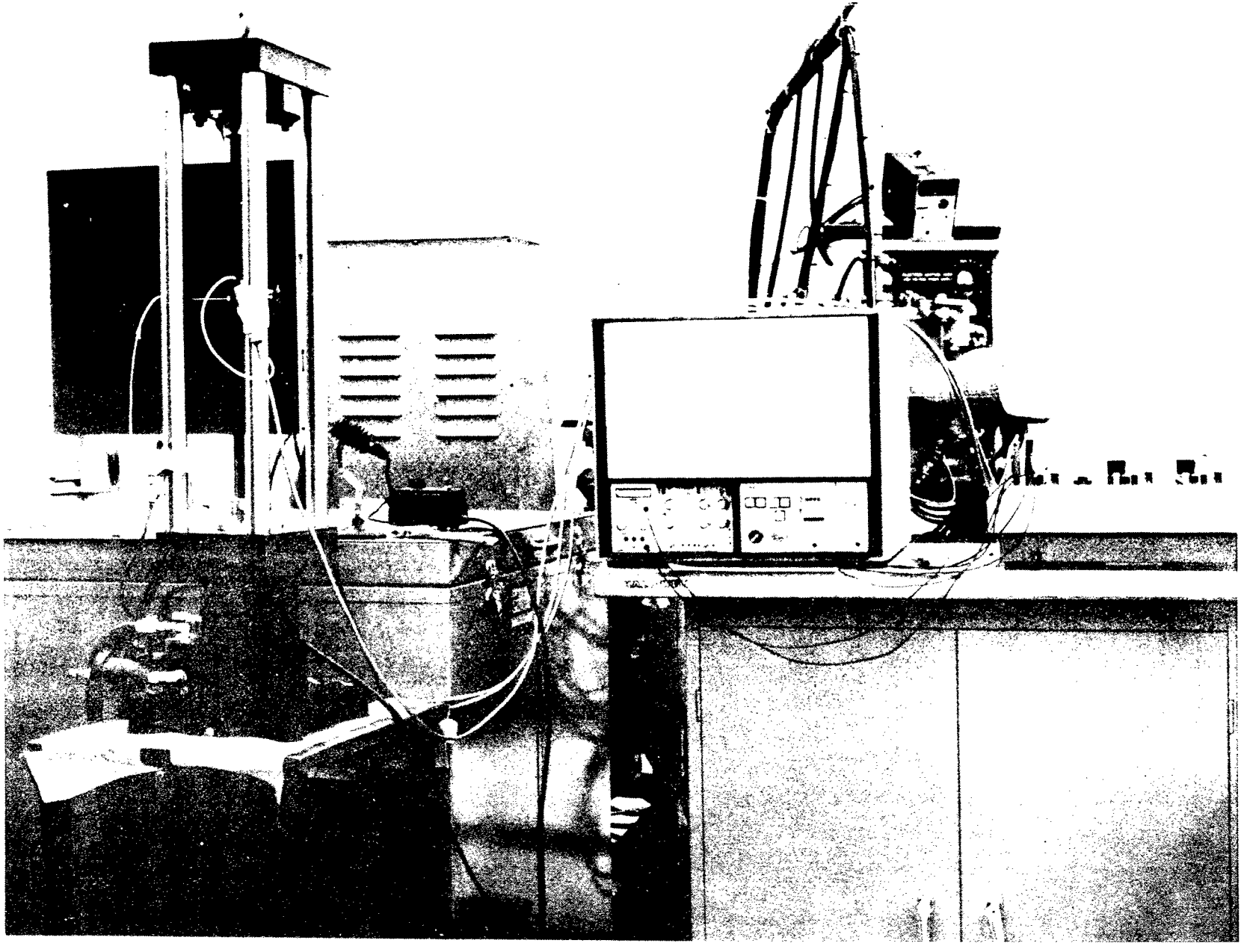

Figure 21. Calibration and Fatigue Pre-Cracking Arrangement

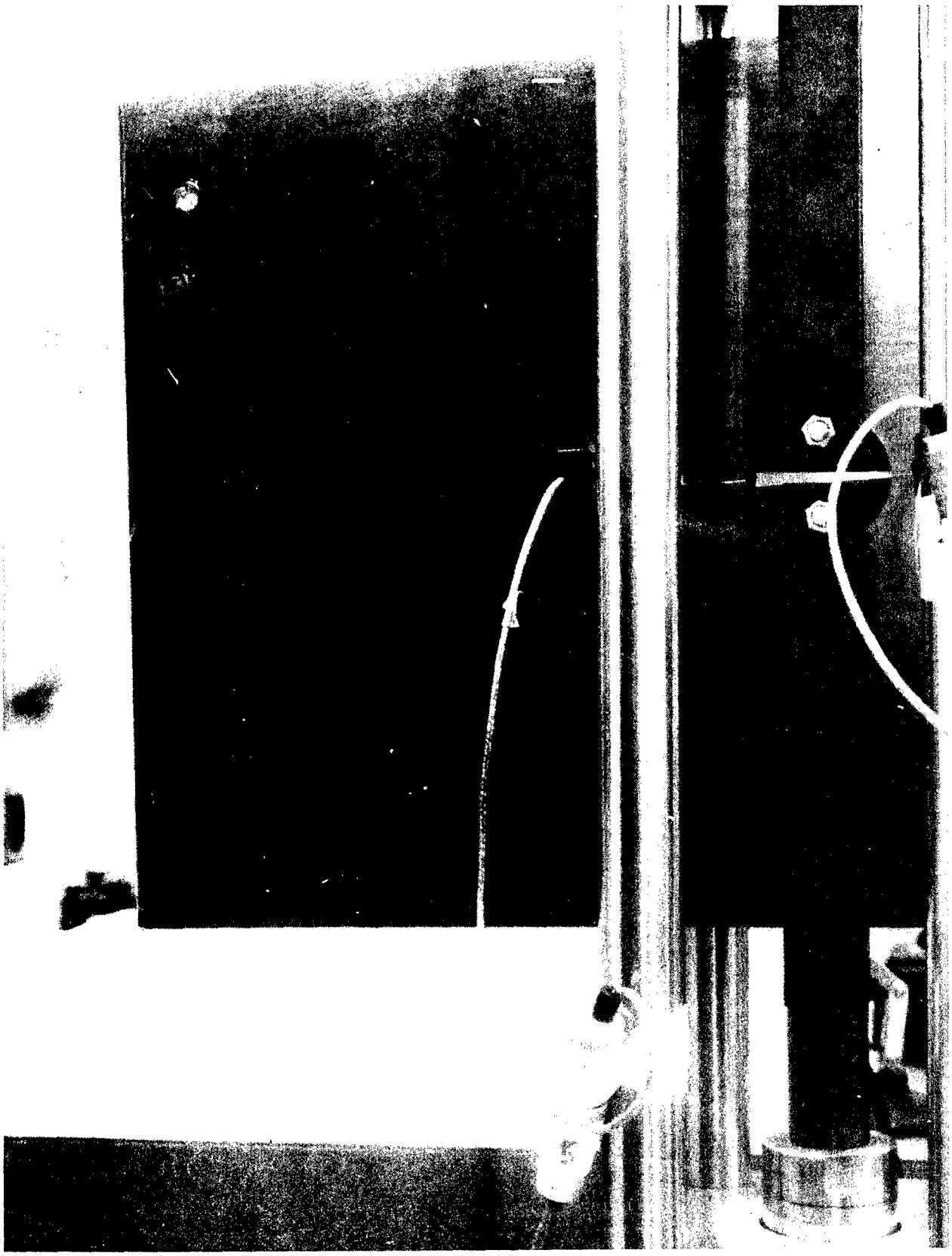

Figure 22. Loading for Calibration and Pre-Cracking CLWL - Compact Type Specimens

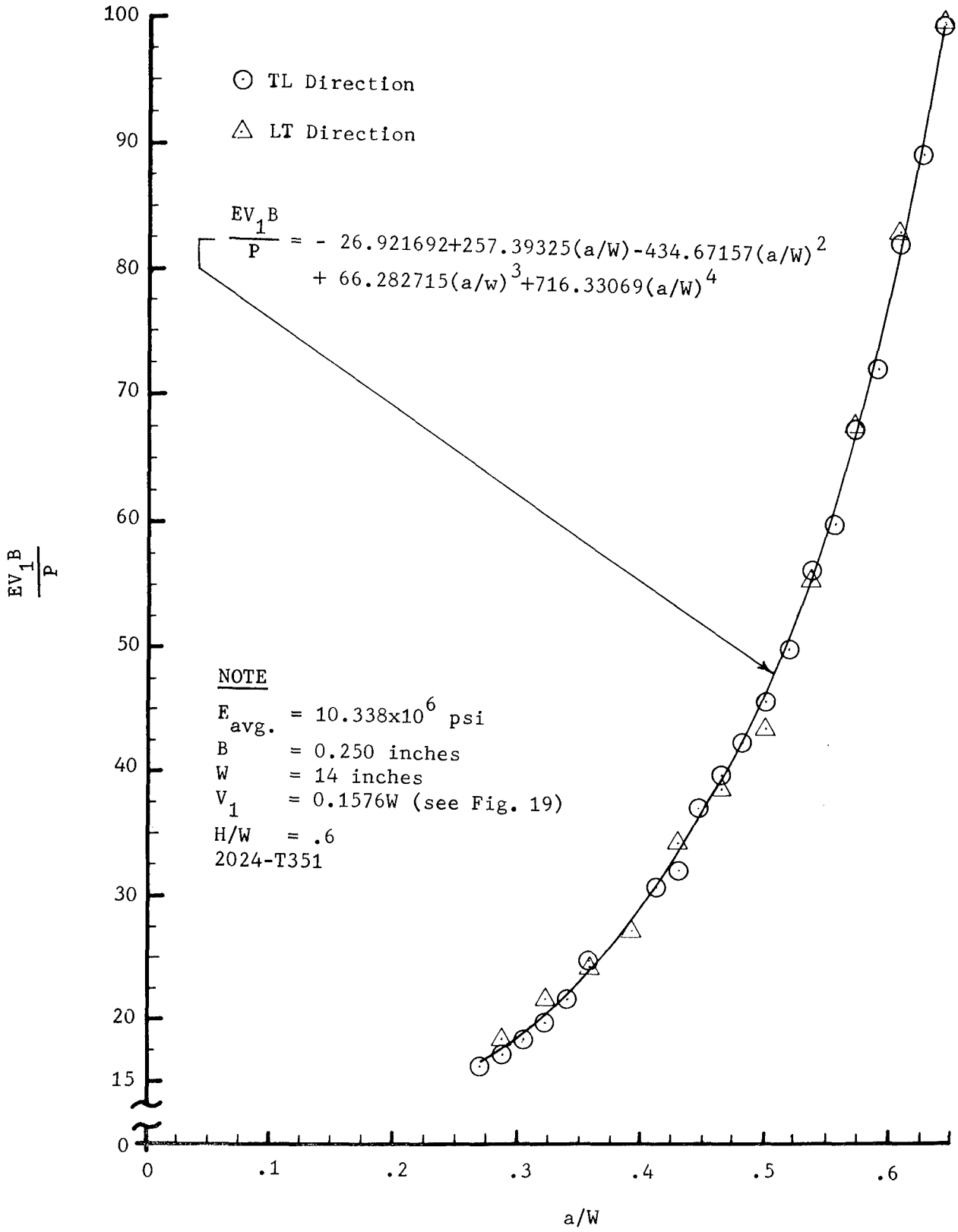

Figure 23. CLWL Compliance Curve for V_1 Probe Location

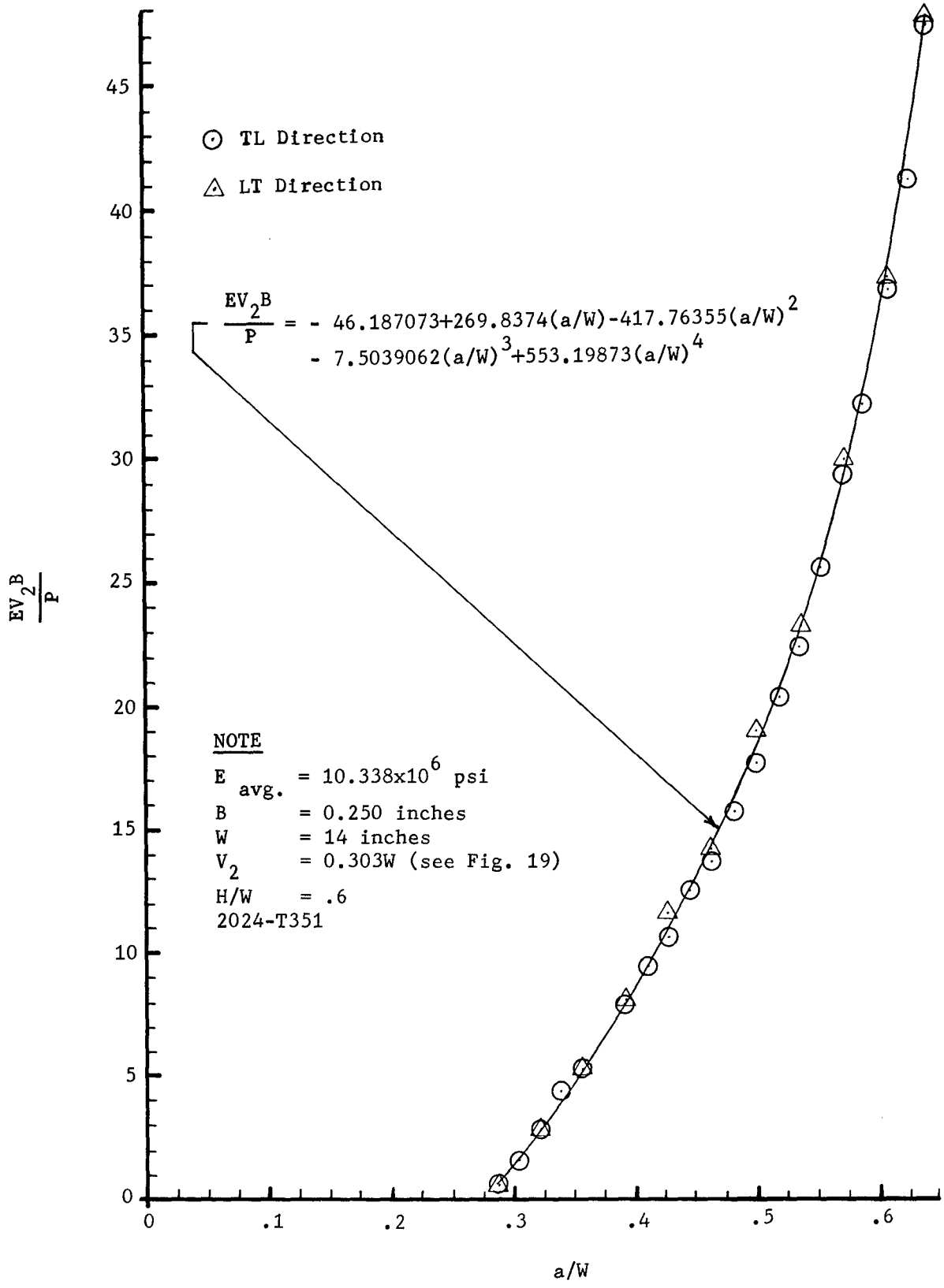

Figure 24. CLWL Compliance Curve for V_2 Probe Location

accuracy of V_n/P slope was maintained. This procedure differs from that of a center crack tension (CCT) specimen, for example, where load (P) is a known quantity and a/W is the factor of interest. In all subsequent calculations the measured deflection at V_1 is used to determine load, and the analytical procedure uses the least square fit equation of Figure 23. The V_1 probe position was selected for these calculations since it's output is more sensitive (larger displacements) to changes in crack size (hence load) than the V_2 location.

The ratio of V_1 to V_2 (return slope after partial unloading in the CLWL test) is used in the double compliance method to determine a/W (see Reference 2). A plot of the data obtained from the 2024-T3 calibration specimen and resulting least squares data fit are shown in Figure 25. For comparison the curve from Reference 2 data is also shown in Figure 25 and indicates slightly larger slopes for a given crack size. This difference could be caused by several factors; one of which could be slight twisting on loading. Although care was exercised in restraining in-plane buckling by guides placed on the specimen faces, some twisting could have taken place. The loading point on the large diameter hole could also have shifted to a radial position other than perpendicular to the slot which also is known to effect displacement at both probe locations (see e.g., the discussion of load distribution for the CLWL specimen geometry in Volume I). However, the data for the two specimens indicate no consistent trends with test conditions (see Figures 23 and 24) so all data of this report was analyzed using the equation of Figure 25.

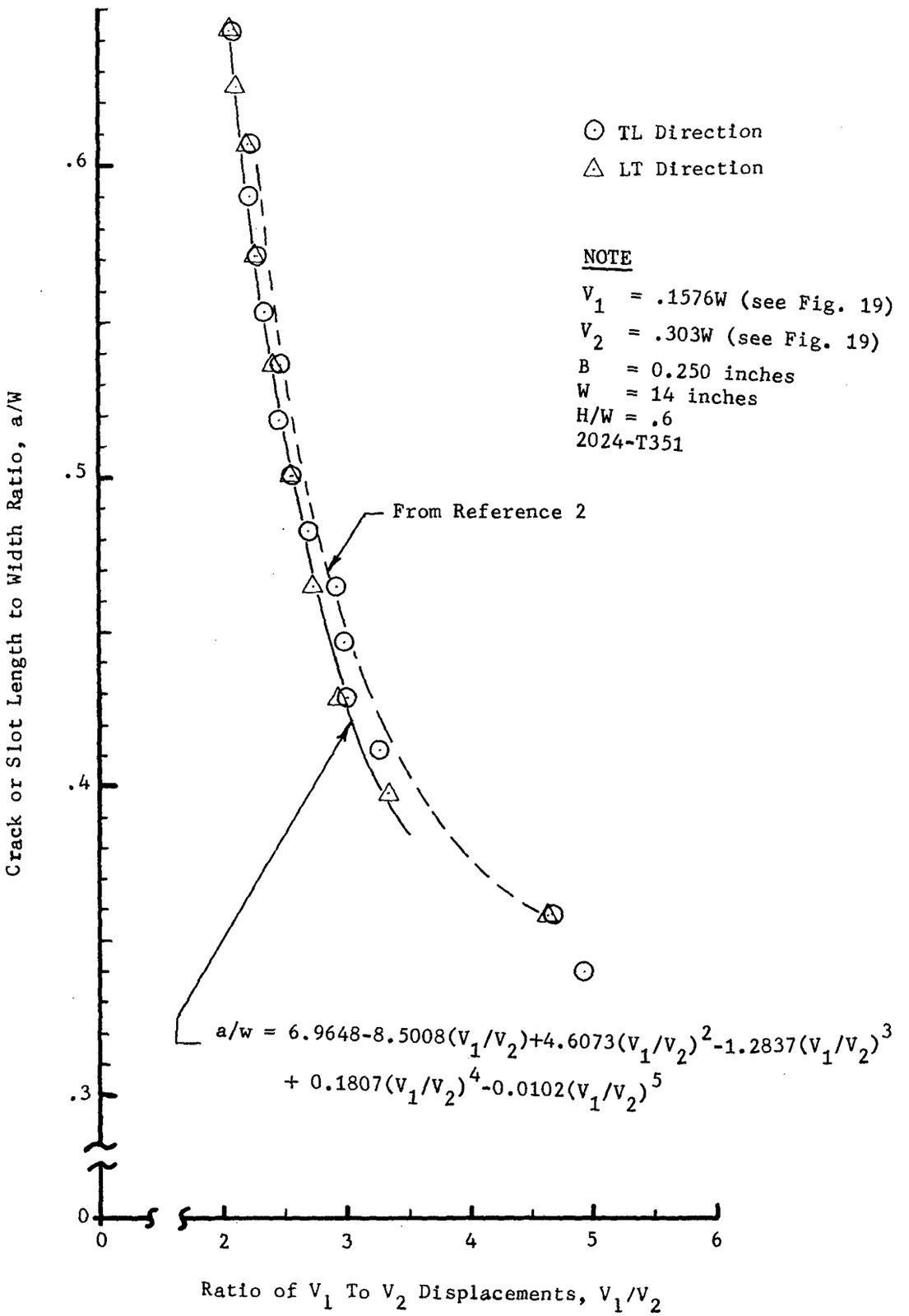

Figure 25. Displacement Ratios for CLWL Specimens As A Function of Crack Length

V CLWL SPECIMEN DATA

5.1 EVALUATION OF DOUBLE COMPLIANCE DATA

. For the crack line wedge loaded (CLWL) specimen, load P, is applied through a wedge and split clevis device and double compliance displacement measured at two points along the crack line, V_1 and V_2 (see Figure 19). A typical sketch of the V_1 versus the V_2 trace is shown in Figure 26. The semi-ductile (or semi-brittle) material of Figure 26(a) shows distinct steps in the V_1 versus the V_2 trace for each increment of crack extension. The ductile material (Figure 26(b)) exhibits few distinct steps but rather consists of a slow tear process represented by the round house nature of the V_1 versus V_2 trace.

At specific times (after physical crack extension), unloading of the specimen is undertaken and a trace recorded as shown in Figure 26. A visual crack length measurement (to within 0.05 inch) is also recorded at the time of unloading as a reference point. In all cases, the slope of the unload line is used to determine the extent of physical crack length. (In our case, a least squares fit to the inverse slope V_1/V_2 is used to compute a/W from a sixth degree polynomial fit to the compliance calibration data (see Figure 25)). Once the crack length is determined (from the V_1/V_2 data), the load P can be determined from the least squares fit to the compliance curve for either the V_1 or V_2 probe position from the following relationship:

$$\frac{E(V_1 \text{ or } V_2)\, B}{P} = f(a/W)$$

$$\text{or} \qquad P = \frac{E(V_1 \text{ or } V_2)\, B}{f(a/W)}, \tag{1}$$

where E is material modulus and B, thickness. In our case, a fifth degree polynomial fit to the V_1 compliance data is used to determine load P (see Figure 23).

At this point, a distinction must be made between what is referred to as a physical crack size ($a_{PHYSICAL}$ or $a_{PHY.}$) and an effective crack size ($a_{effective}$ or $a_{eff.}$).

5.1.1 Physical Crack Length

As mentioned previously, the slope of the unload line (see Figure 26) is used to calculate a/W where "a" in this case is $a_{PHY.}$. The value of displacement $V_{1\ PHY.}$, used to calculate load P is that value after crack extension and is normally the same as the value prior to crack extension except at the longer crack lengths (see Figure 26(a) for example).

The exception to this behavior occurs for ductile materials where slow tear takes place in an almost continuous manner. In those cases (see Figure 26(b)), the value of $V_{1\ PHY.}$ is taken from the point of intersection of the unloading and loading lines.

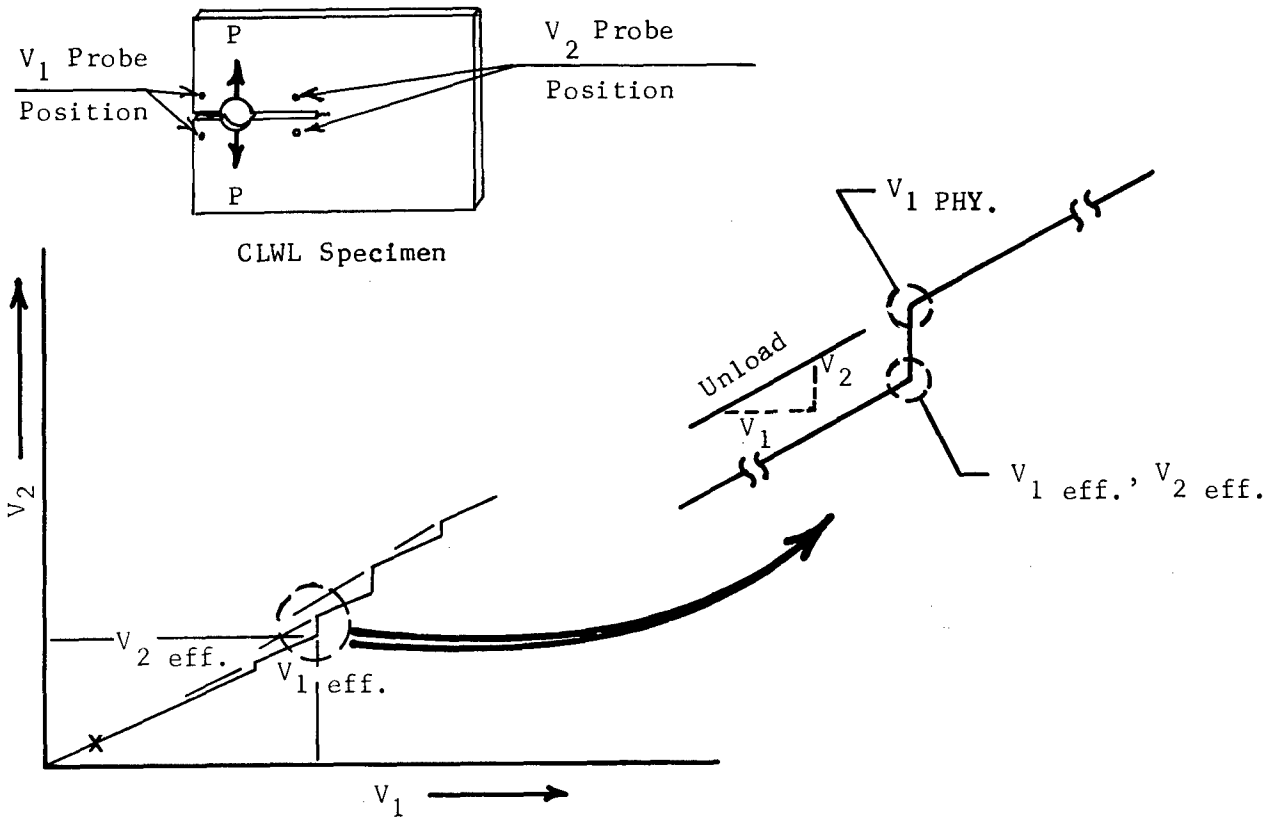

(a) Semi-ductile

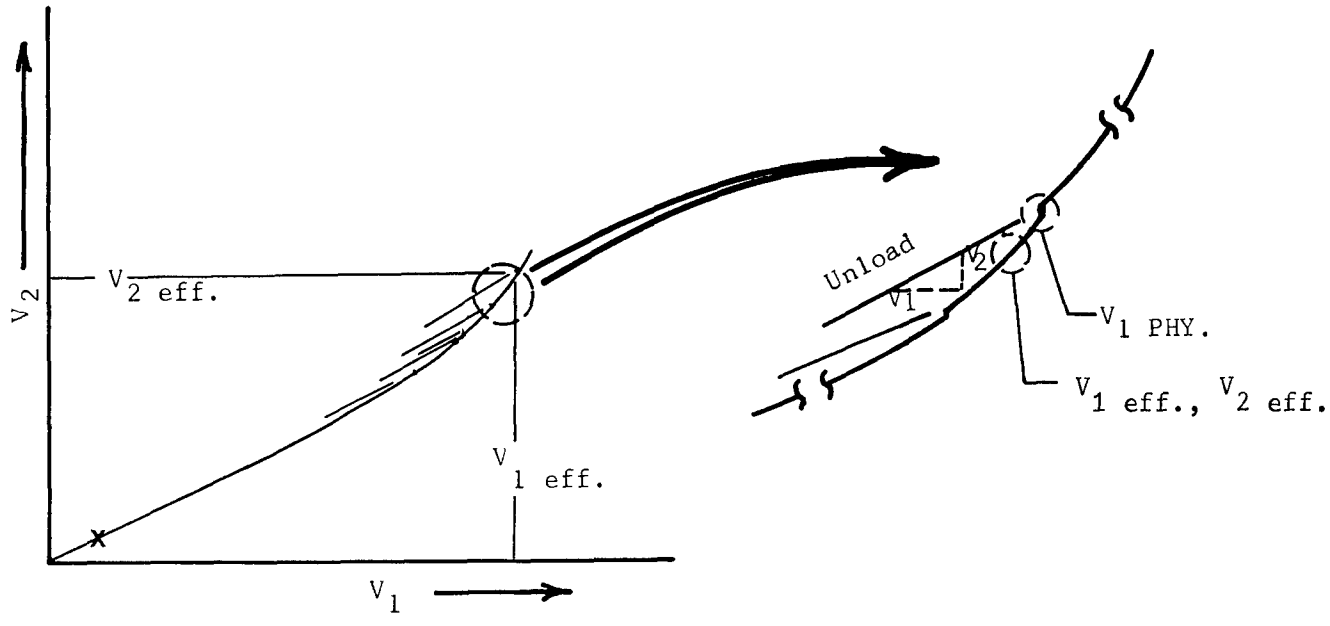

(b) Ductile

Figure 26. Typical V_1, V_2 Plots for a Semi-Ductile and Ductile Material

The reference crack length for physical crack extension is the physical crack length (starter slot plus fatigue precrack) at the start of testing, a_o. This length is readily determined from post examination of the fracture surface to determine fatigue crack length.

Thus the incremental crack extension $\Delta a_{PHY.}$ is determined from successive, computed values of a/W or $a_{PHY.}$. Each successive value has the initial physical crack size a_o subtracted to establish incremental, physical crack growth $\Delta a_{PHY.}$.

5.2.2 Effective Crack Length

To determine effective crack size (physical + plastic zone), the ratio of the deflection at points V_1 and V_2 is used directly in the inverse polynomial expression for a/W. The initial (linear) portion of the trace prior to plastic zone development (see Figure 26, Point X) is used to establish an effective crack length data base, a_{oe}. This value of effective crack length is generally within 5% of the physical crack length; i.e., slot + fatigue crack.

At each increment of crack extension, the ratio of displacements at those points can be used to calculate the respective value of a/W, where the crack length "a" is the value of effective crack size (physical + plastic zone), $a_{eff.}$. Incremental crack extension is then determined by subtracting the initial, effective crack size (a_{oe}) from the respective values of $a_{eff.}$.

The value of V_1 used in the compliance equation to determine load, P is that value of displacement just prior to crack extension that is $V_{1\ eff.}$ (see Figure 26(a)) since this is the value of displacement which occurs when the maximum load is reached prior to slow tear. This load then corresponds to the maximum value of $a_{eff.}$ for the given value of maximum load.

For ductile material behavior, the point at which V_1 and V_2 displacements are employed to determine effective a/W are as noted in Figure 26(b). The point on the V_1/V_2 trace at which the measurement is taken corresponds to some point prior to a rapid change in slope of the V_1/V_2 trace. This point is readily detected for the materials tested during this program. The sketch of Figure 26(b) has been purposely exaggerated to point out the differences between the semi-ductile and ductile materials.

5.2 DEFLECTION TRACES FOR CLWL SPECIMENS

Traces of the actual V_1 versus V_2 deflection curves are reproduced here so that comparisons can be made between the various materials tested. In most cases, the overall specimen dimensions shown in Figure 19 have been maintained and in those specimens where specimen width (W) was altered, all other dimensions were also changed to maintain geometric similarity (e.g., H/W remained 0.6, V_2 probe position remained at .303W, etc.).

To maintain consistency in data presentation, the thinner gage, LT and TL data are shown first, followed by the thicker gage data for each alloy class. These data are consistent with the mechanical property data given in Tables III through V. It will be noted that in many cases, traces are of small crack

extension. In these cases, the crack was deviating significantly out of plane and no further data was taken. This will be discussed further in Section VI.

In order to extend the measurement range at the longer crack lengths, it was necessary to change the bolt heads at the V_1 probe position to a large diameter head (hence producing a smaller gap) for the tougher materials. This is reflected by a series of additional traces on the V_1 versus V_2 plots which follow. This procedure extended the useful range of data for a given magnification. The majority of the displacement data was recorded at a magnification of 0.020 inches/inch at the V_1 and V_2 clip gages. Prior to each CLWL test, a calibration was performed on each clip gage using an extensometer calibrator (high magnification) with an accuracy of $\pm$ 0.00002 inches. This calibration is noted as the tick marks on each V_1 versus V_2 trace which follow.

5.2.1 V_1 versus V_2 Deflection Data - Aluminum Alloys

Figures 27-28 are data for 0.63 inch gage 7075-T6 in the LT direction and Figures 29-31 in the TL direction. Deflection traces for .195 inch gage 7075-T651 in the LT direction are presented in Figures 32-34 and in Figures 35-38 for the TL direction.

The heat treated 7075-T73 deflection data are shown in Figures 39-41 for the LT, thin gage and Figures 42-43 for the TL test direction. V_1 versus V_2 traces for the thicker (.195 inch) 7075-T7351 material tested in the LT direction are shown in Figures 44-46 and in the TL direction in Figures 47-52.

The 2024-T3 aluminum alloy data are shown in Figures 53-55 for the .064 inch gage LT and Figures 56-57 for the TL direction. Figures 58-61 include the .258 inch gage LT data and Figures 62-67 the TL data traces. This same 2024-T351 (plate) material, chem milled to .083 nominal thickness has deflection data as shown in Figures 68-70 for the LT direction and Figure 71 for the TL direction.

5.2.2 V_1 versus V_2 Deflection Data - Titanium Alloys

Deflection data from the beta processed Ti-6Al-4V has not been included in this report since additional testing of this material was not attempted. The beta mill annealed 6Al-4V, V_1 versus V_2 traces are shown in Figures 72-73 for the thin LT direction and in Figures 74-75 for the TL direction. The thicker gage material data is shown in Figures 76-79 for the LT direction and Figures 80-83 for the TL direction.

Displacement data for the mill annealed Ti-6Al-6V-2Sn, .063 inch gage, LT direction data are shown in Figures 84-86 and TL data in Figures 87-91. The thick LT data traces are shown in Figures 92-94 and TL data in Figures 95-100.

5.2.3 V_1 versus V_2 Deflection Data - Steel Alloy

All of the deflection data for the 9 nickel steel tested during this program are shown in Figures 101-103 for the LT direction and Figures 104-106 for the TL direction.

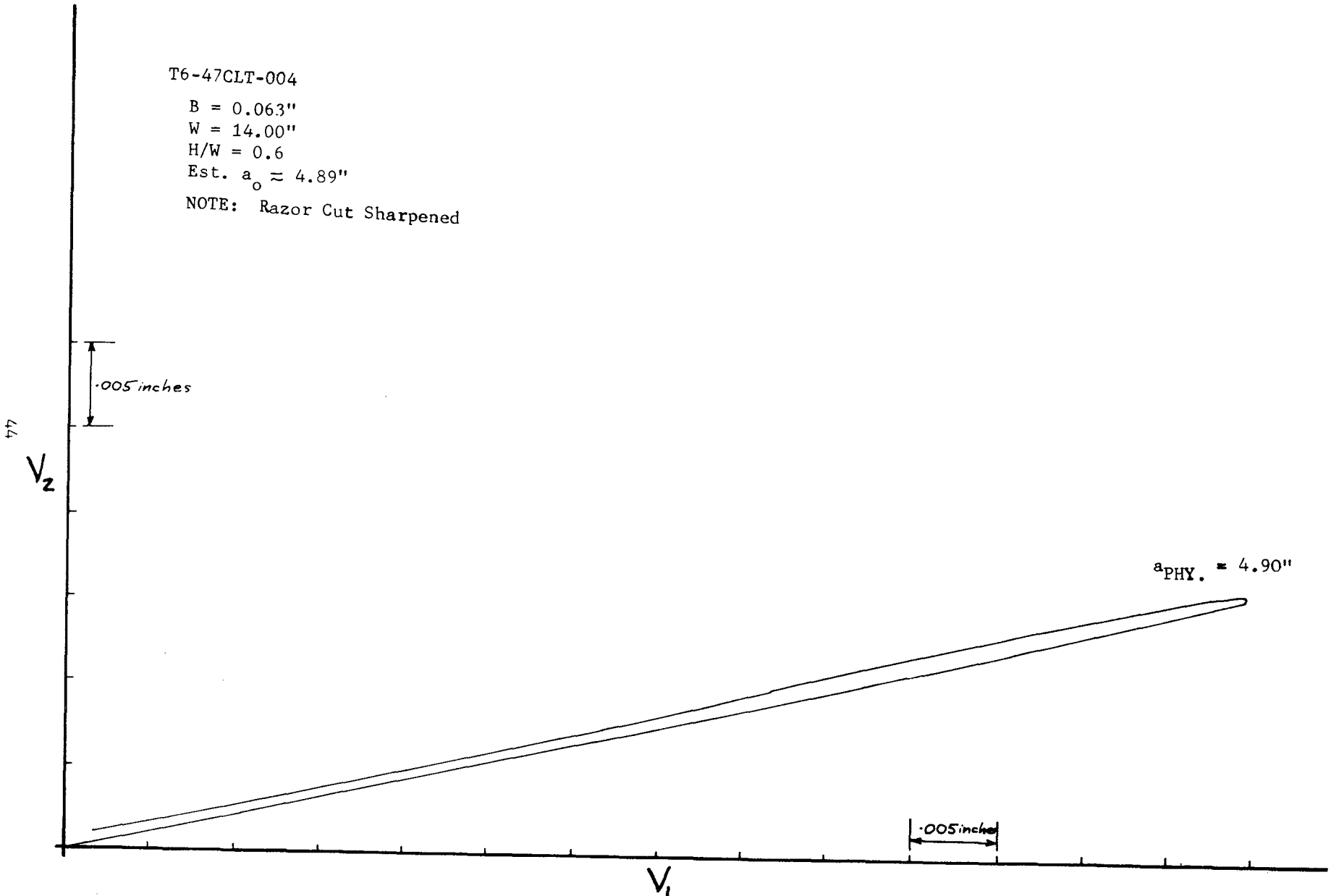

Figure 27. Deflection Curve - 0.063 Inch, 7075-T6 (LT)

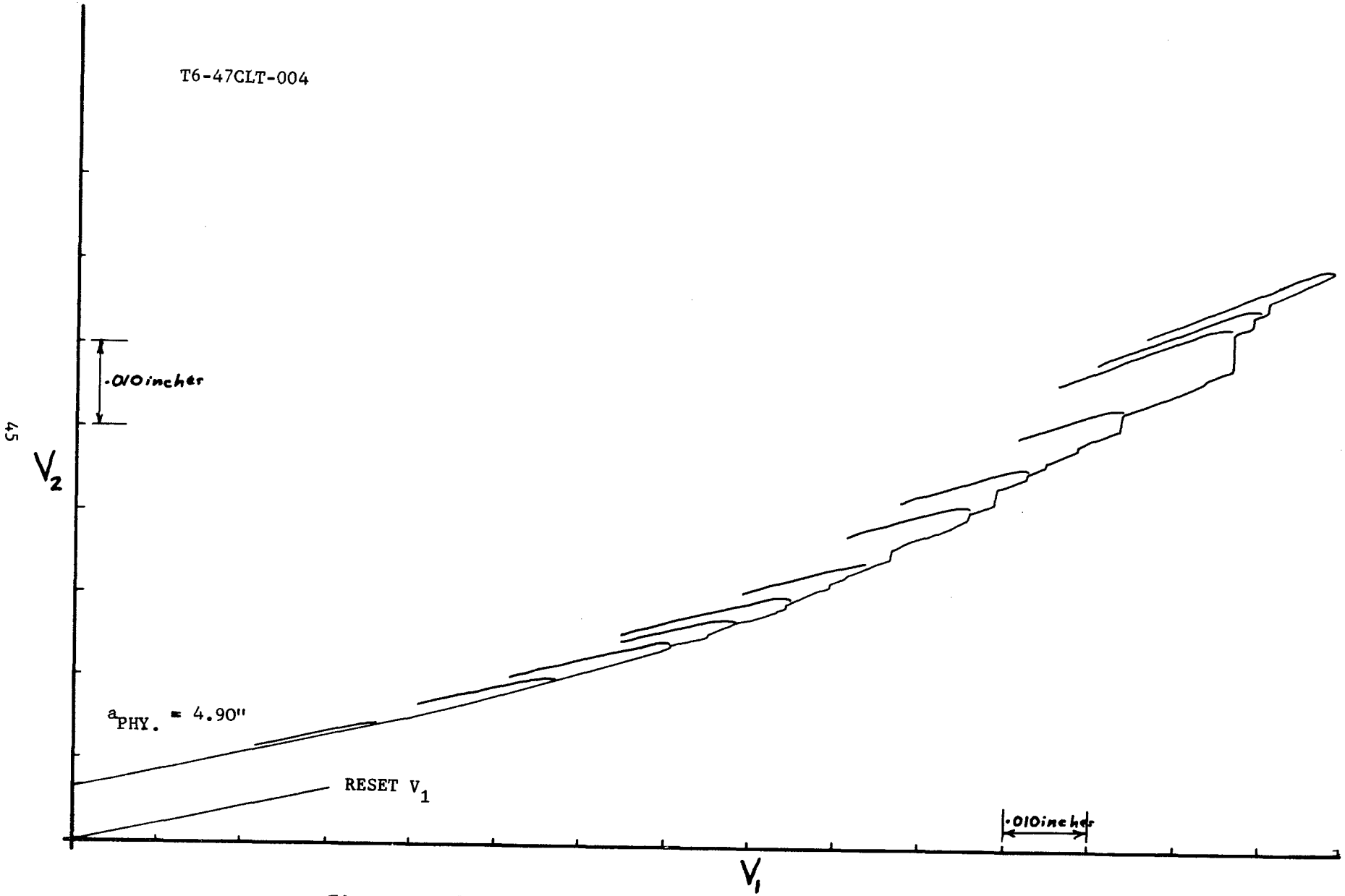

Figure 27. Deflection Curve - 0.063 Inch, 7075-T6 (LT) (Continued)

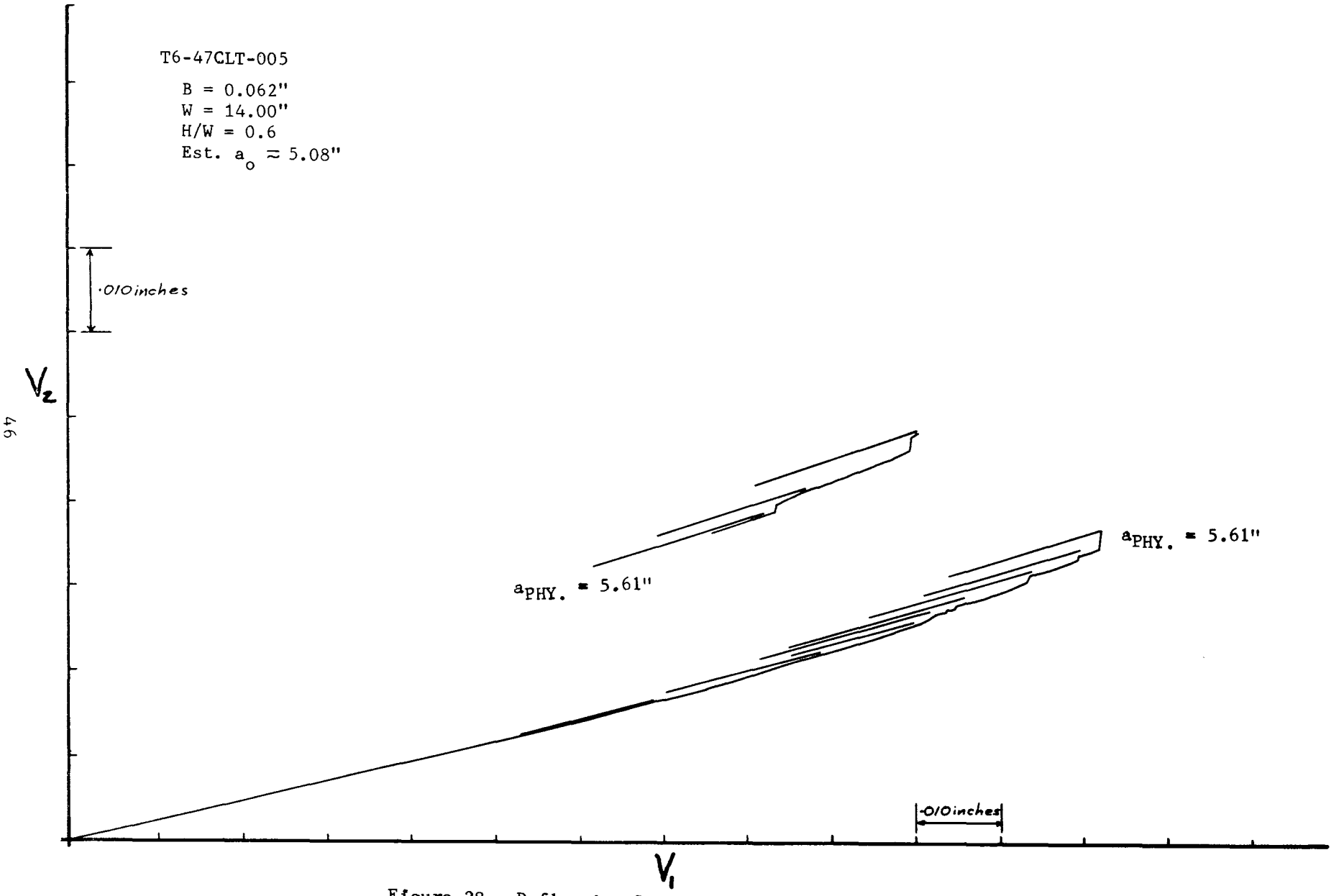

Figure 28. Deflection Curve - 0.062 Inch, 7075-T6 (LT)

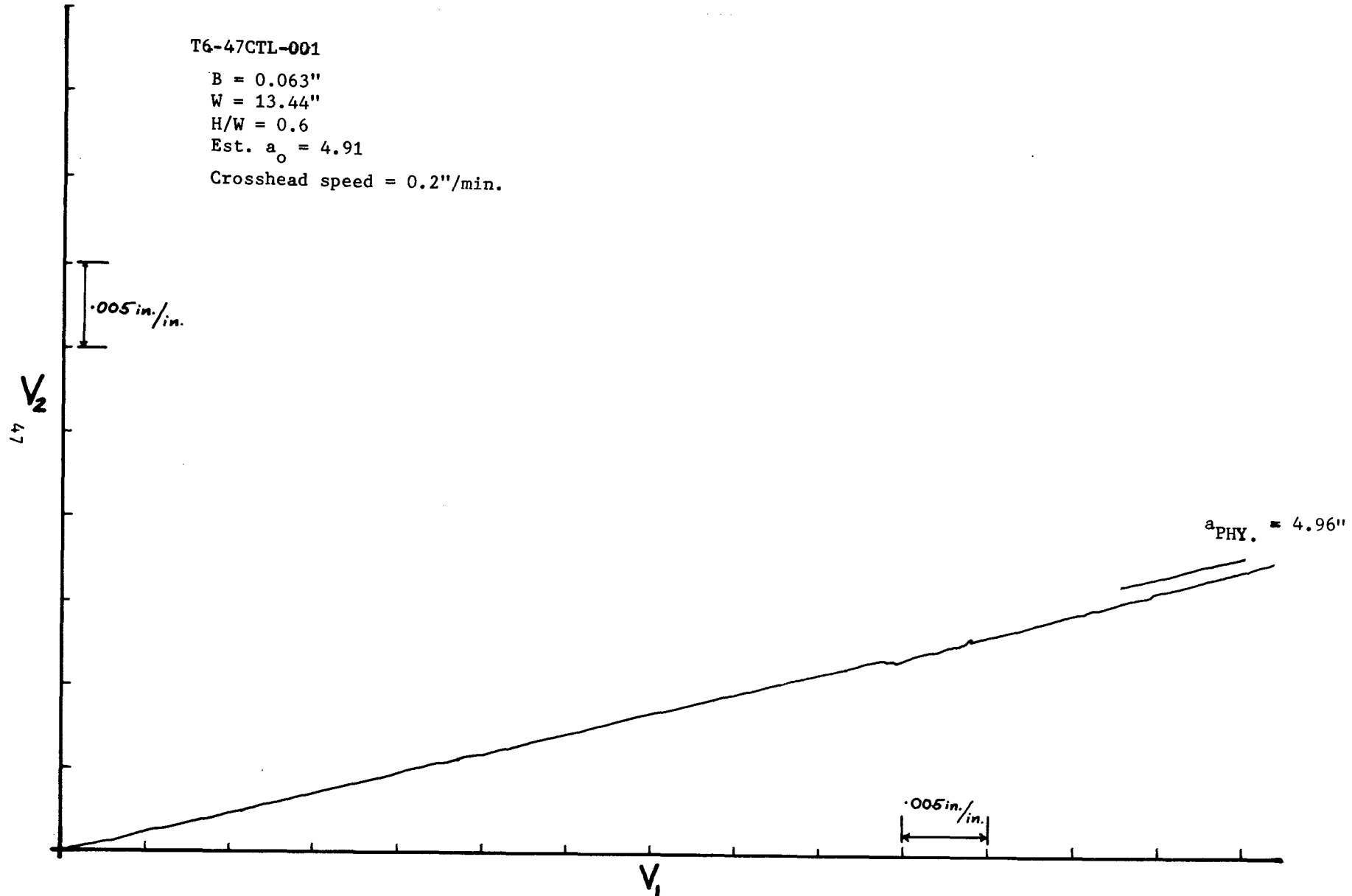

Figure 29. Deflection Curve - 0.063 Inch, 7075-T6 (TL)

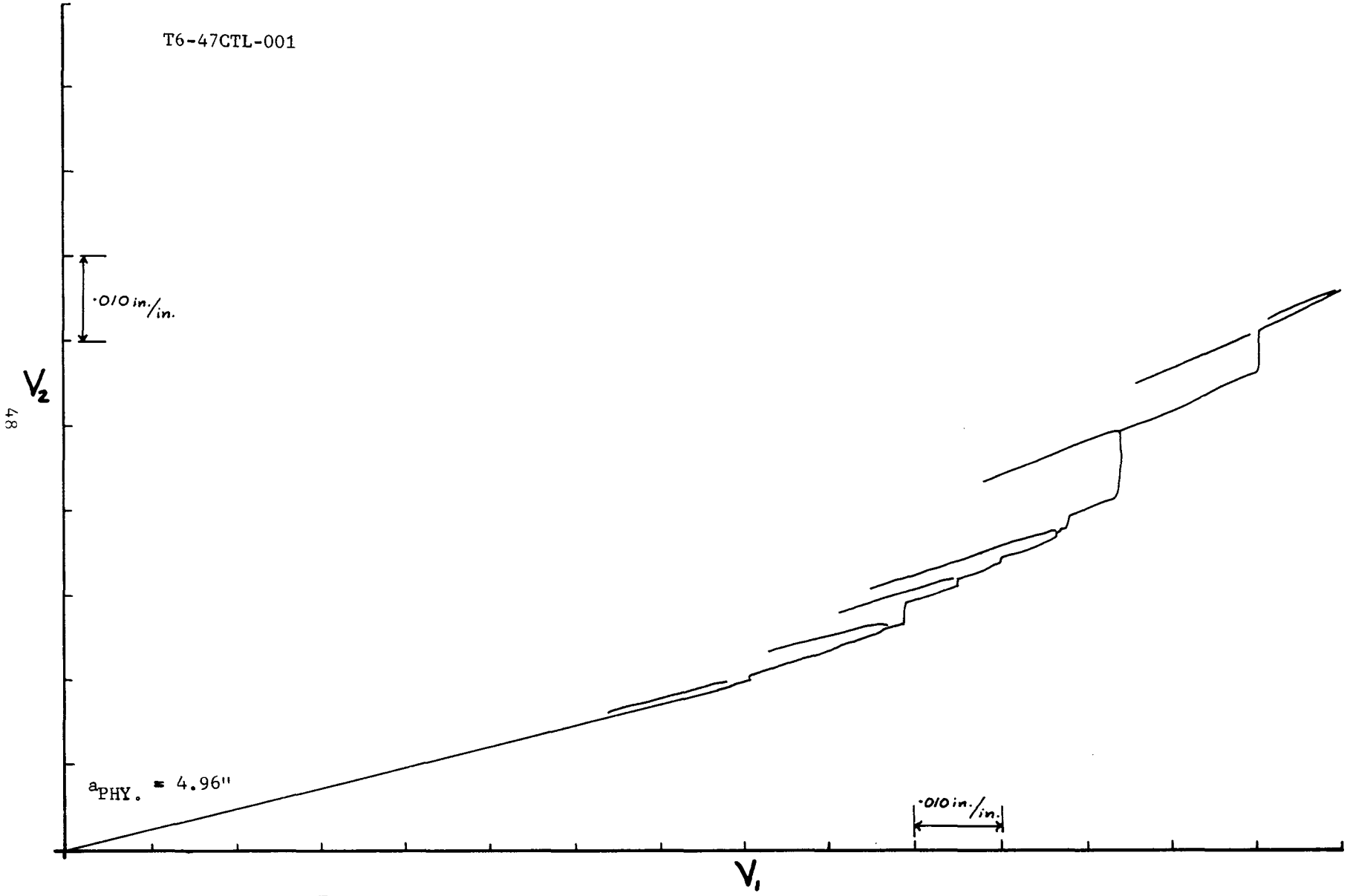

Figure 29. Deflection Curve - 0.063 Inch, 7075-T6 (TL) (Continued)

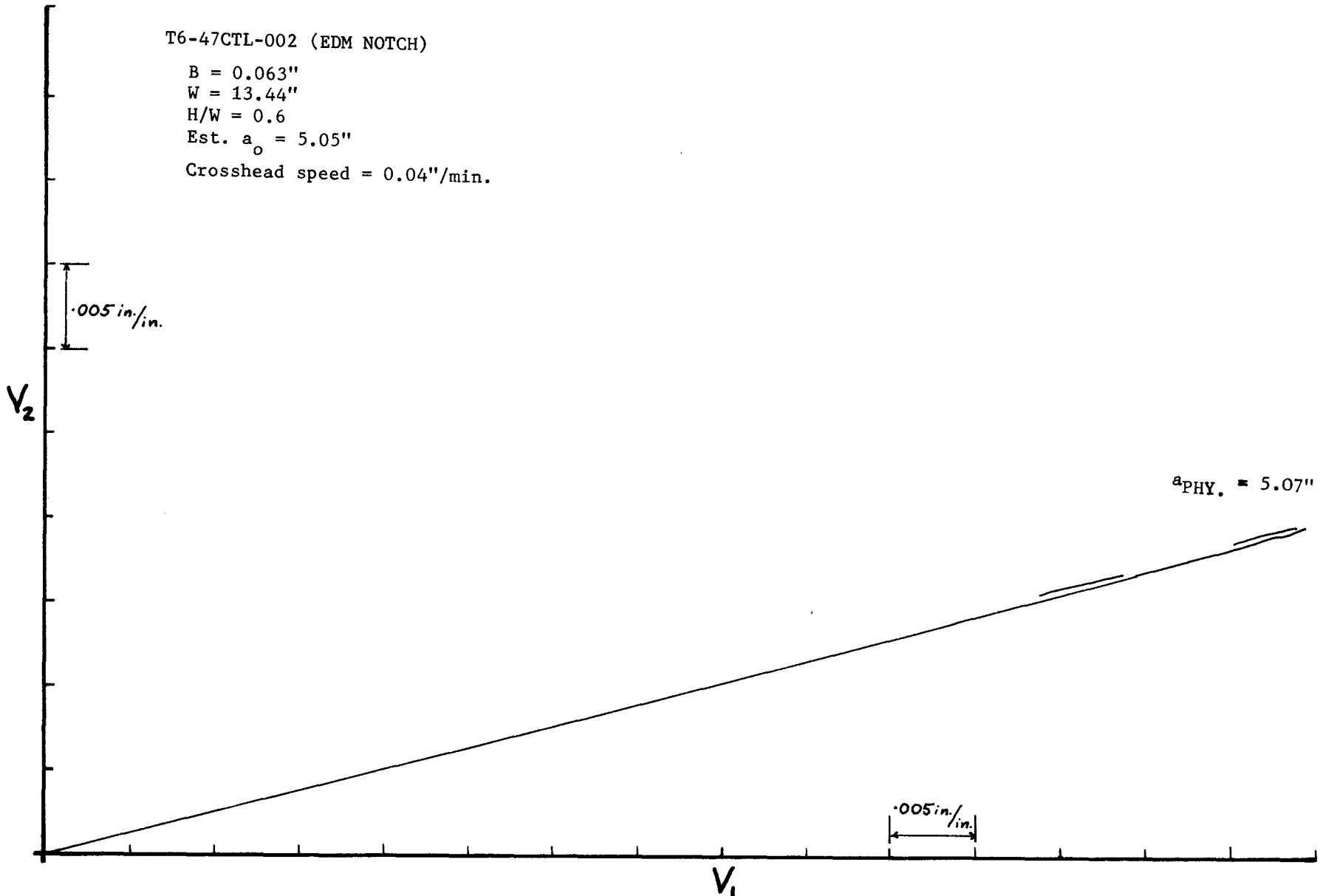

Figure 30. Deflection Curve - 0.063 Inch, 7075-T6 (TL)

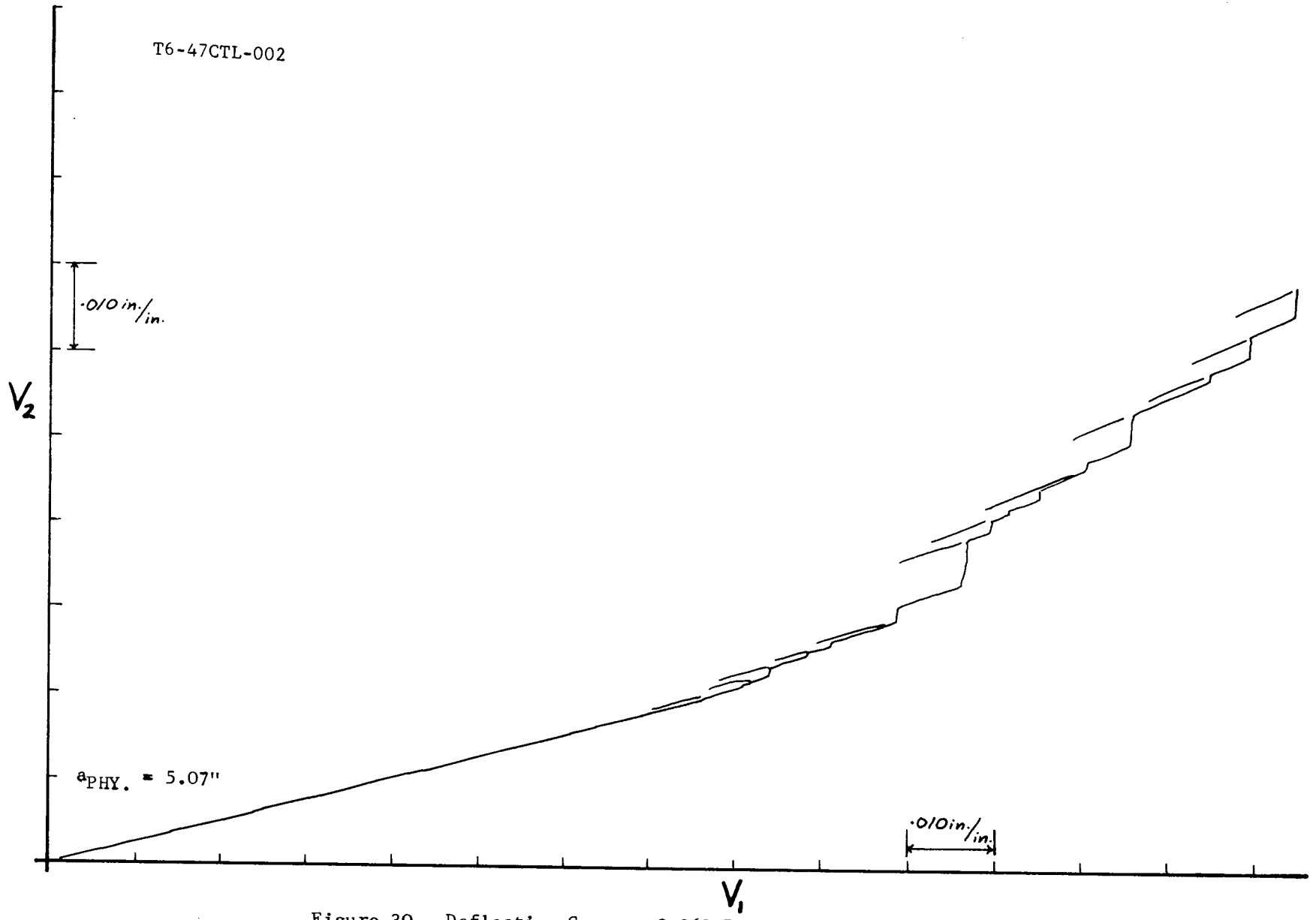

Figure 30. Deflection Curve - 0,063 Inch, 7075-T6 (TL) (Continued)

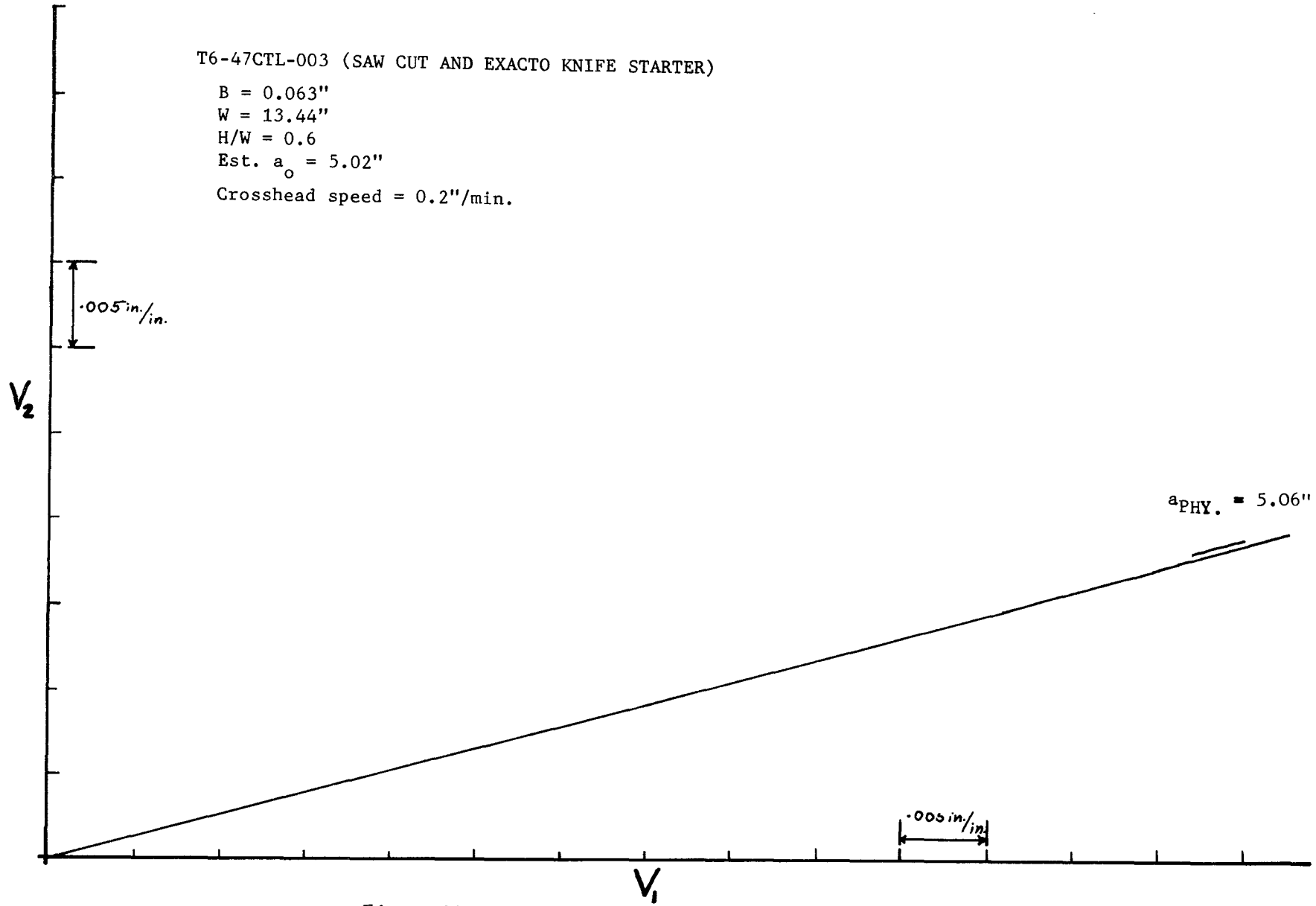

Figure 31. Deflection Curve - 0.063 Inch, 7075-T6 (TL)

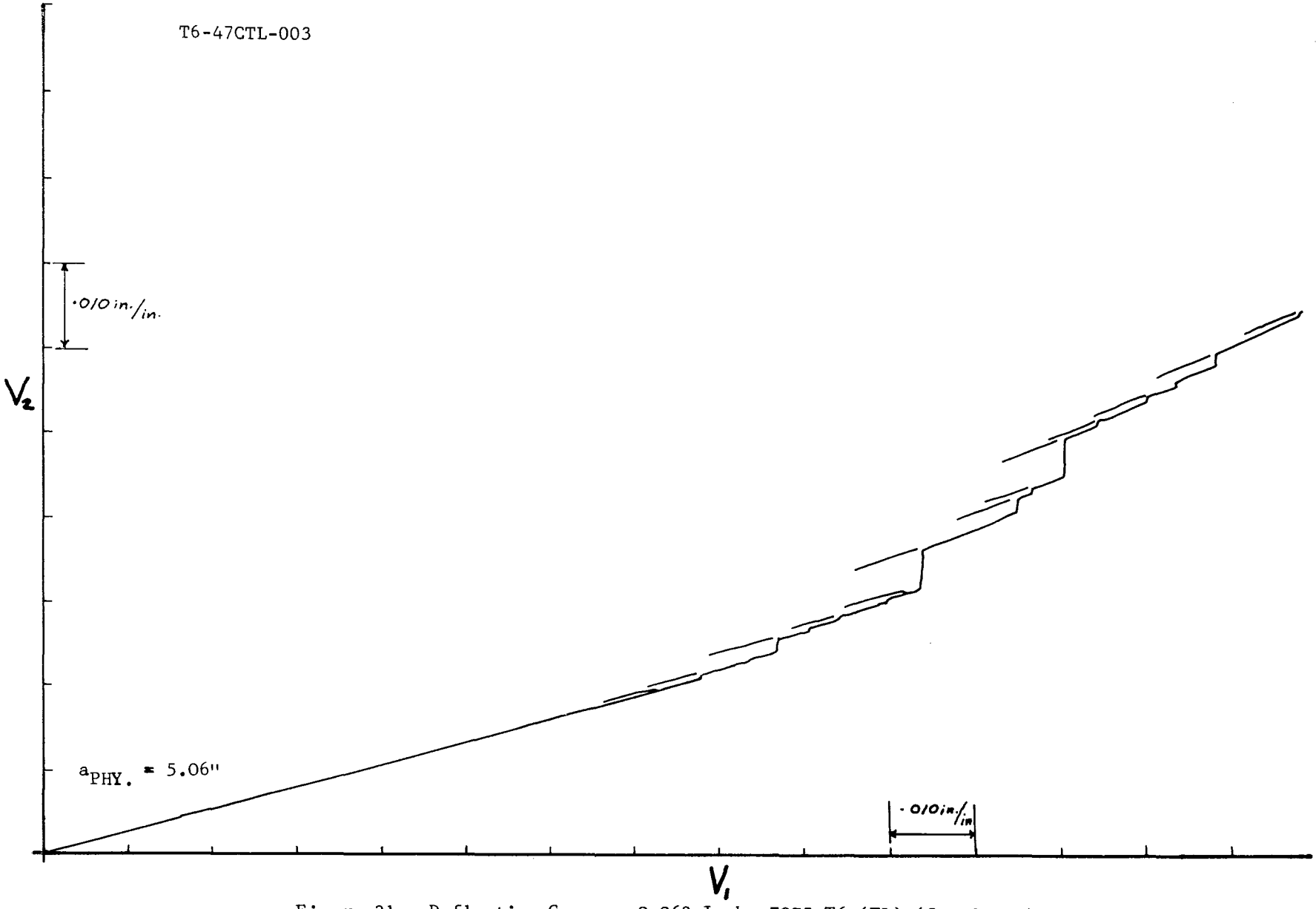

Figure 31. Deflection Curve - 0.063 Inch, 7075-T6 (TL) (Continued)

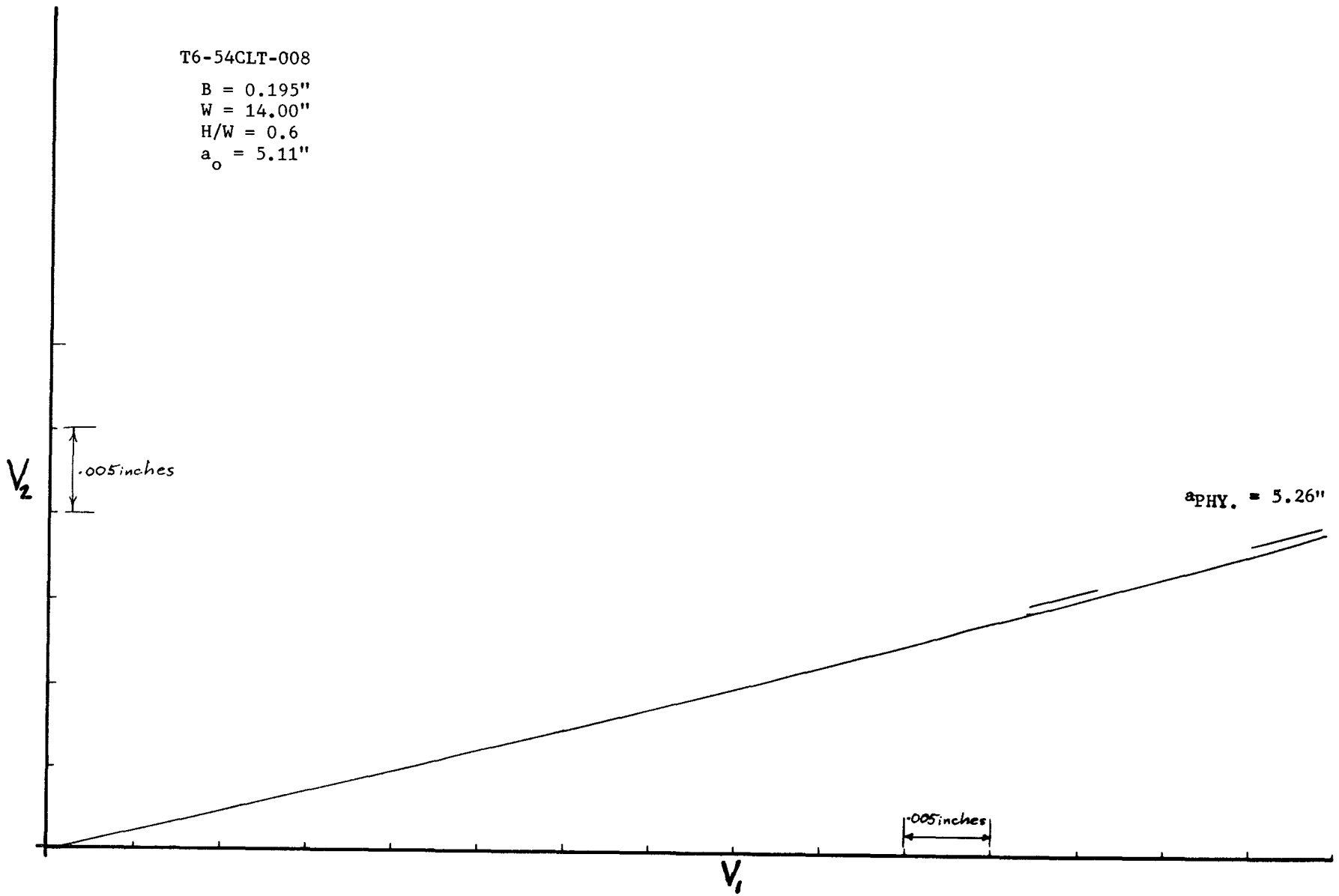

Figure 32. Deflection Curve - 0.195 Inch, 7075-T651 (LT)

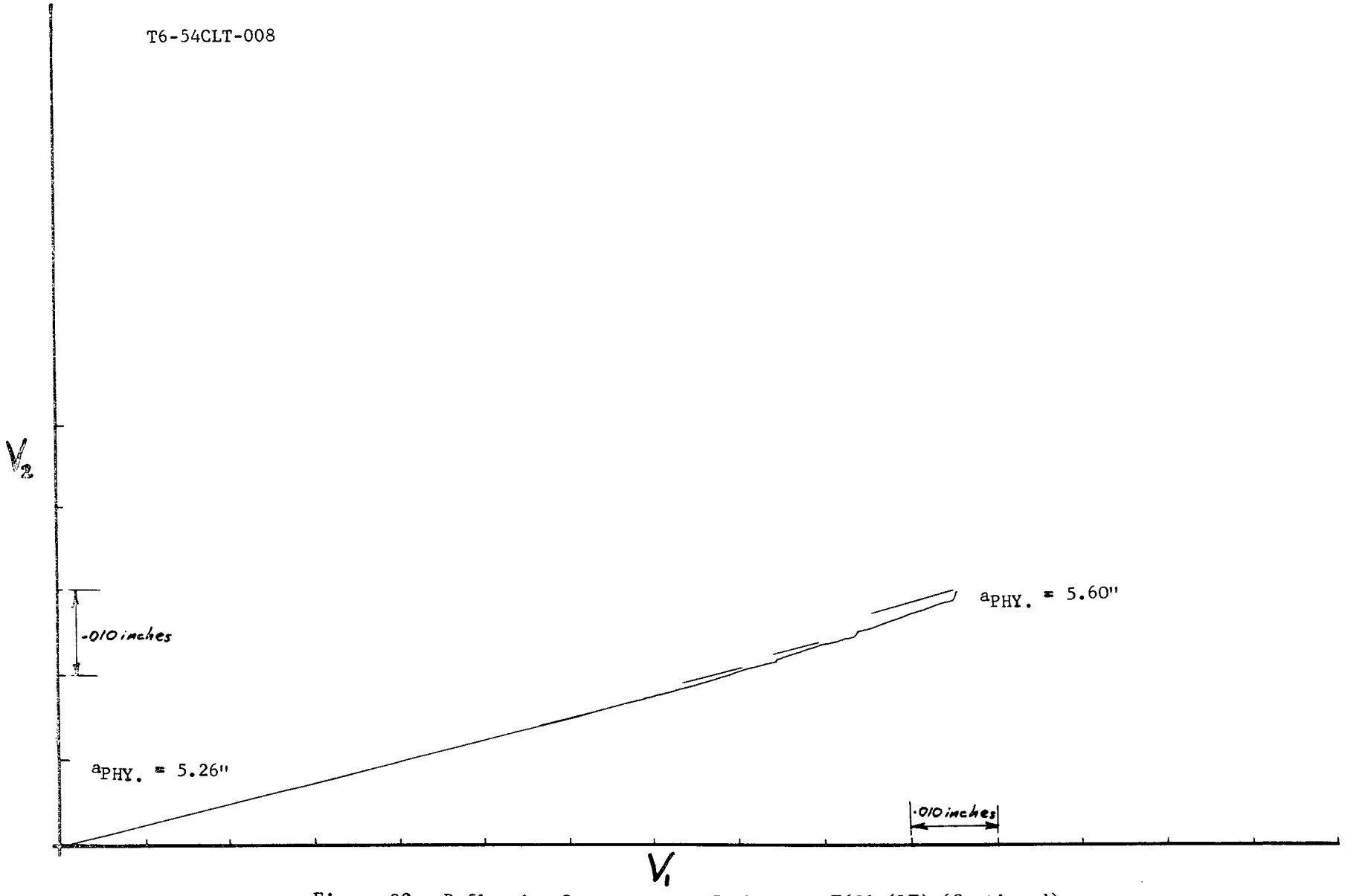

Figure 32. Deflection Curve - 0.195 Inch, 7075-T651 (LT) (Continued)

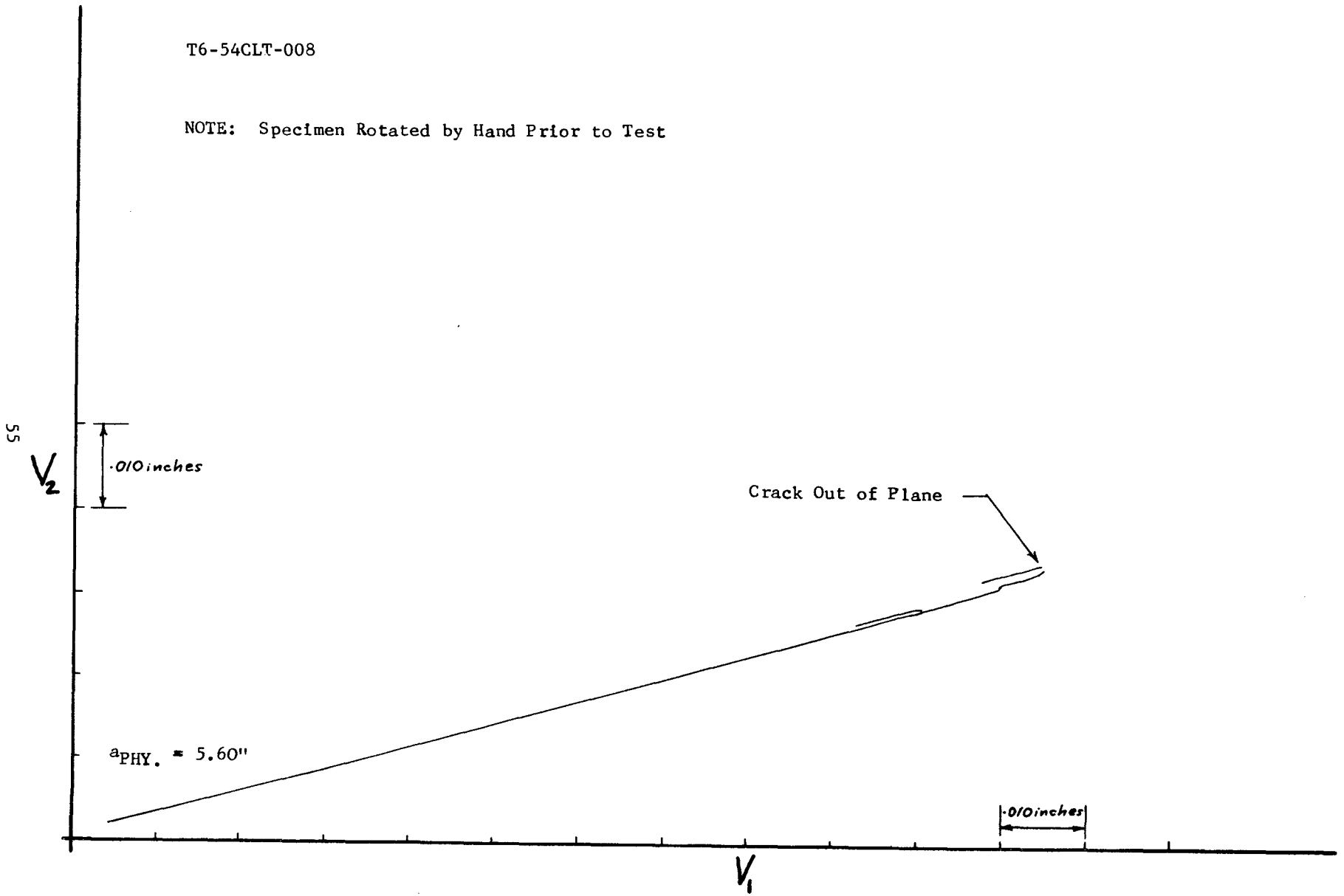

Figure 32. Deflection Curve - 0.195 Inch, 7075-T651 (LT) (Continued)

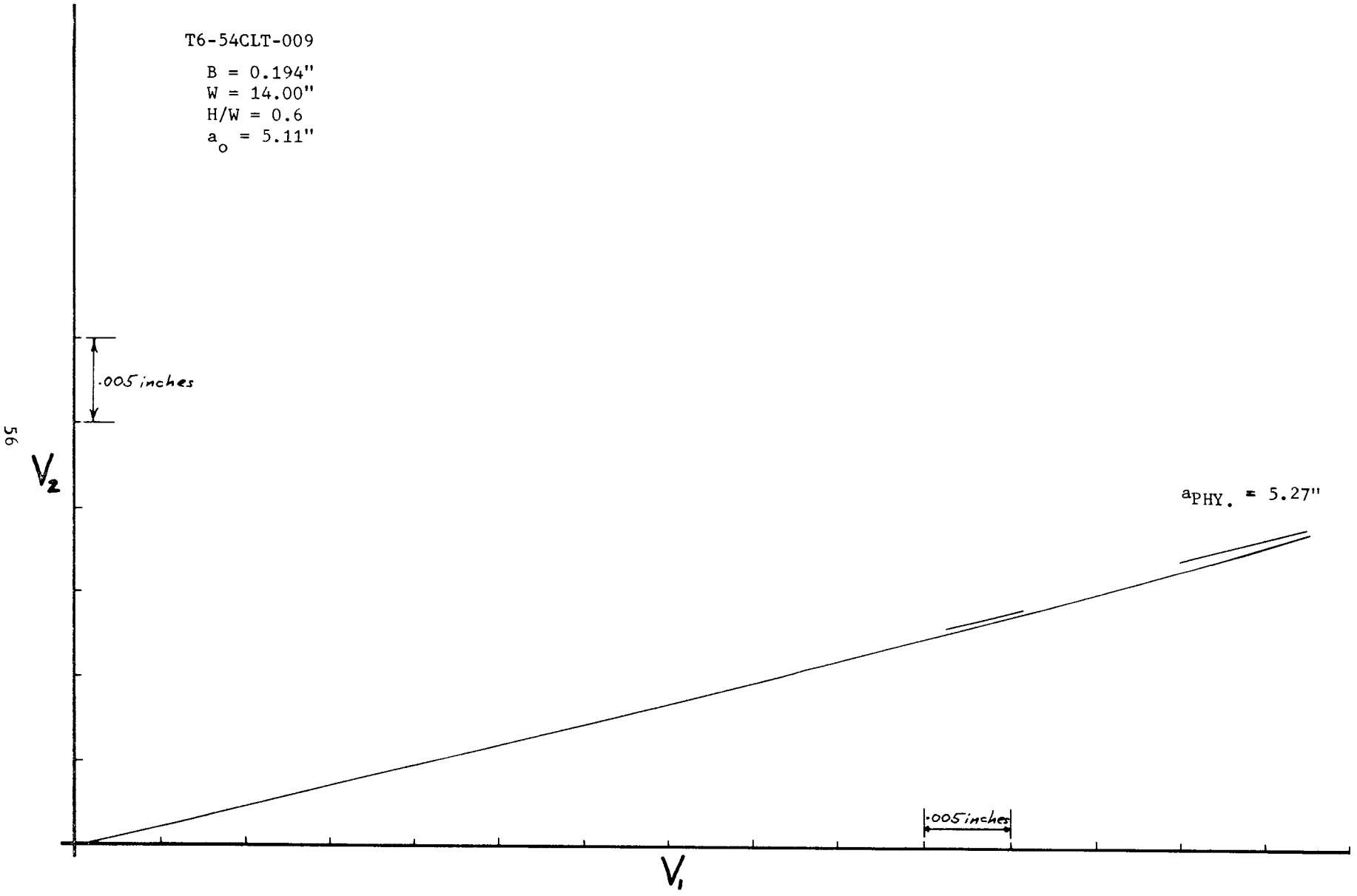

Figure 33. Deflection Curve - 0.194 Inch, 7075-T651 (LT)

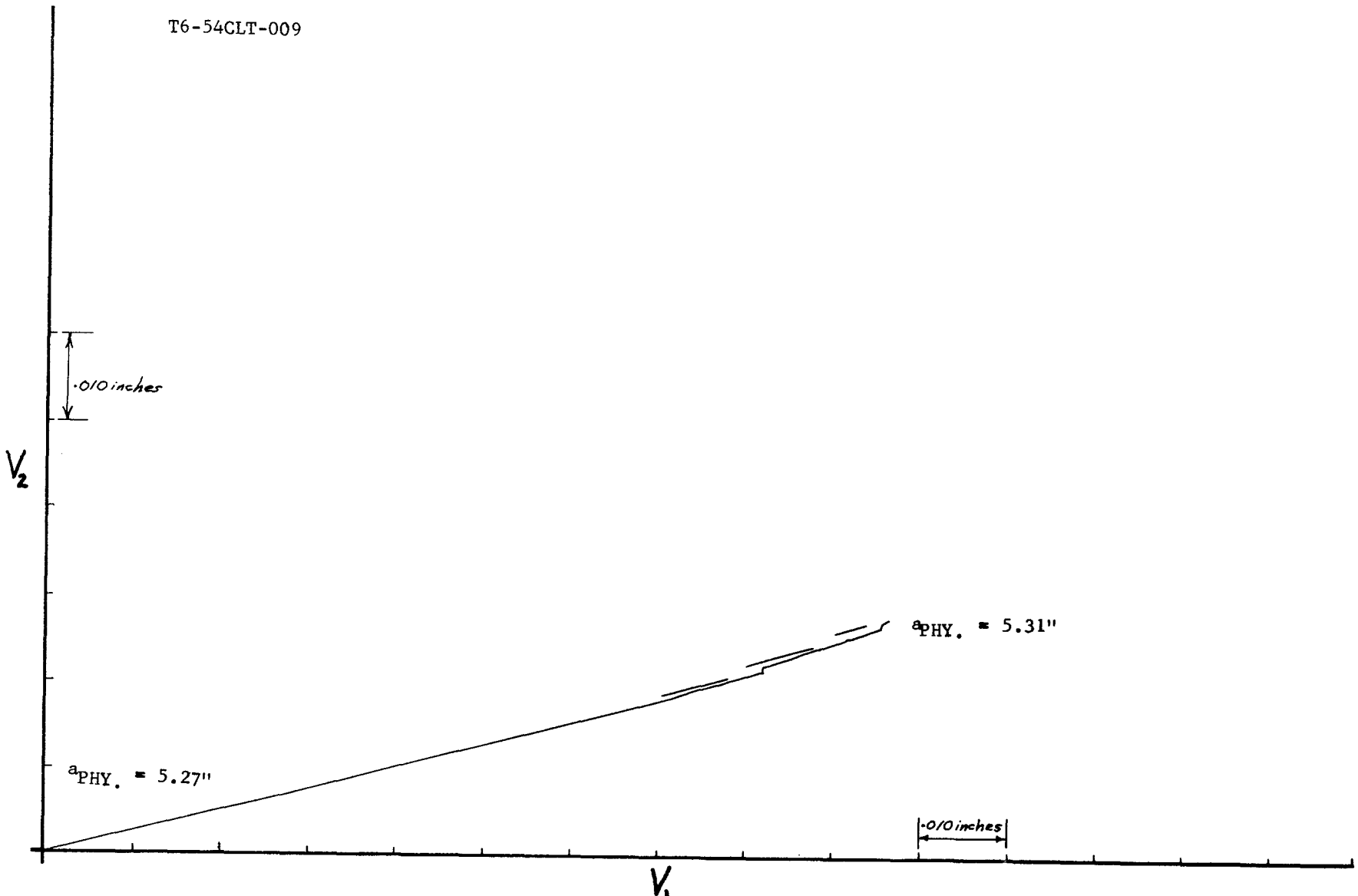

Figure 33. Deflection Curve - 0.194 Inch, 7075-T651 (LT) (Continued

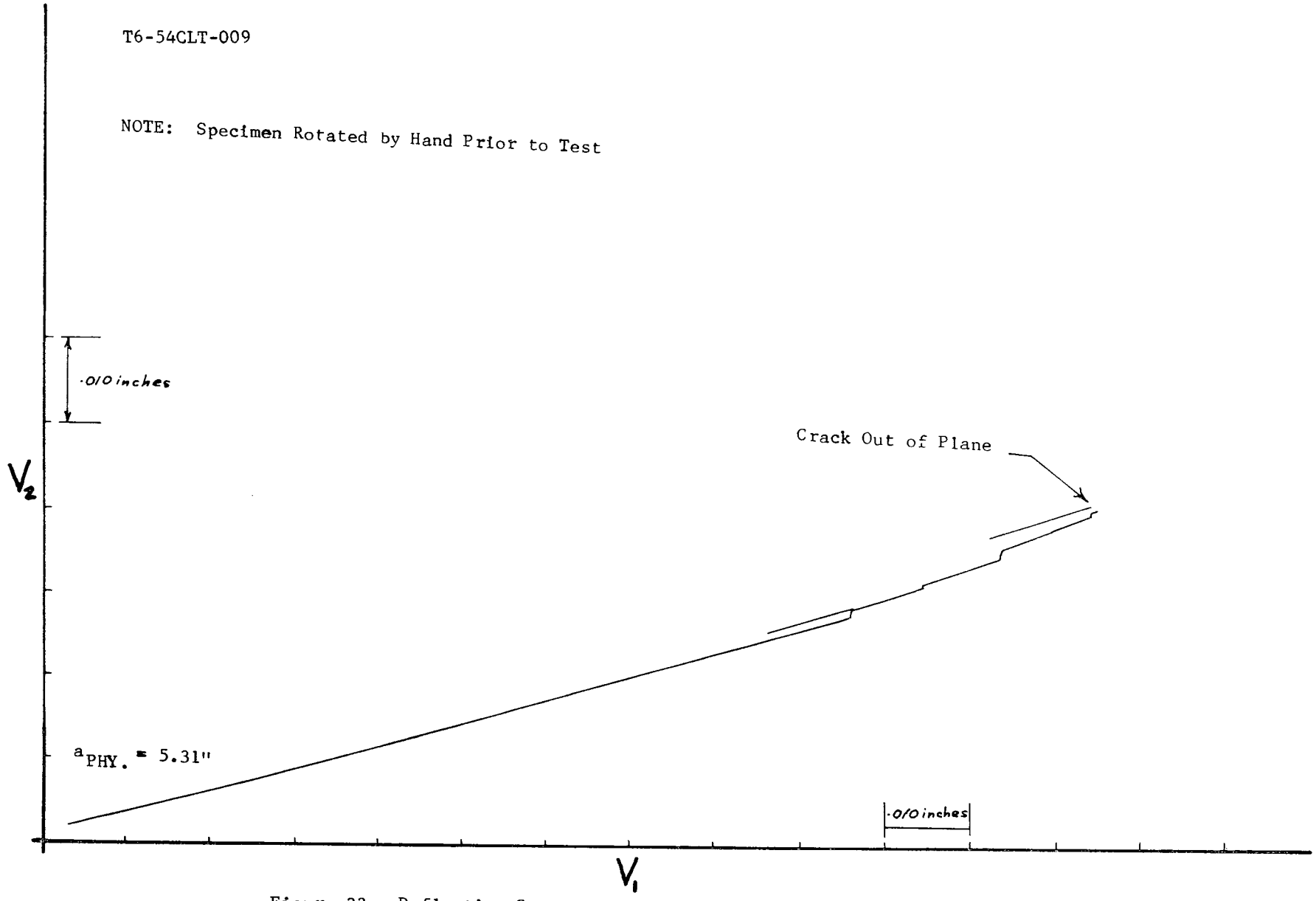

Figure 33. Deflection Curve - 0.194 Inch, 7075-T651 (LT) (Continued)

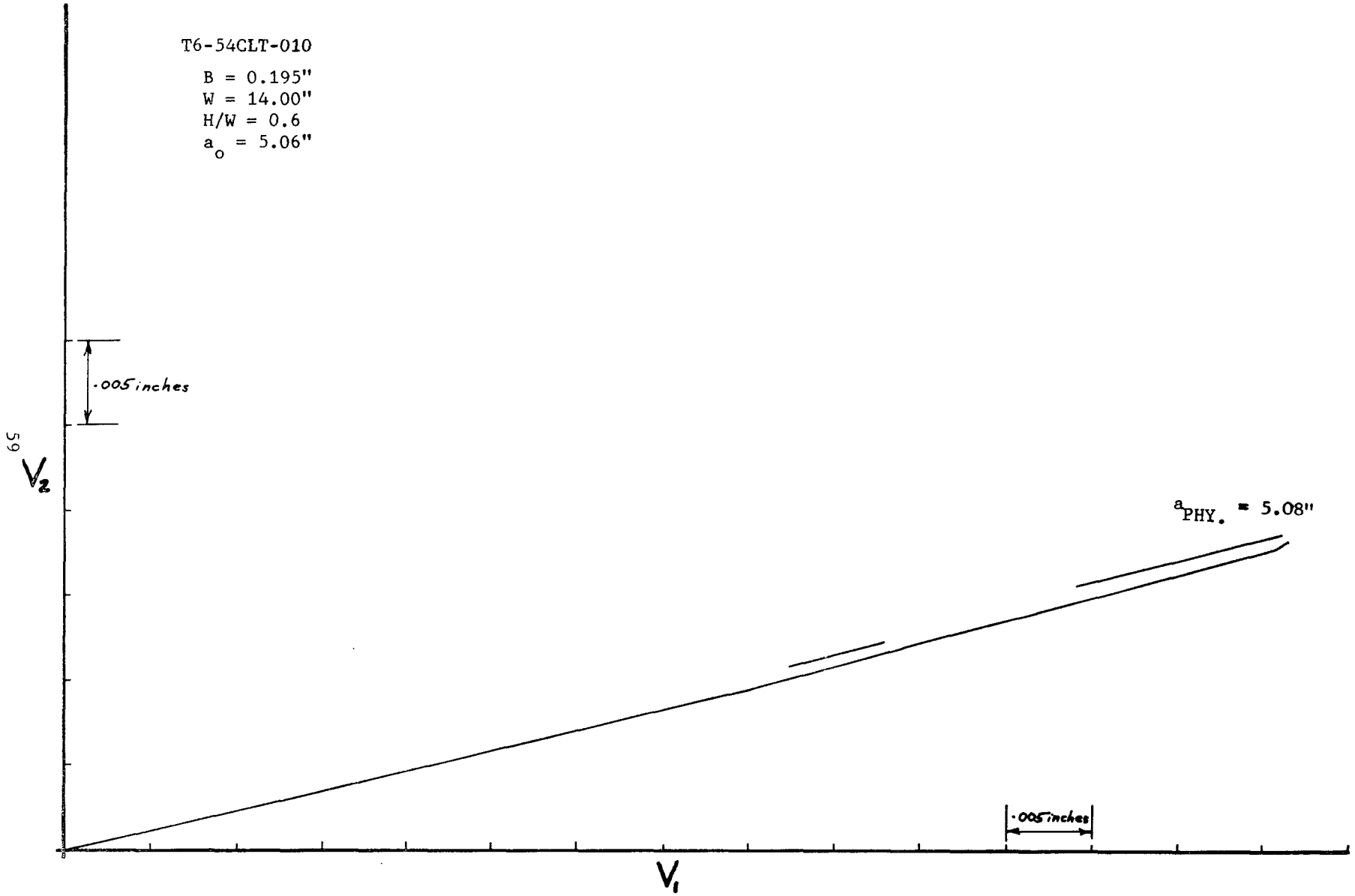

Figure 34. Deflection Curve - 0.195 Inch, 7075-T651 (LT)

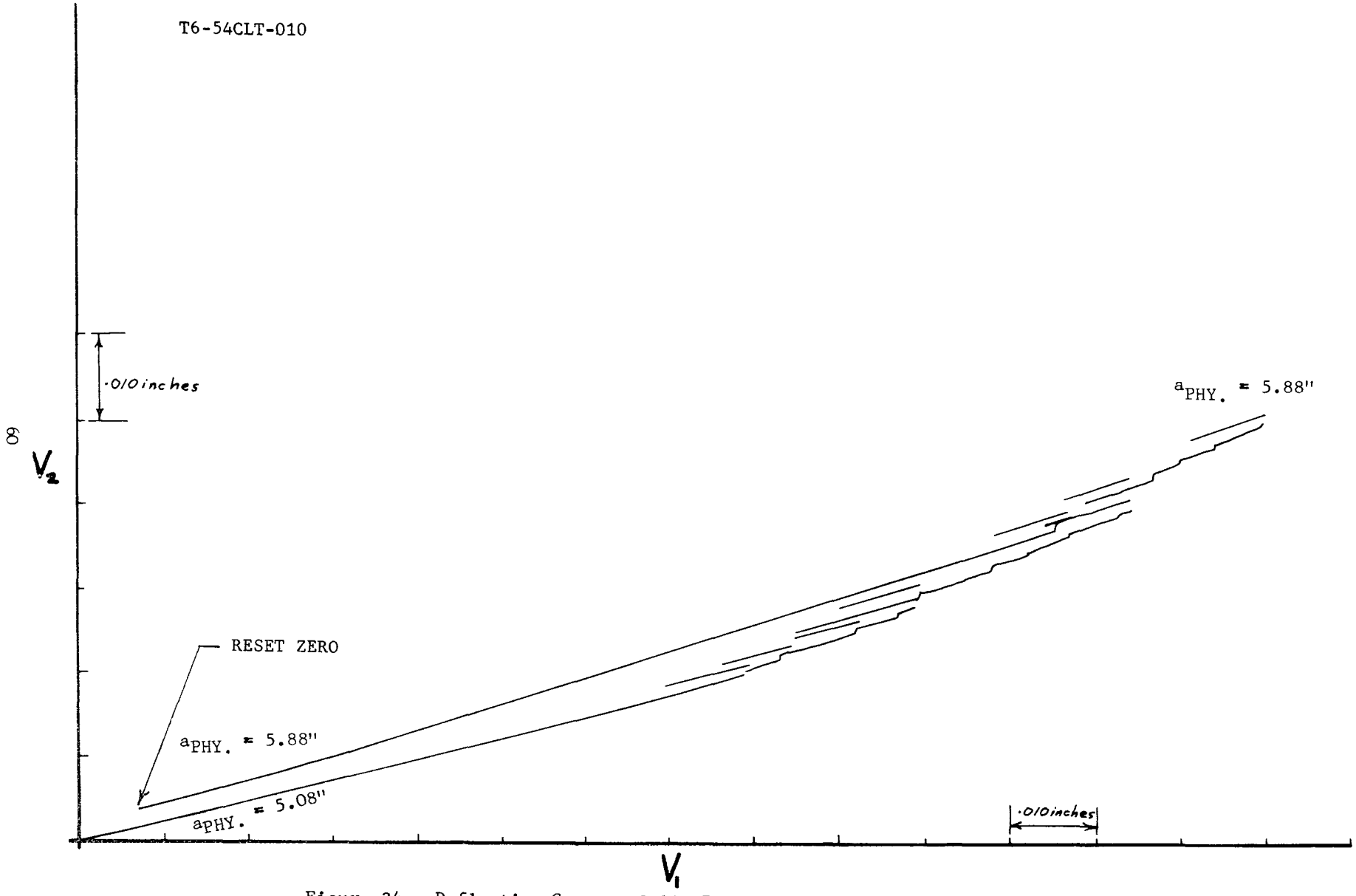

Figure 34. Deflection Curve - 0.195 Inch, 7075-T651 (LT) (Continued)

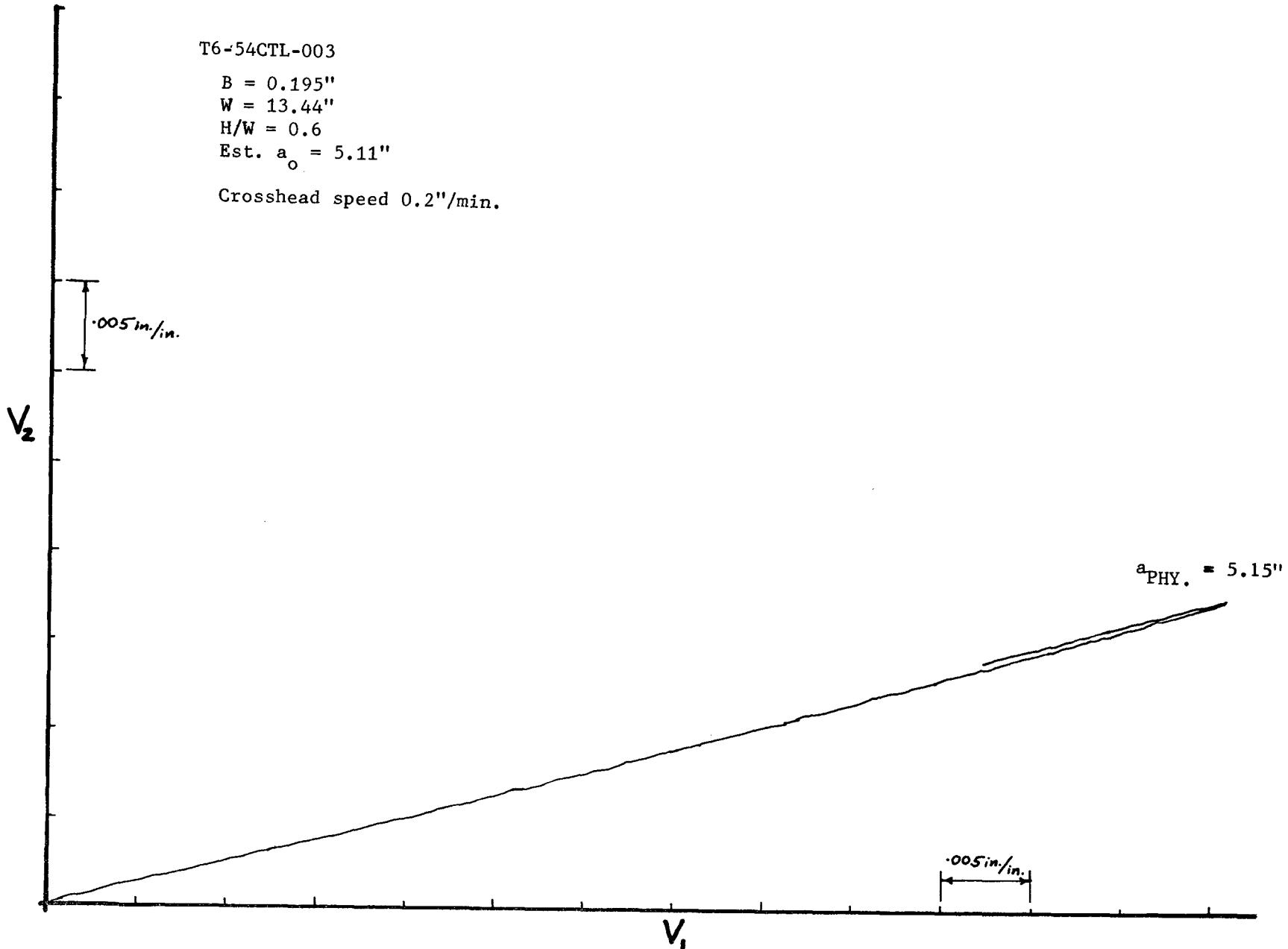

Figure 35. Deflection Curve - 0.195 Inch, 7075-T651 (TL)

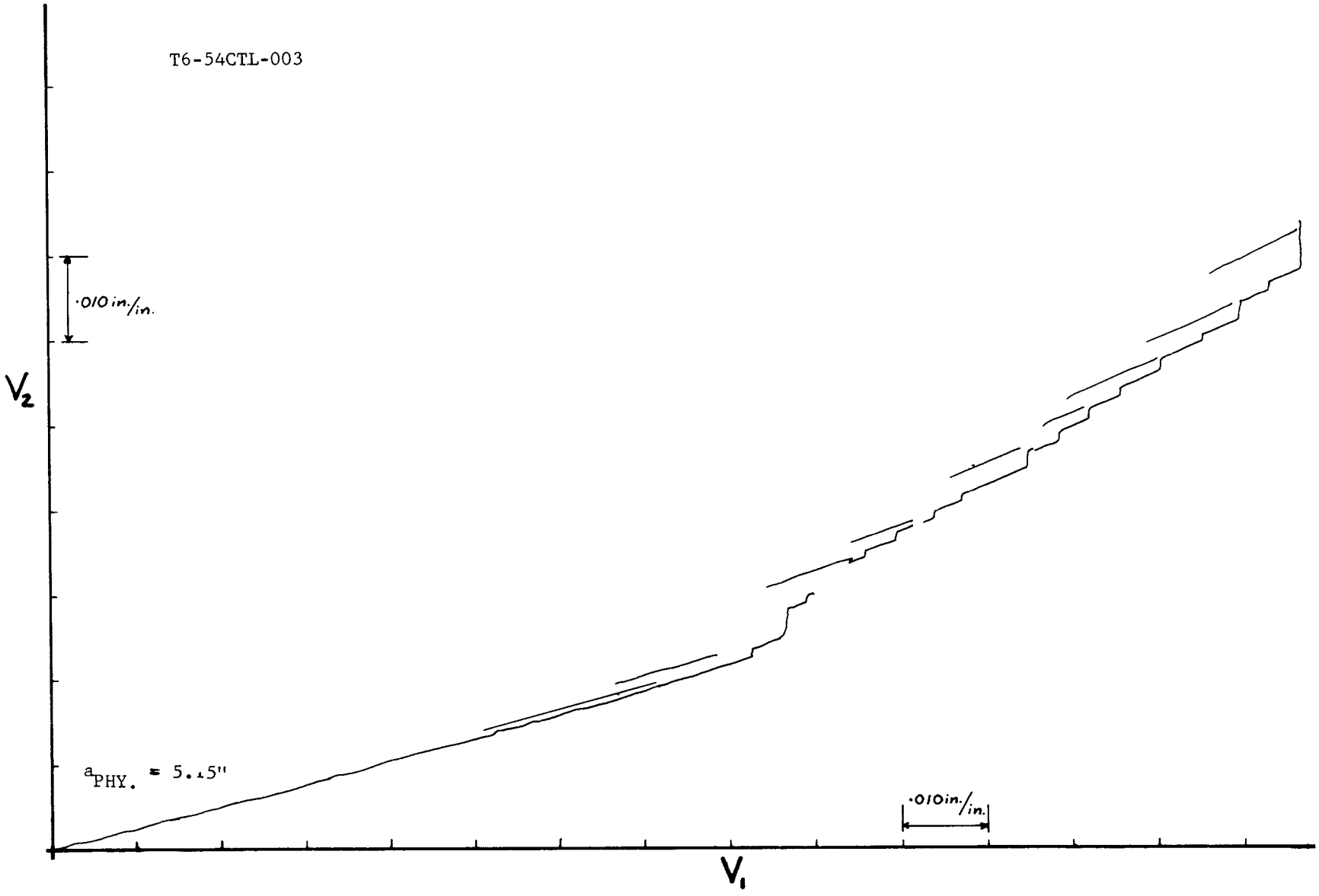

Figure 35. Deflection Curve - 0.195 Inch, 7075-T651 (TL) (Continued)

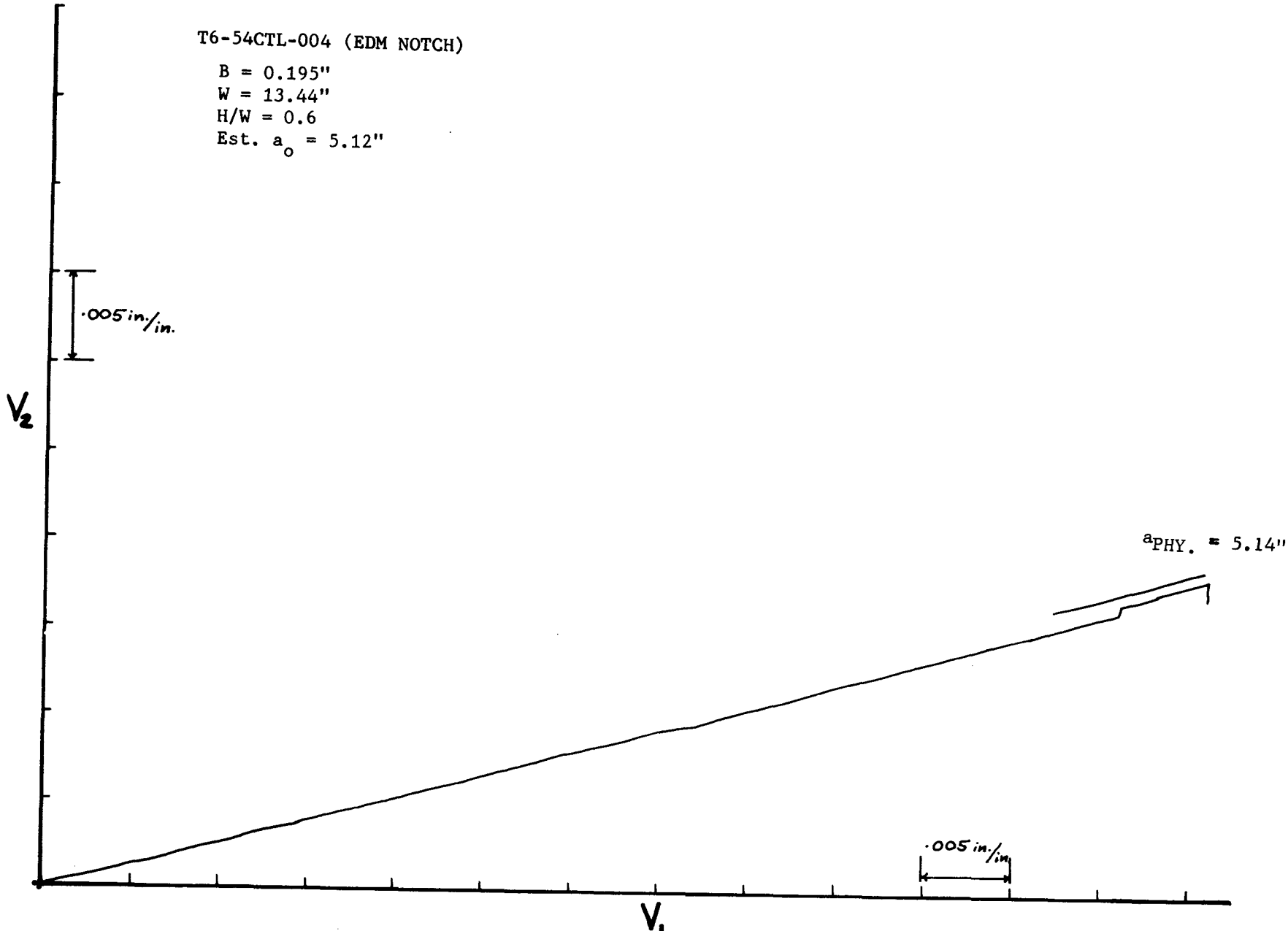

Figure 36. Deflection Curve - 0.195 Inch, 7075-T651 (TL)

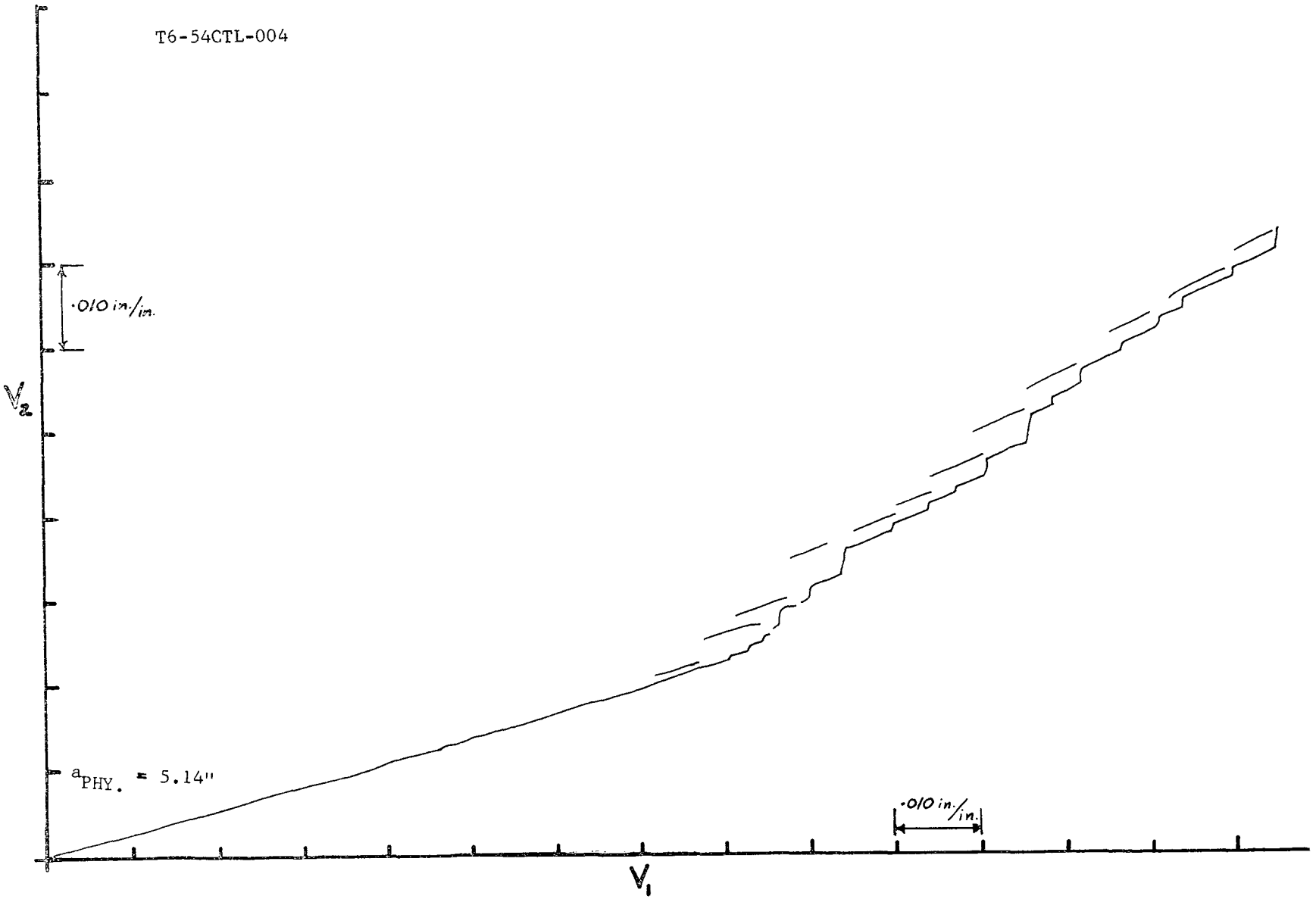

Figure 36. Deflection Curve - 0.195 Inch, 7075-T651 (TL) (Continued)

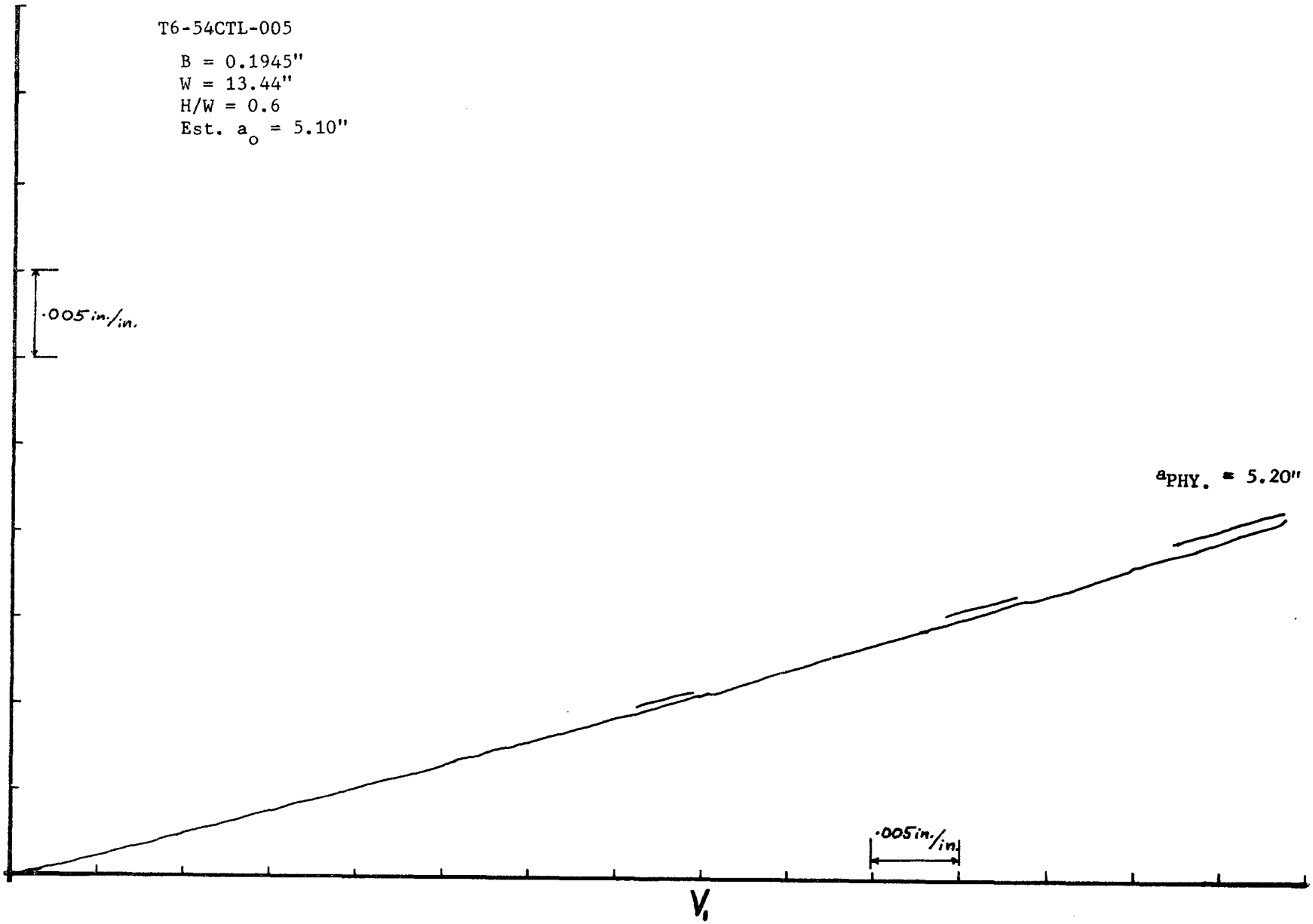

Figure 37. Deflection Curve - 0.1945 Inch, 7075-T651 (TL)

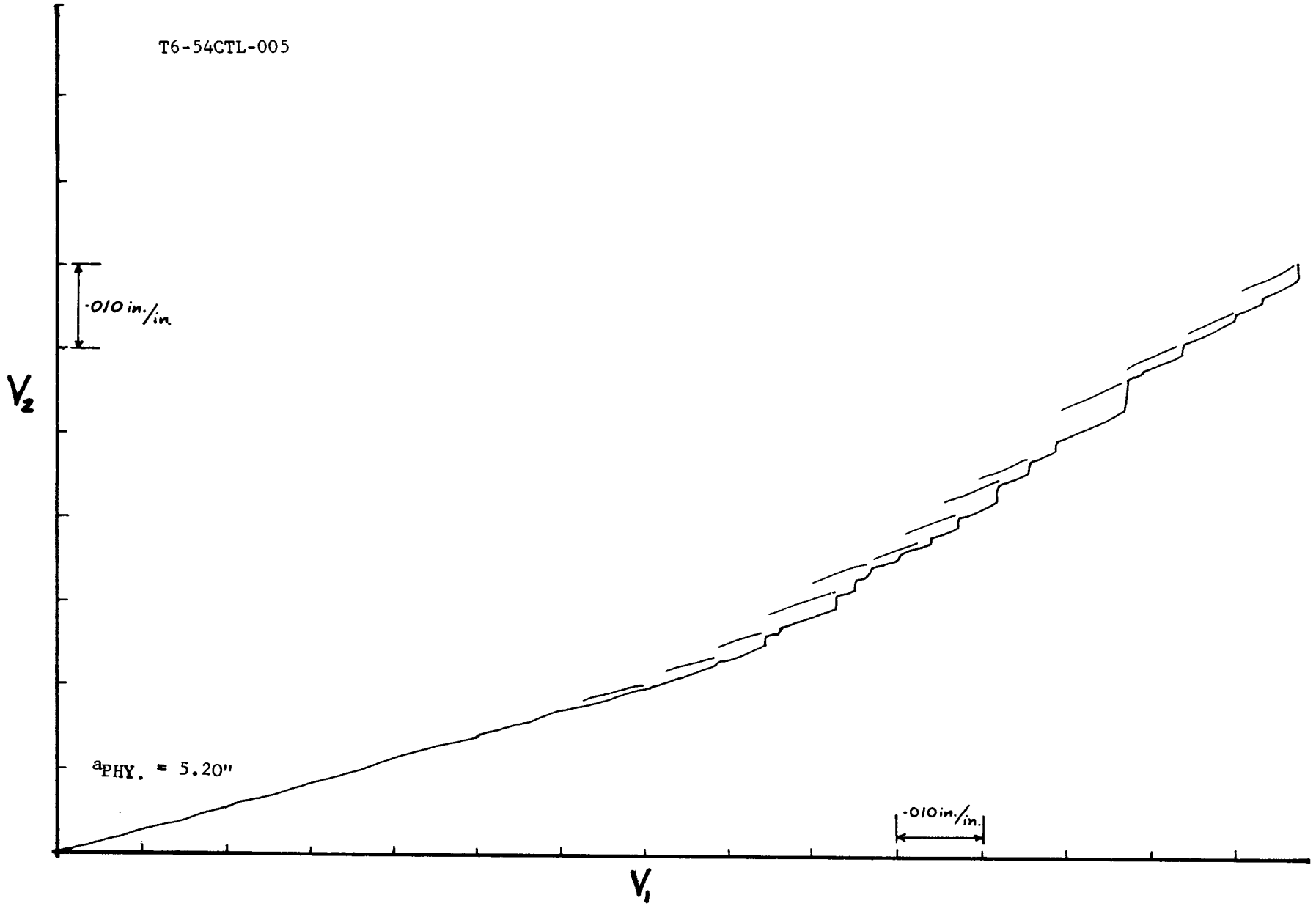

Figure 37. Deflection Curve - 0.1945 Inch, 7075-T651 (TL) (Continued)

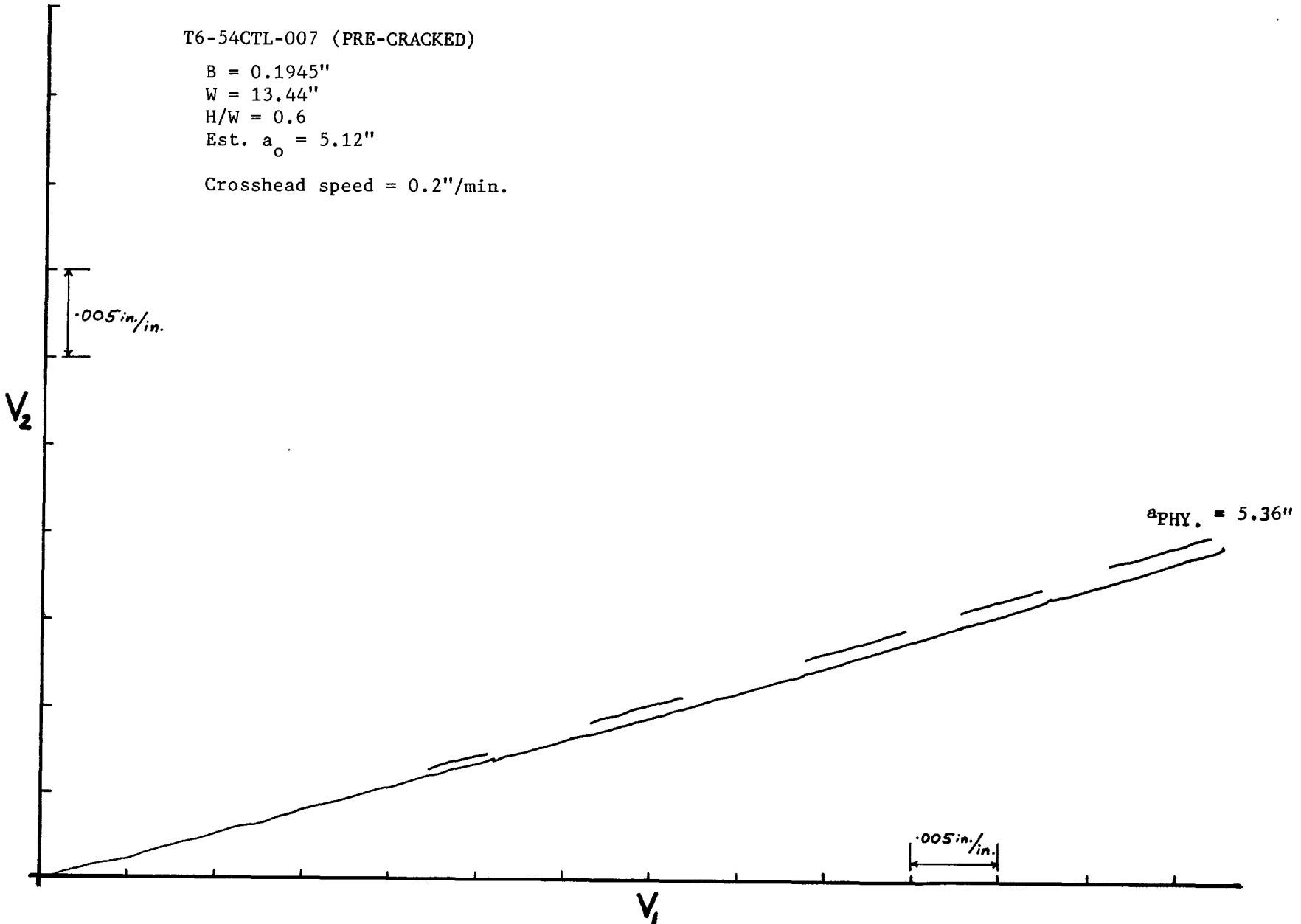

Figure 38. Deflection Curve - 0.1945 Inch, 7075-T651 (TL)

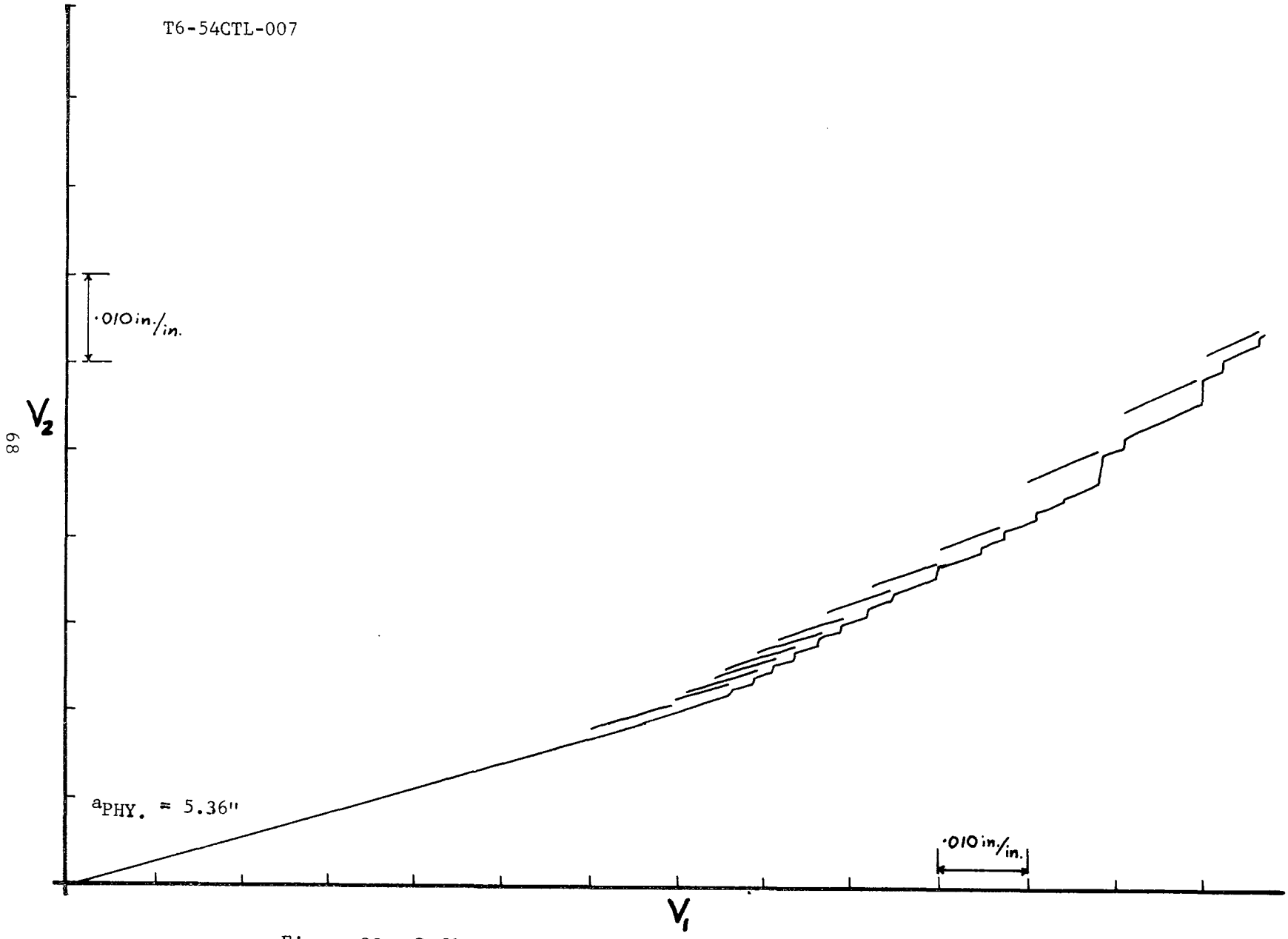

Figure 38. Deflection Curve - 0.1945 Inch, 7075-T651 (TL) (Continued)

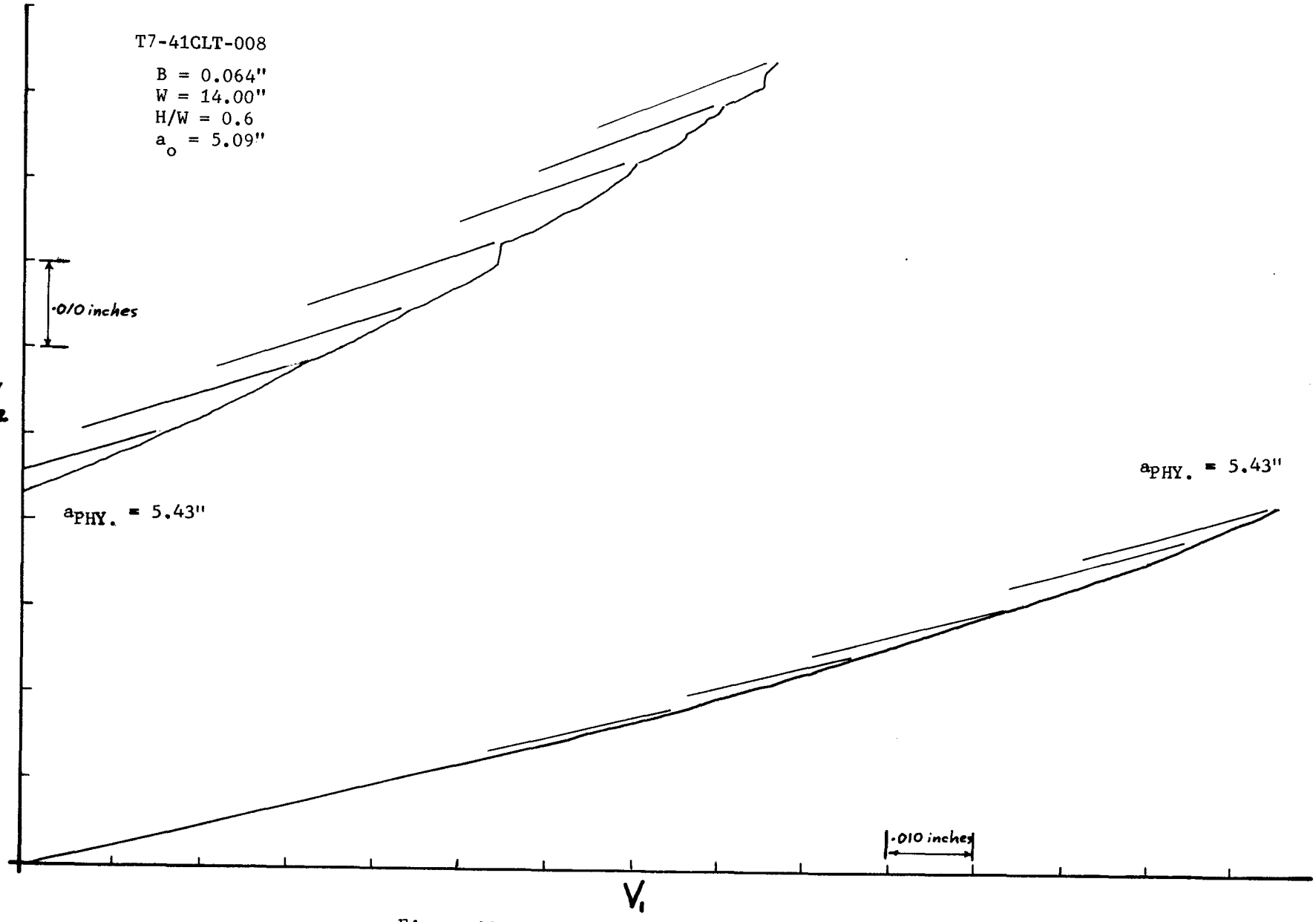

Figure 39. Deflection Curve - 0.064 Inch, 7075-T73 (LT)

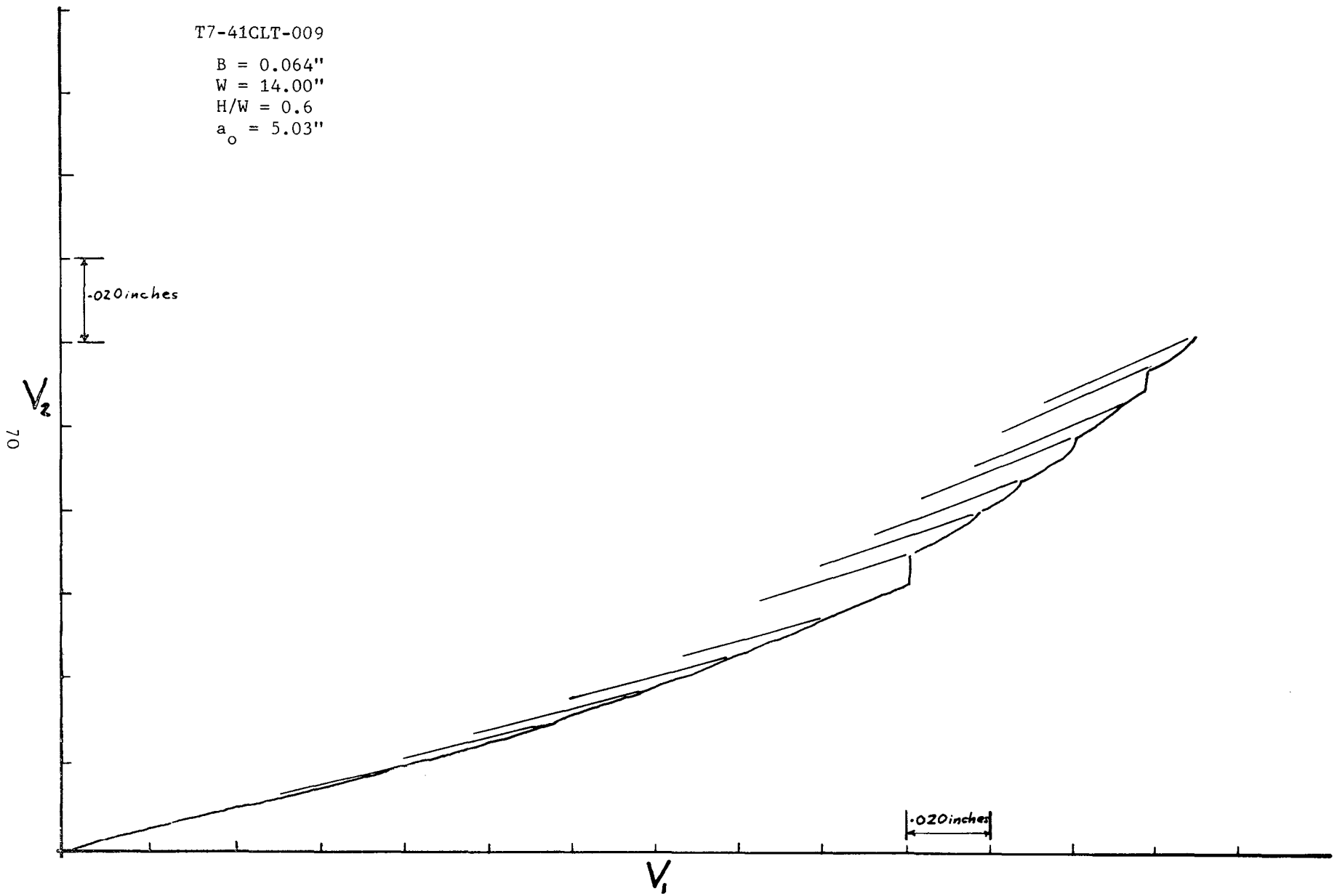

Figure 40. Deflection Curve - 0.064 Inch, 7075-T73 (LT)

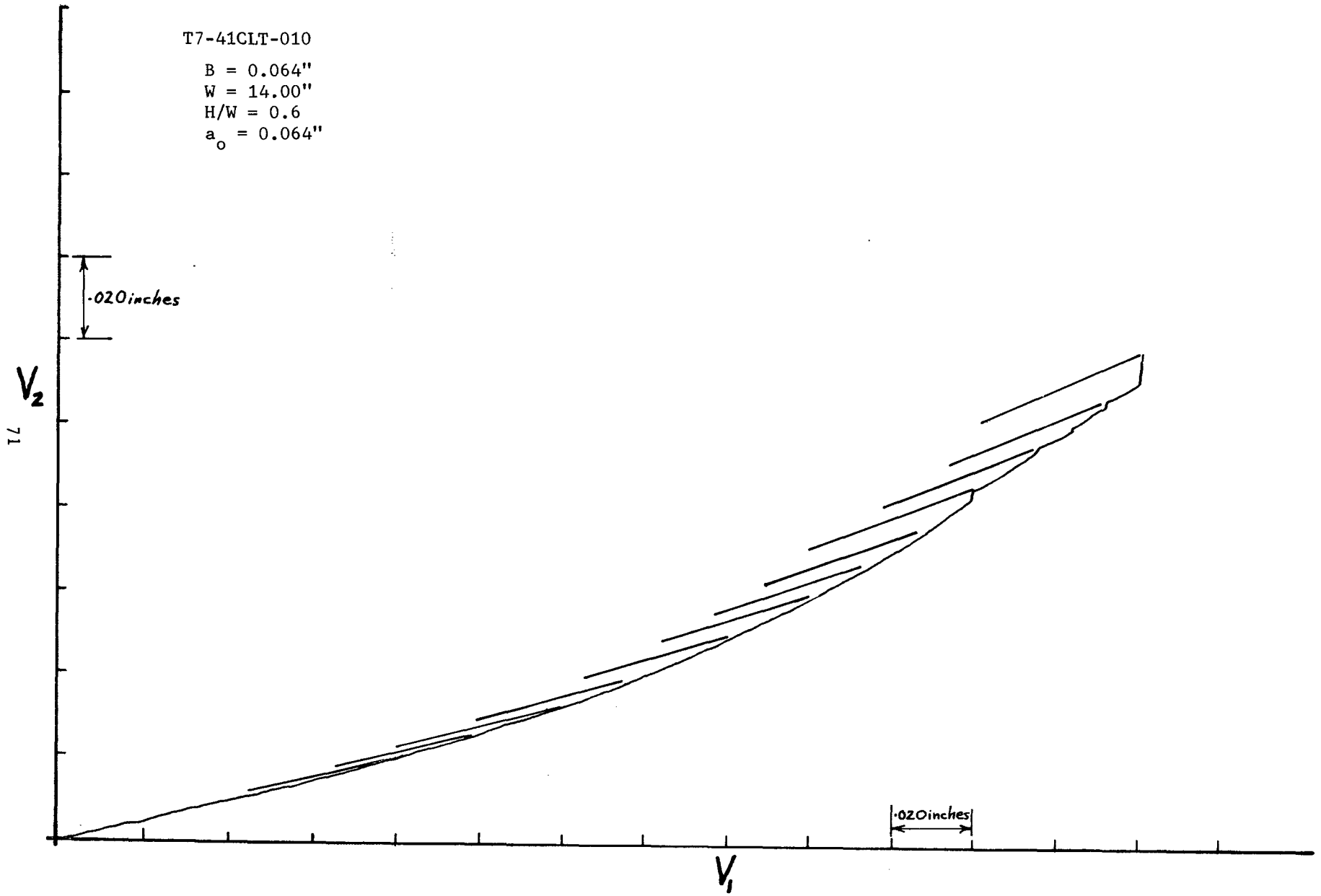

Figure 41. Deflection Curve - 0.064 Inch, 7075-T73 (LT)

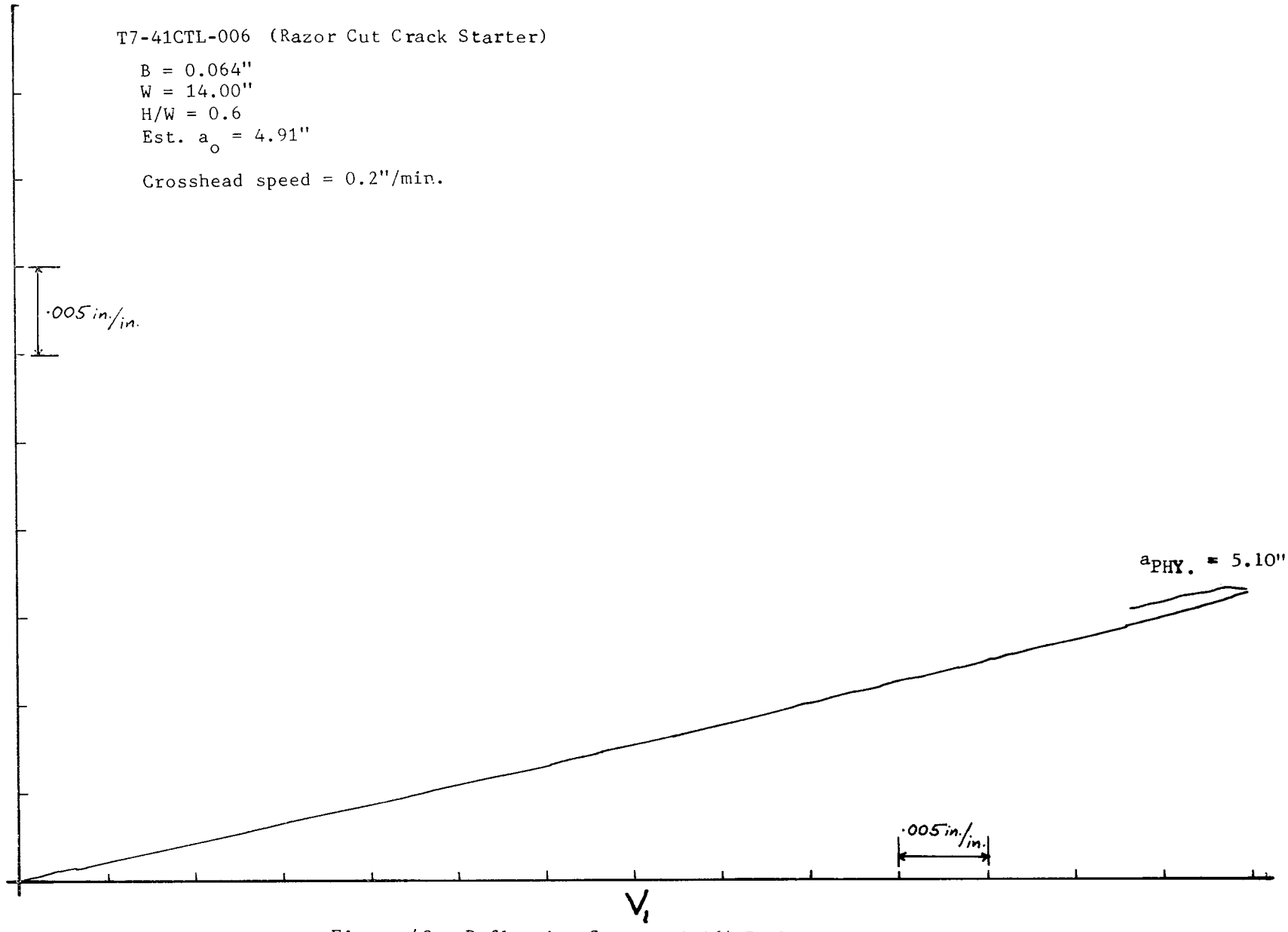

Figure 42. Deflection Curve - 0.064 Inch, 7075-T53 (LT)

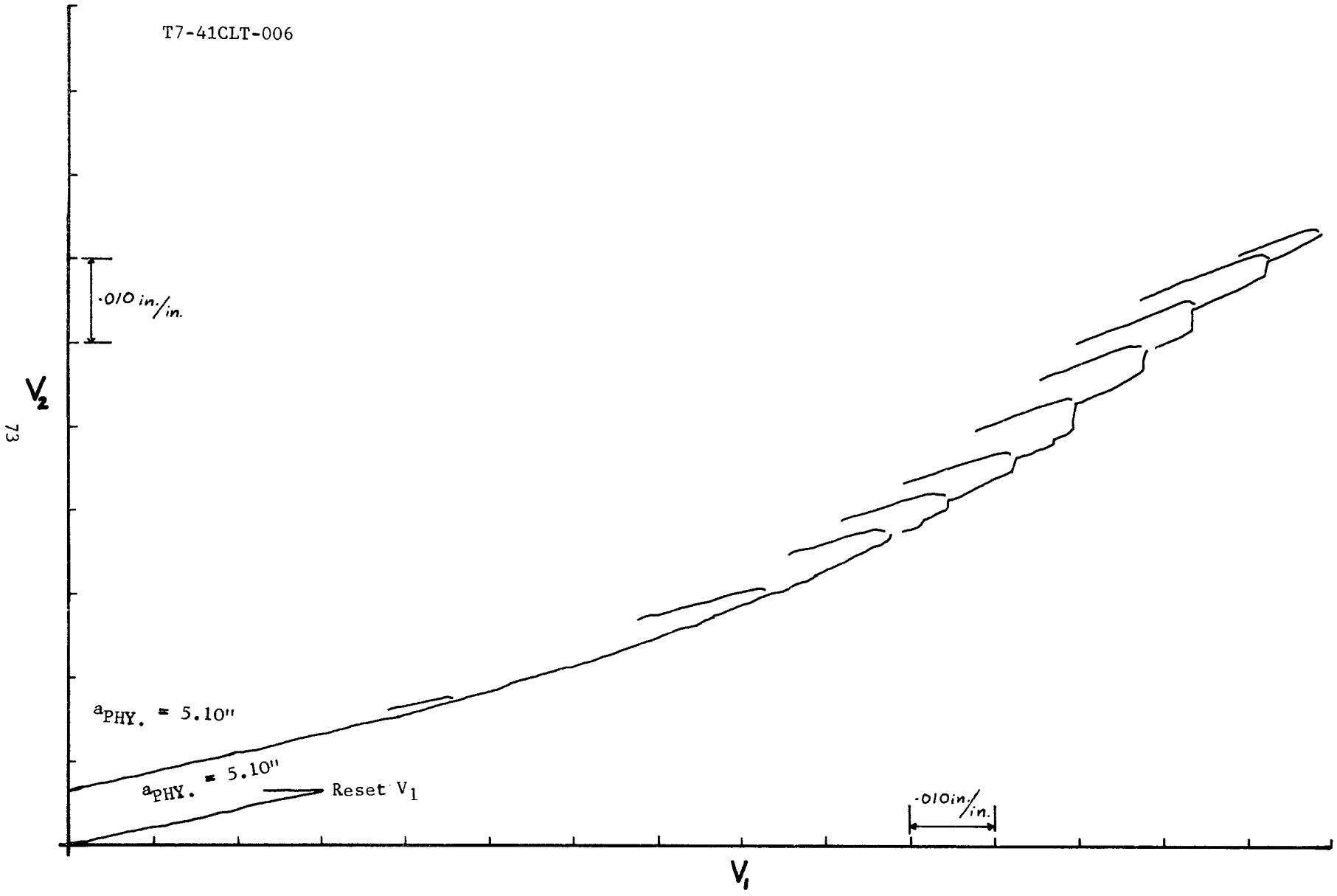

Figure 42. Deflection Curve - 0.064 Inch, 7075-T73 (LT) (Continued)

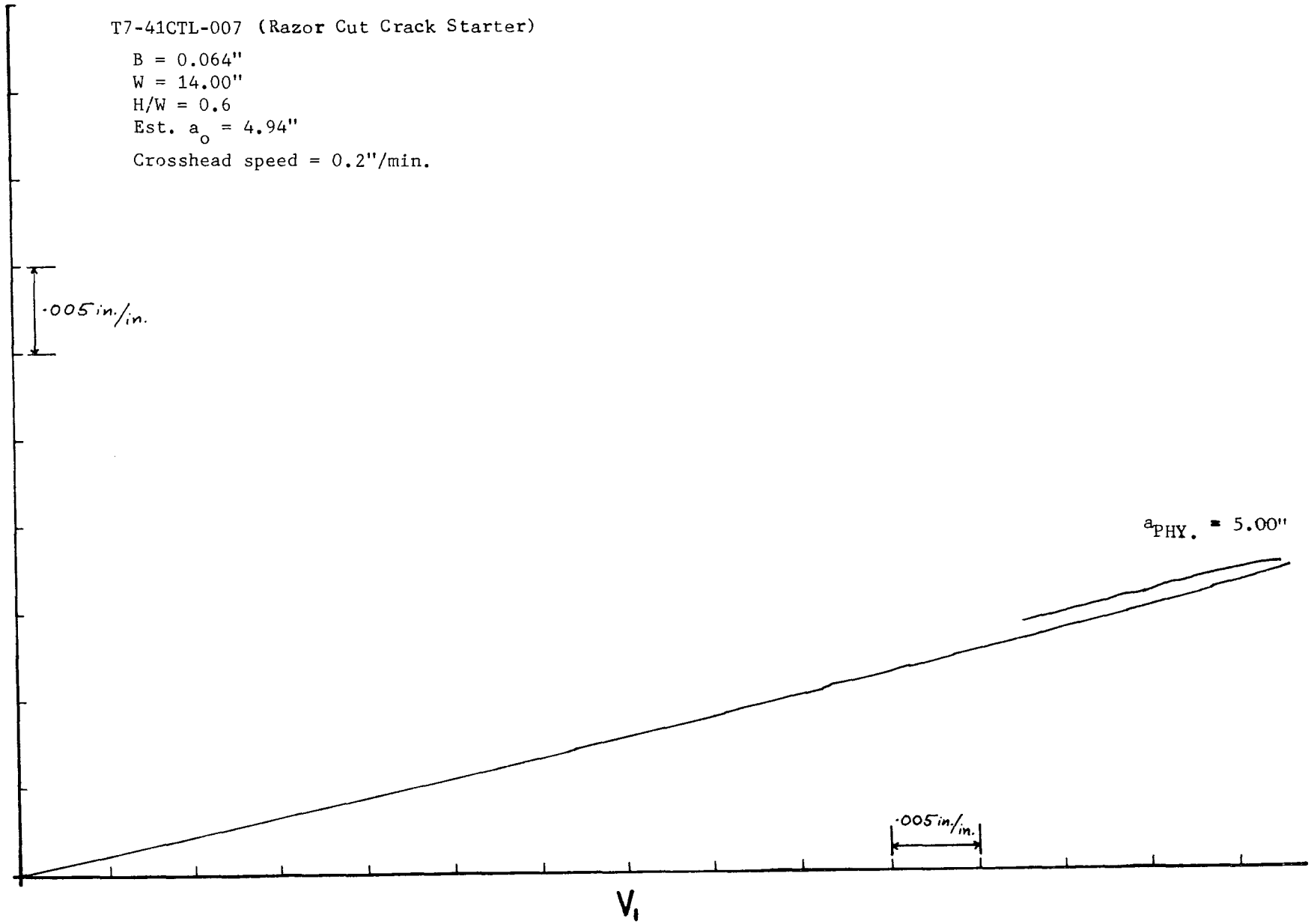

Figure 43. Deflection Curve - 0.064 Inch, 7075-T73 (TL)

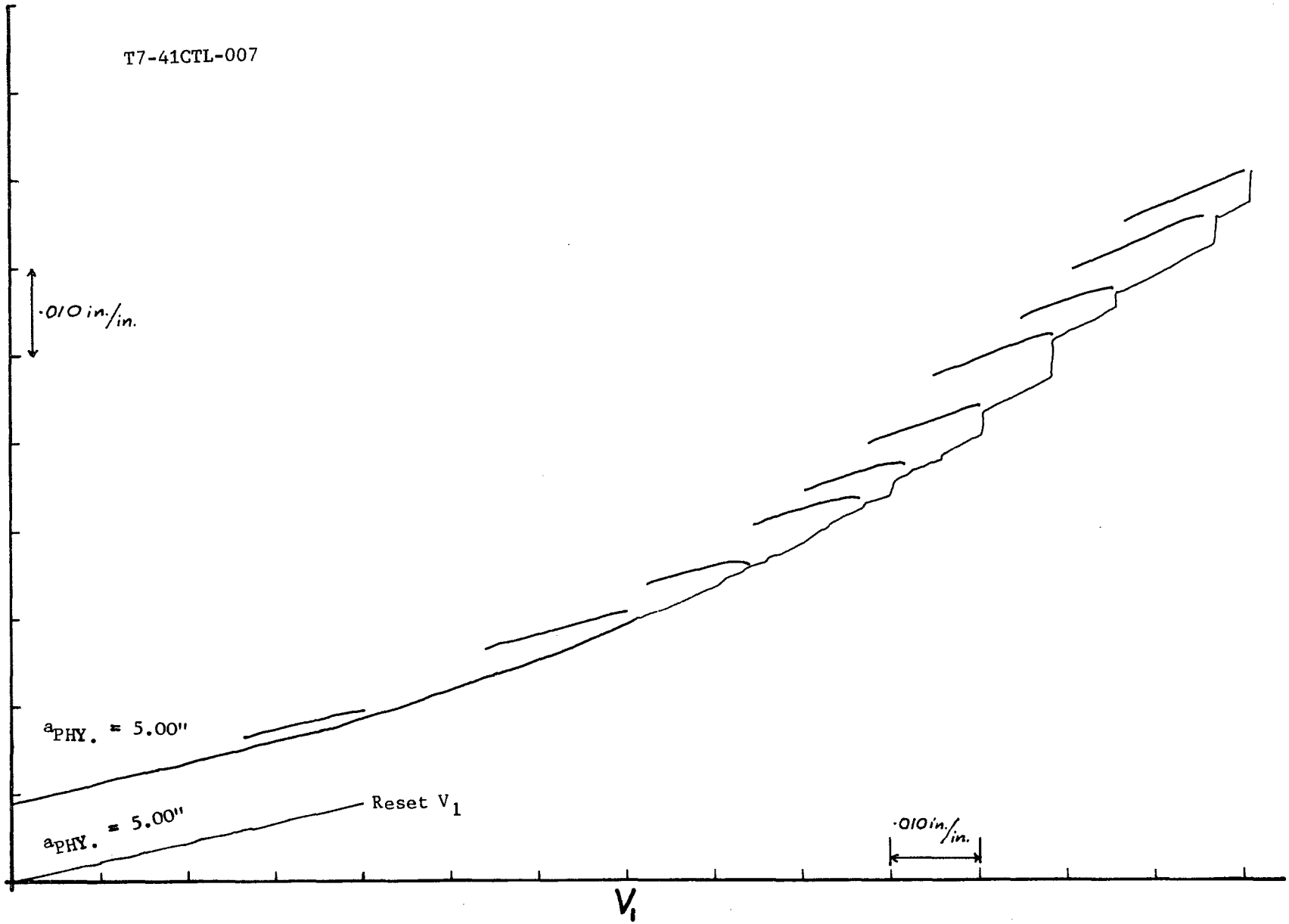

Figure 43. Deflection Curve - 0.064 Inch, 7075-T73 (TL) (Continued)

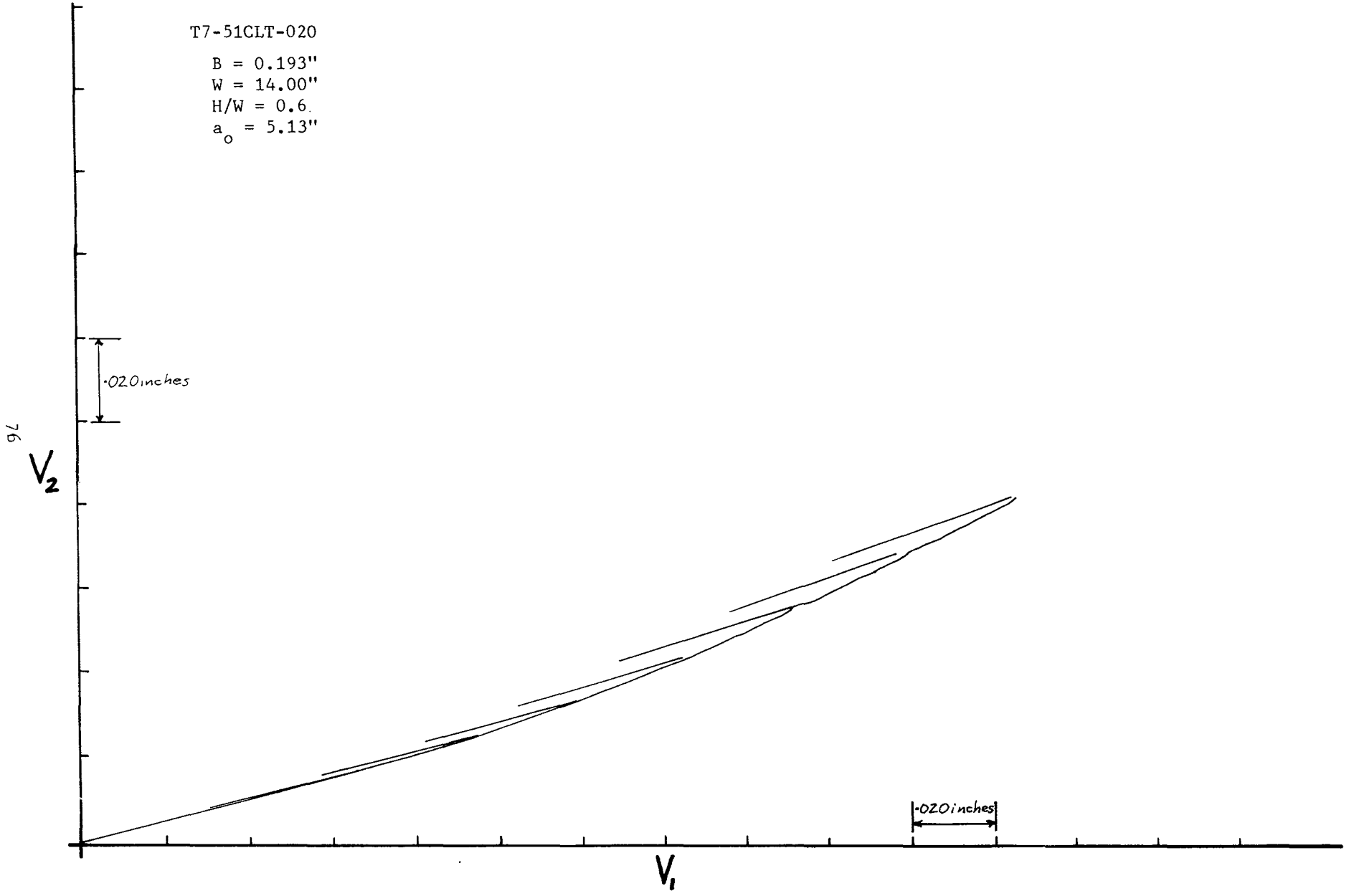

Figure 44. Deflection Curve - 0.193 Inch, 7075-T731 (LT)

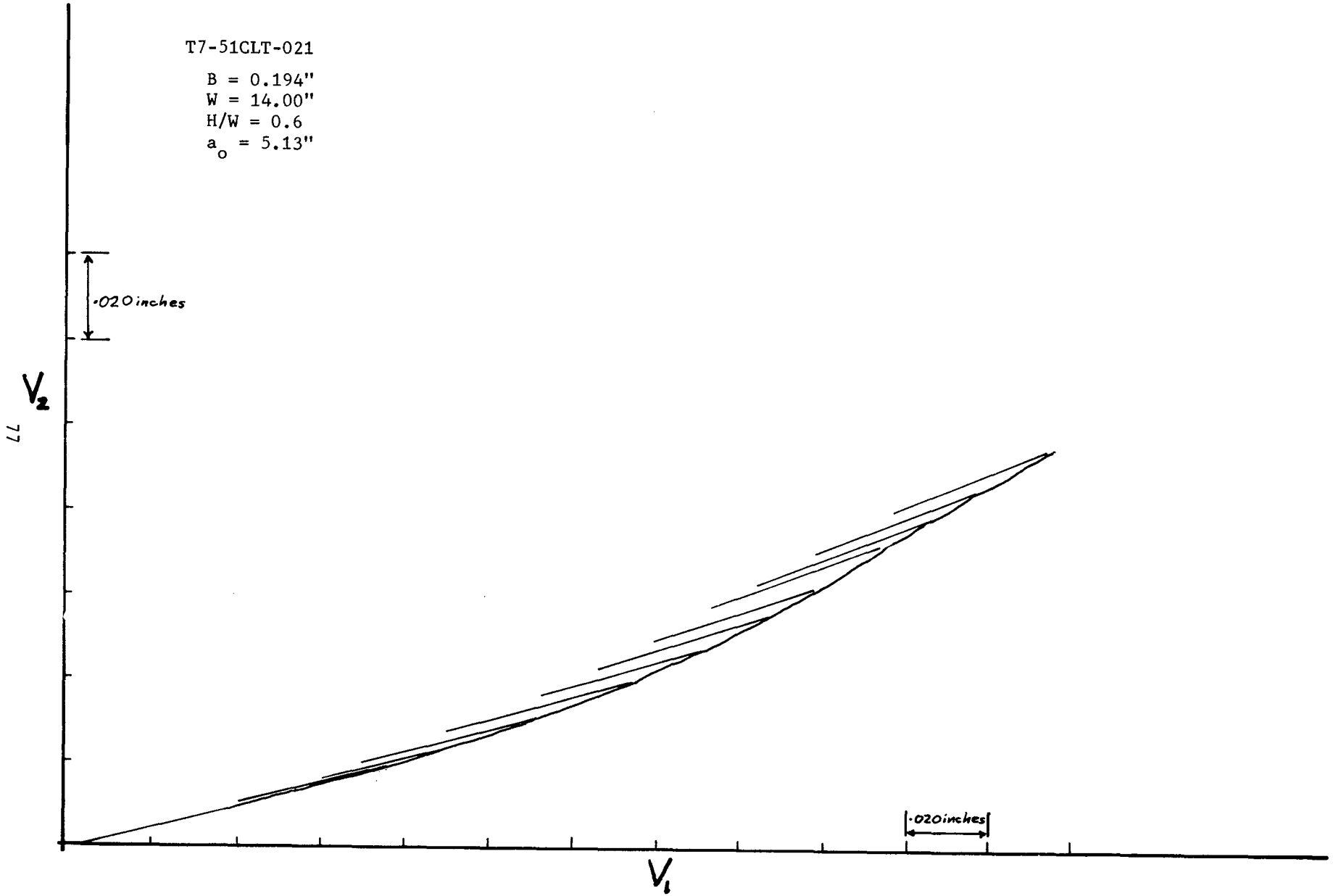

Figure 45. Deflection Curve - 0.194 Inch, 7075-T7351 (LT)

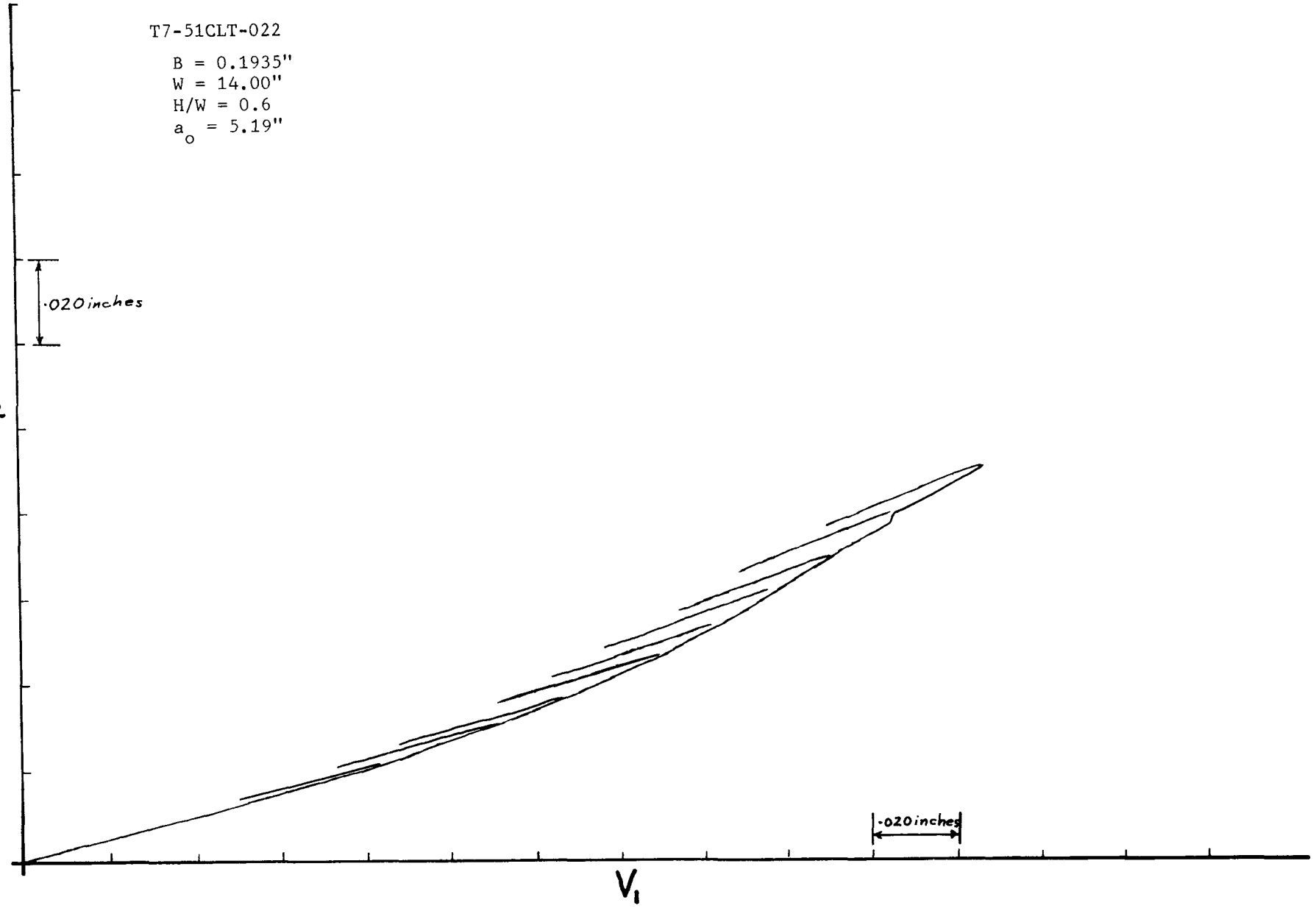

Figure 46. Deflection Curve - 0.1935 Inch, 7075-T7351 (LT)

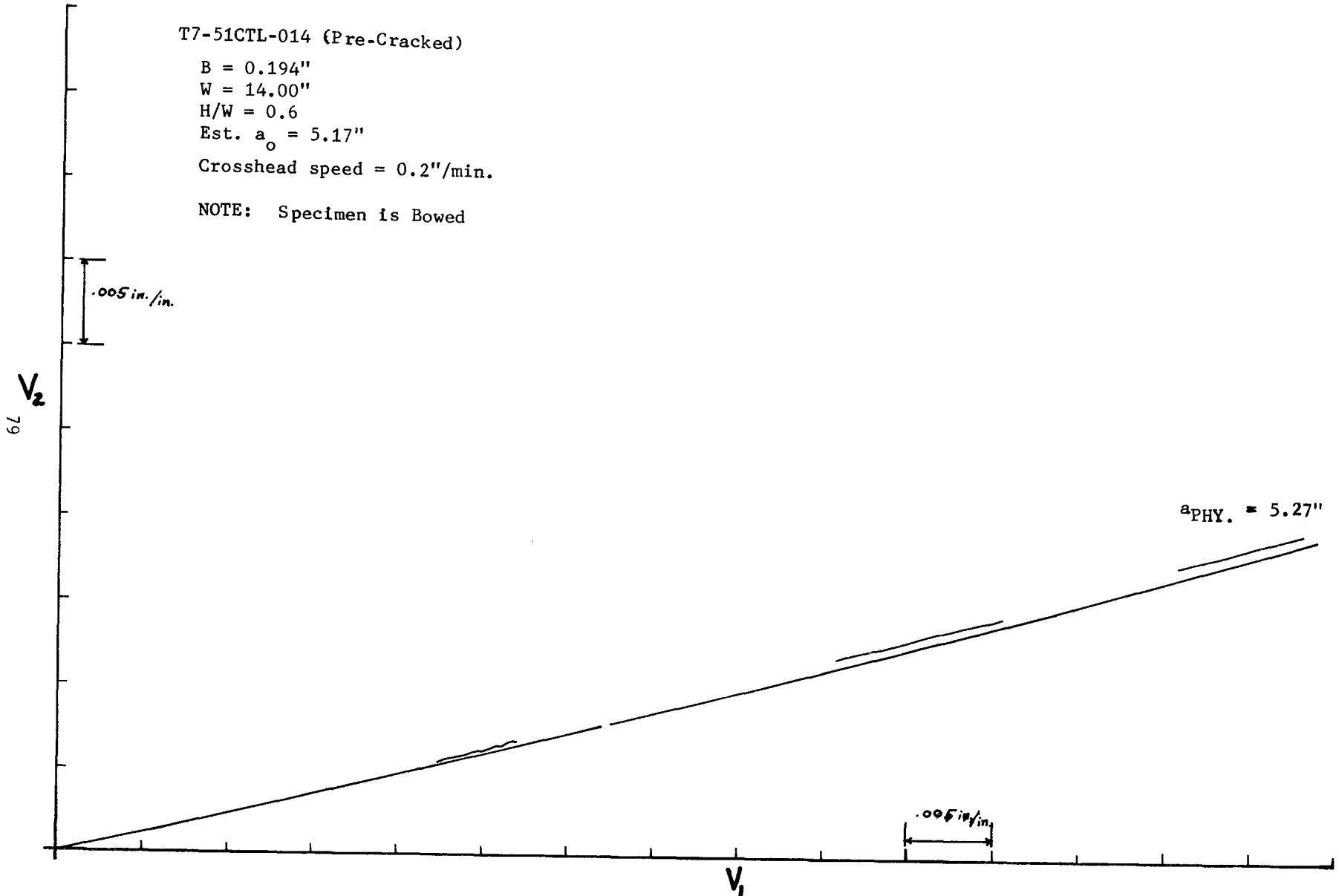

Figure 47. Deflection Curve - 0.194 Inch, 7075-T7351 (TL)

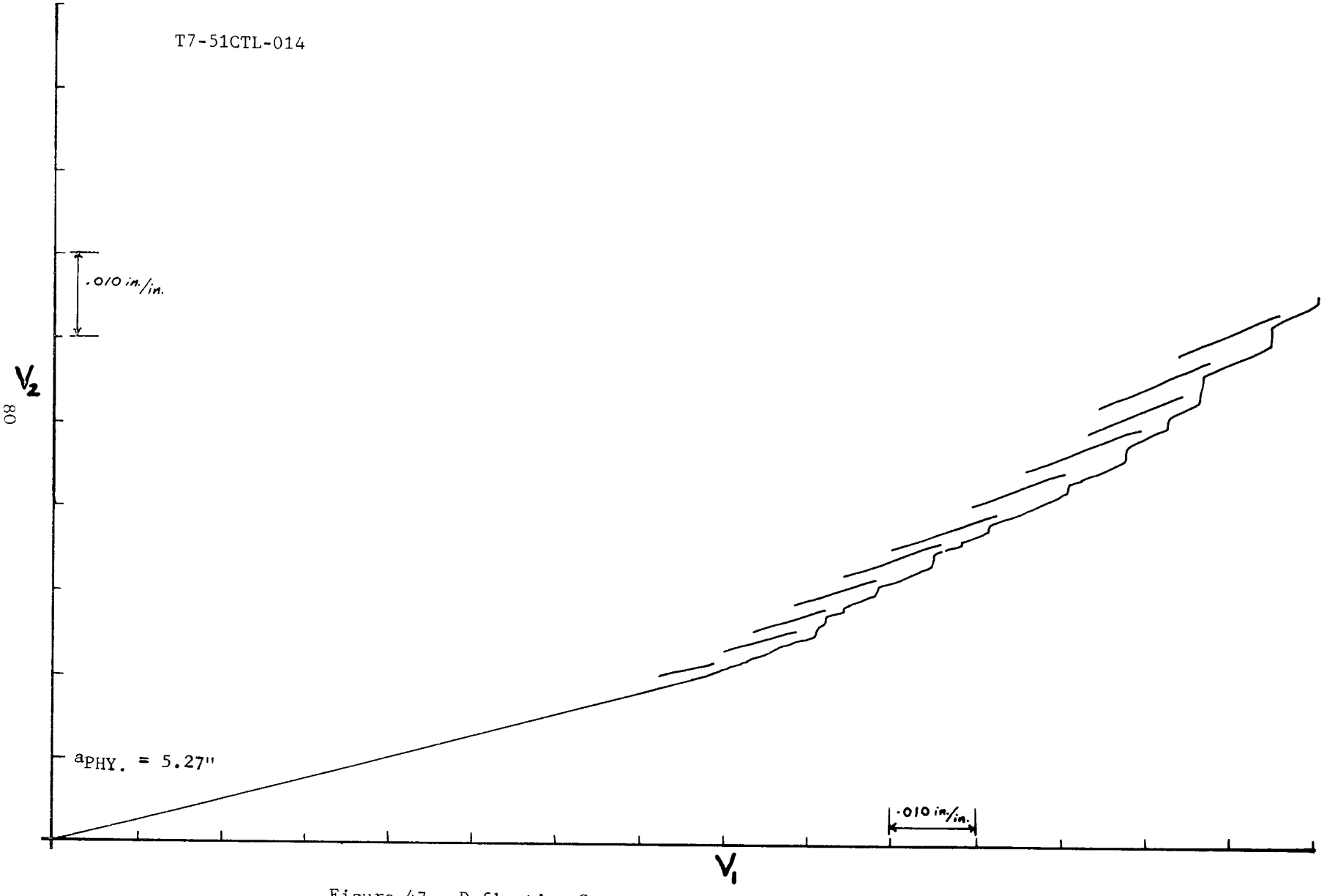

Figure 47. Deflection Curve - 0.194 Inch, 7075-T7351 (TL) Continued)

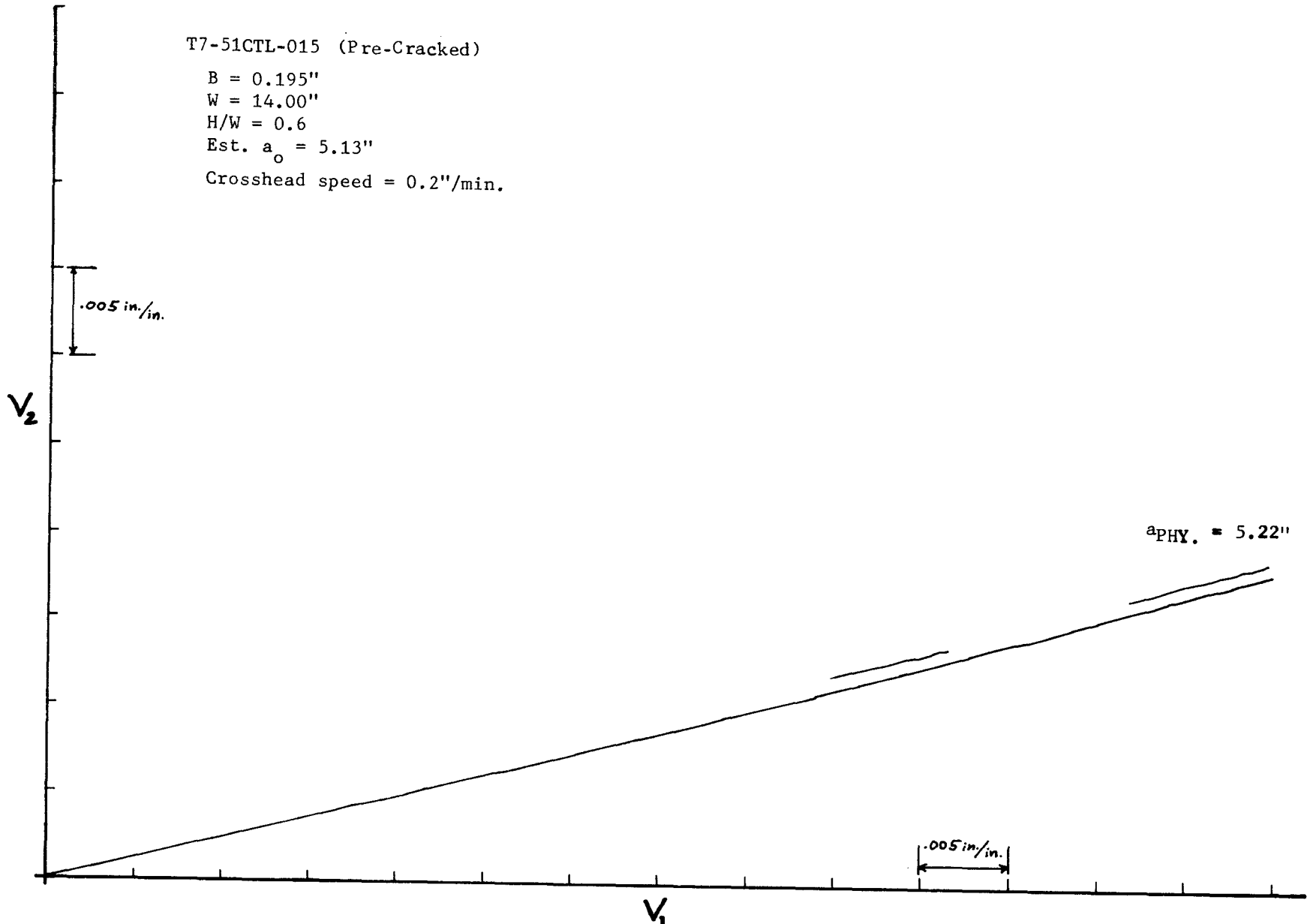

Figure 48. Deflection Curve - 0.195 Inch, 7075-T7351 (TL)

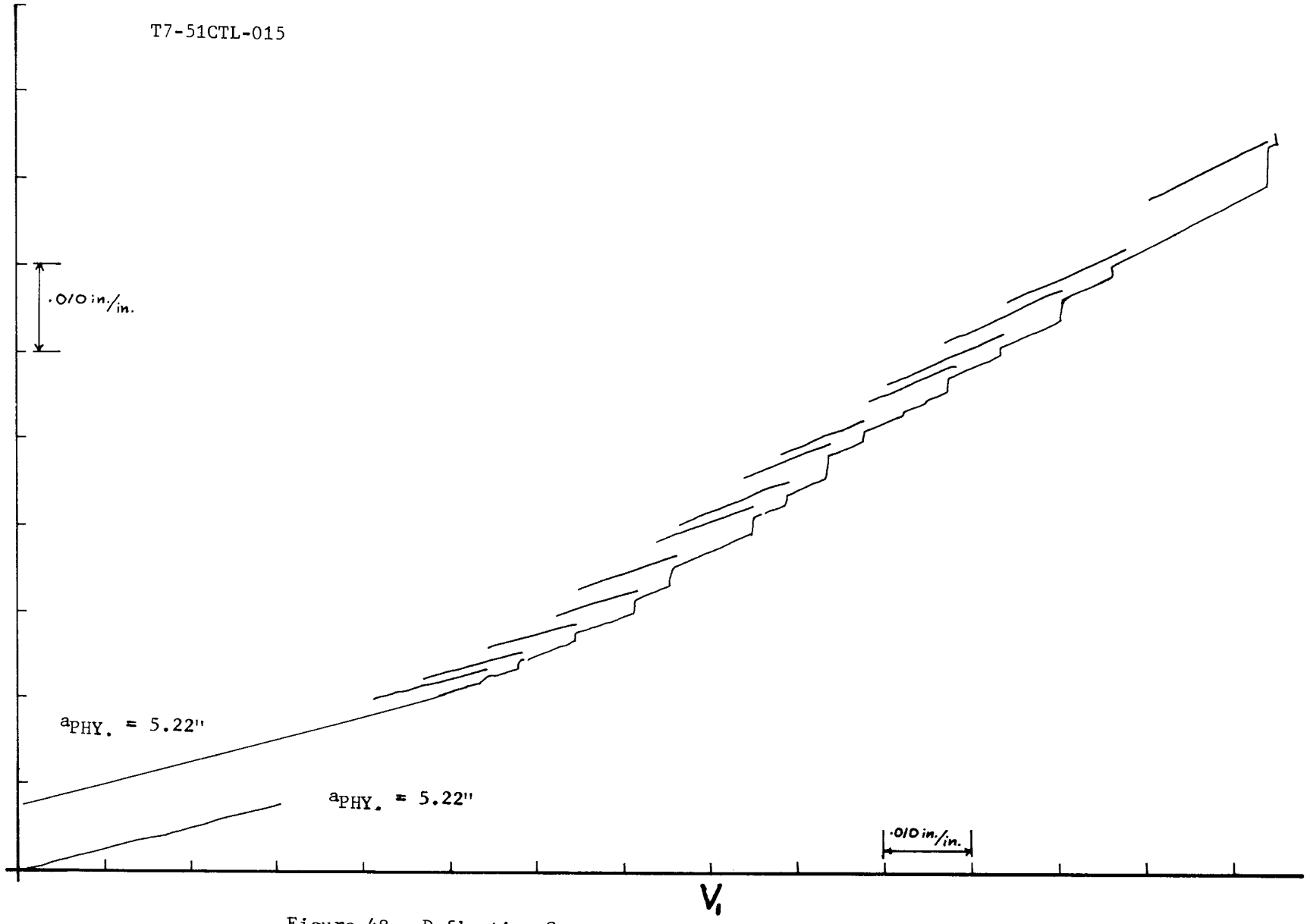

Figure 48. Deflection Curve - 0.195 Inch, 7075-T7351 (TL) (Continued)

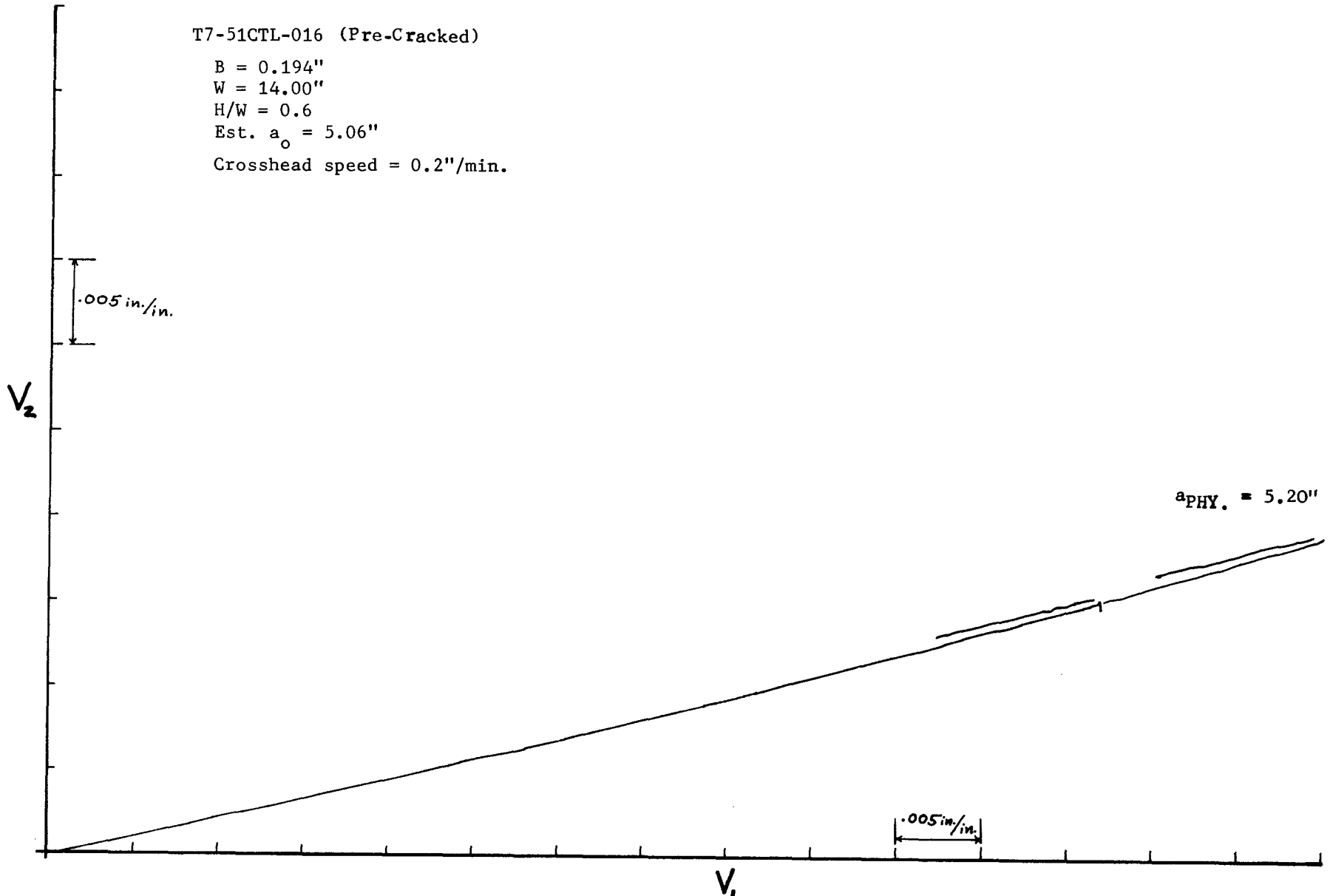

Figure 49. Deflection Curve - 0.194 Inch, 7075-T7351 (TL)

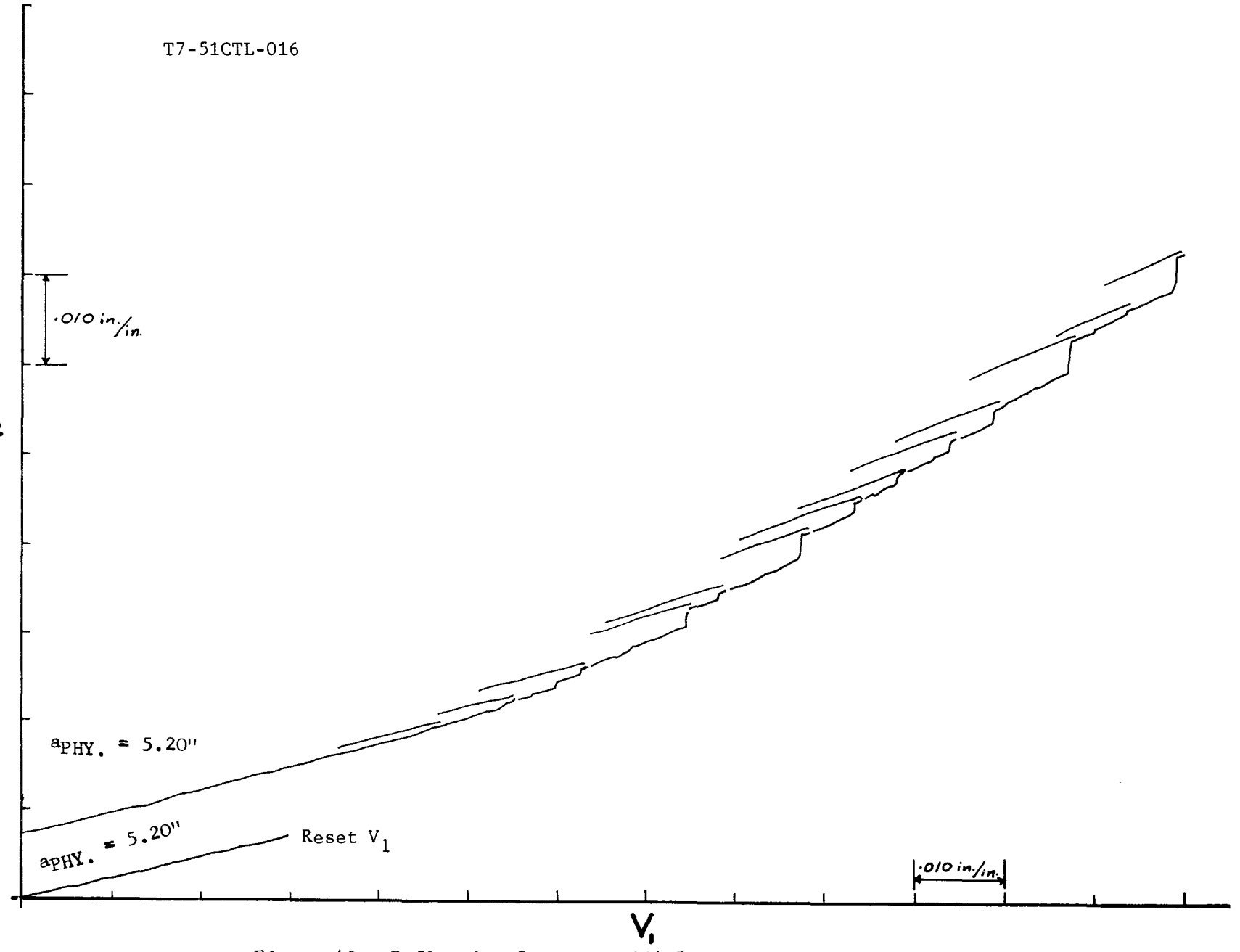

Figure 49. Deflection Curve - 0.194 Inch, 7075-T7351 (TL) (Continued)

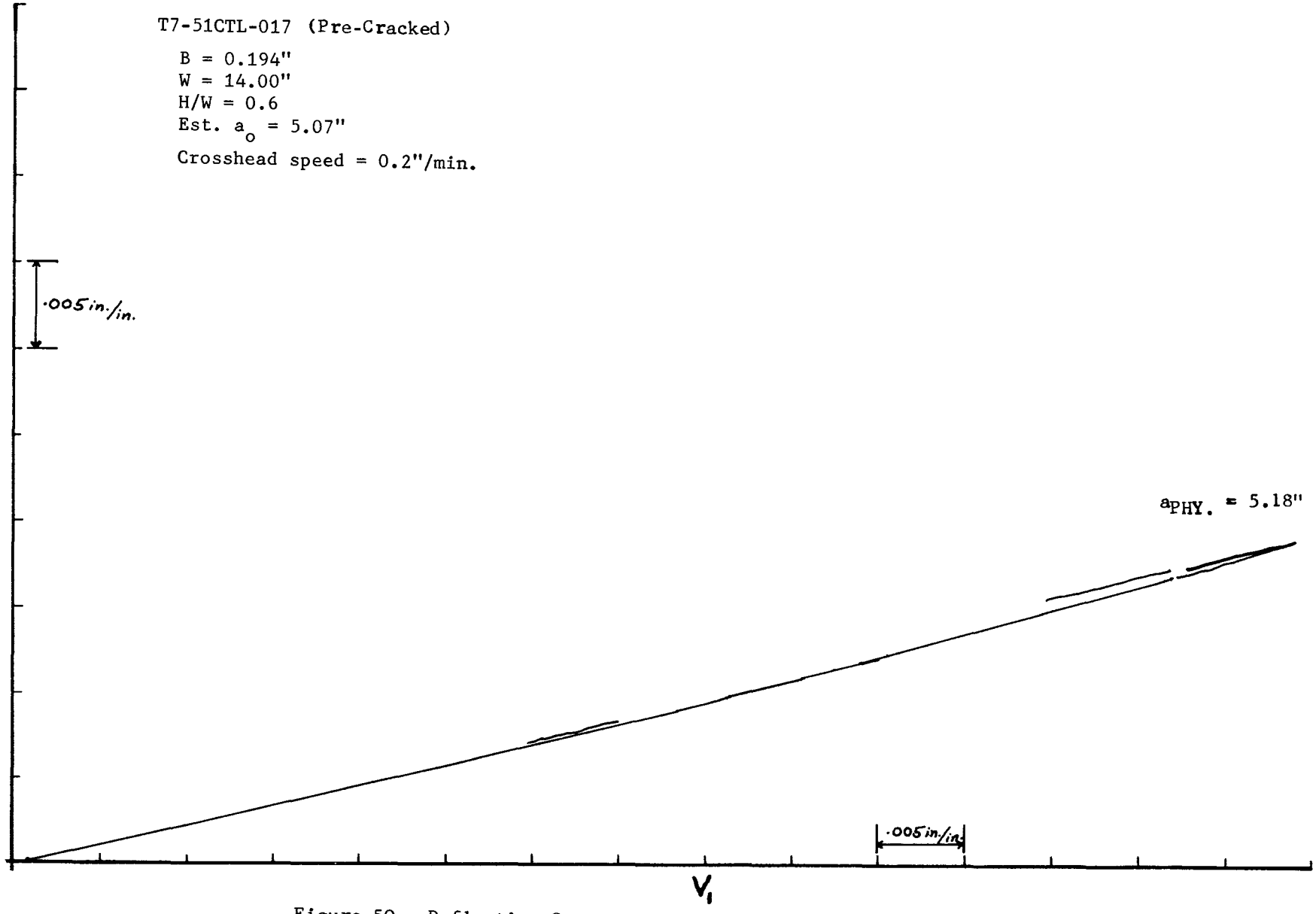

Figure 50. Deflection Curve - 0.194 Inch, 7075-T7351 (TL)

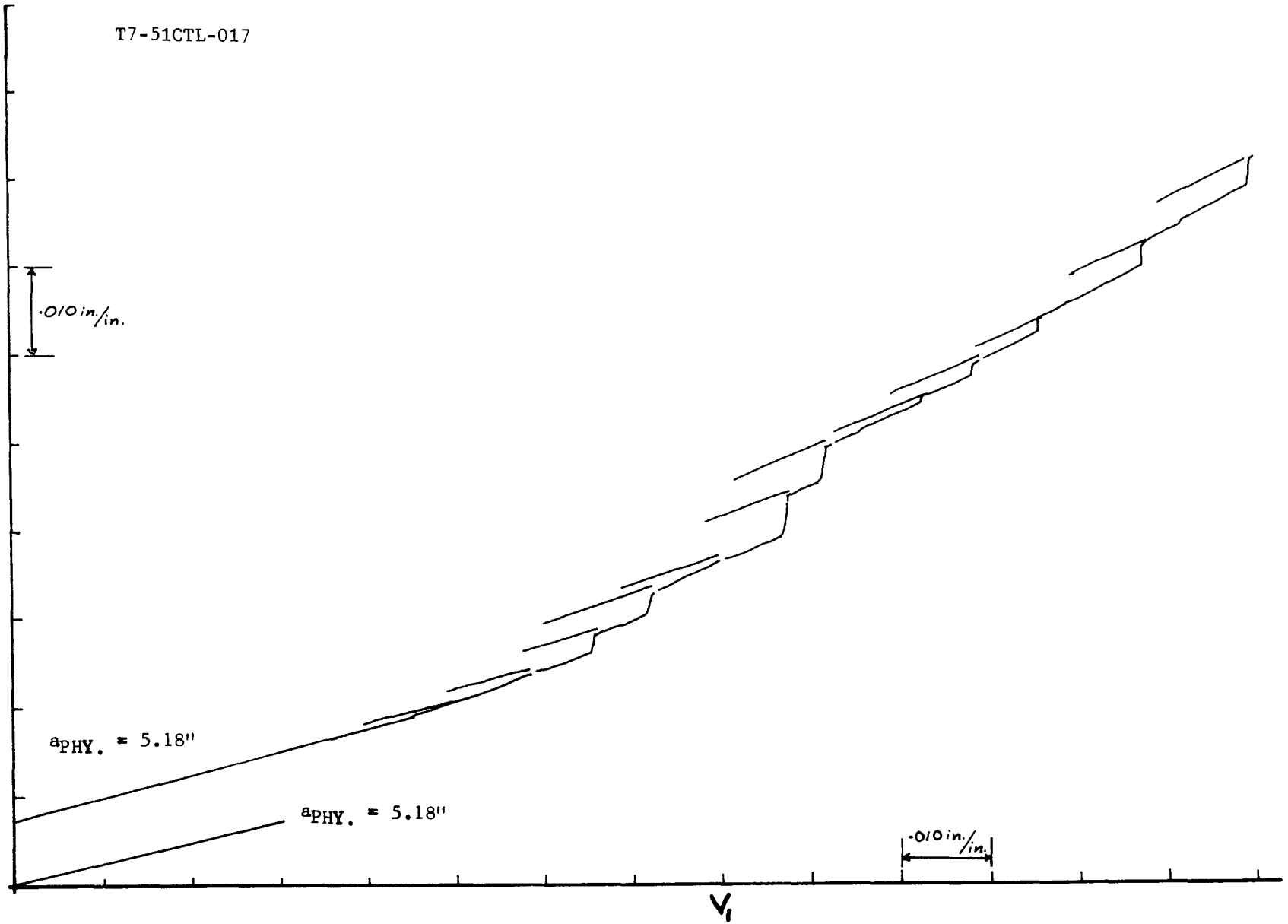

Figure 50. Deflection Curve - 0.194 Inch, 7075-T7351 (TL) (Continued)

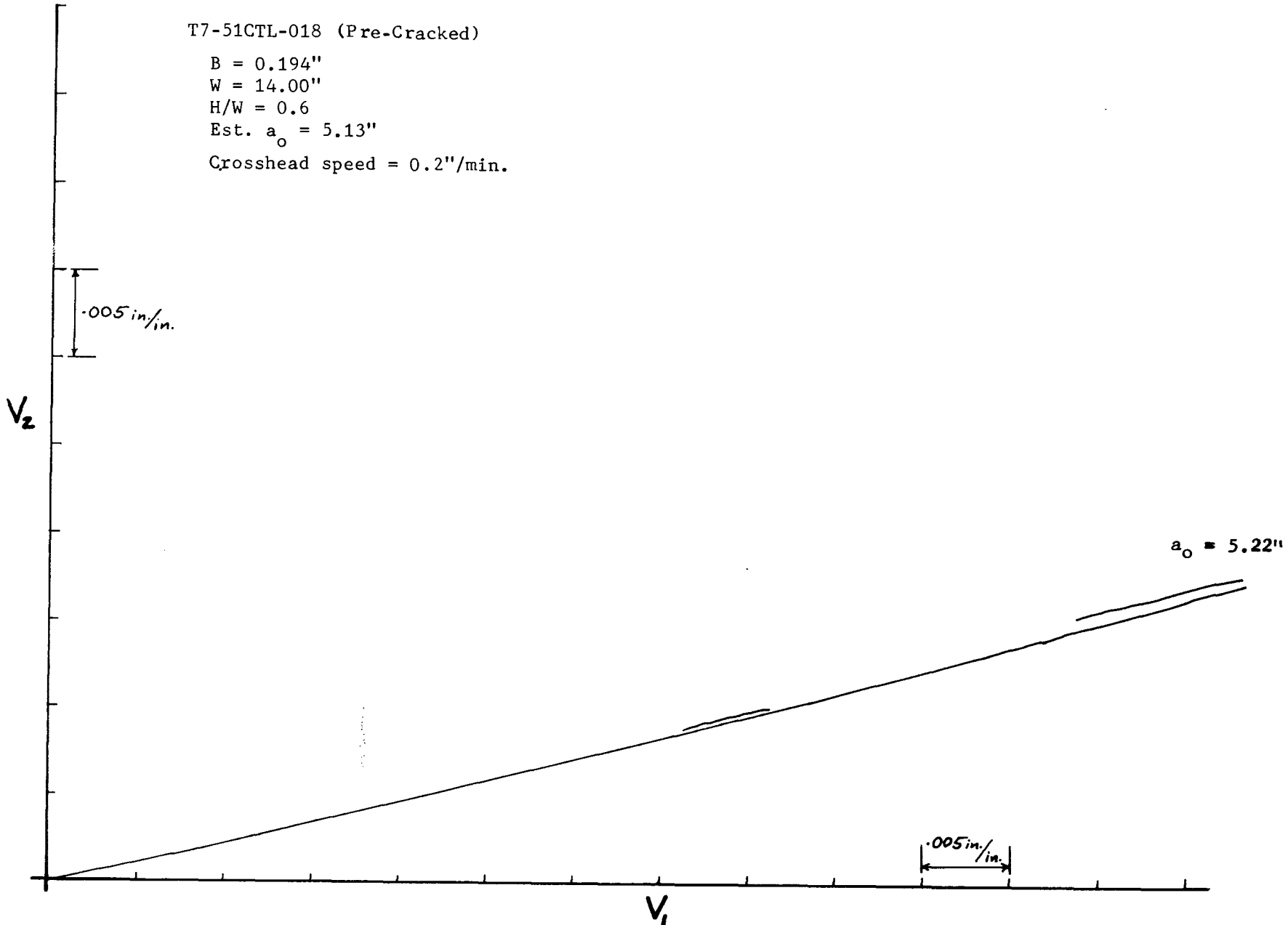

Figure 51. Deflection Curve - 0.194 Inch, 7075-T7351 (TL)

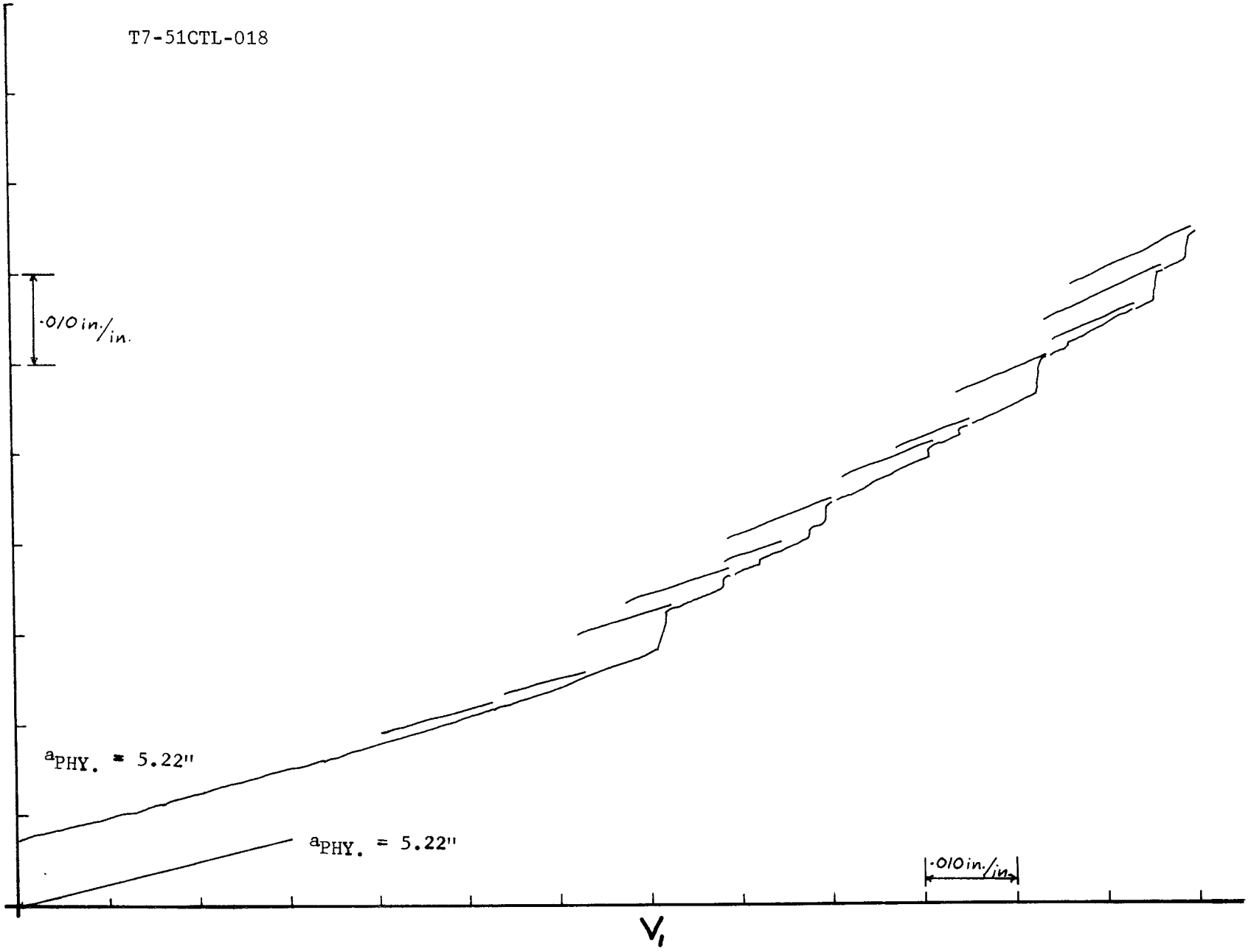

Figure 51. Deflection Curve - 0.194 Inch, 7075-T7351 (TL) (Continued)

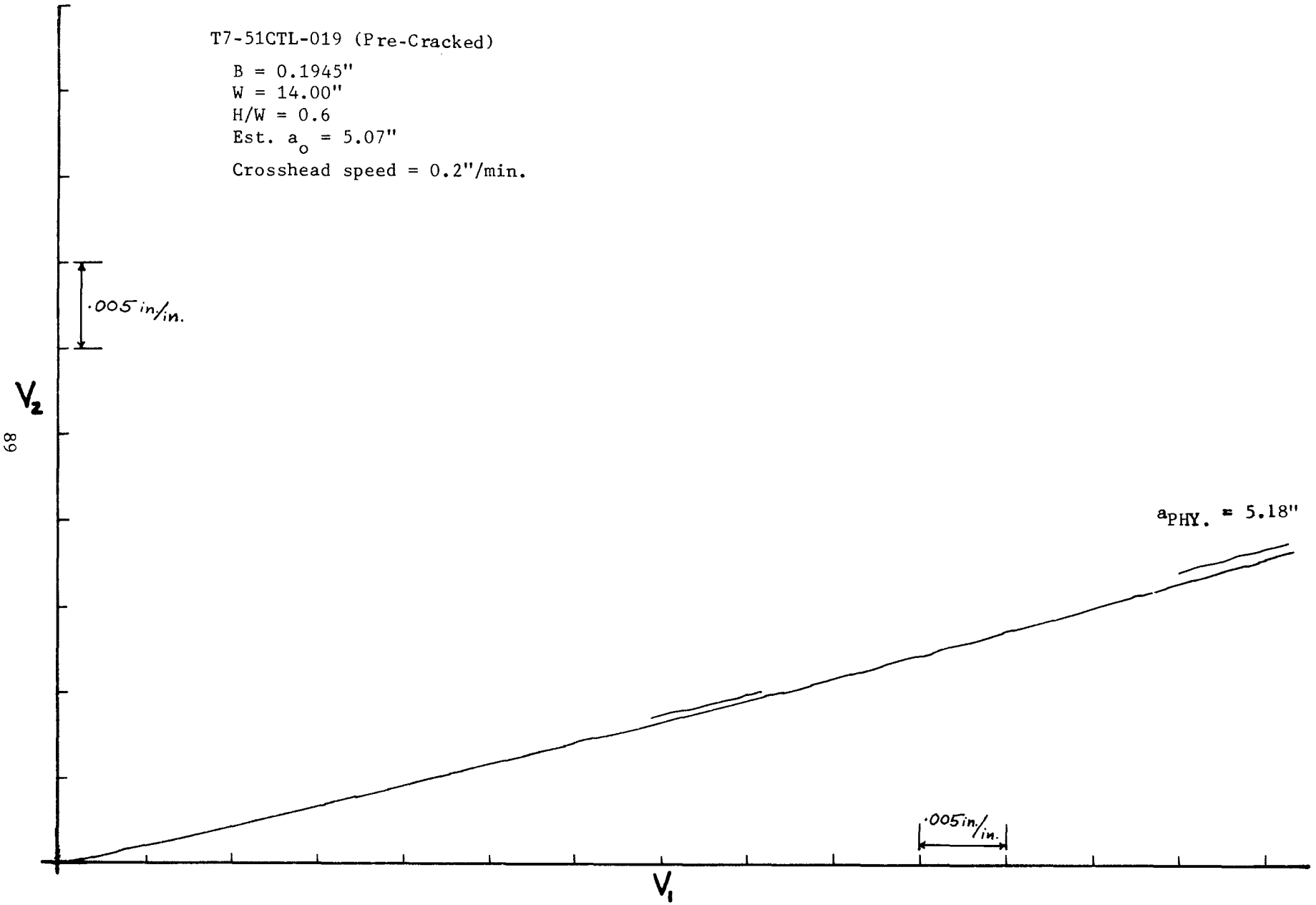

Figure 52. Deflection Curve - 0.1945 Inch, 7075-T7351 (TL)

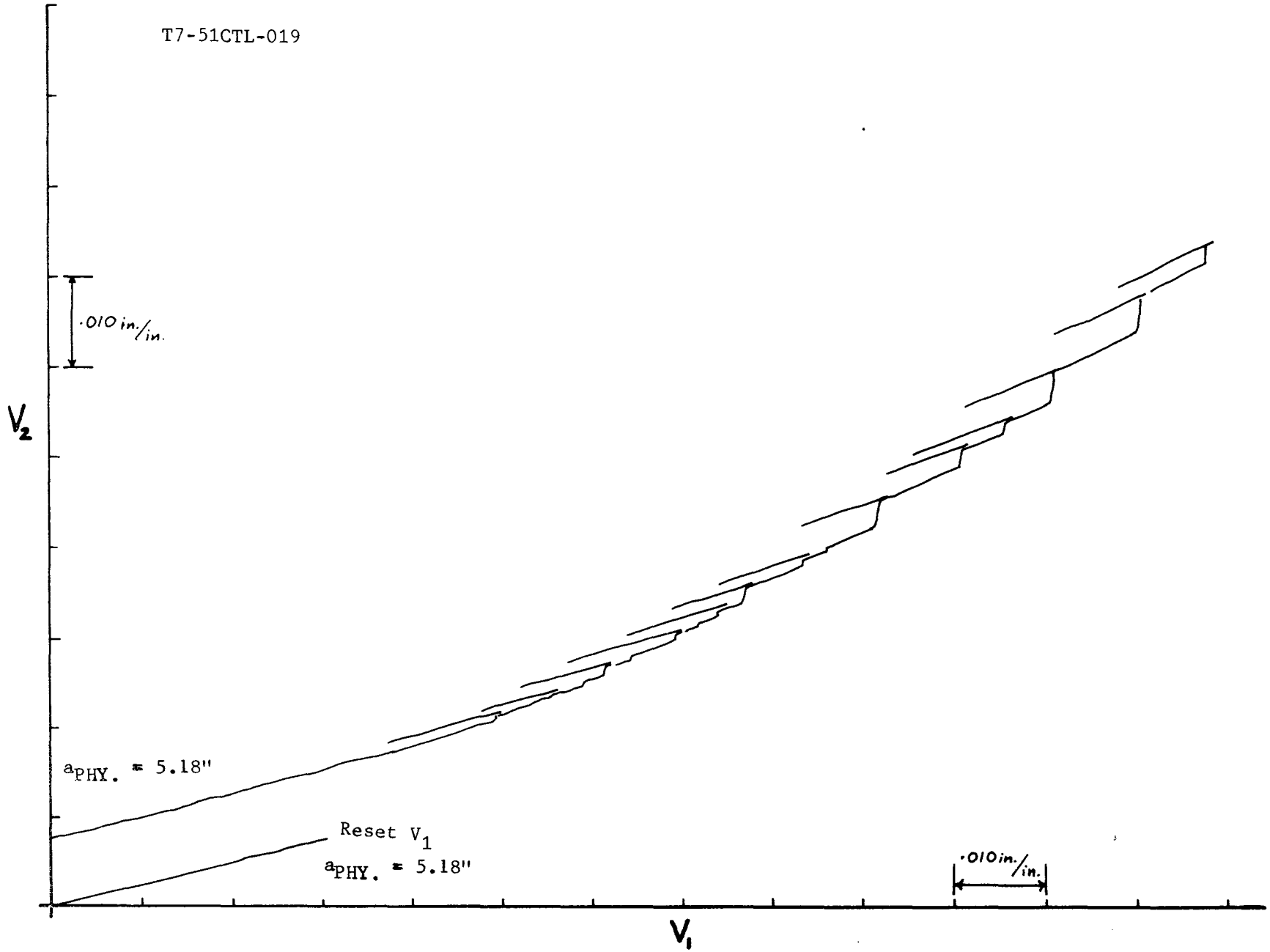

Figure 52. Deflection Curve - 0.1945 Inch, 7075-T7351 (TL) (Continued)

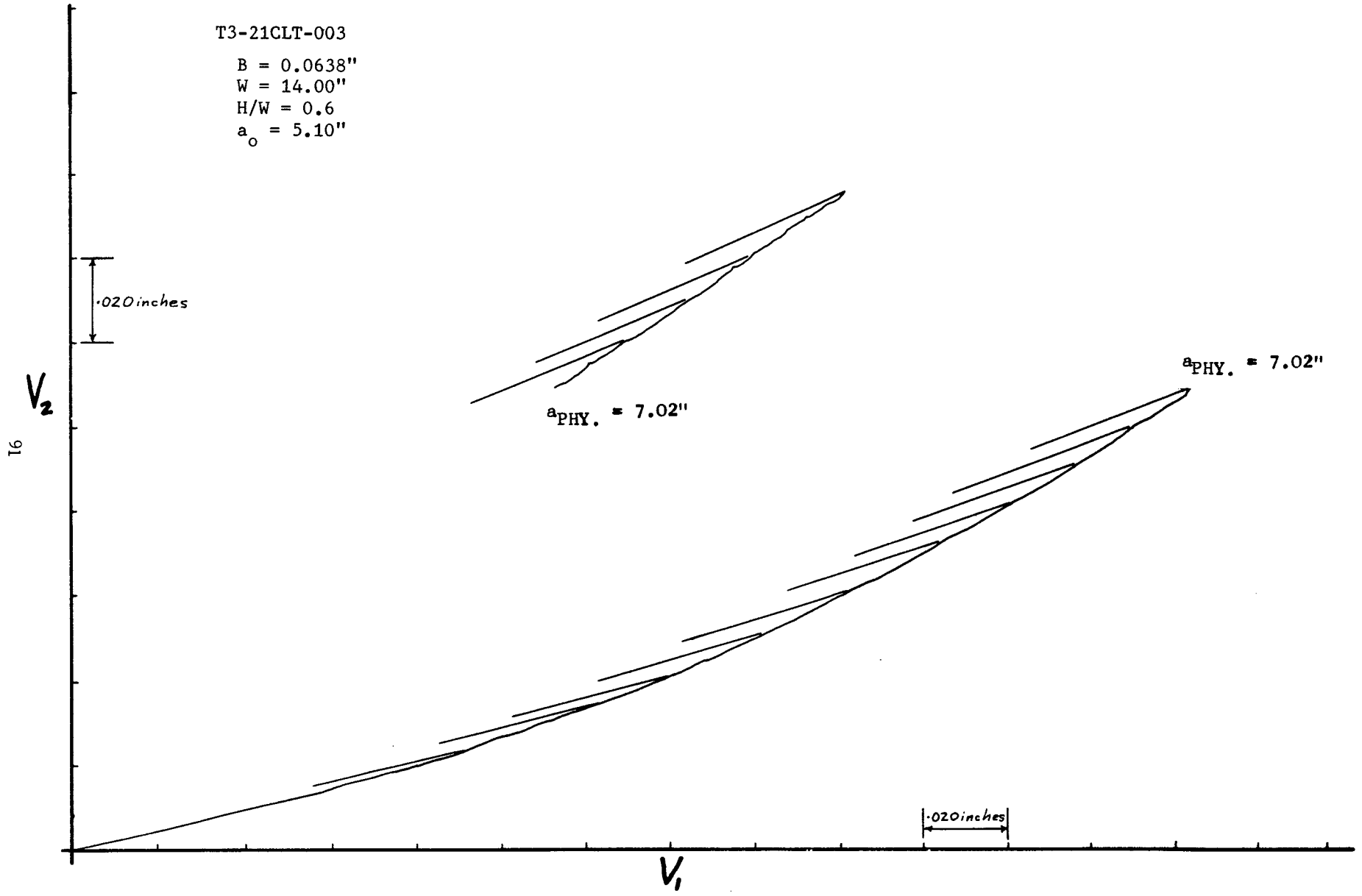

Figure 53. Deflection Curve - 0.0638 Inch, 2024-T3 (LT)

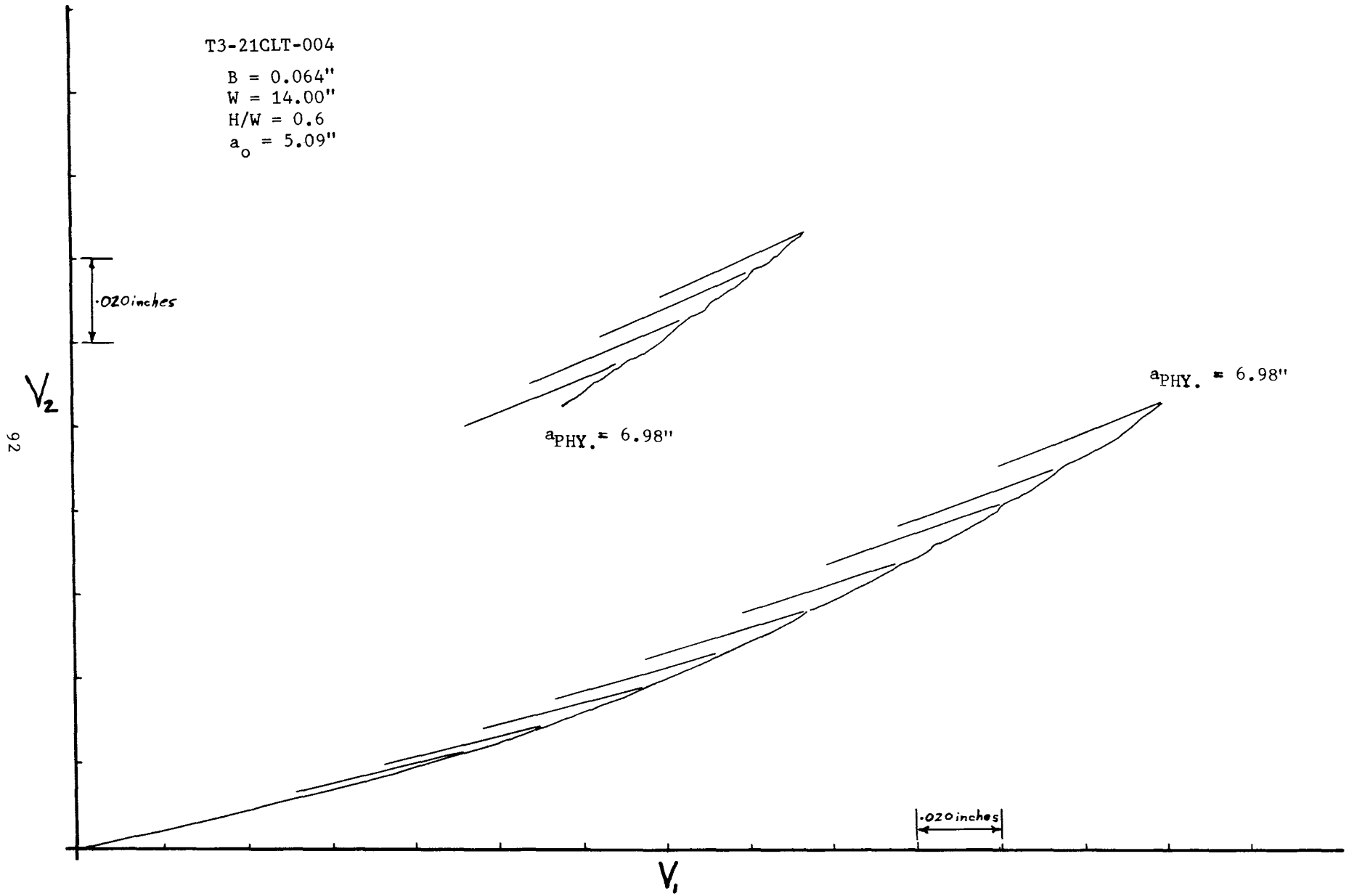

Figure 54. Deflection Curve - 0.064 Inch, 2024-T3 (LT)

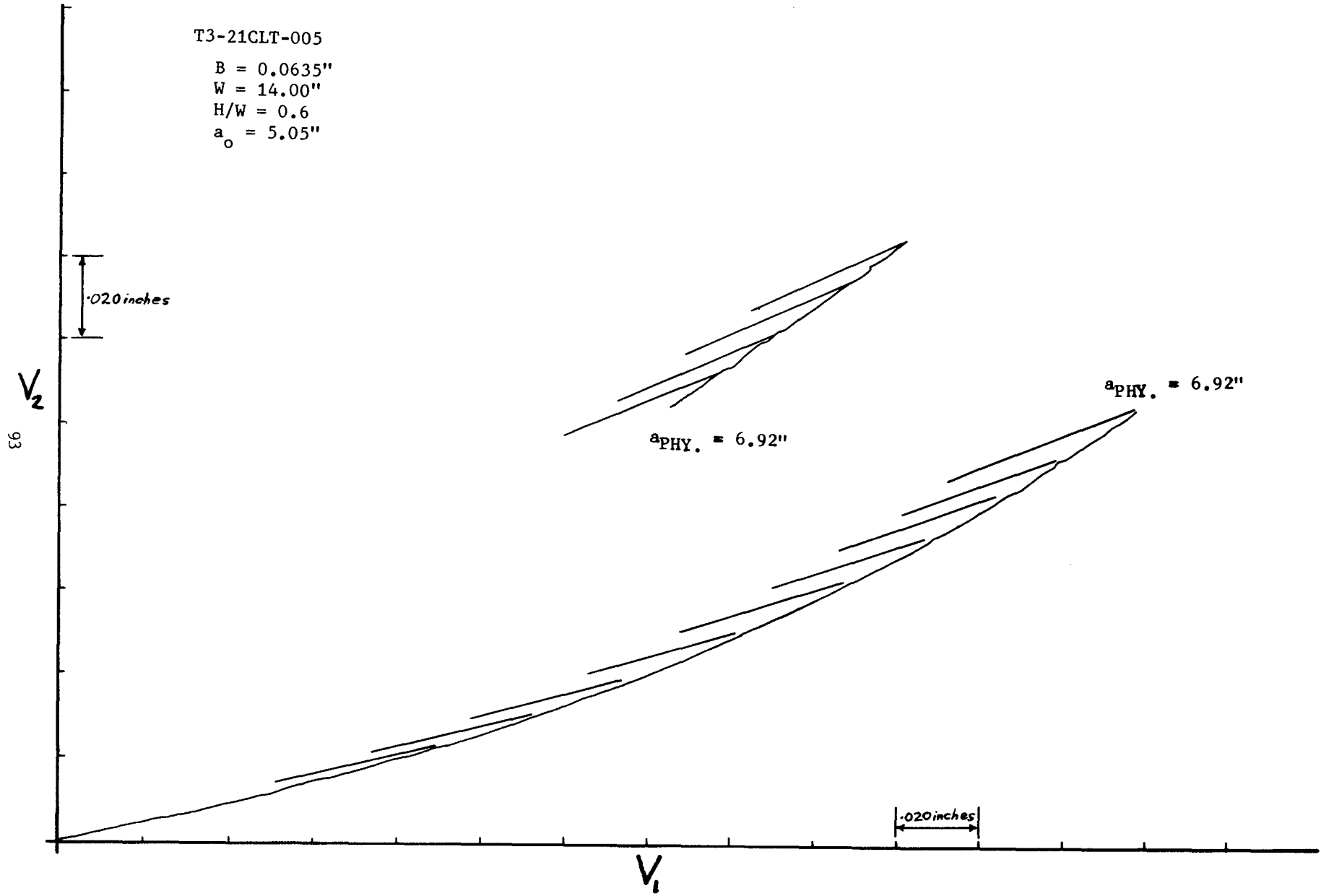

Figure 55. Deflection Curve - 0.0635 Inch, 2024-T3 (LT)

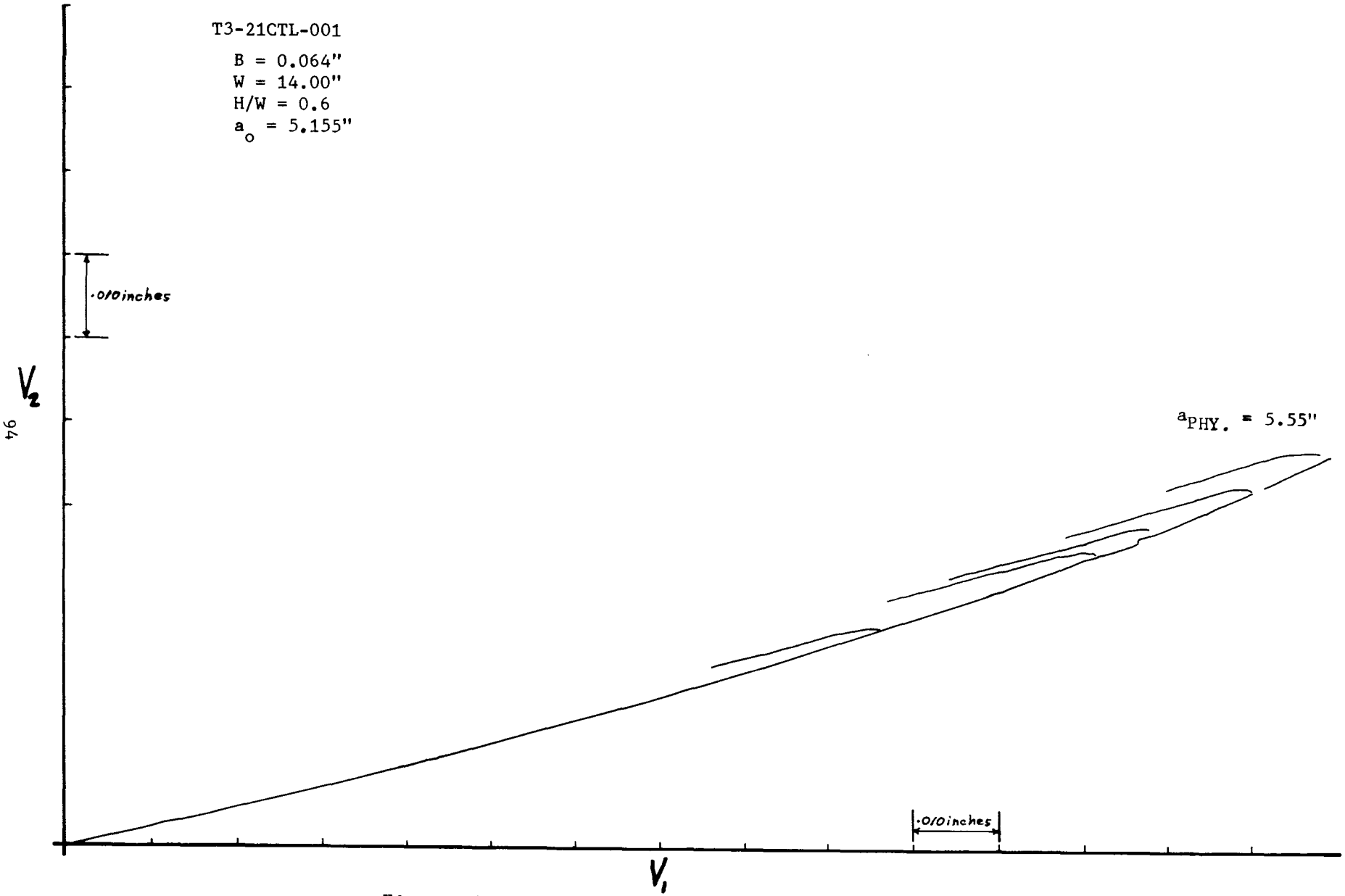

Figure 56. Deflection Curve - 0.064 Inch, 2024-T3 (TL)

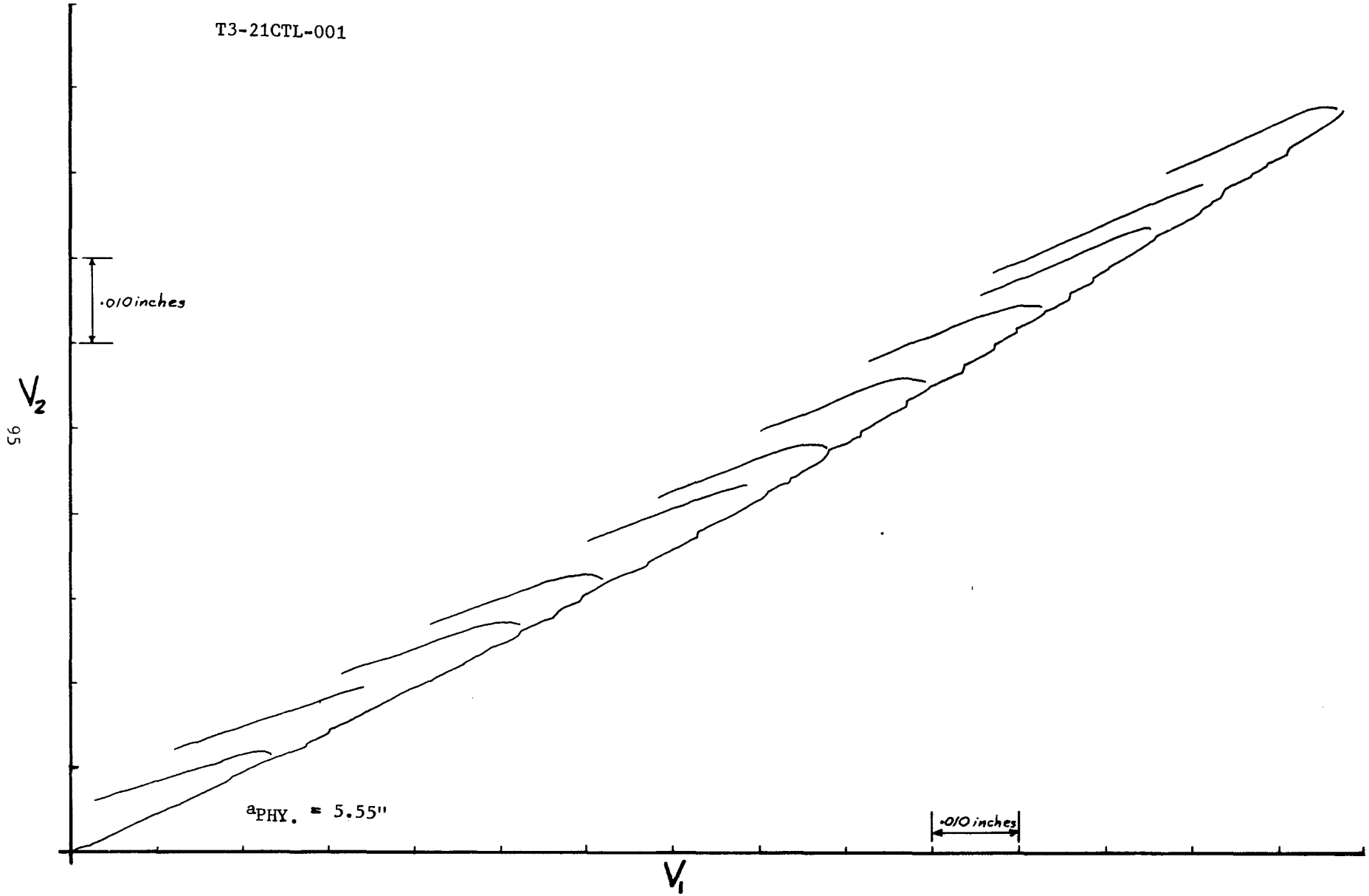

Figure 56. Deflection Curve - 0.064 Inch, 2024-T3 (TL) (Continued)

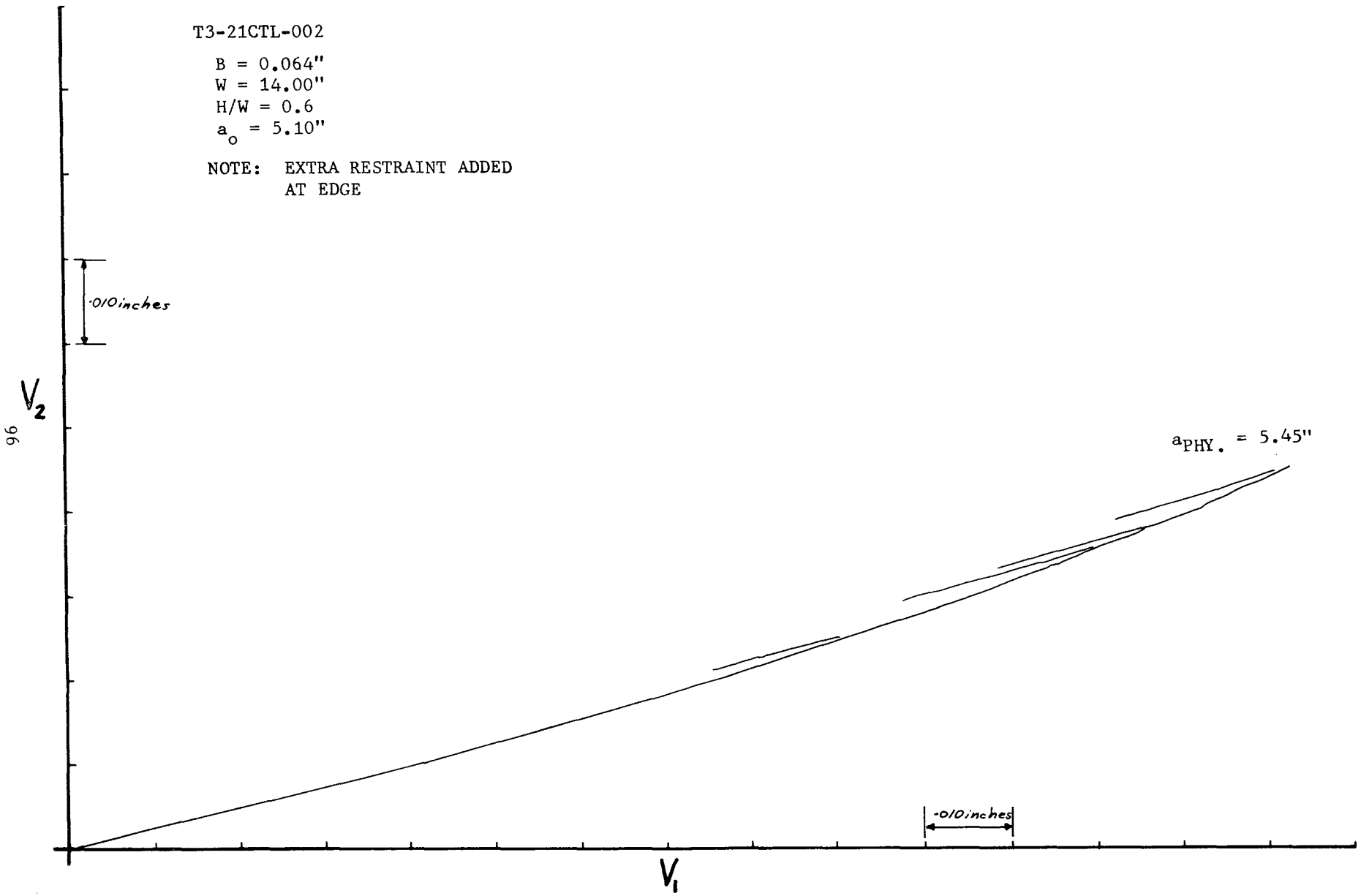

Figure 57. Deflection Curve - 0.064 Inch, 2024-T3 (TL)

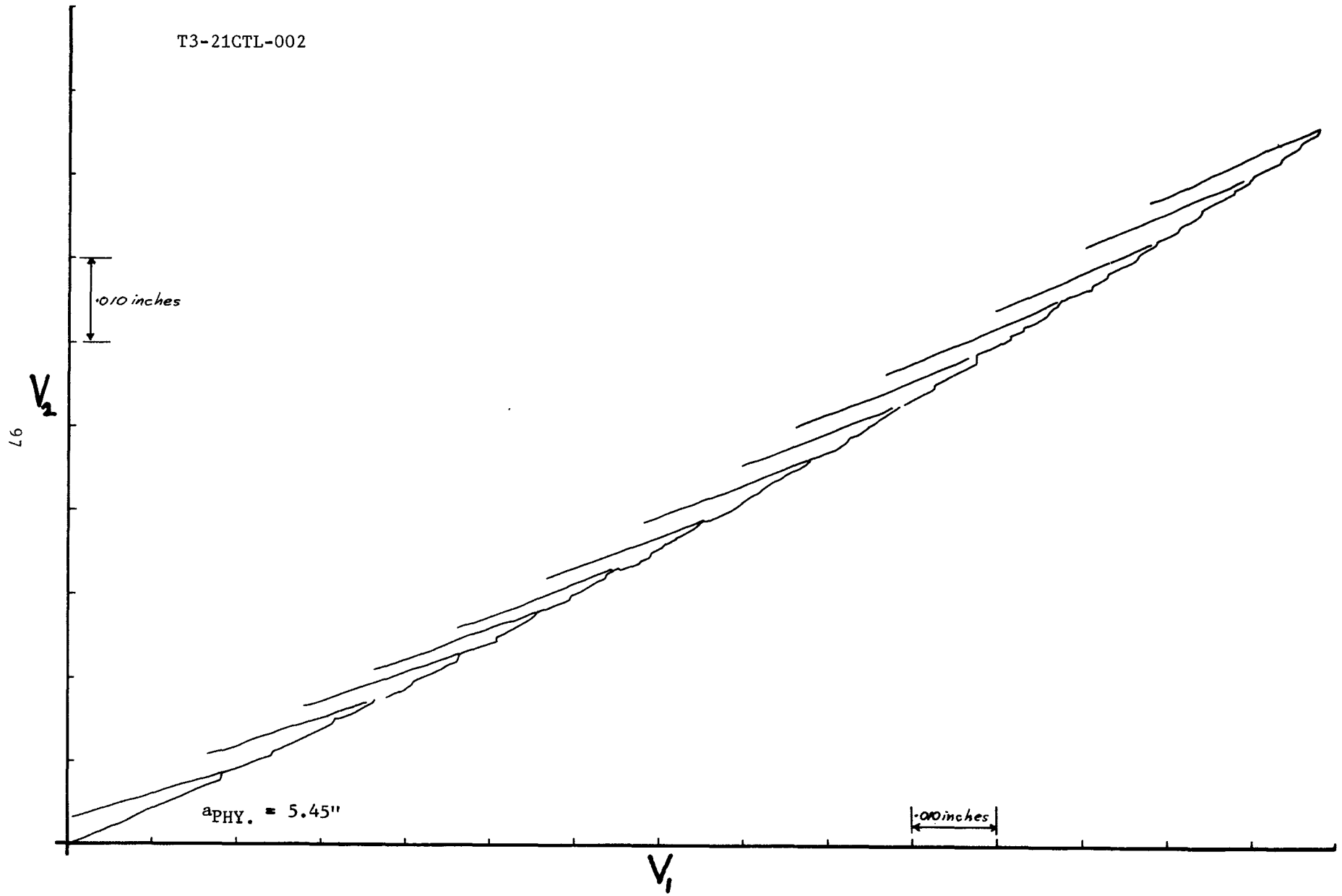

Figure 57. Deflection Curve - 0.064 Inch, 2024-T3 (TL) (Continued)

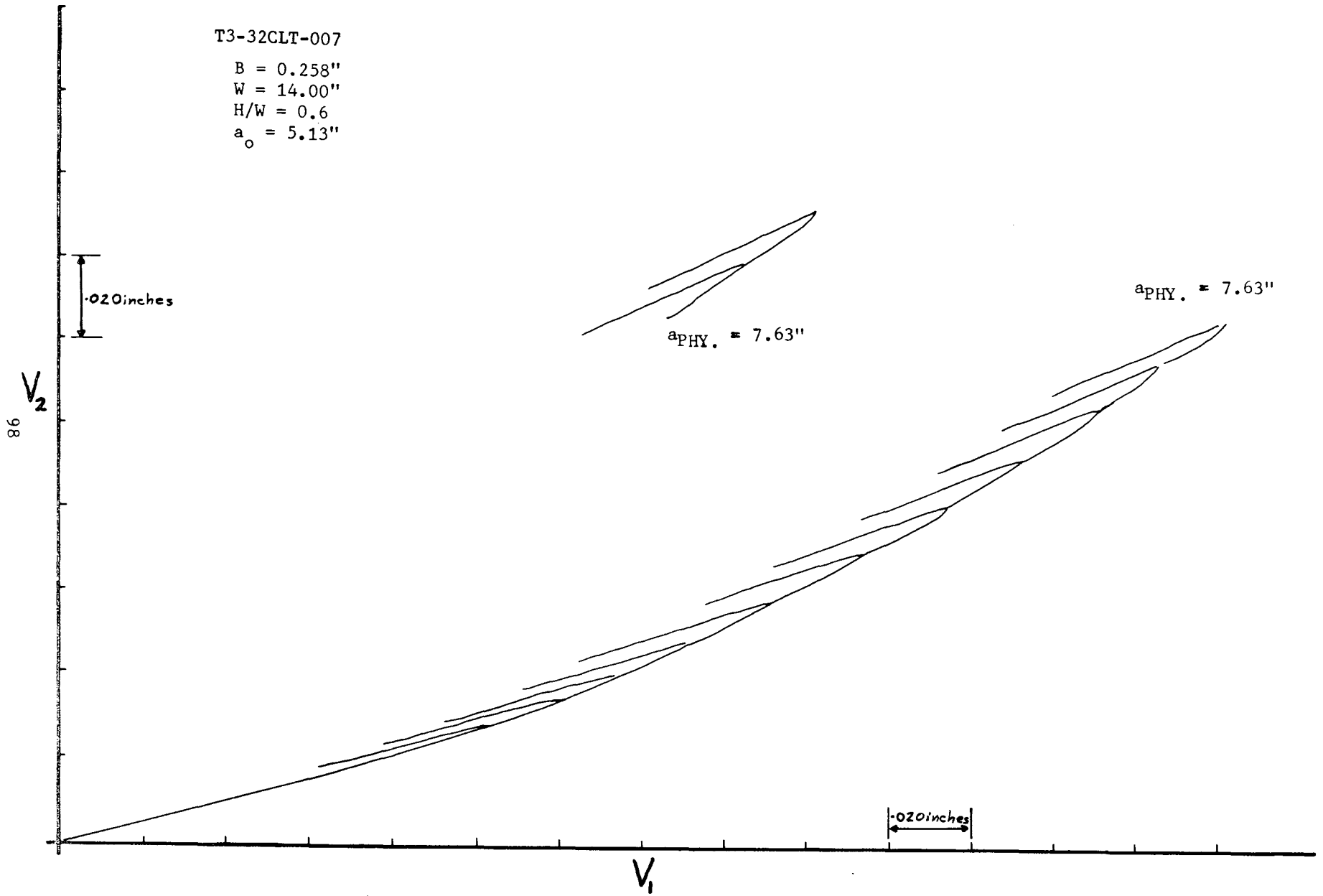

Figure 58. Deflection Curve - 0.258 Inch, 2024-T351 (LT)

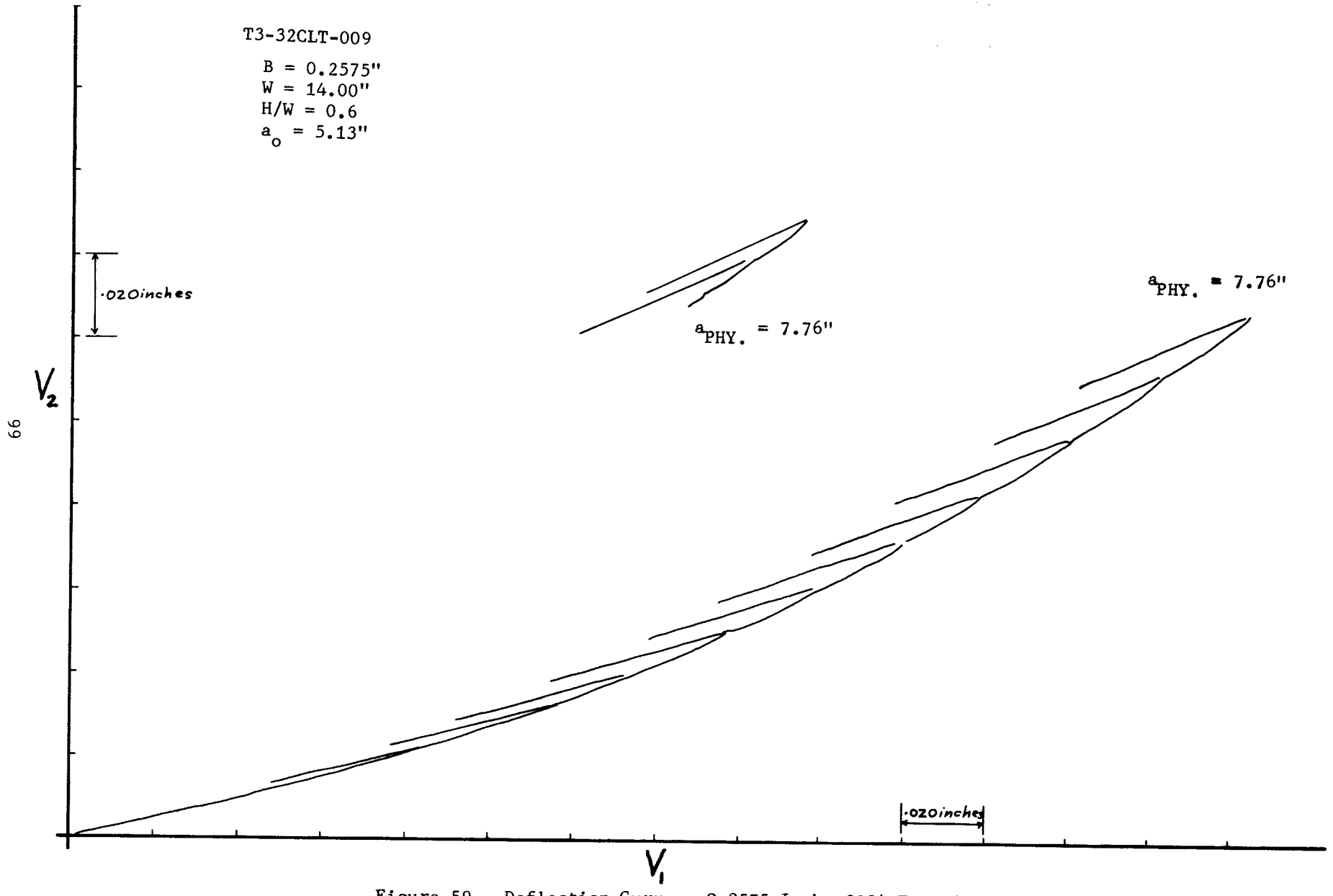

Figure 59. Deflection Curve - 0.2575 Inch, 2024-T351 (LT)

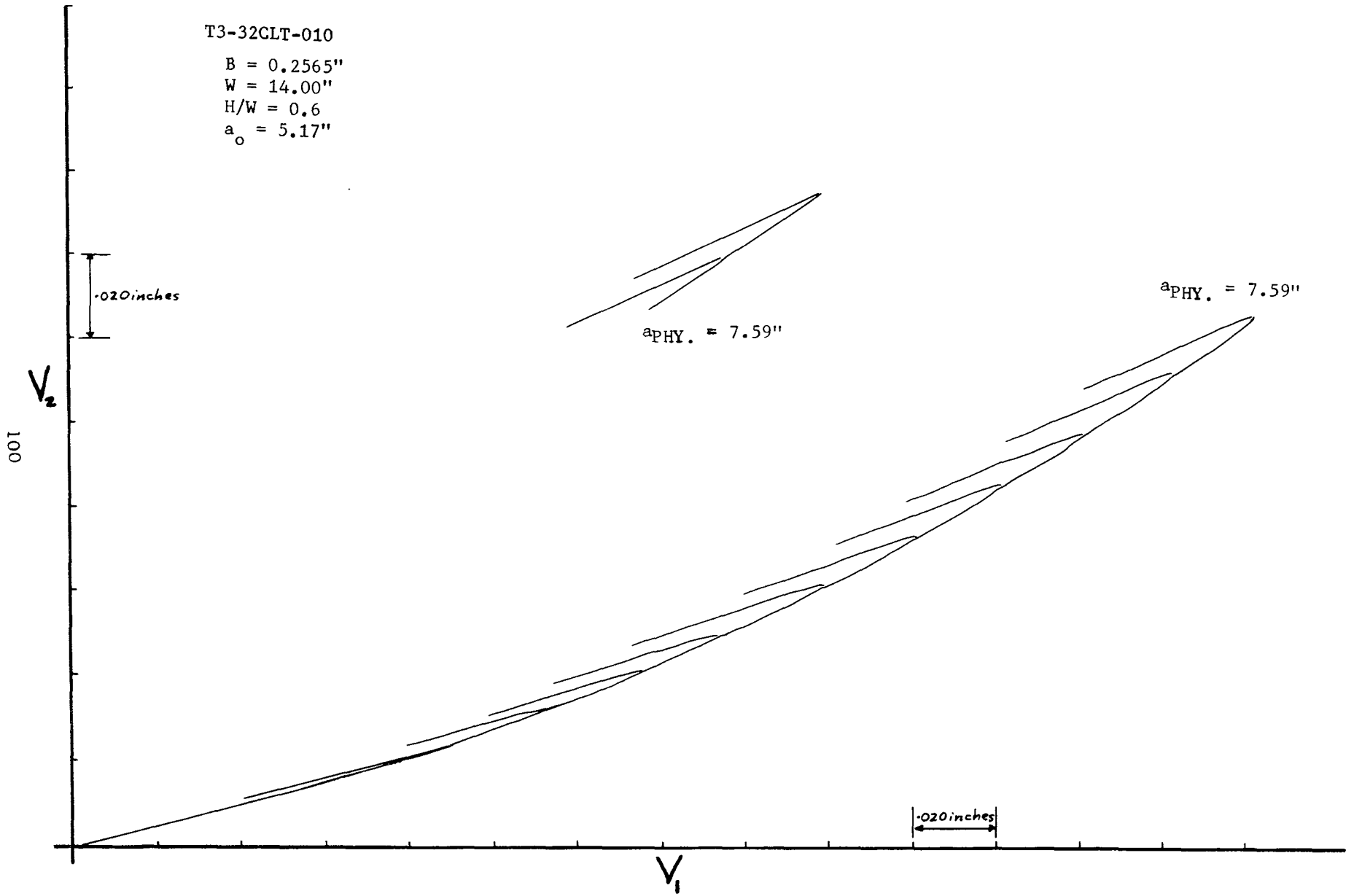

Figure 60. Deflection Curve - 0.2565 Inch, 2024-T351 (LT)

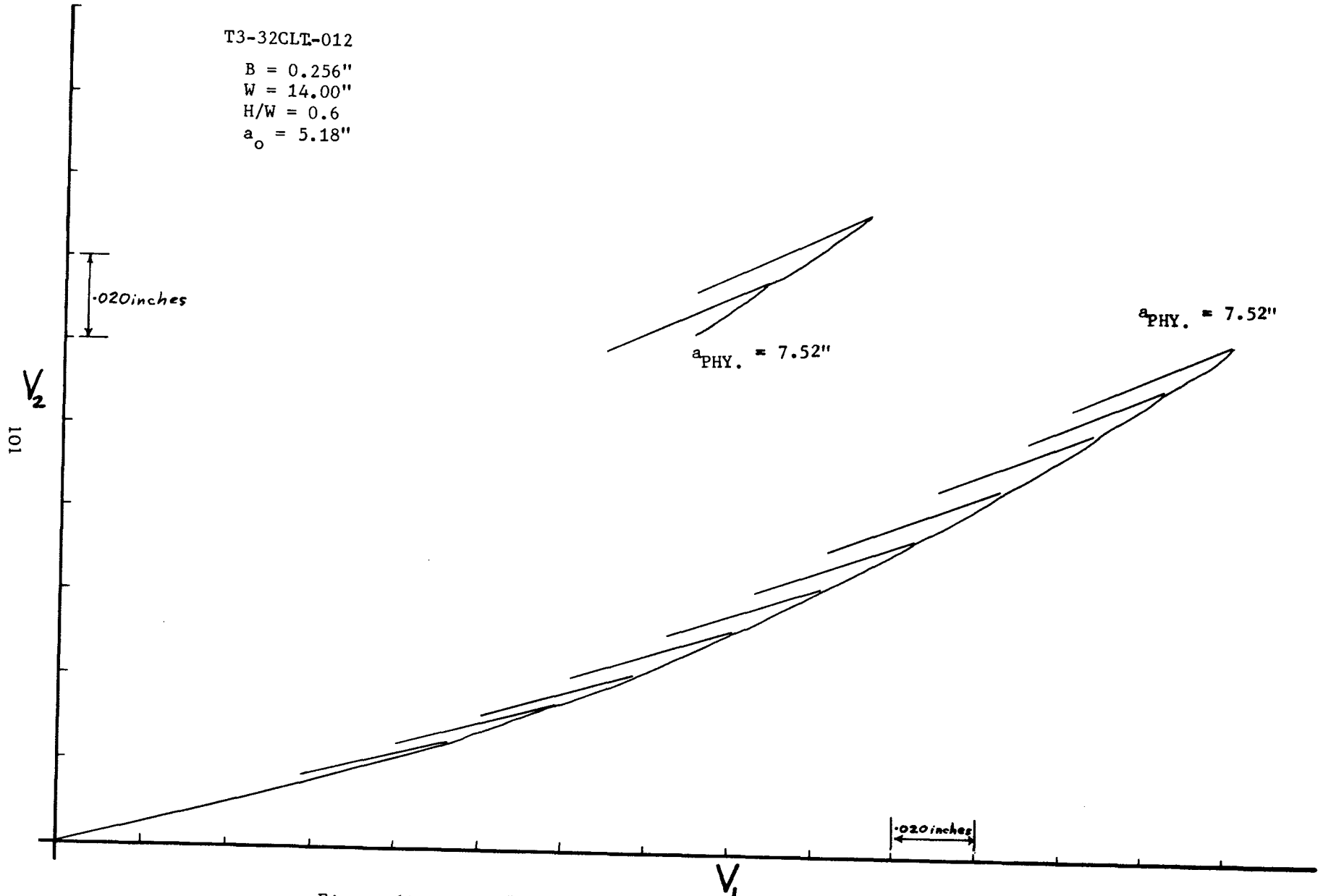

Figure 61. Deflection Curve - 0.256 Inch, 2024-T351 (LT)

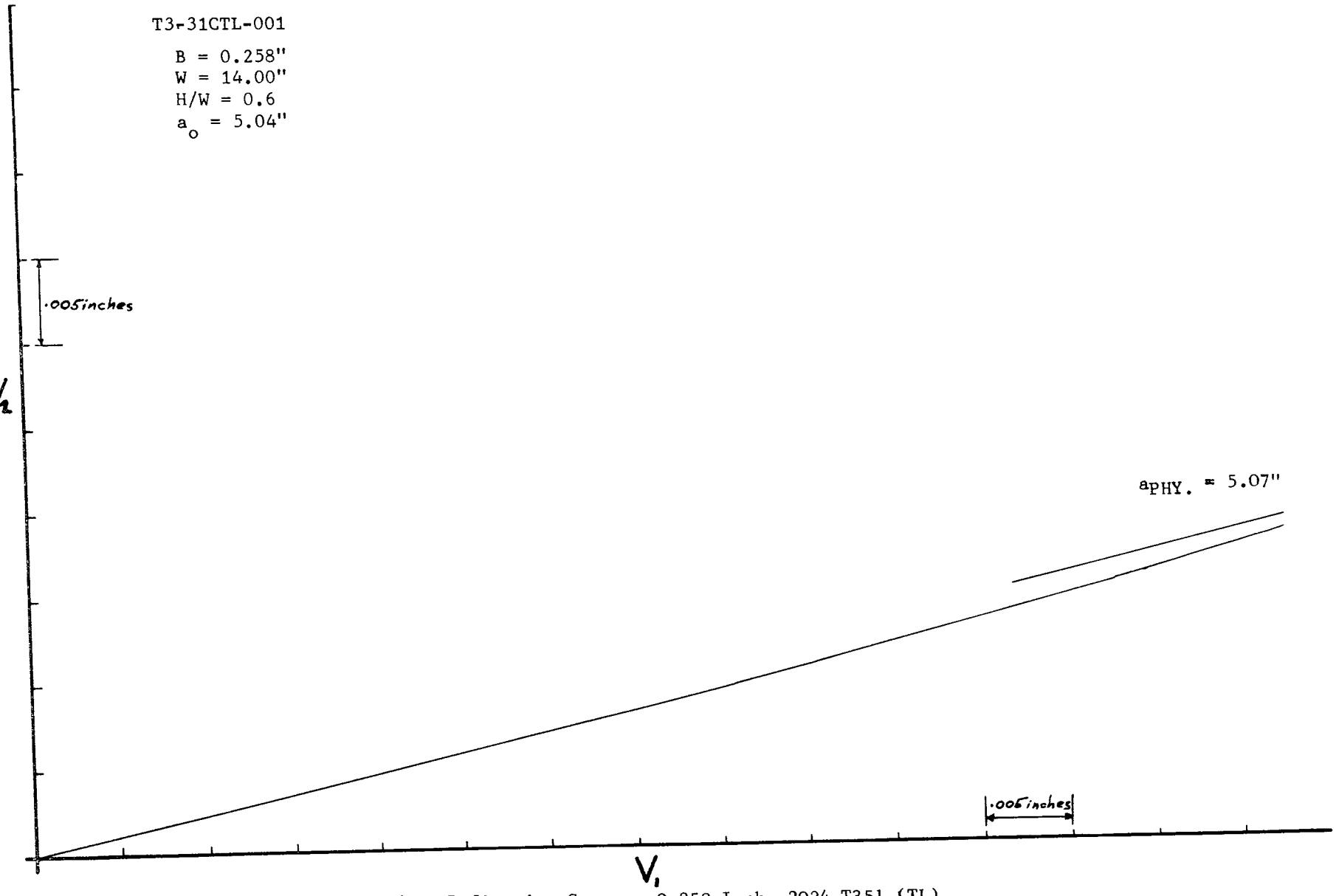

Figure 62. Deflection Curve - 0.258 Inch, 2024-T351 (TL)

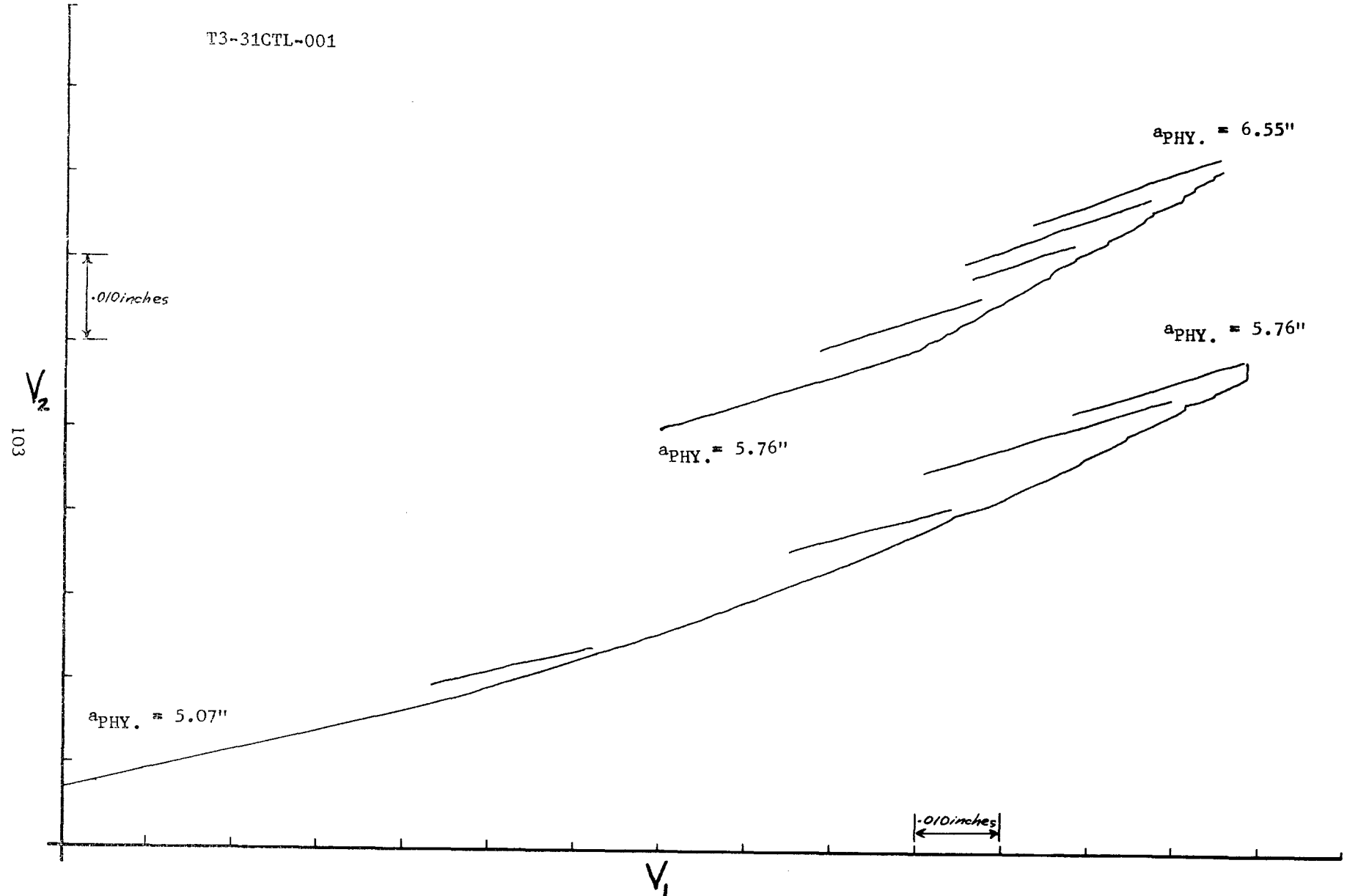

Figure 62. Deflection Curve - 0.258 Inch, 2024-T351 (TL) (Continued)

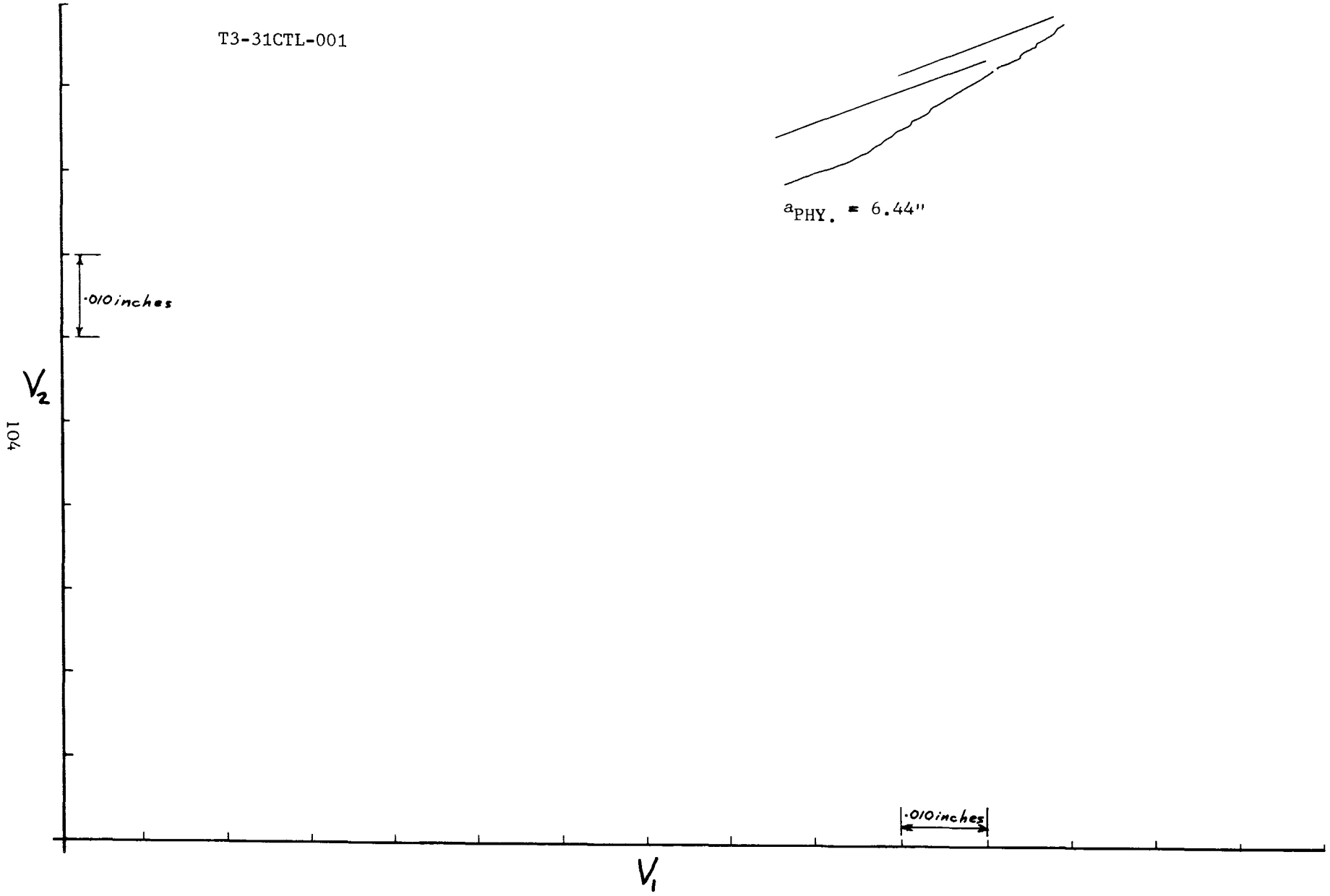

Figure 62. Deflection Curve - 0.258 Inch, 2024-T351 (TL) (Continued)

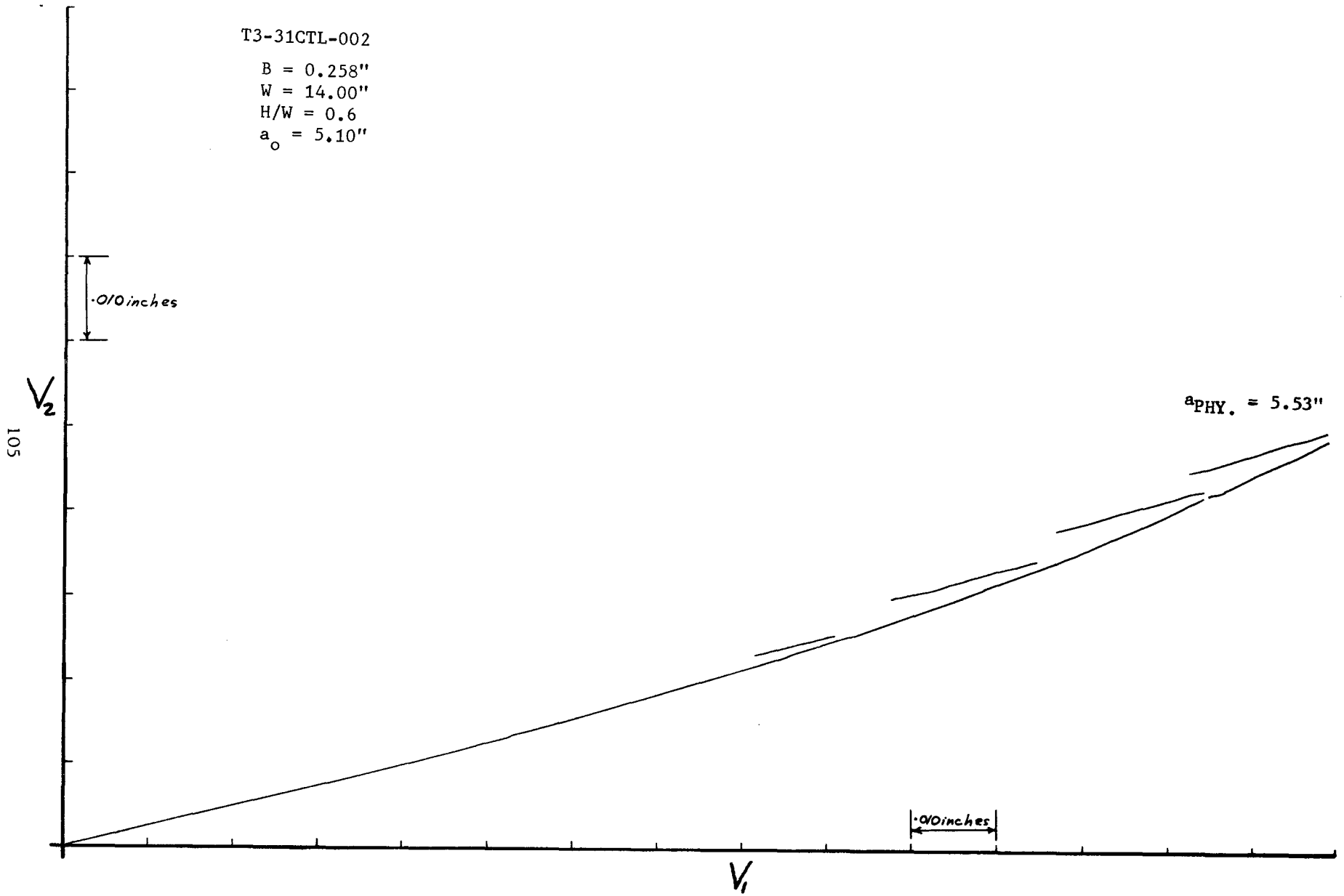

Figure 63. Deflection Curve - 0.258 Inch, 2024-T351 (TL)

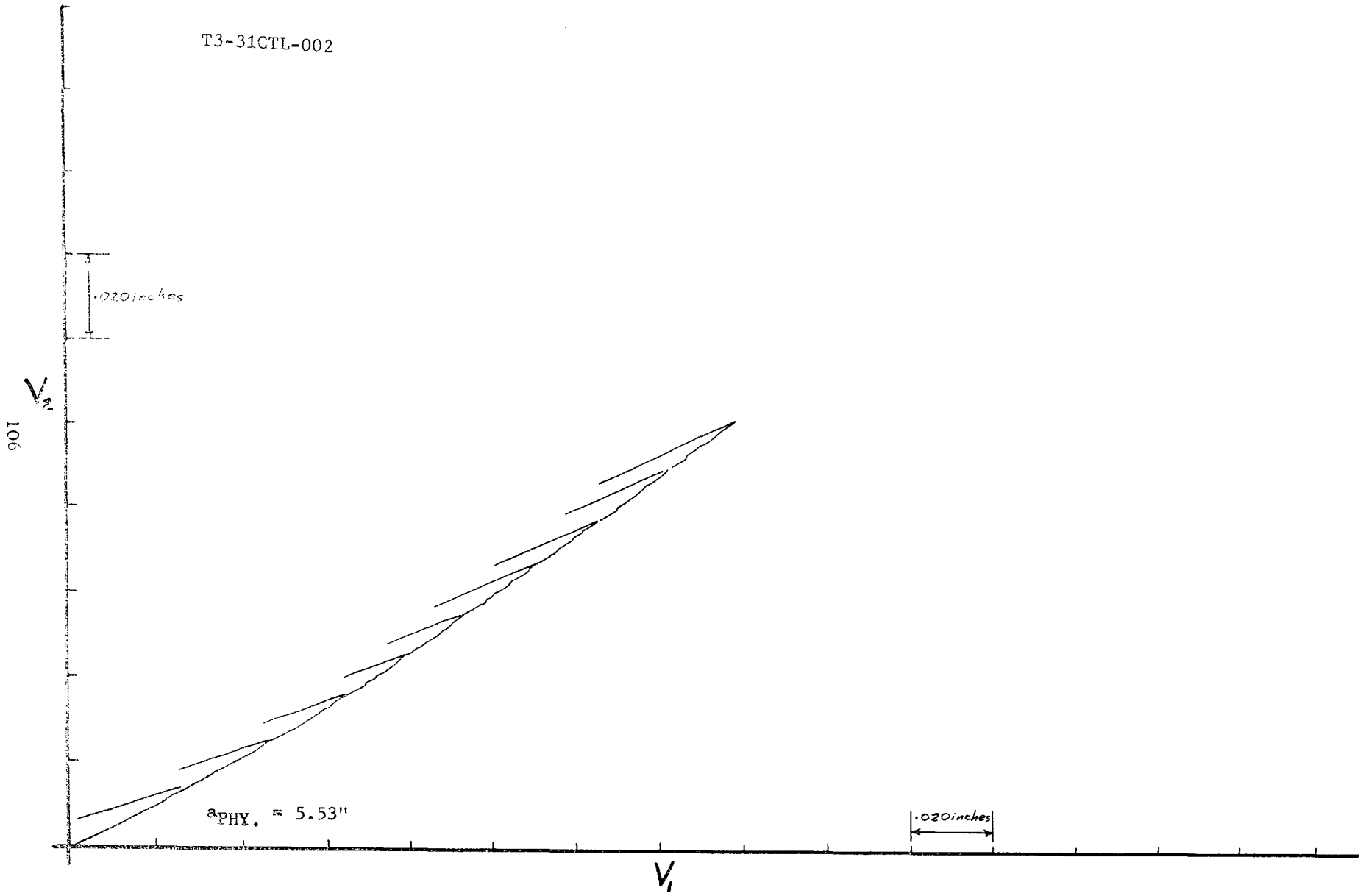

Figure 63. Deflection Curve - 0.258 Inch, 2024-T351 (TL) (Continued)

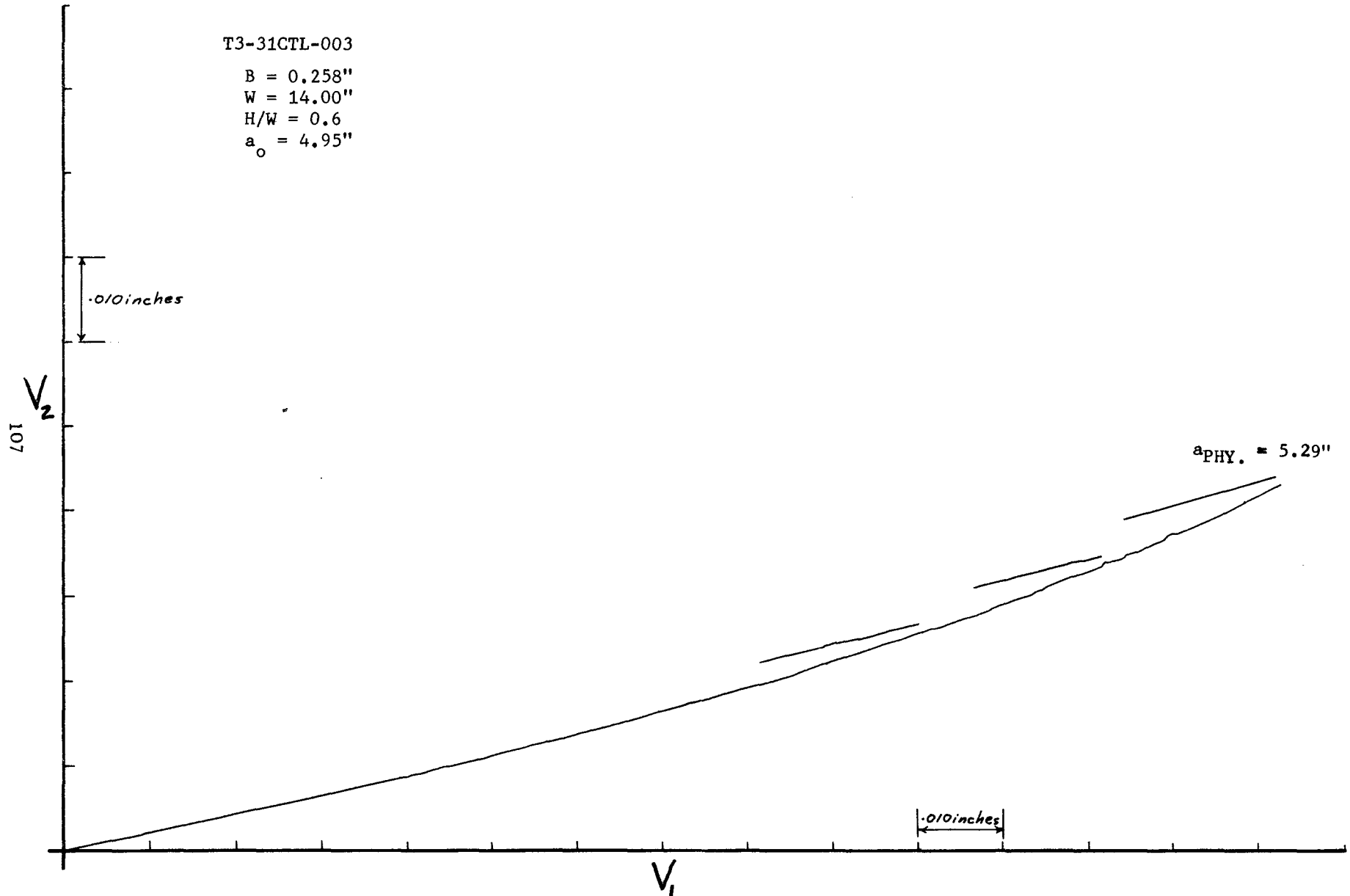

Figure 64. Deflection Curve - 0.258 Inch, 2024-T351 (TL)

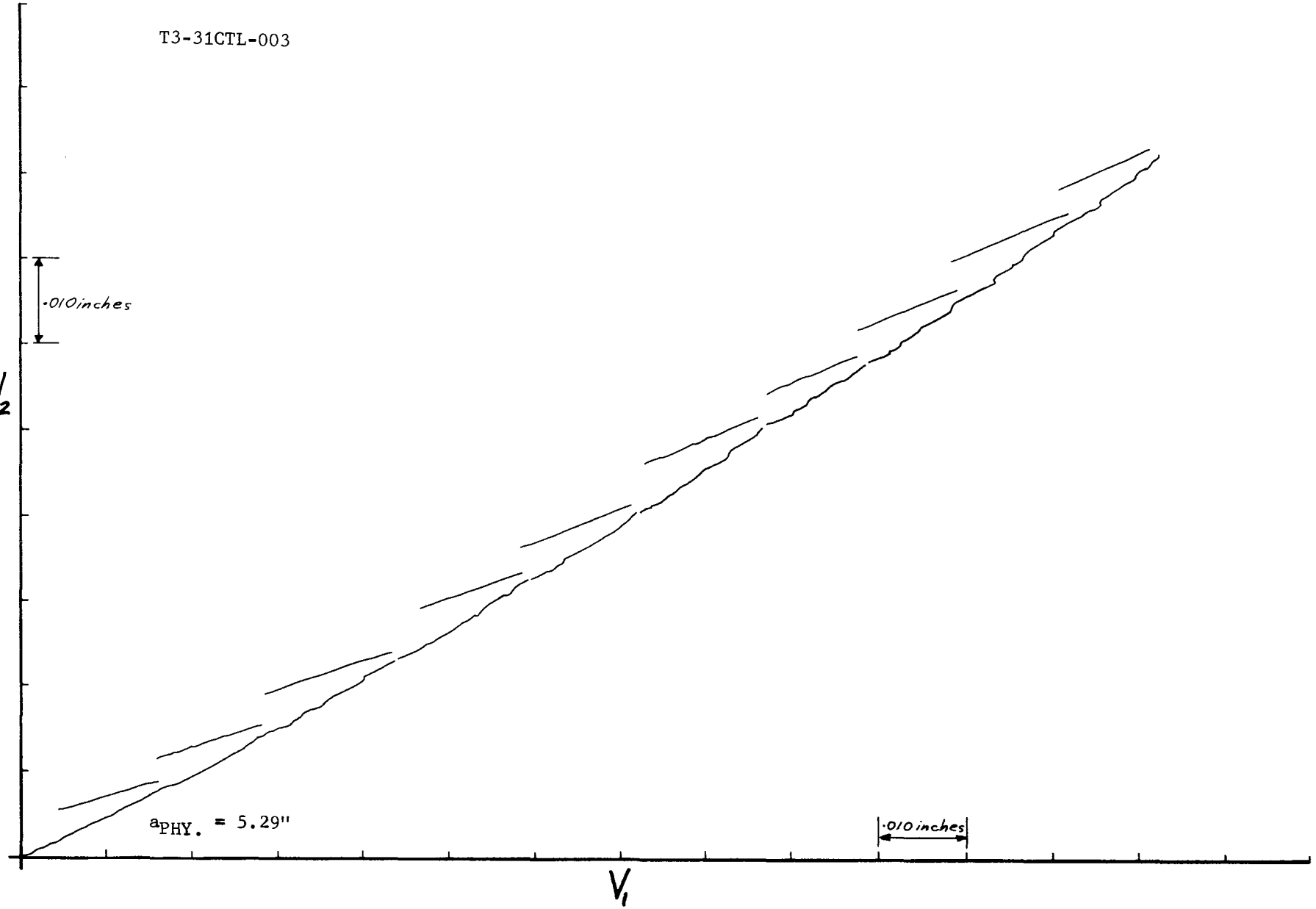

Figure 64. Deflection Curve - 0.258 Inch, 2024-T351 (TL) (Continued)

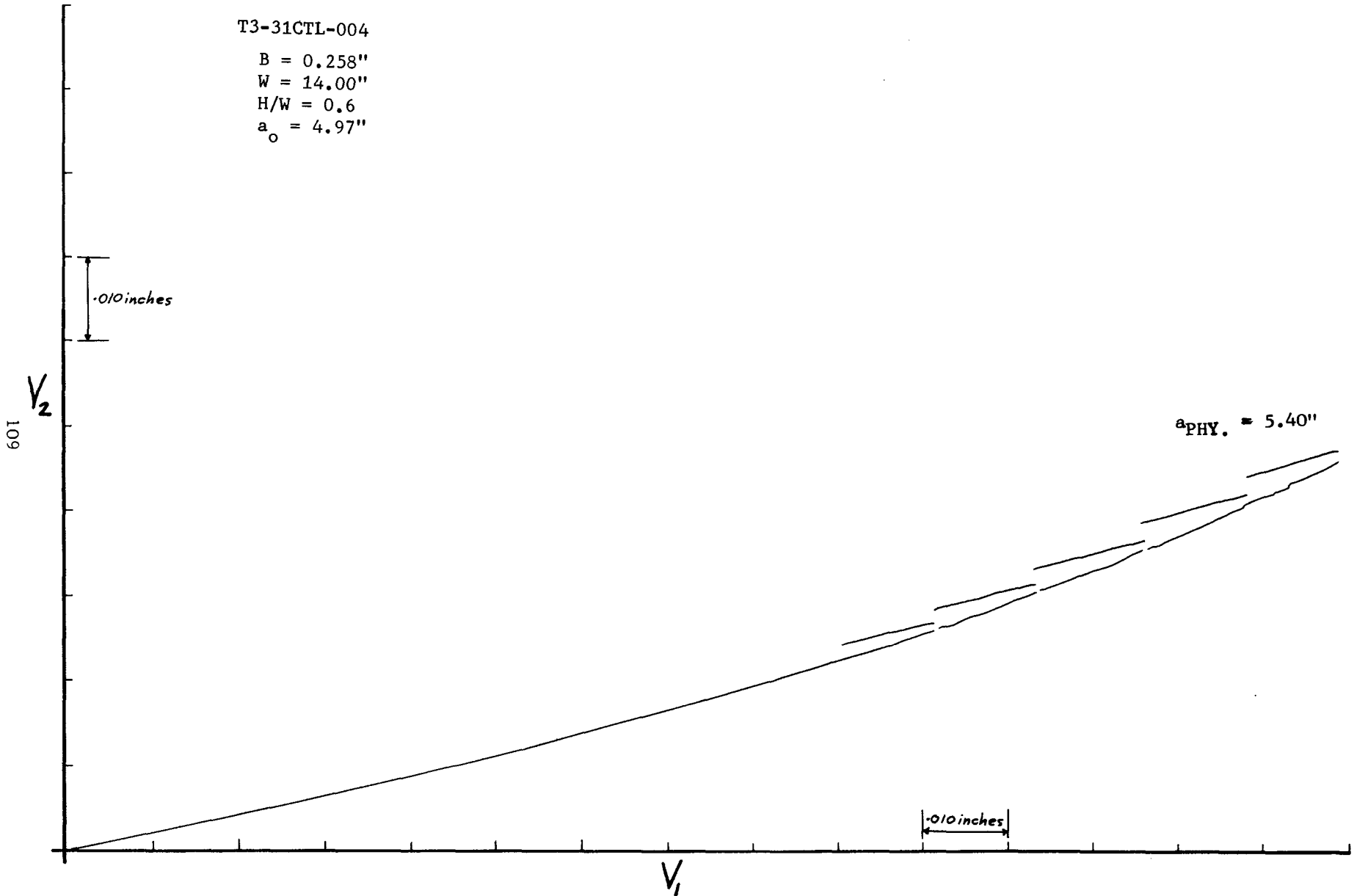

Figure 65. Deflection Curve - 0.258 Inch, 2024-T351 (TL)

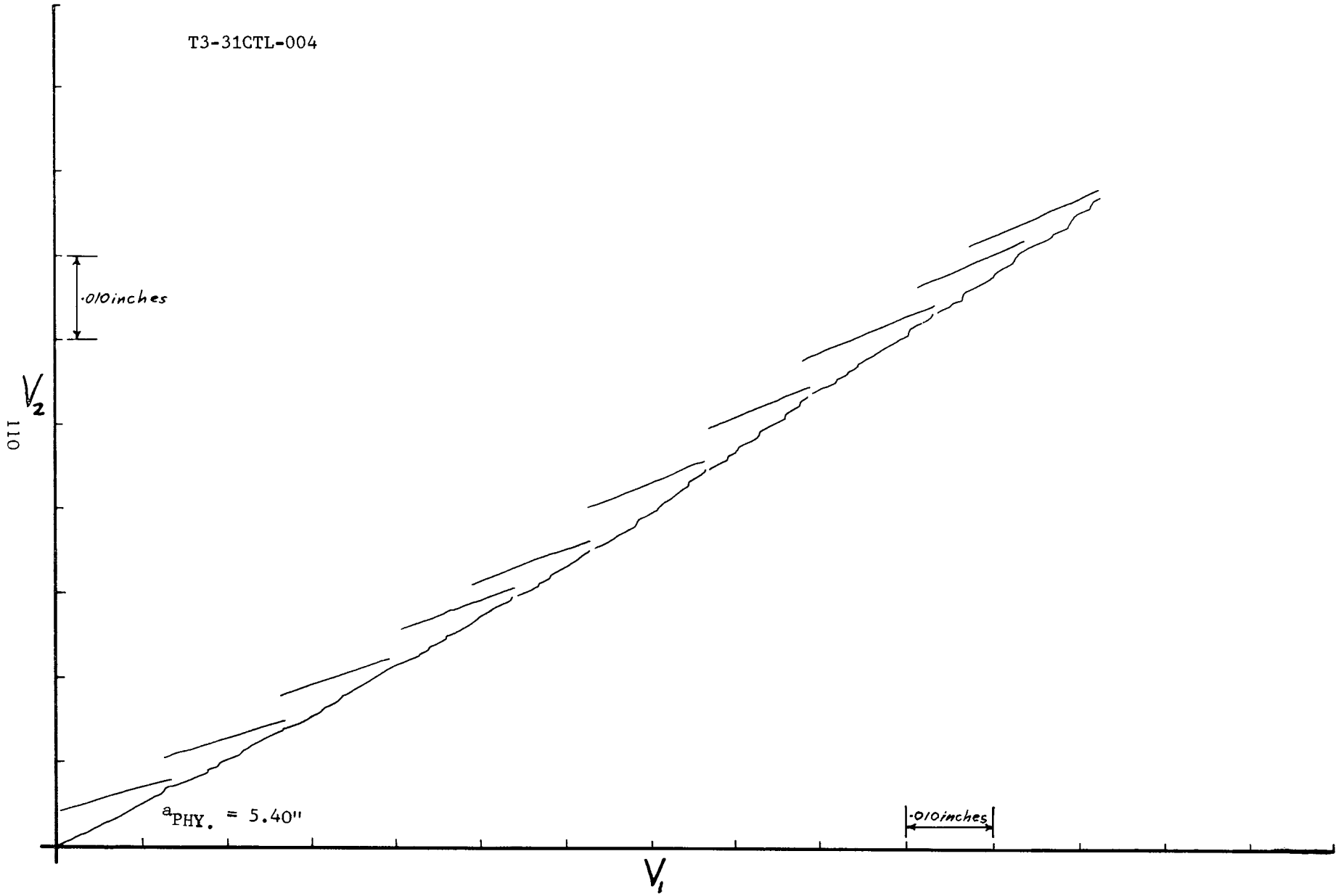

Figure 65. Deflection Curve - 0.258 Inch, 2024-T351 (TL) (Continued)

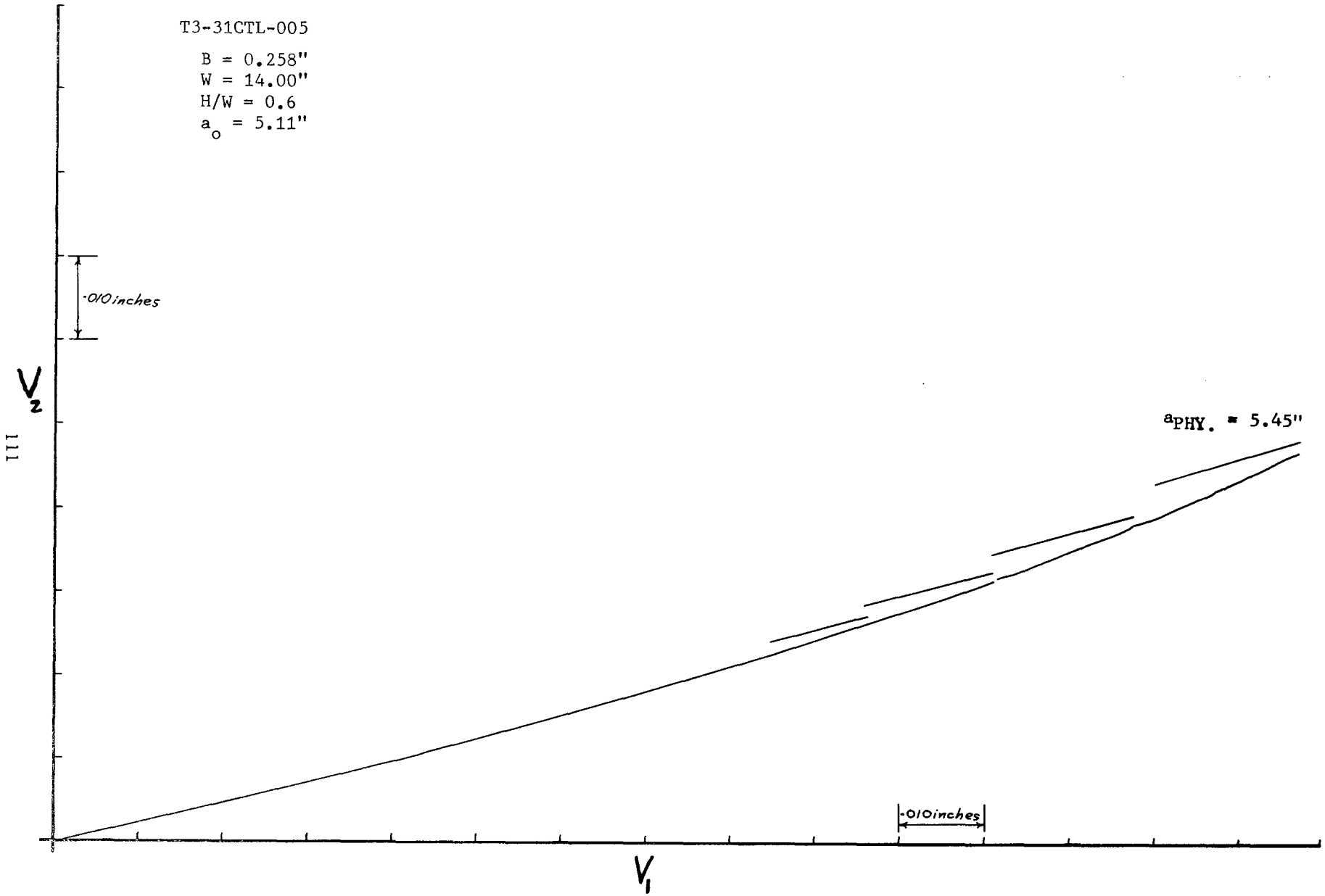

Figure 66. Deflection Curve - 0.258 Inch, 2024-T351 (TL)

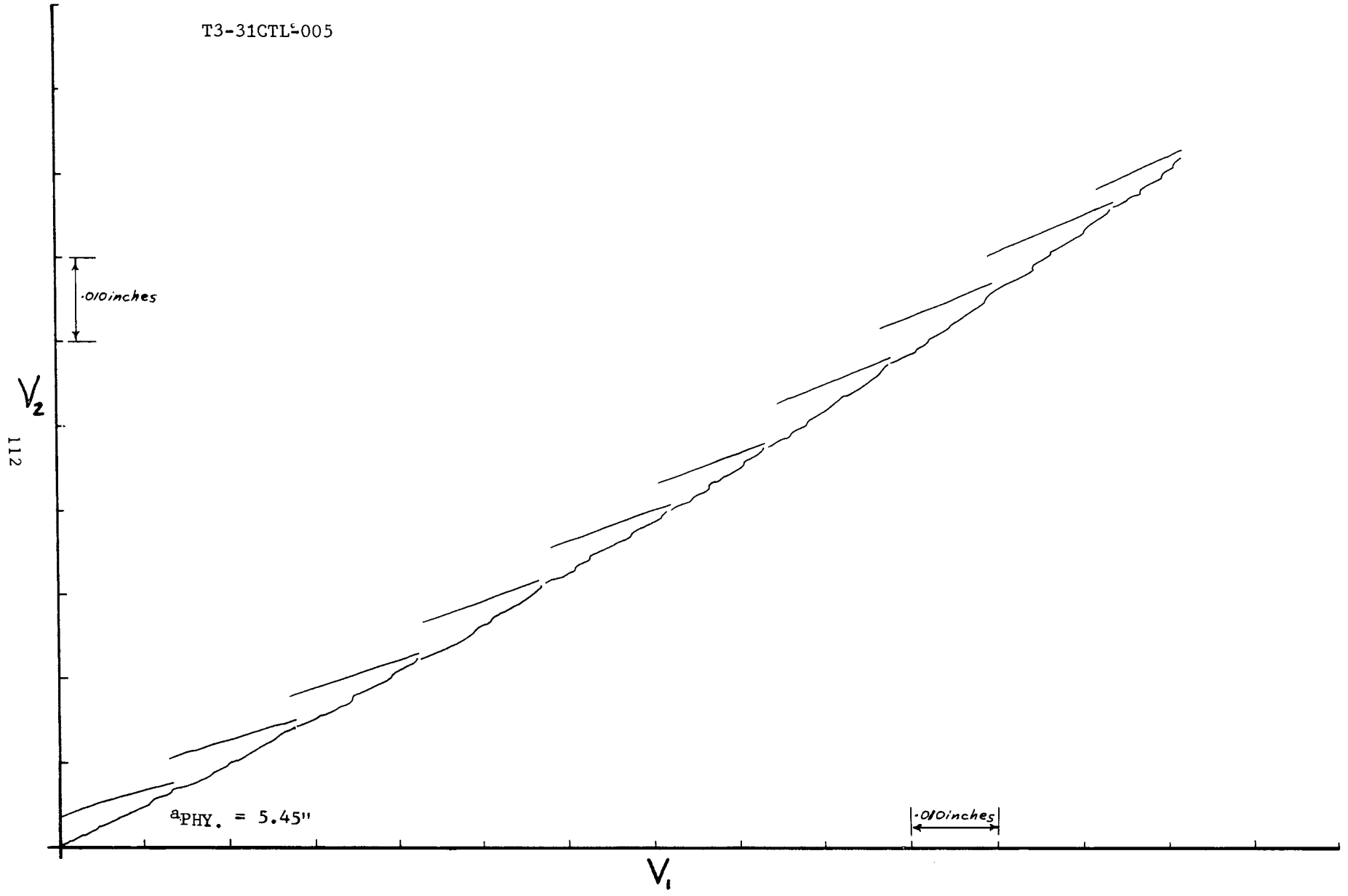

Figure 66. Deflection Curve - 0.258 Inch, 2024-T351 (TL) (Continued)

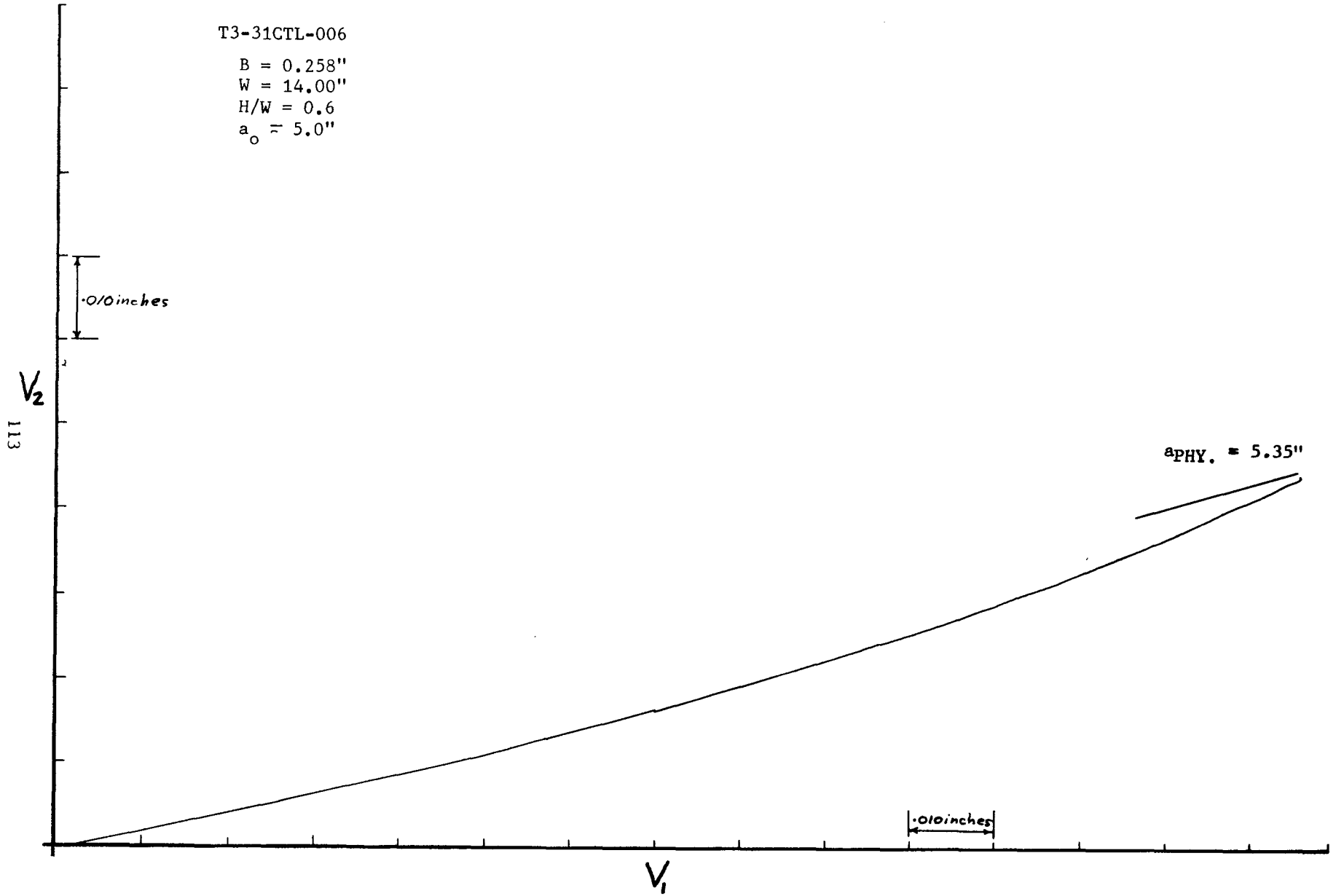

Figure 67. Deflection Curve - 0.258 Inch, 2024-T351 (TL)

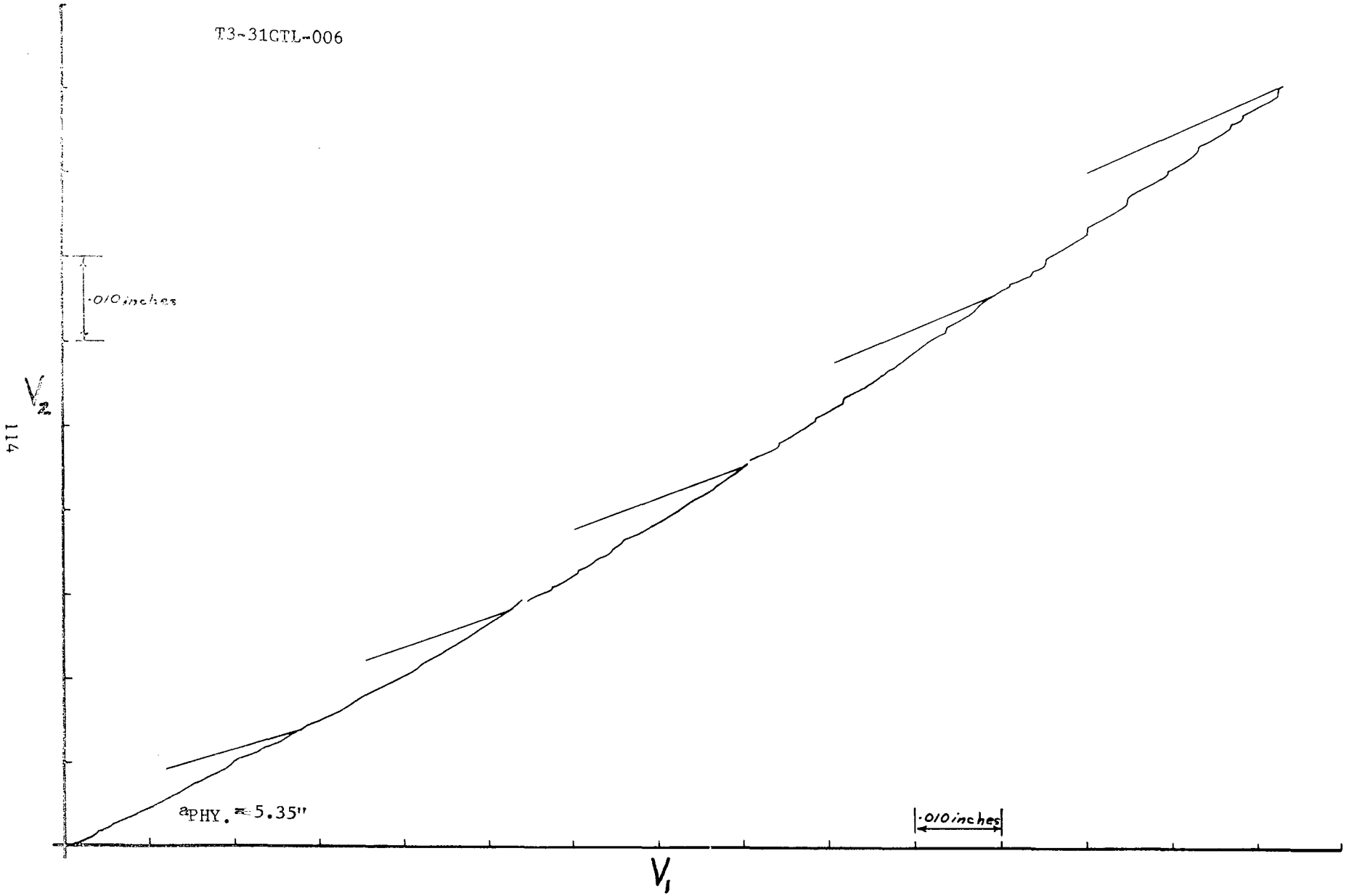

Figure 67. Deflection Curve - 0.258 Inch, 2024-T351 (TL_t) (Continued)

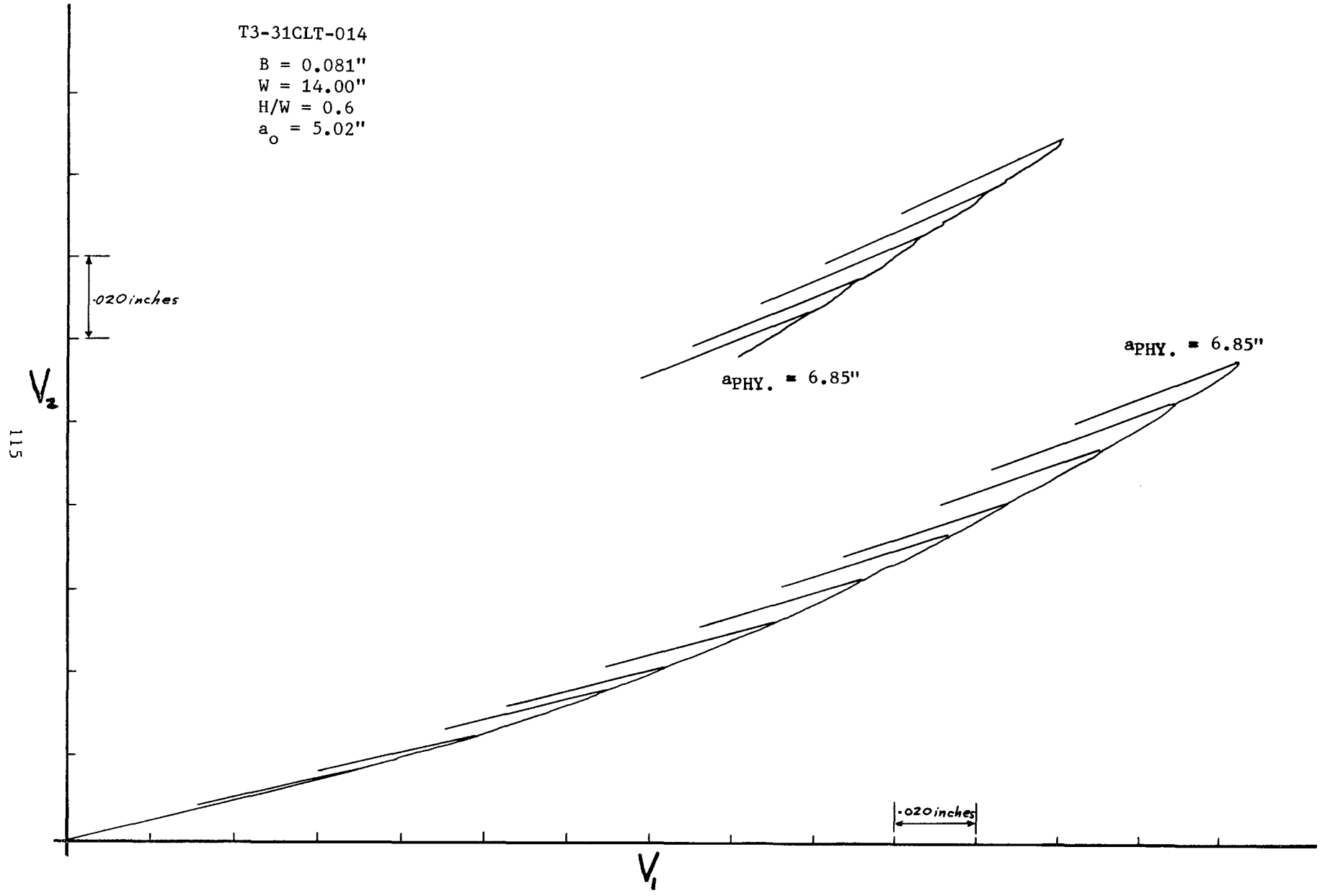

Figure 68. Deflection Curve - 0.081 Inch, Chem Milled 2024-T351 (LT)

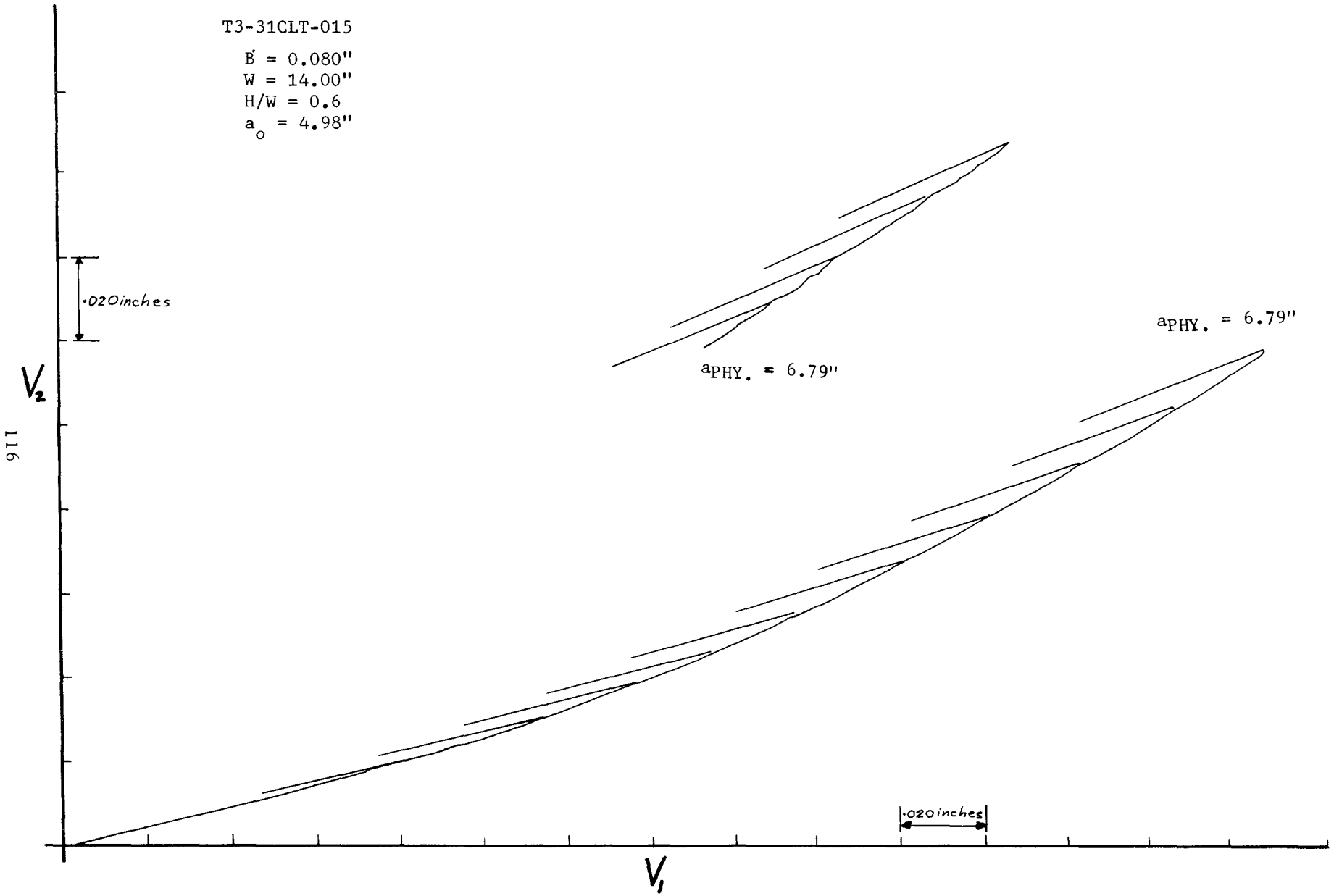

Figure 69. Deflection Curve - 0.080 Inch, Chem Milled 2024-T351 (LT)

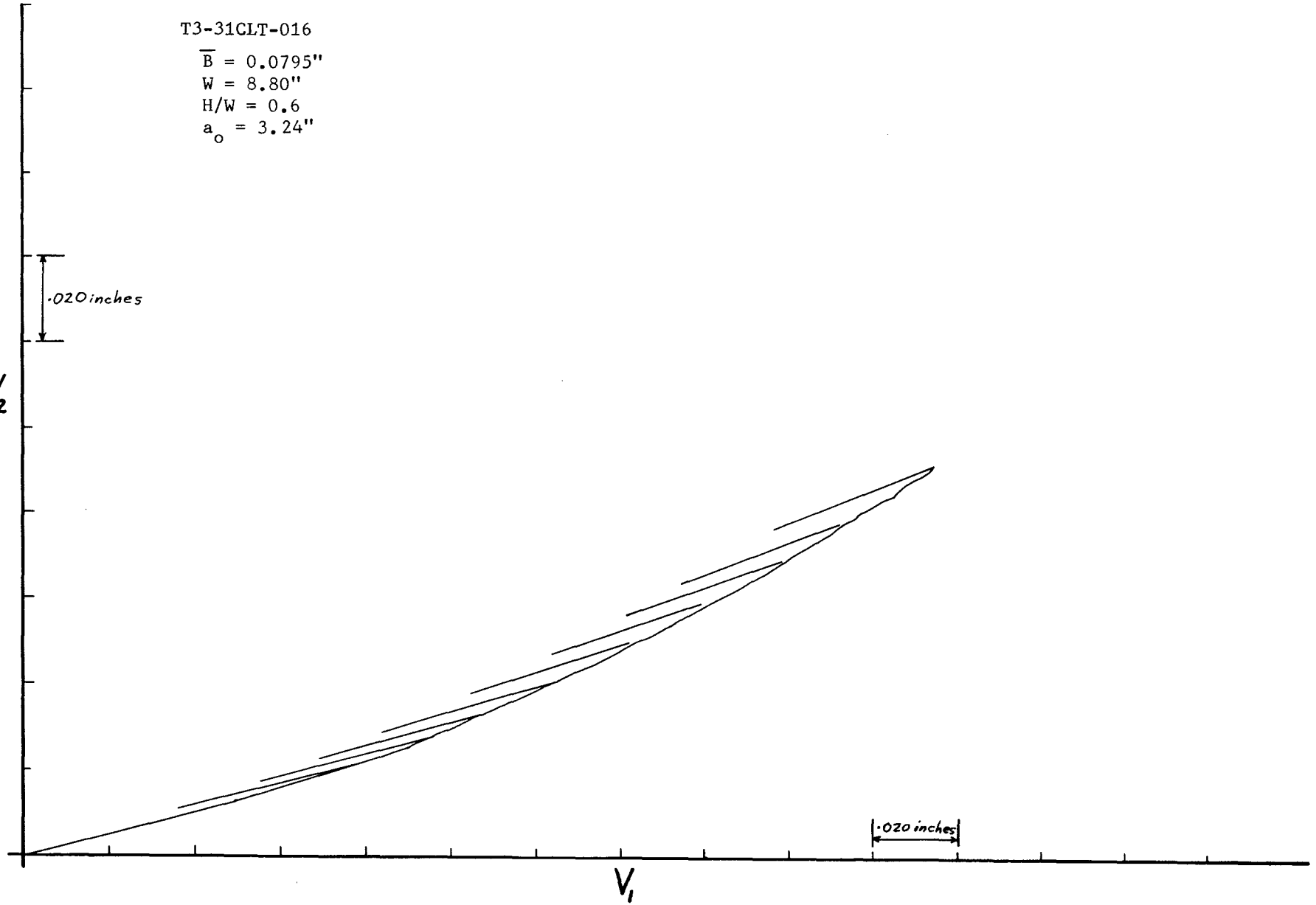

Figure 70. Deflection Curve - 0.0795 Inch, Chem Milled 2024-T351 (LT)

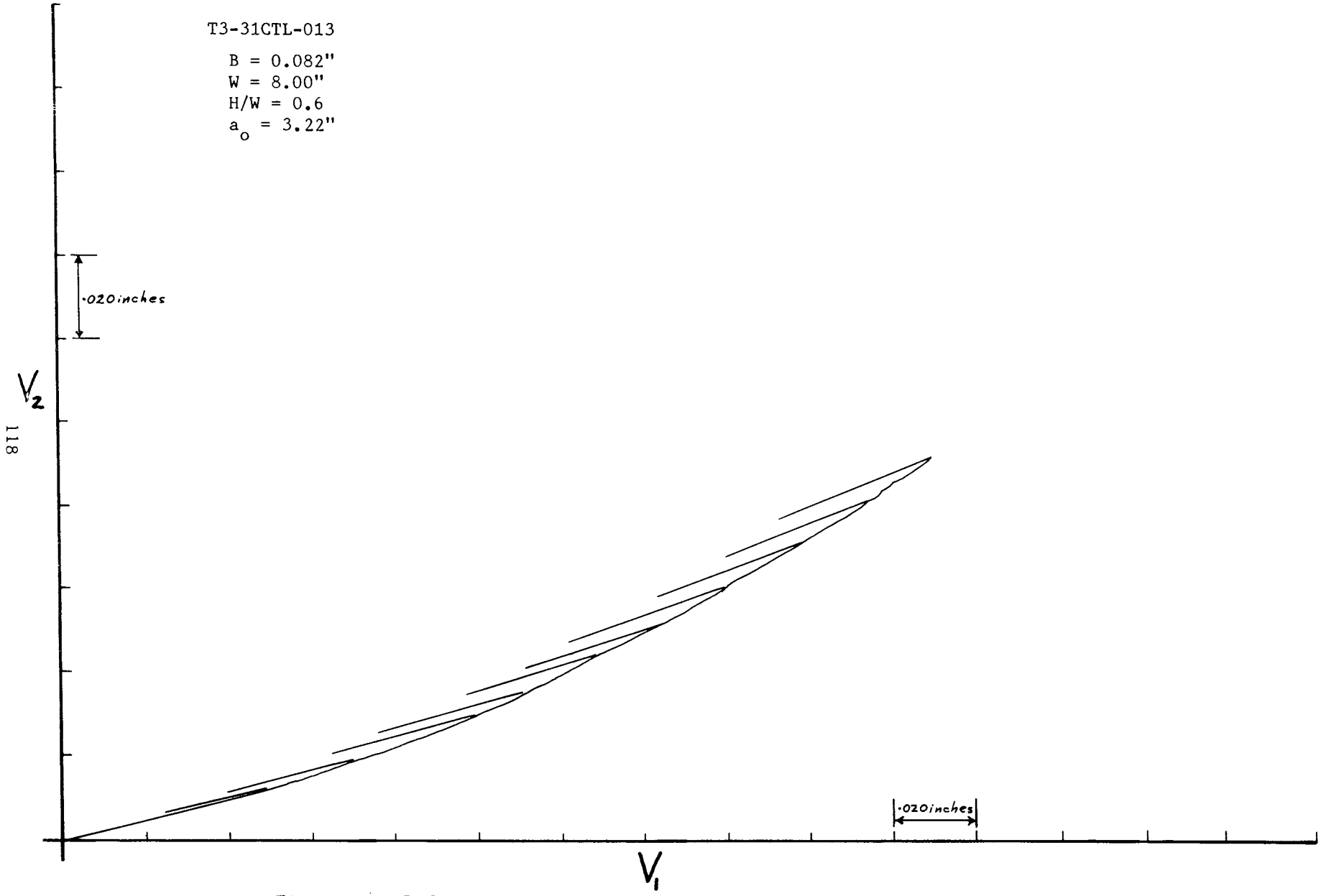

Figure 71. Deflection Curve - 0.082 Inch, Chem Milled 2024-T351 (TL)

4V-93CLT-007

B = 0.053"
W = 14.00"
H/W = 0.6
a_o = 5.07"

NOTE: Specimen Bowed

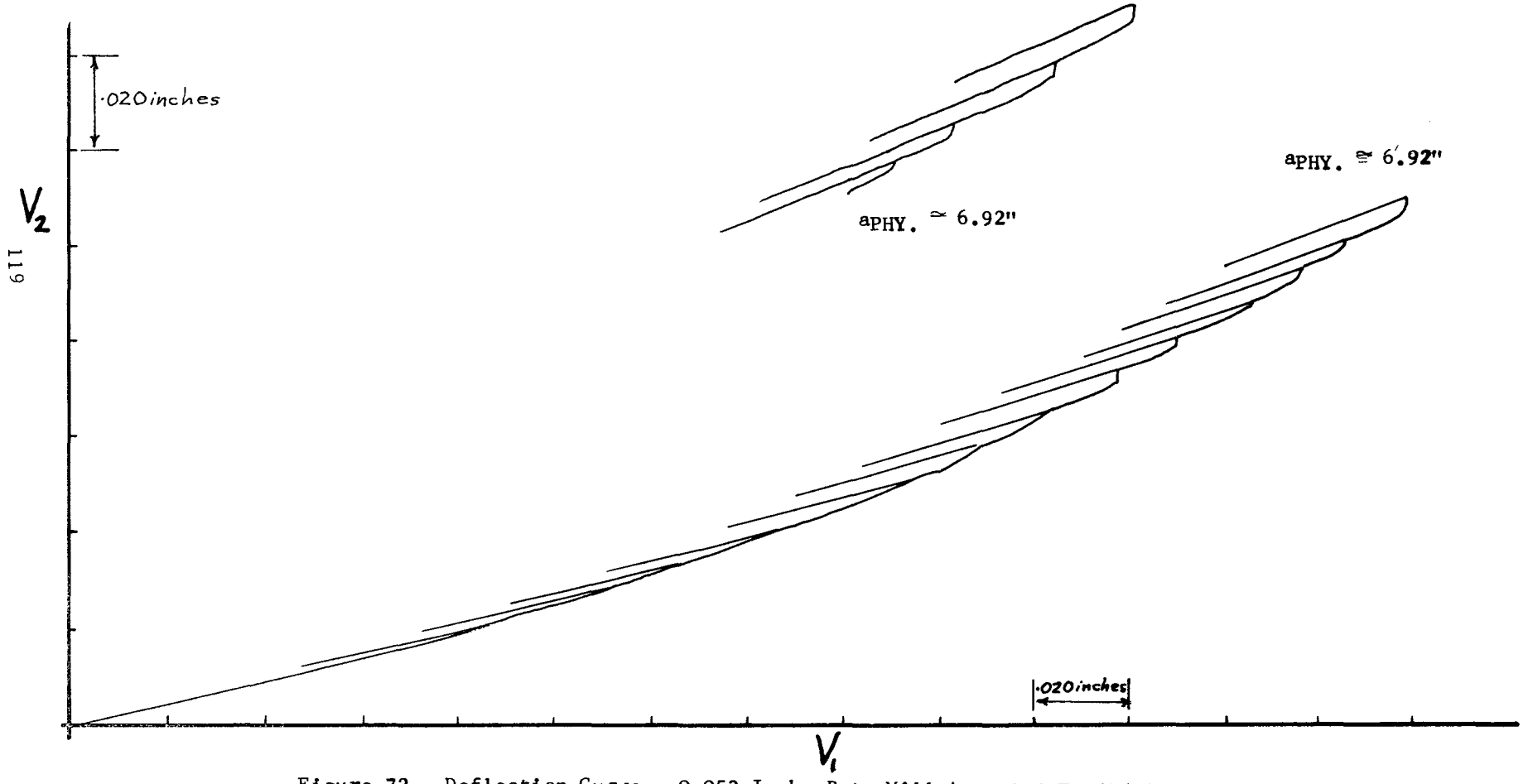

Figure 72. Deflection Curve - 0.053 Inch, Beta Mill Annealed Ti-6Al-4V (LT)

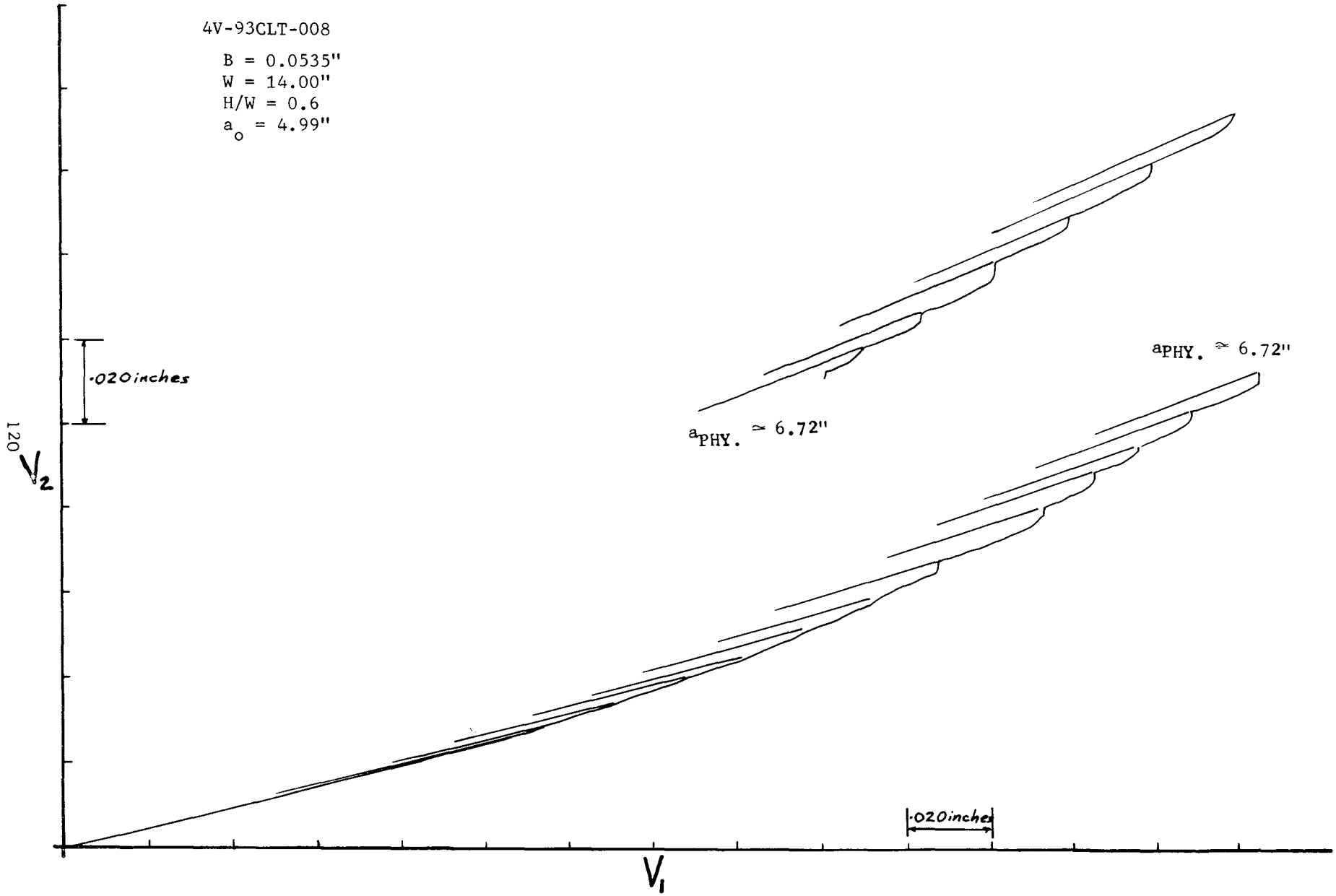

Figure 73. Deflection Curve - 0.0535 Inch, Beta Mill Annealed Ti-6Aℓ-4V (LT)

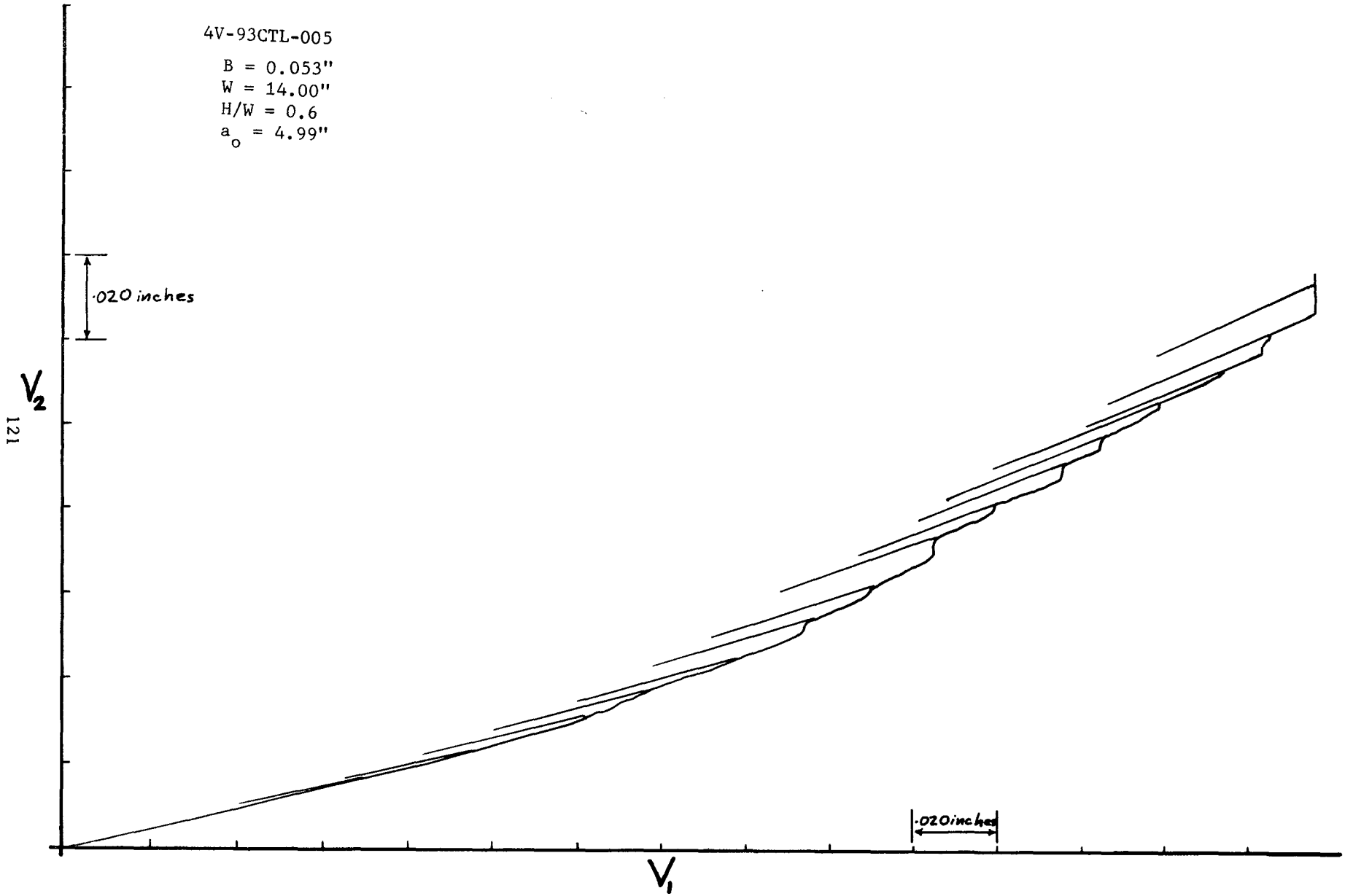

Figure 74. Deflection Curve - 0.053 Inch, Beta Mill Annealed Ti-6Al-4V (TL)

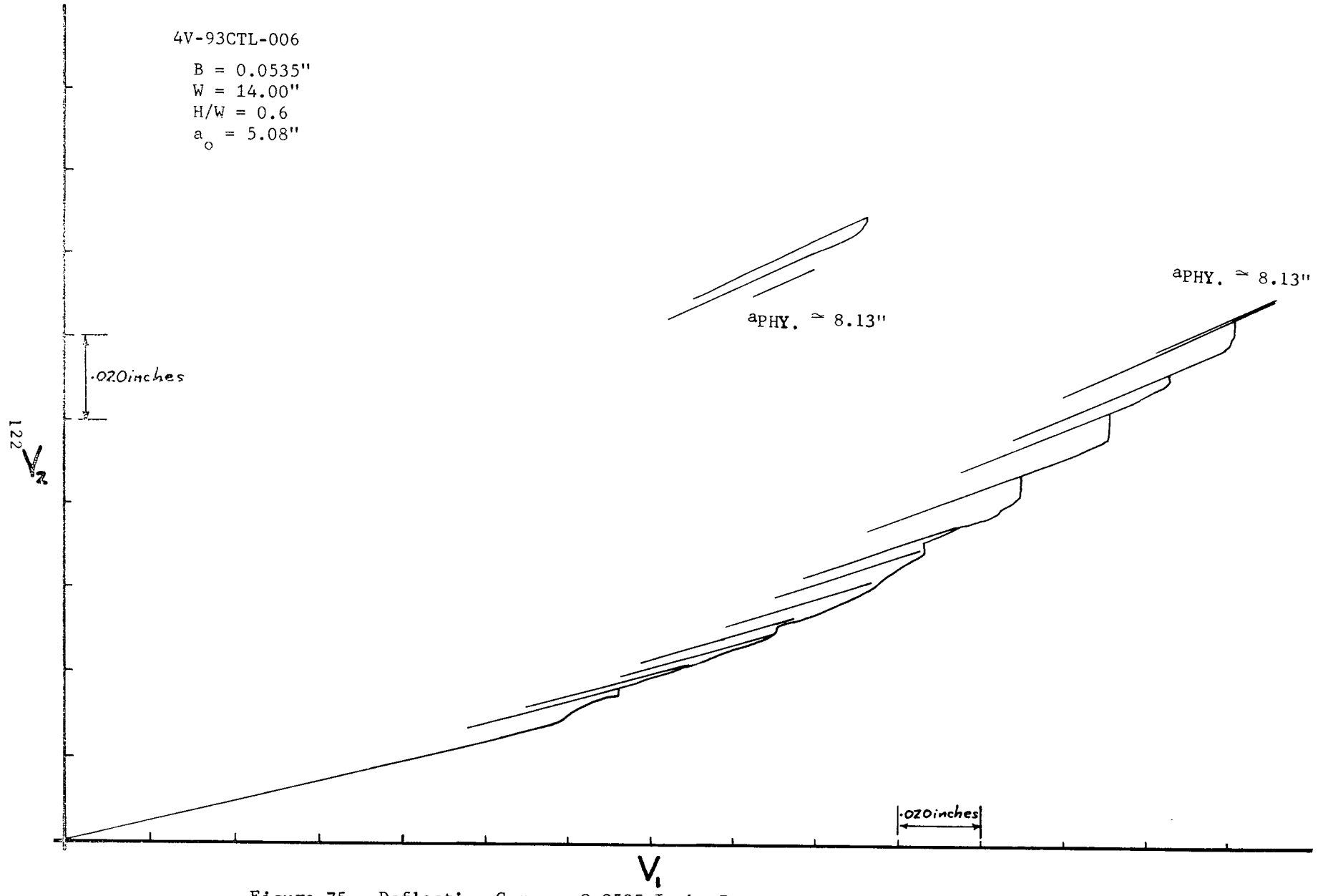

Figure 75. Deflection Curve - 0.0535 Inch, Beta Mill Annealed Ti-6Al-4V (TL)

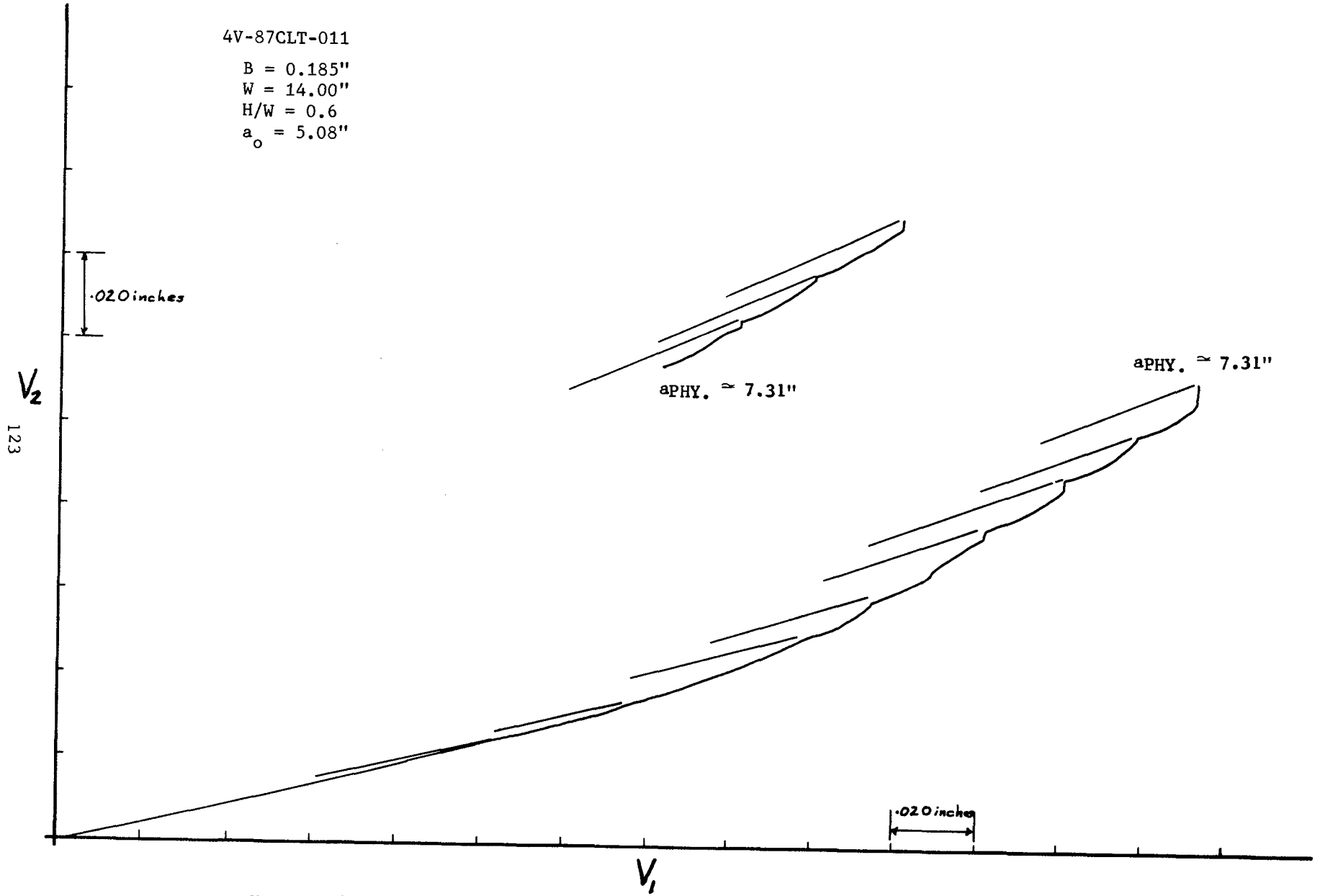

Figure 76. Deflection Curve - 0.185 Inch, Beta Mill Annealed Ti-6Al-4V (LT)

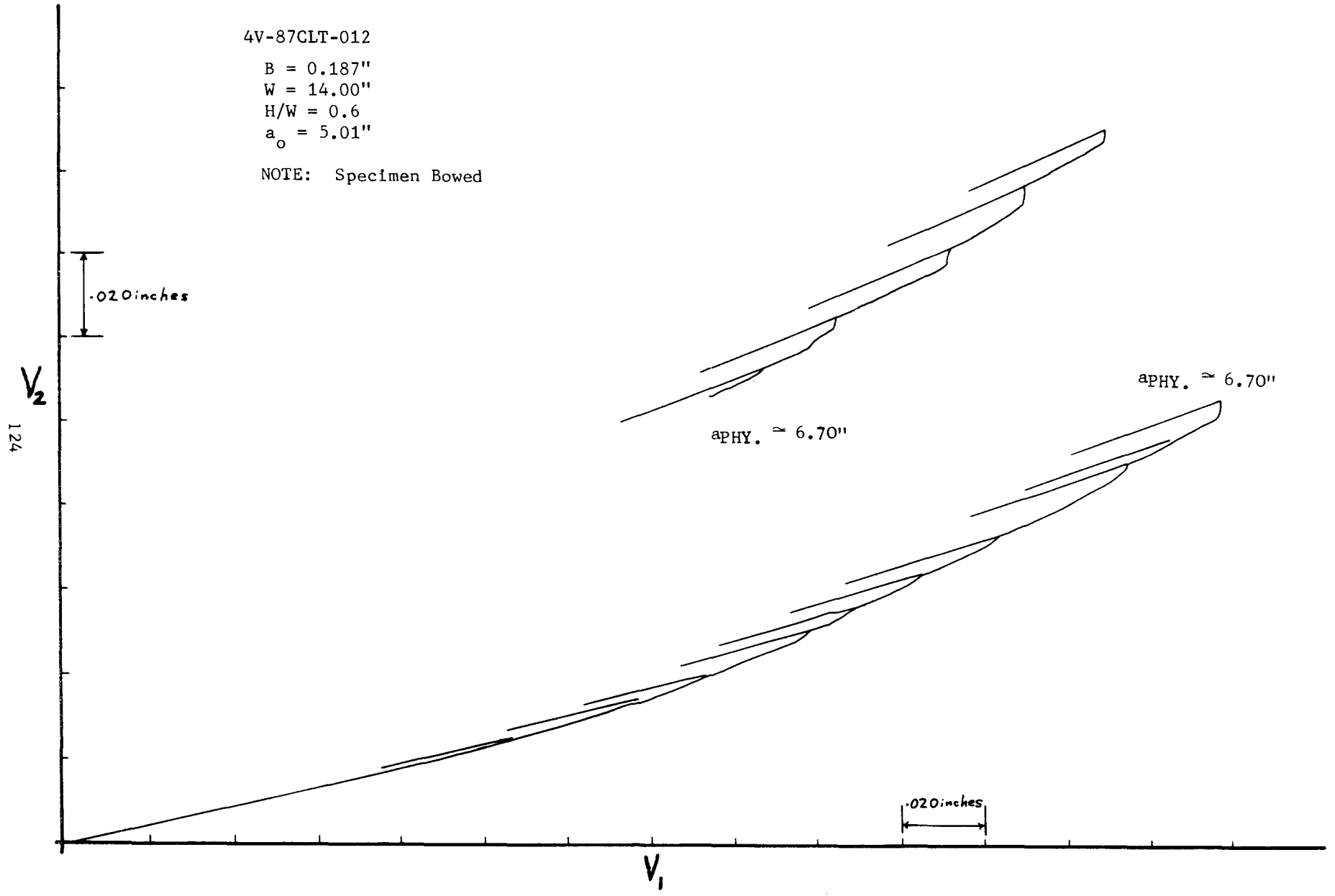

Figure 77. Deflection Curve - 0.187 Inch, Beta Mill Annealed Ti-6Al-4V (LT)

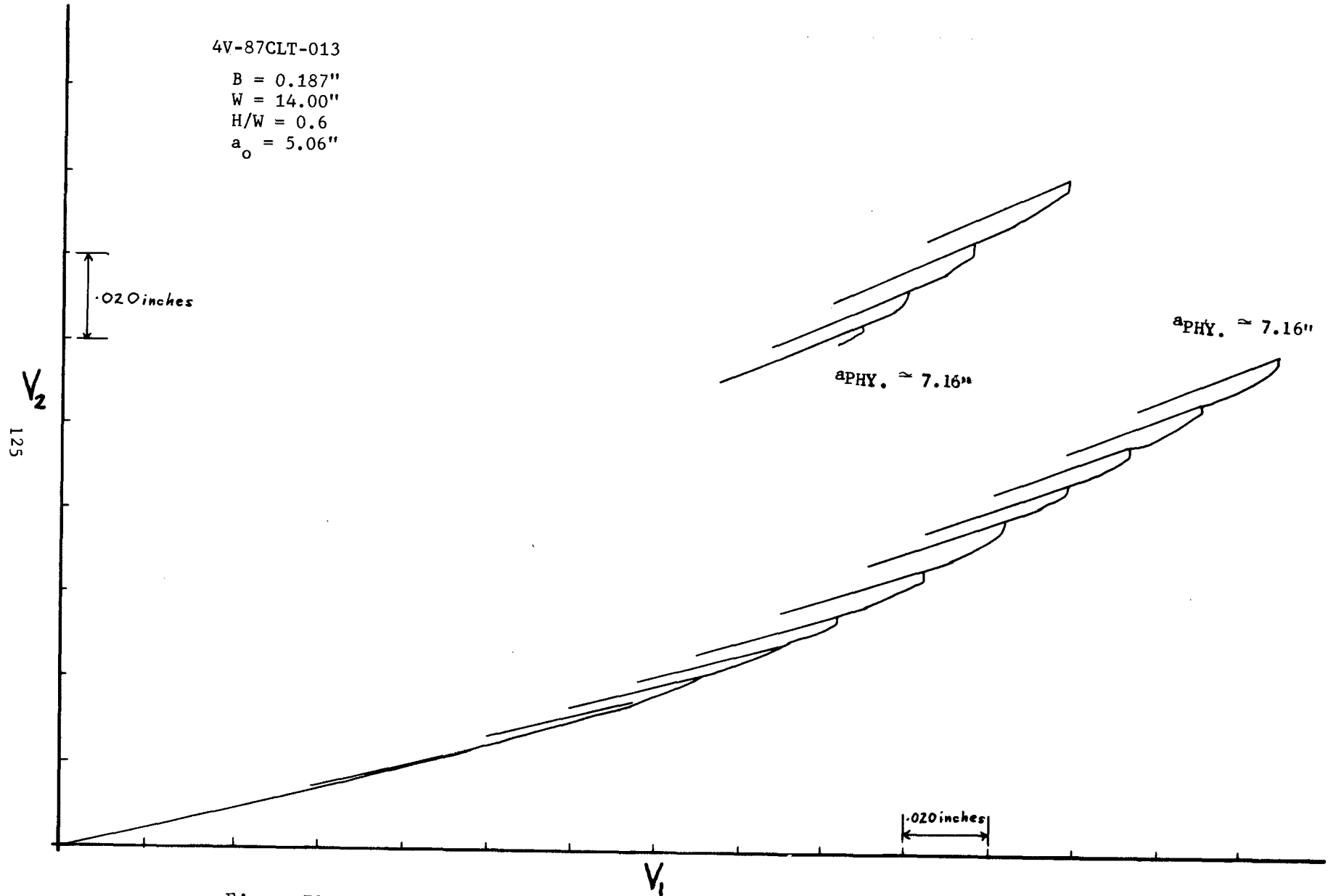

Figure 78. Deflection Curve - 0.187 Inch, Beta Mill Annealed Ti-6Al-4V (LT)

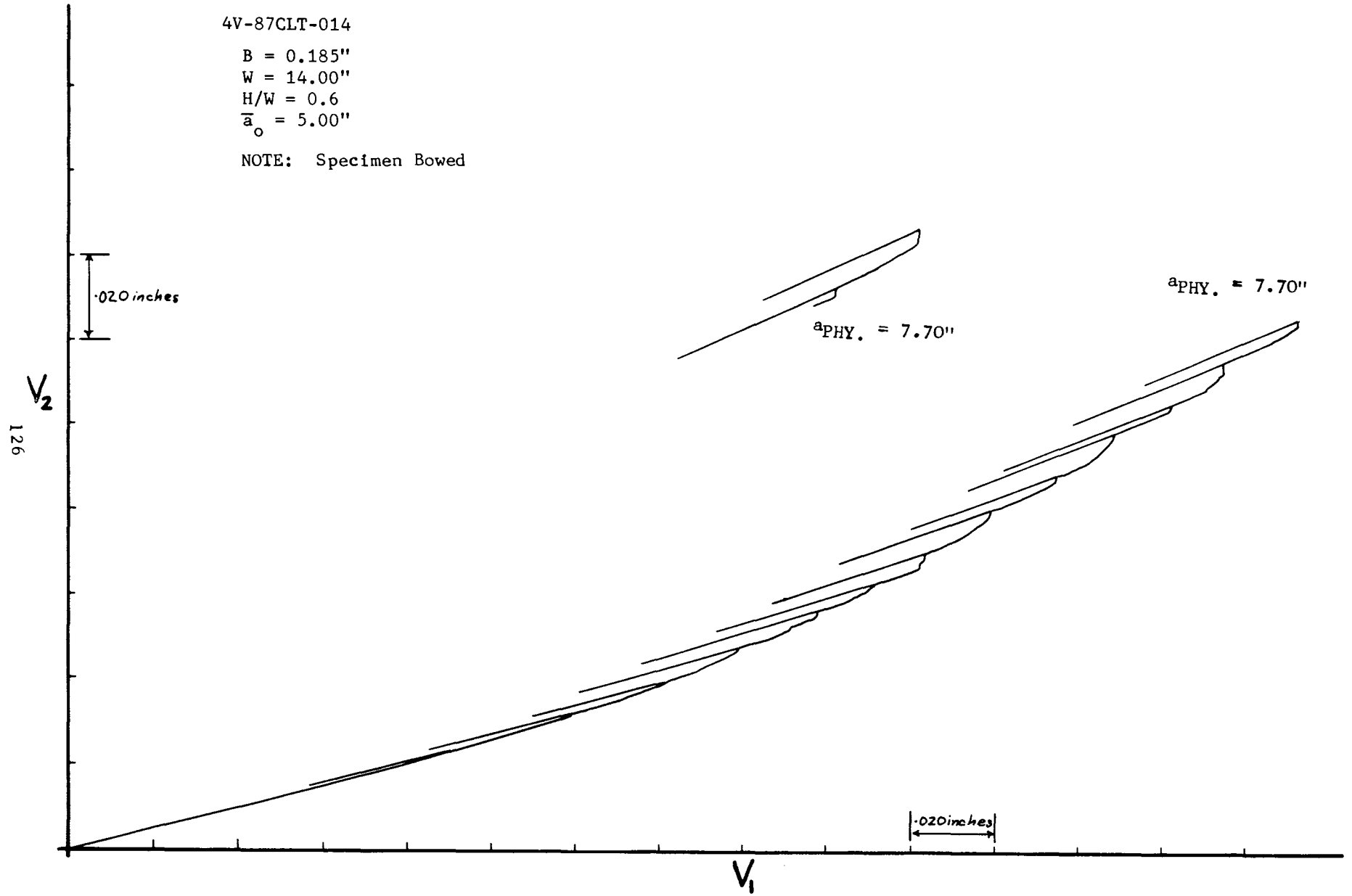

Figure 79. Deflection Curve - 0.185 Inch, Beta Mill Annealed Ti-6Al-4V (LT)

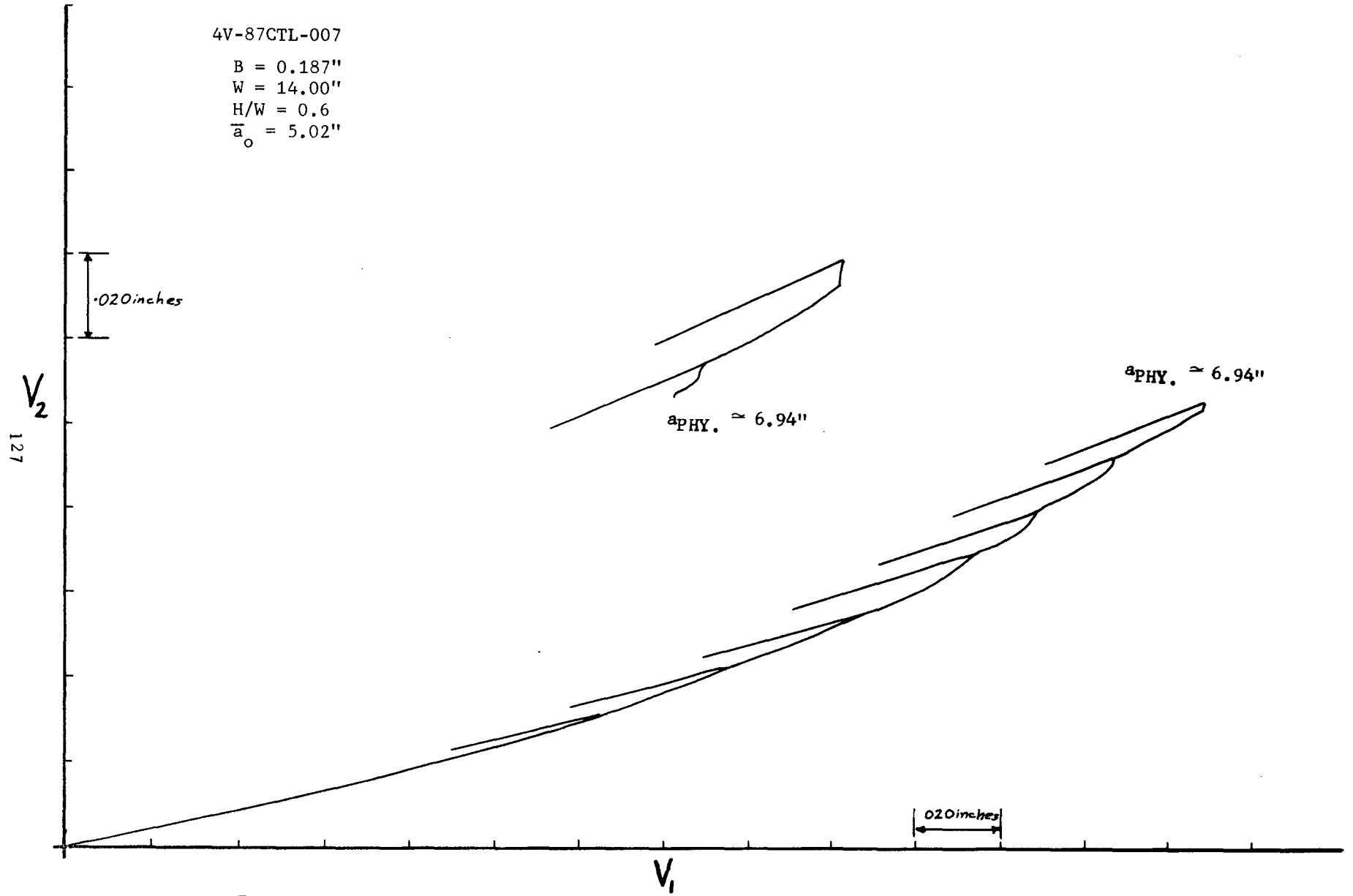

Figure 80. Deflection Curve - 0.187 Inch, Beta Mill Annealed Ti-6Al-4V (TL0)

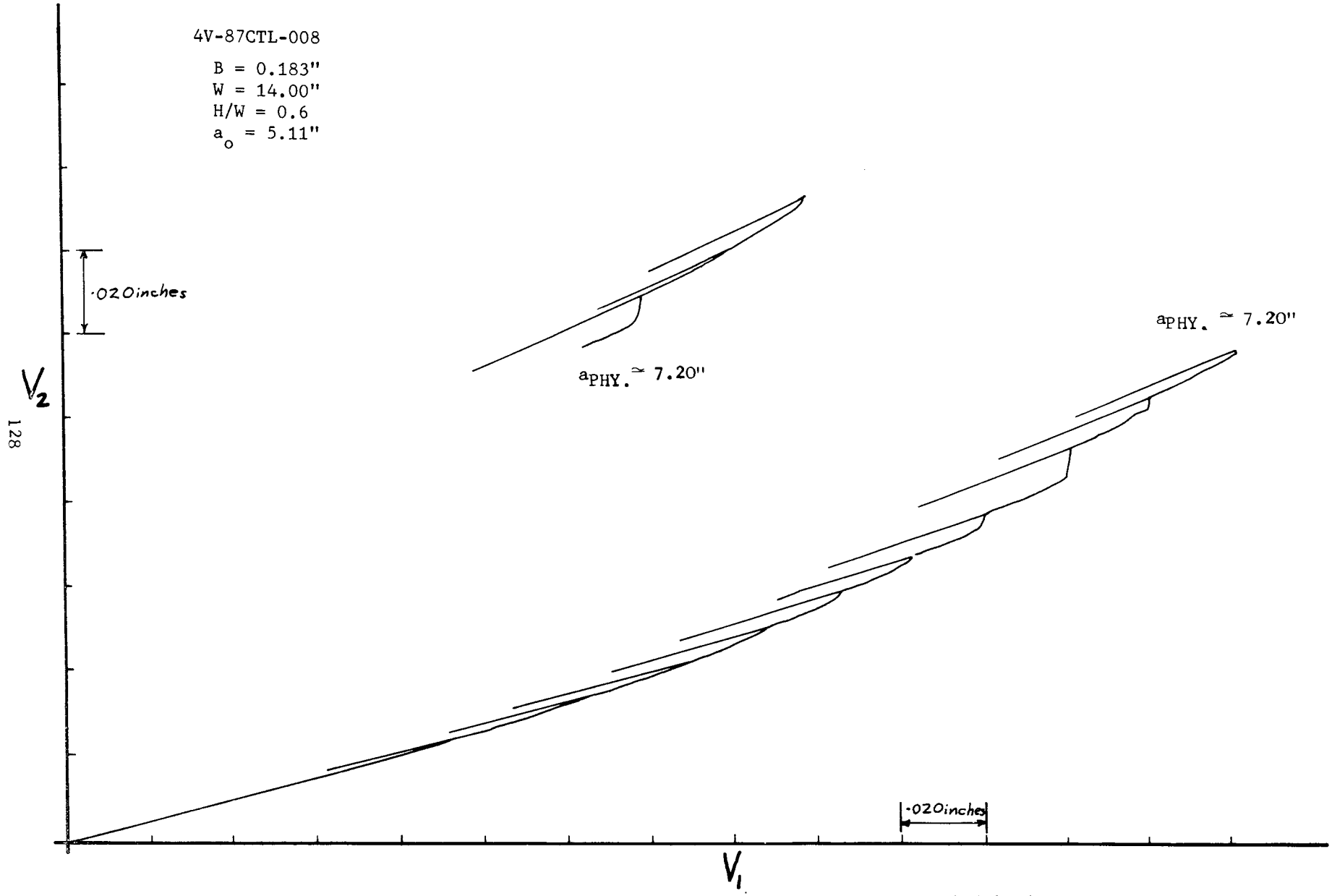

Figure 81. Deflection Curve - 0.183 Inch, Beta Mill Annealed Ti-6Aℓ-4V (TL)

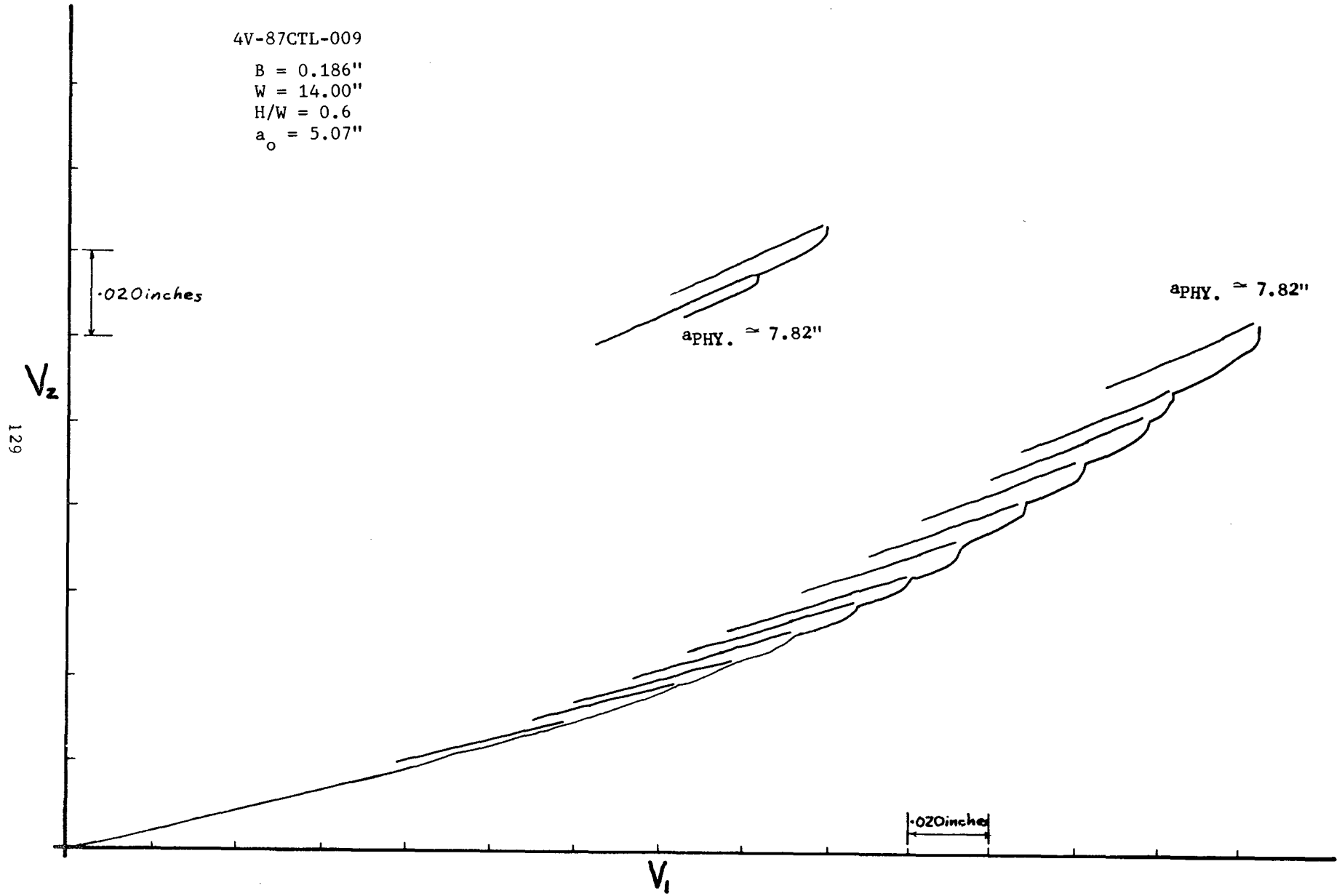

Figure 82. Deflection Curve - 0.186 Inch, Beta Mill Annealed Ti-6Al-4V (TL)

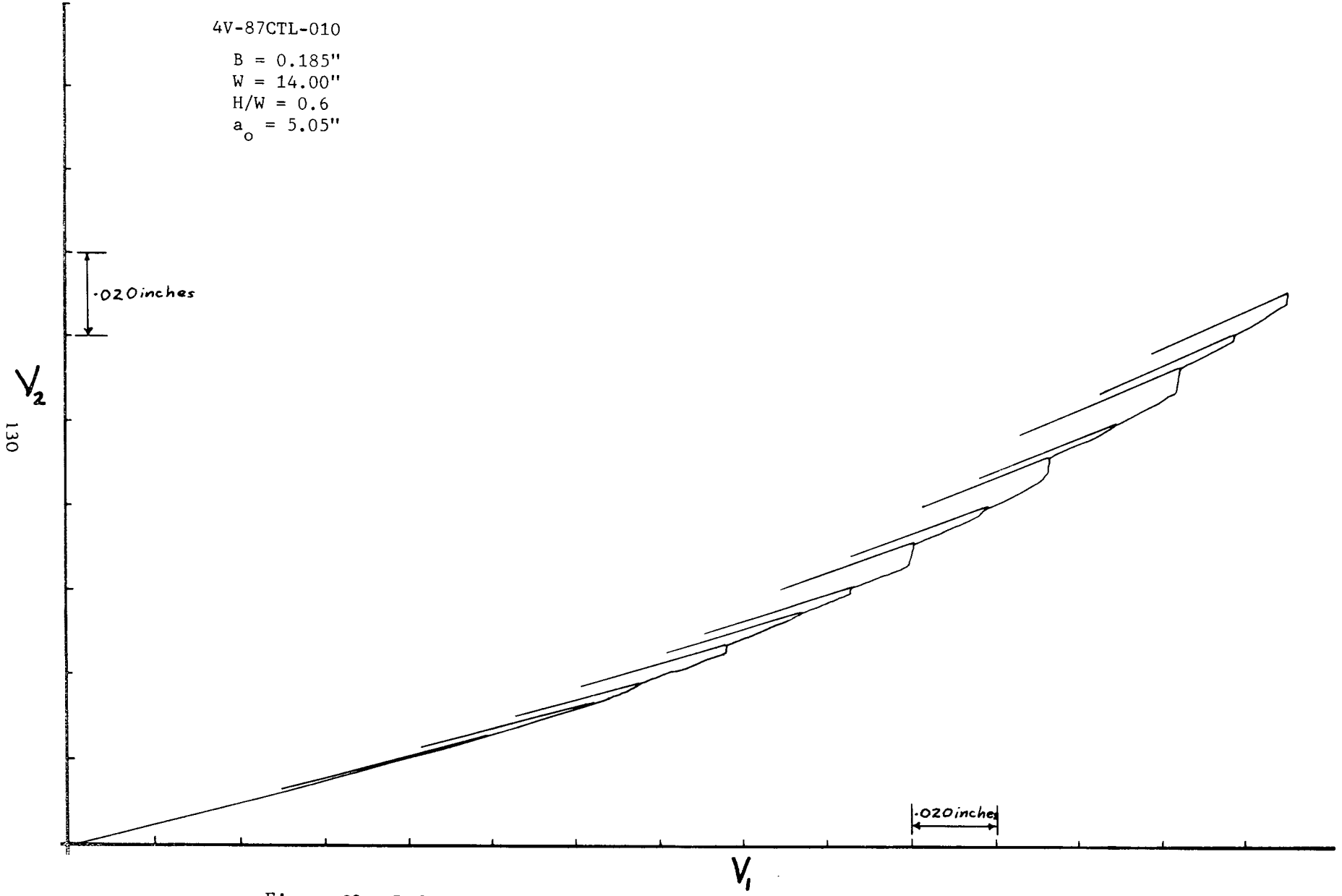

Figure 83. Deflection Curve - 0.185 Inch, Beta Mill Annealed Ti-6Al-4V (TL)

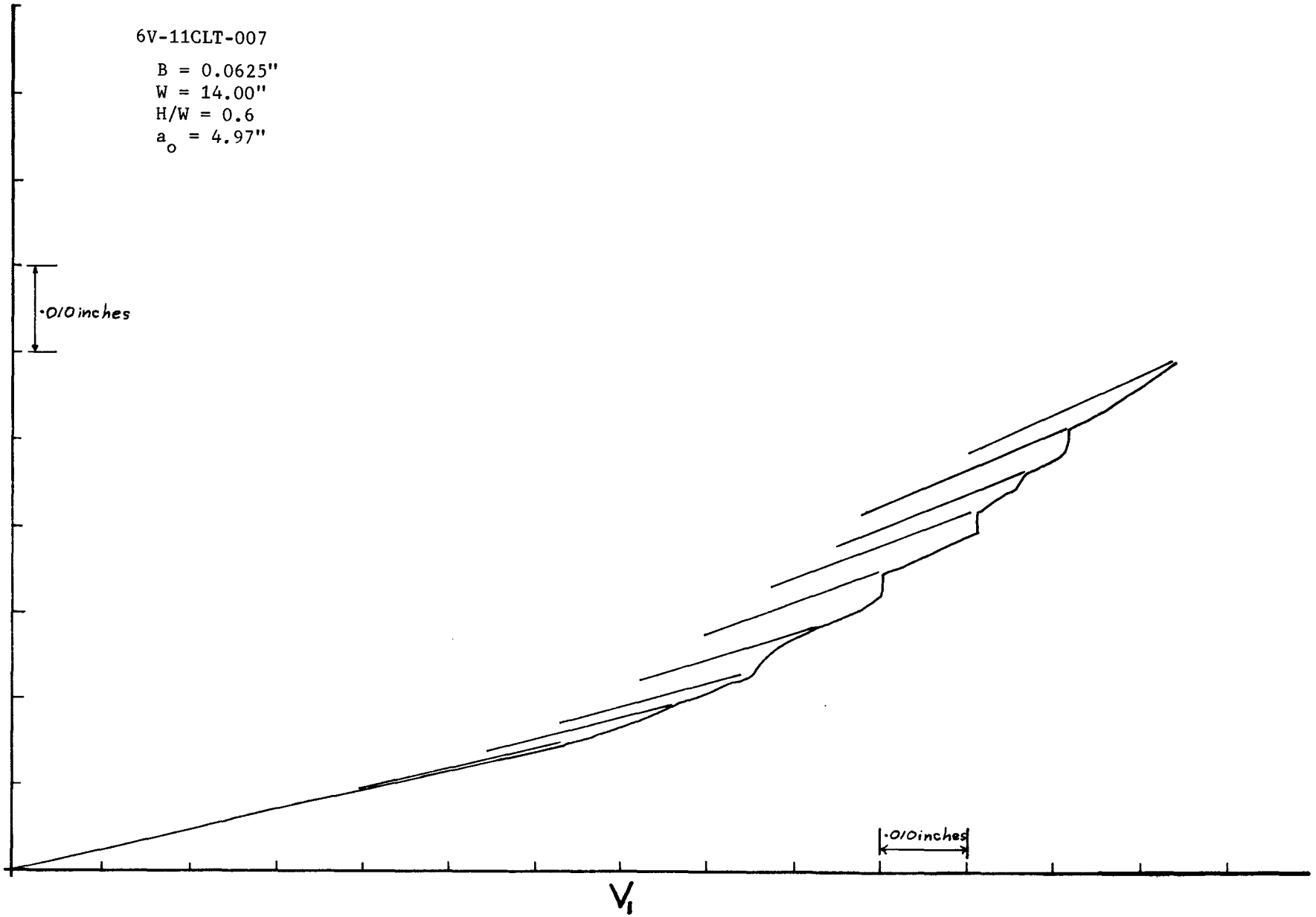

Figure 84. Deflection Curve - 0.0625 Inch, Mill Annealed Ti-6Al-6V-2Sn (LT)

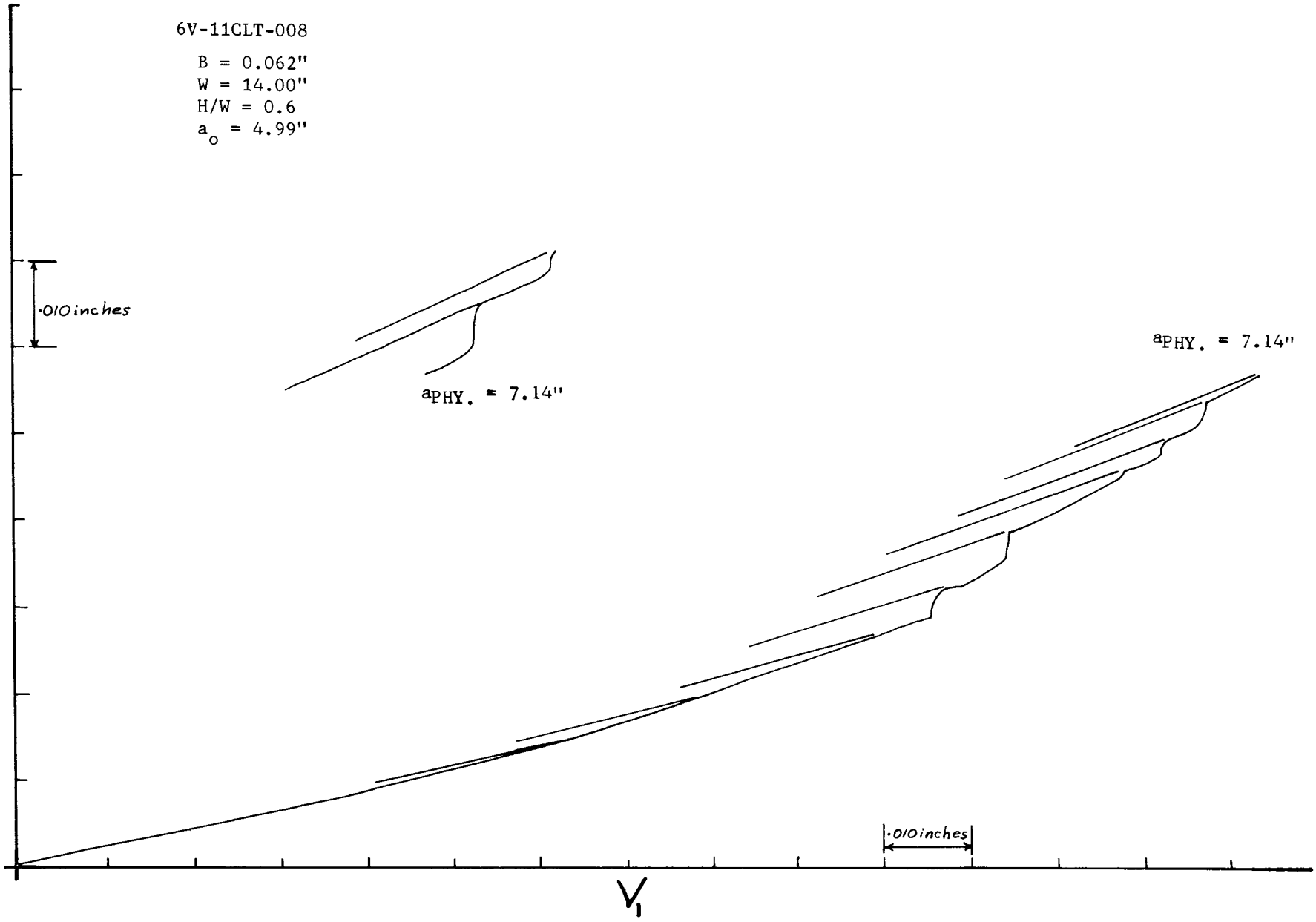

Figure 85. Deflection Curve - 0.062 Inch, Mill Annealed Ti-6Aℓ-6V-2Sn (LT)

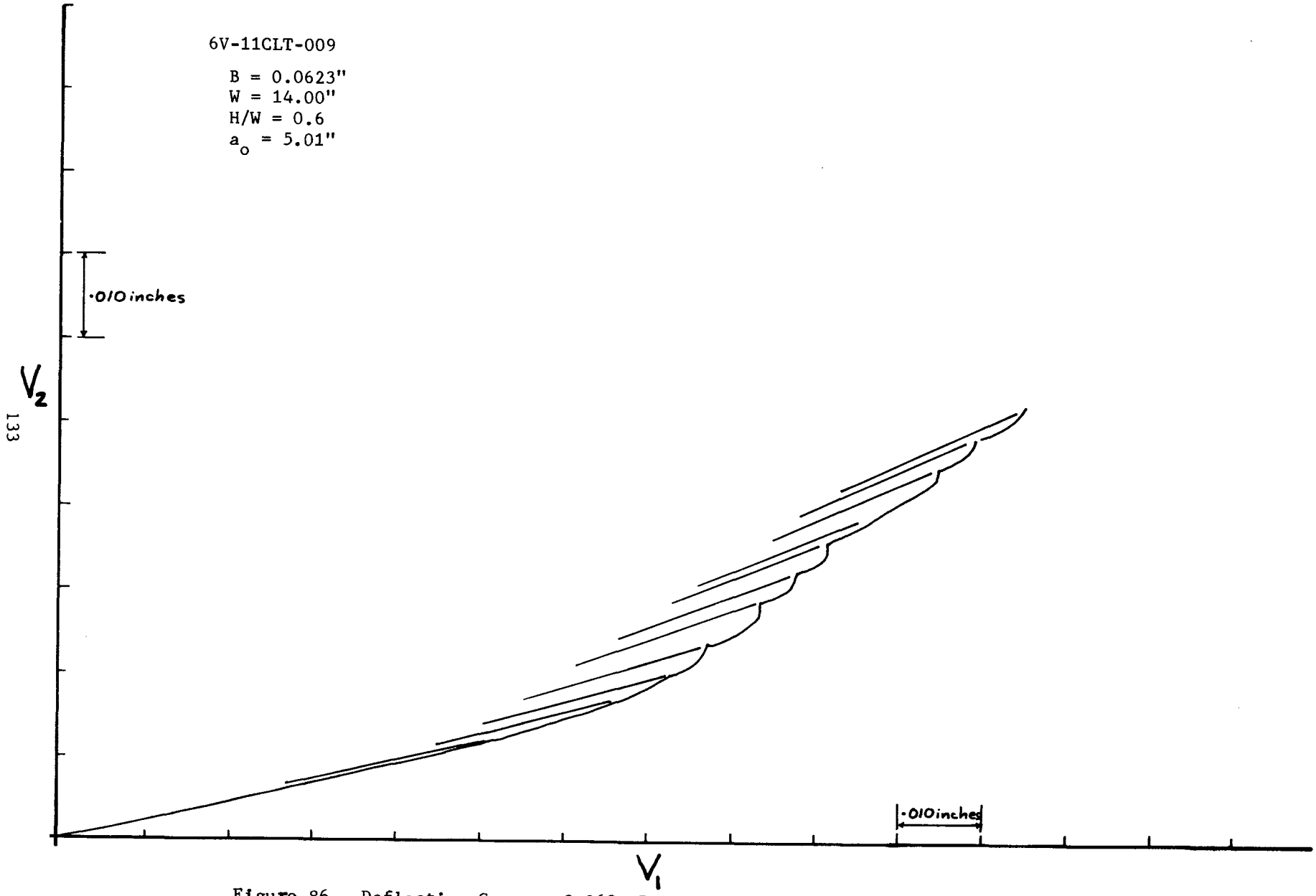

Figure 86. Deflection Curve - 0.0623 Inch, Mill Annealed Ti-6Al-6V-2Sn (LT)

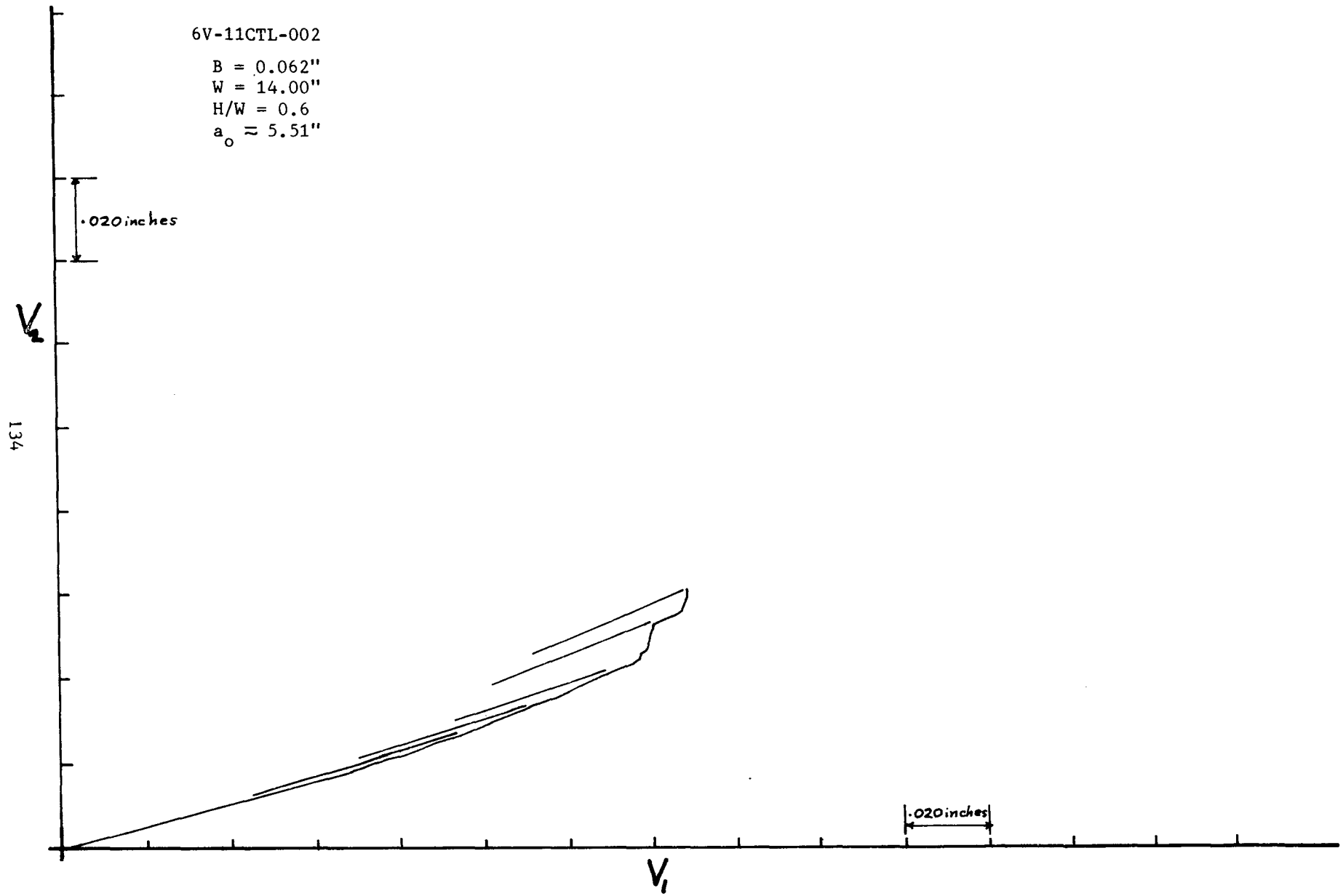

Figure 87. Deflection Curve - 0.062 Inch, Mill Annealed Ti-6Al-6V-2Sn (TL)

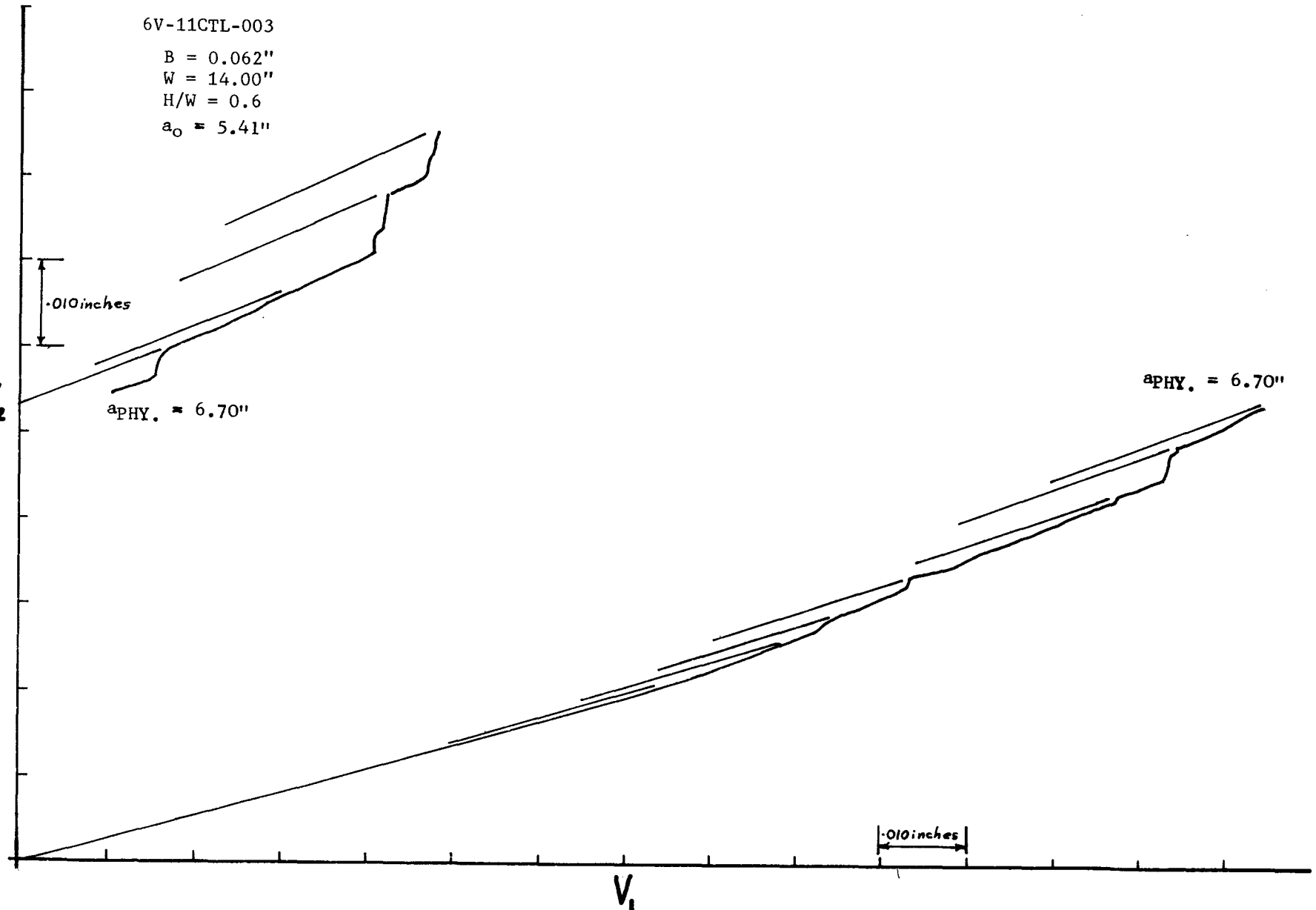

Figure 88. Deflection Curve - 0.062 Inch, Mill Annealed Ti-6Al-6V-2Sn (TL)

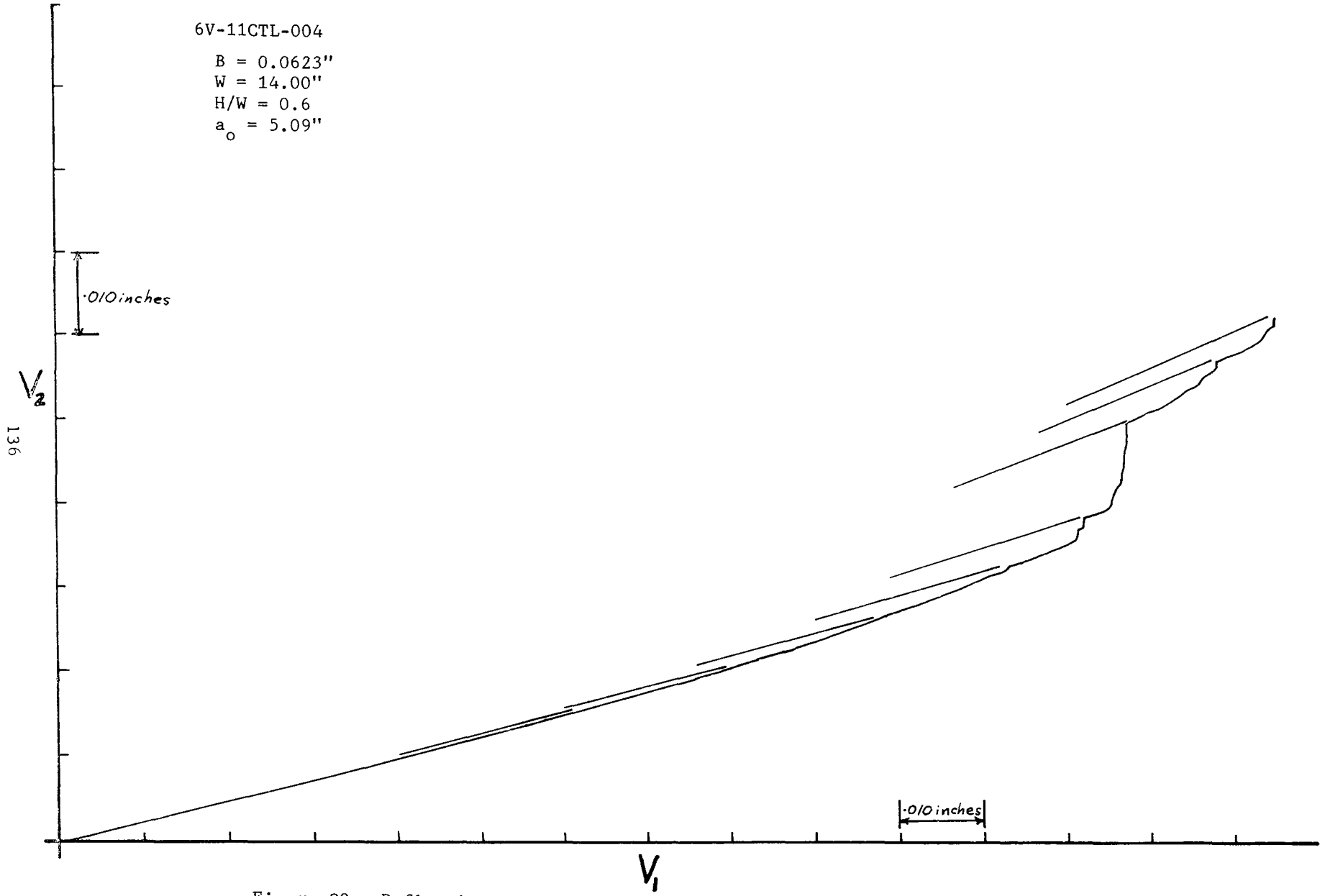

Figure 89. Deflection Curve - 0.0623 Inch, Mill Annealed Ti-6Aℓ-6V-2Sn (TL)

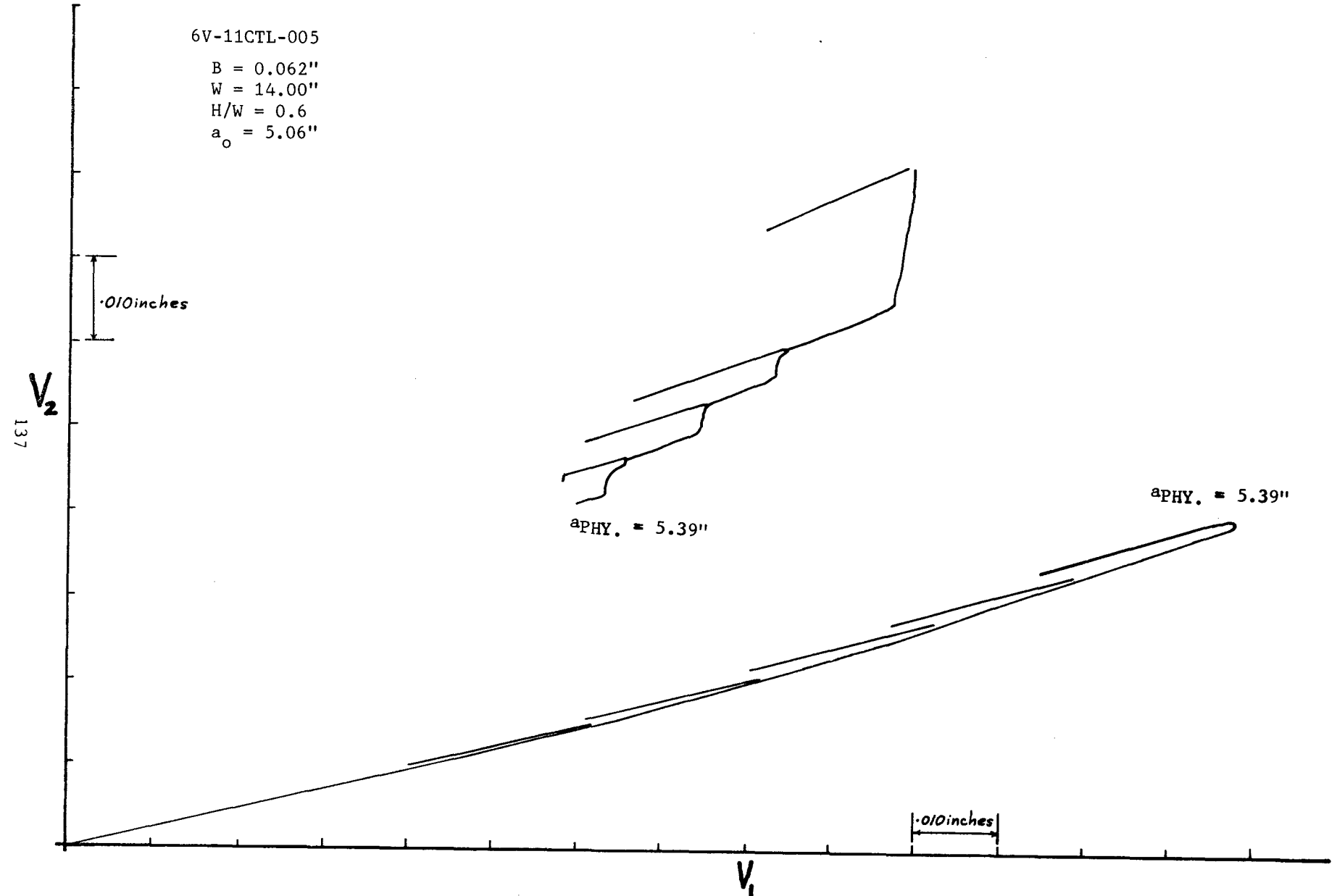

Figure 90. Deflection Curve - 0.062 Inch, Mill Annealed Ti-6Al-4V-2Sn (TL)

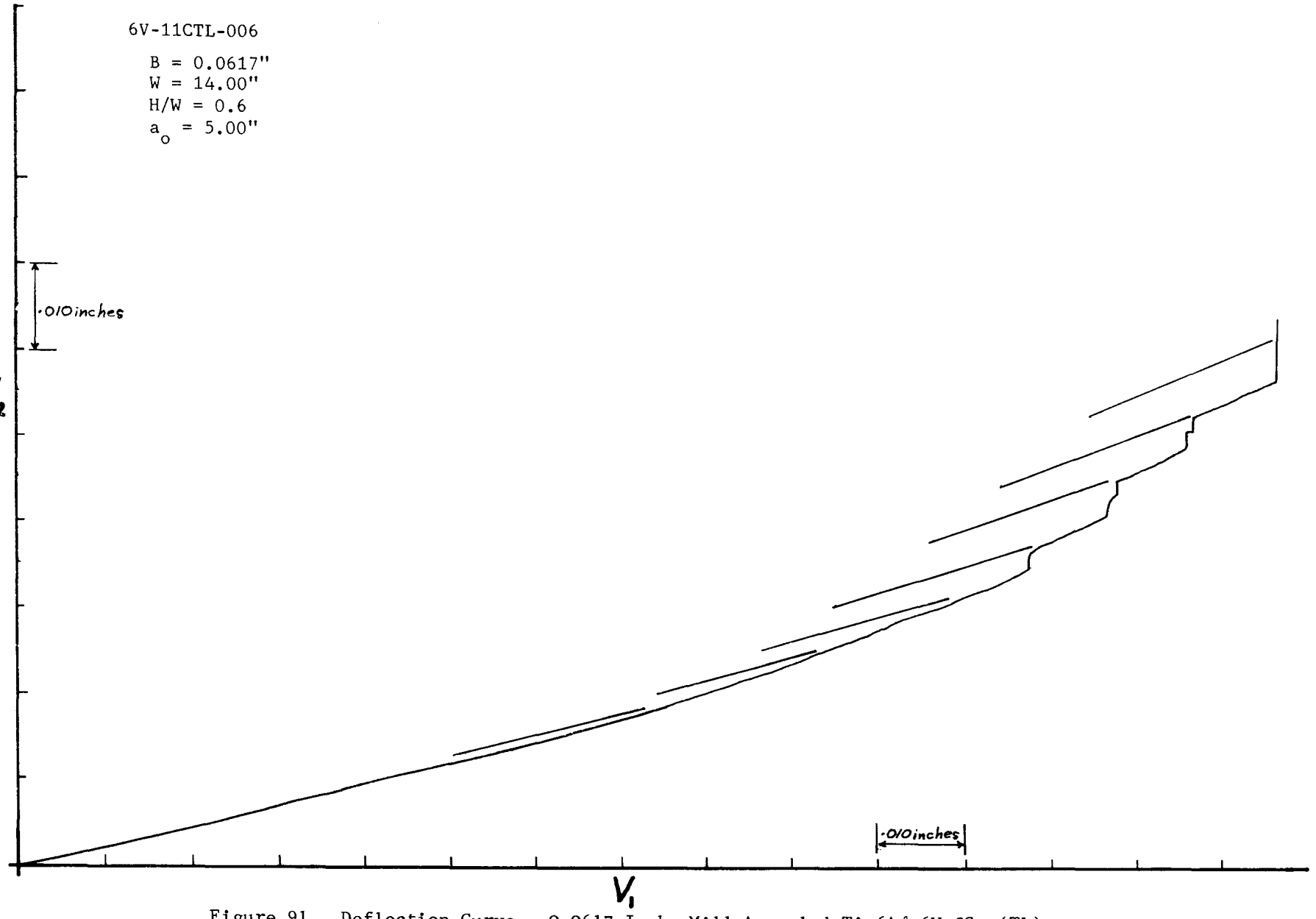

Figure 91. Deflection Curve - 0.0617 Inch, Mill Annealed Ti-6Aℓ-6V-2Sn (TL)

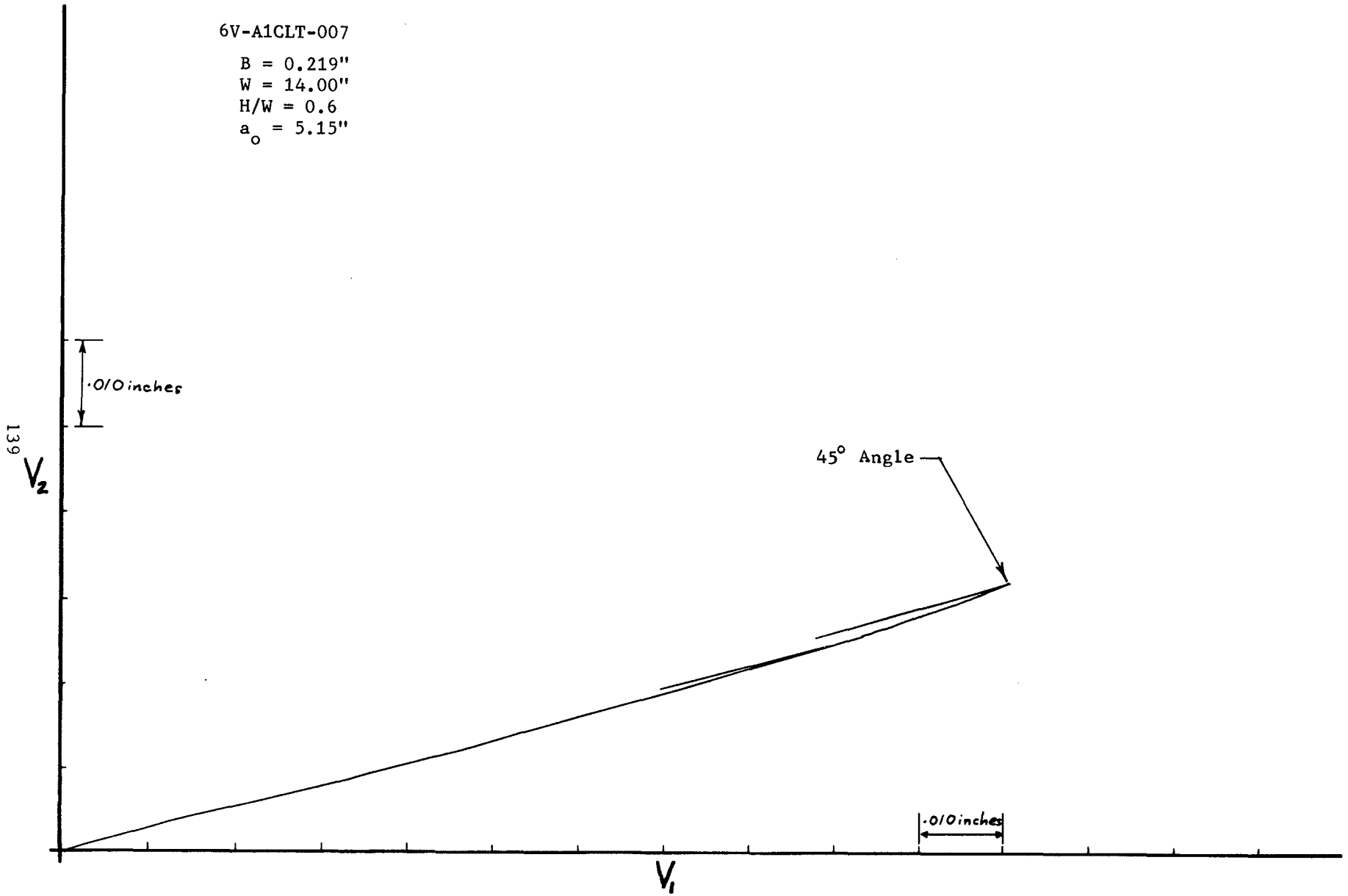

Figure 92. Deflection Curve - 0.219 Inch, Mill Annealed Ti-6Aℓ-6V-2Sn (LT)

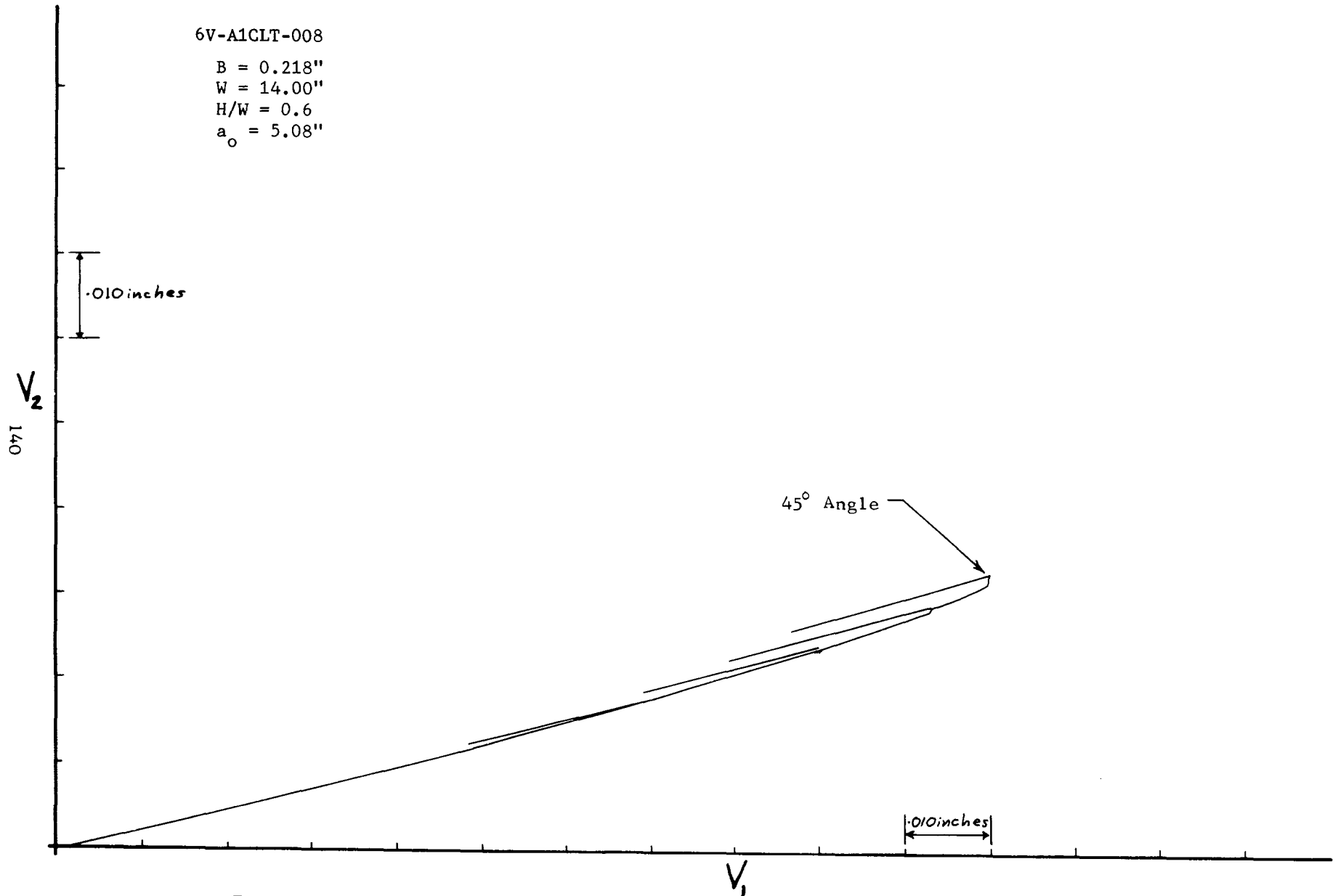

Figure 93. Deflection Curve - 0.218 Inch, Mill Annealed Ti-6Al-6V-2Sn (LT)

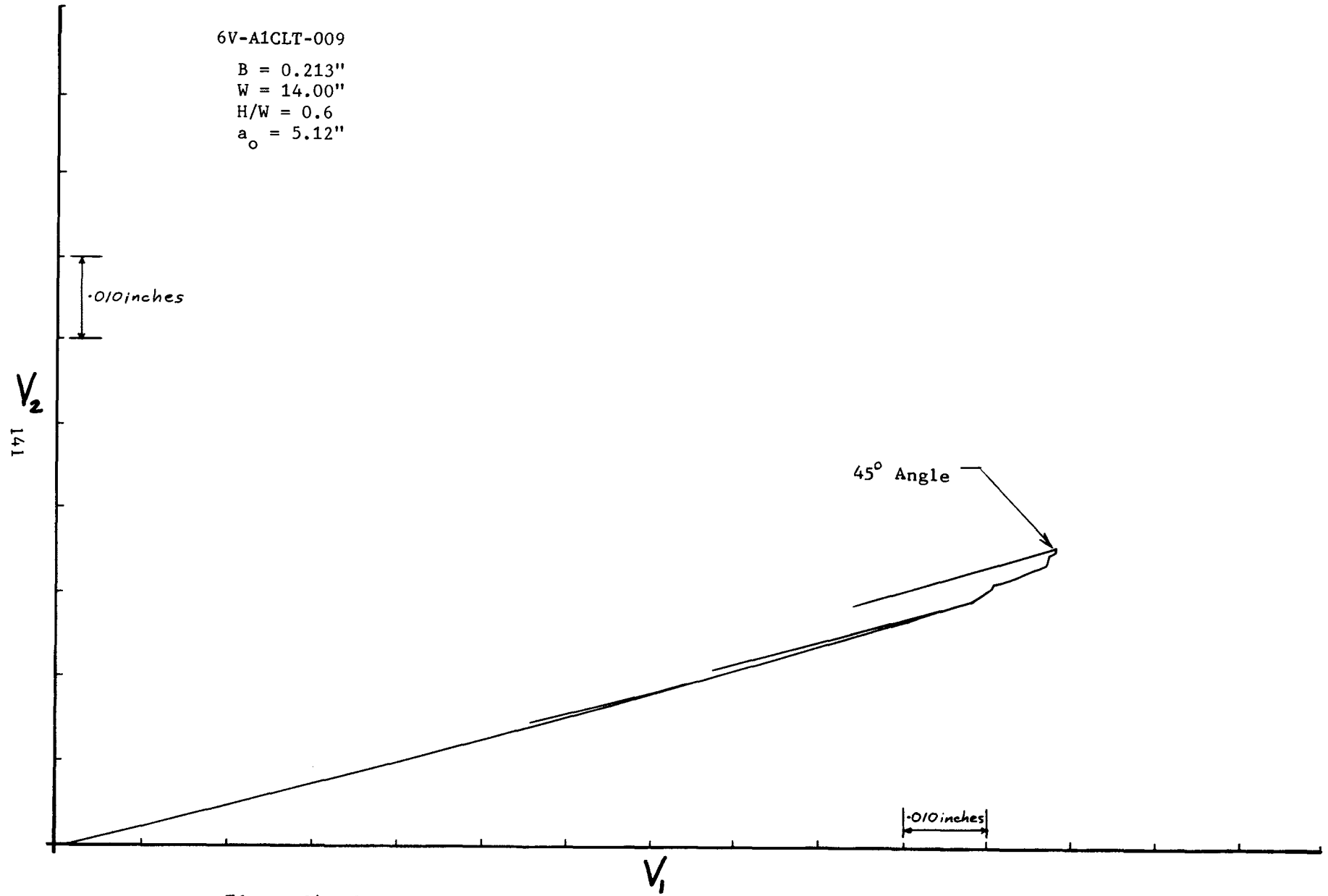

Figure 94. Deflection Curve - 0.213 Inch, Mill Annealed Ti-6Al-6V-2Sn (LT)

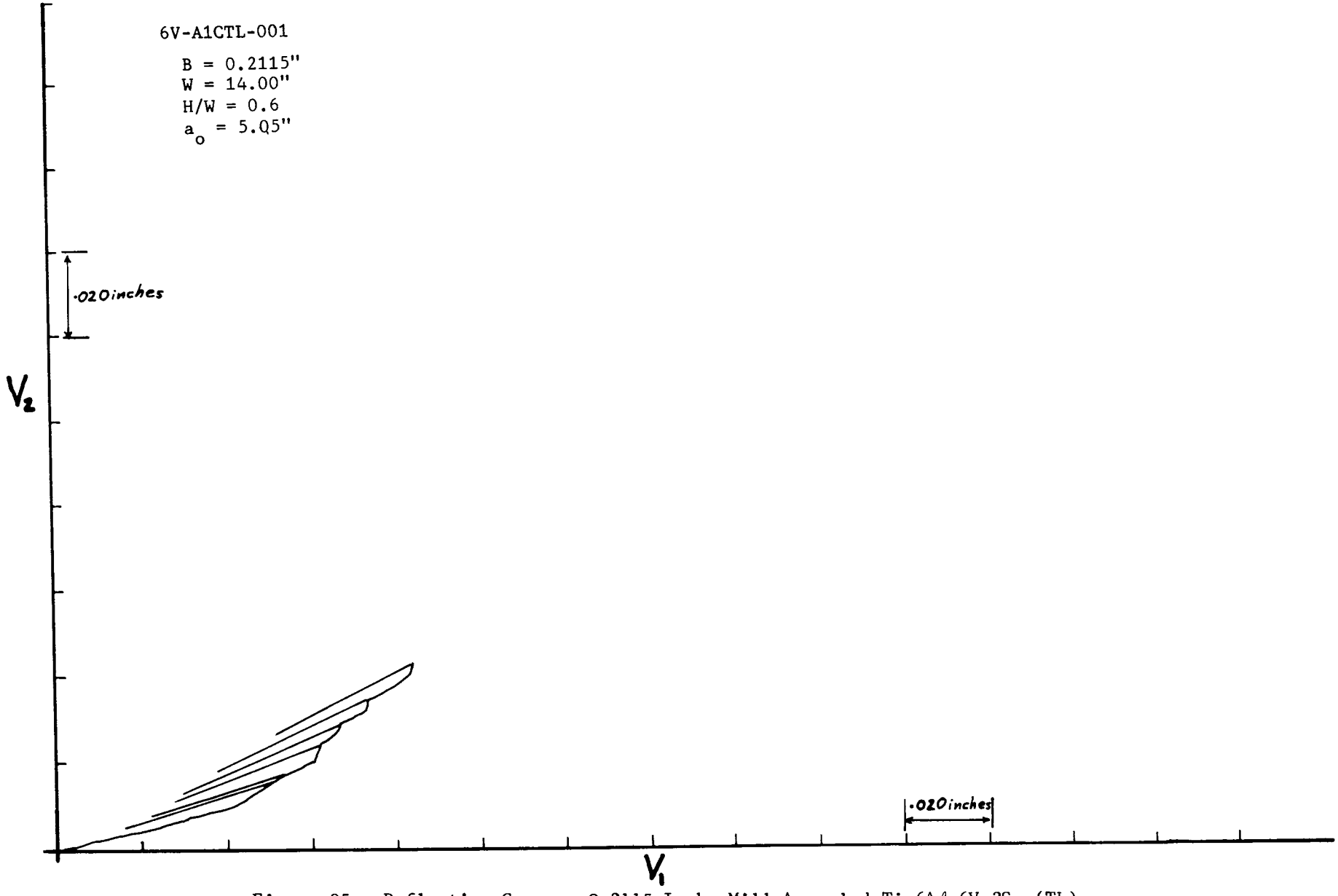

Figure 95. Deflection Curve - 0.2115 Inch, Mill Annealed Ti-6Aℓ-6V-2Sn (TL)

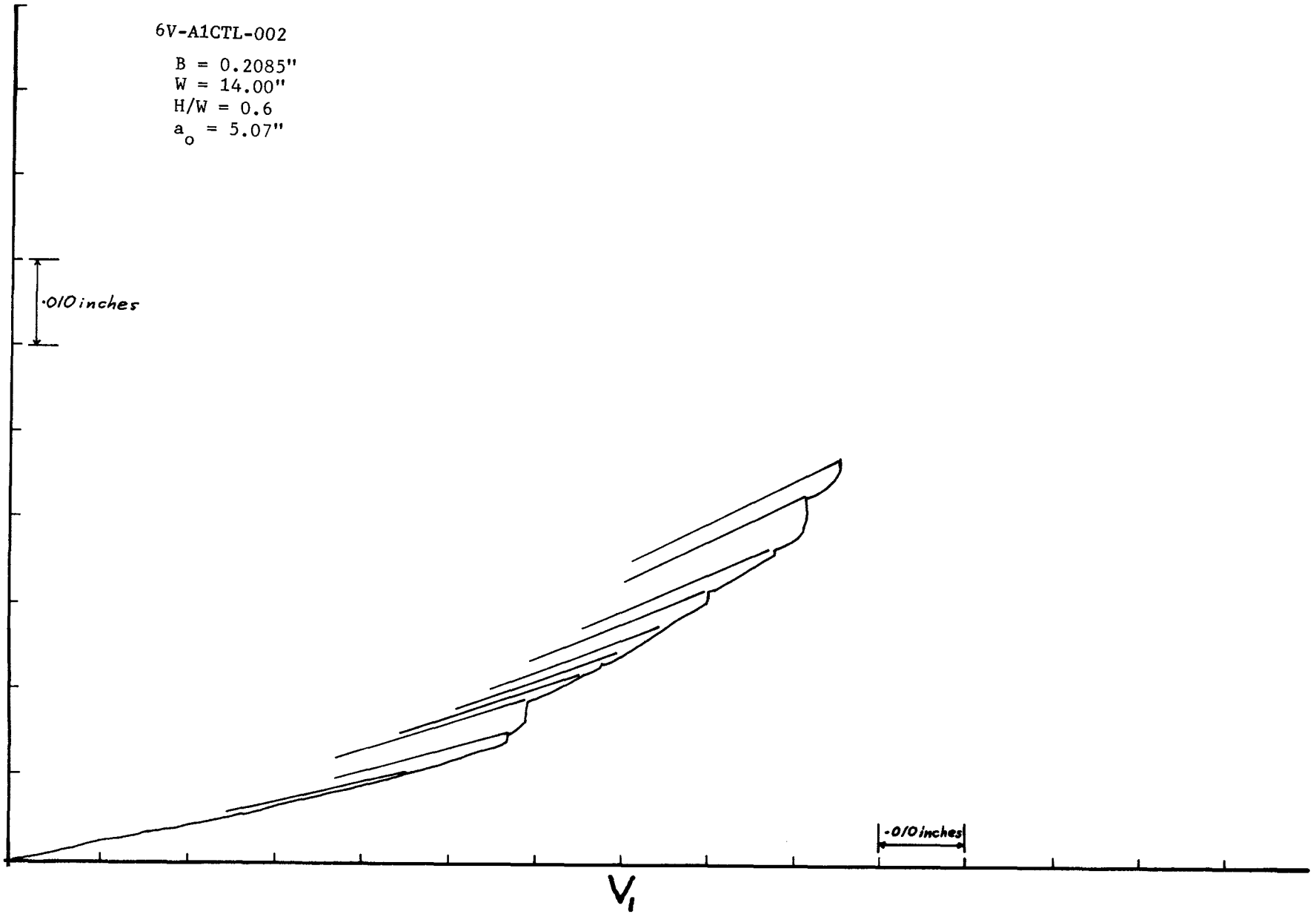

Figure 96. Deflection Curve - 0.2085 Inch, Mill Annealed Ti-6Al-6V-2Sn (TL)

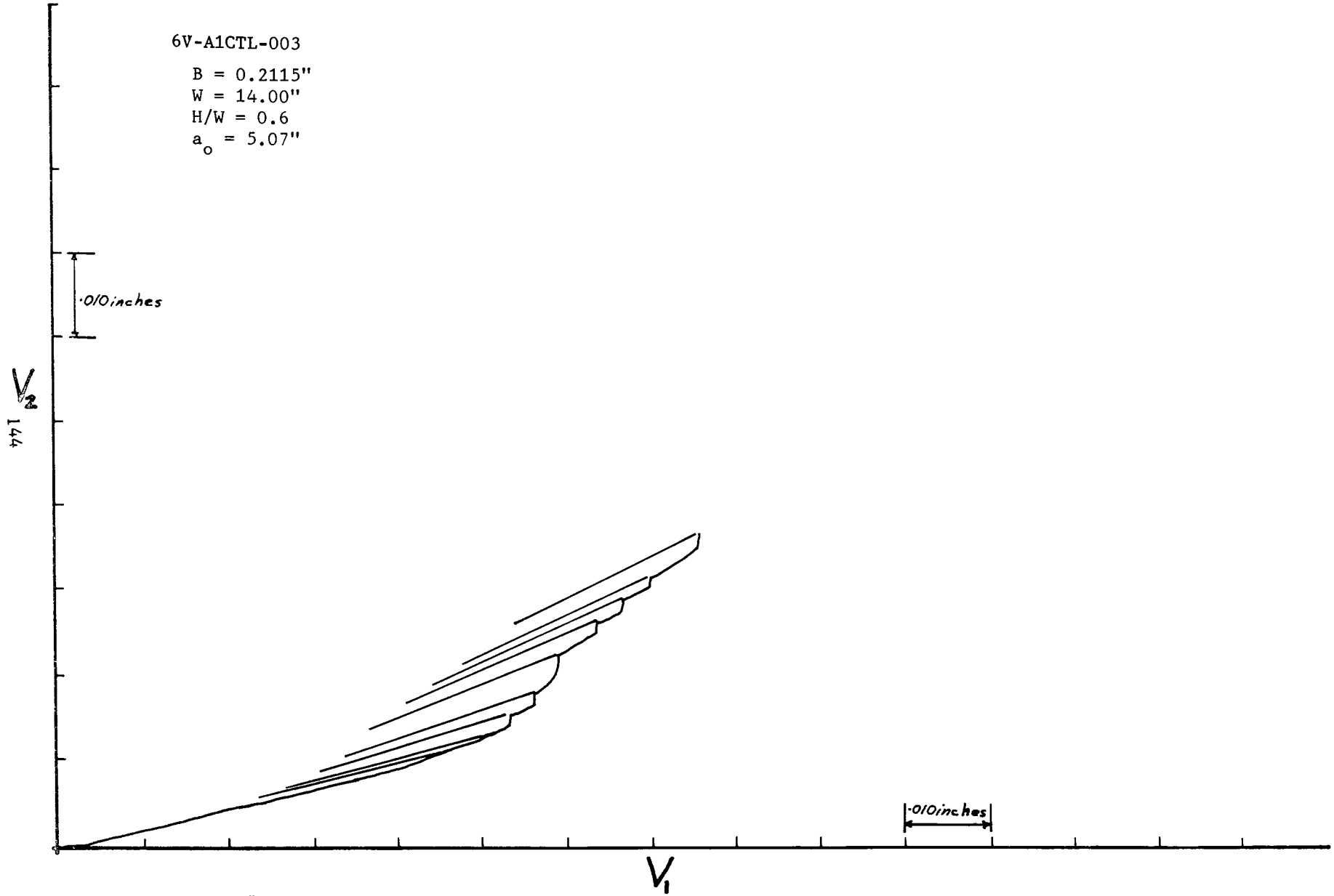

Figure 97. Deflection Curve - 0.2115 Inch, Mill Annealed Ti-6Al-6V-2Sn (TL)

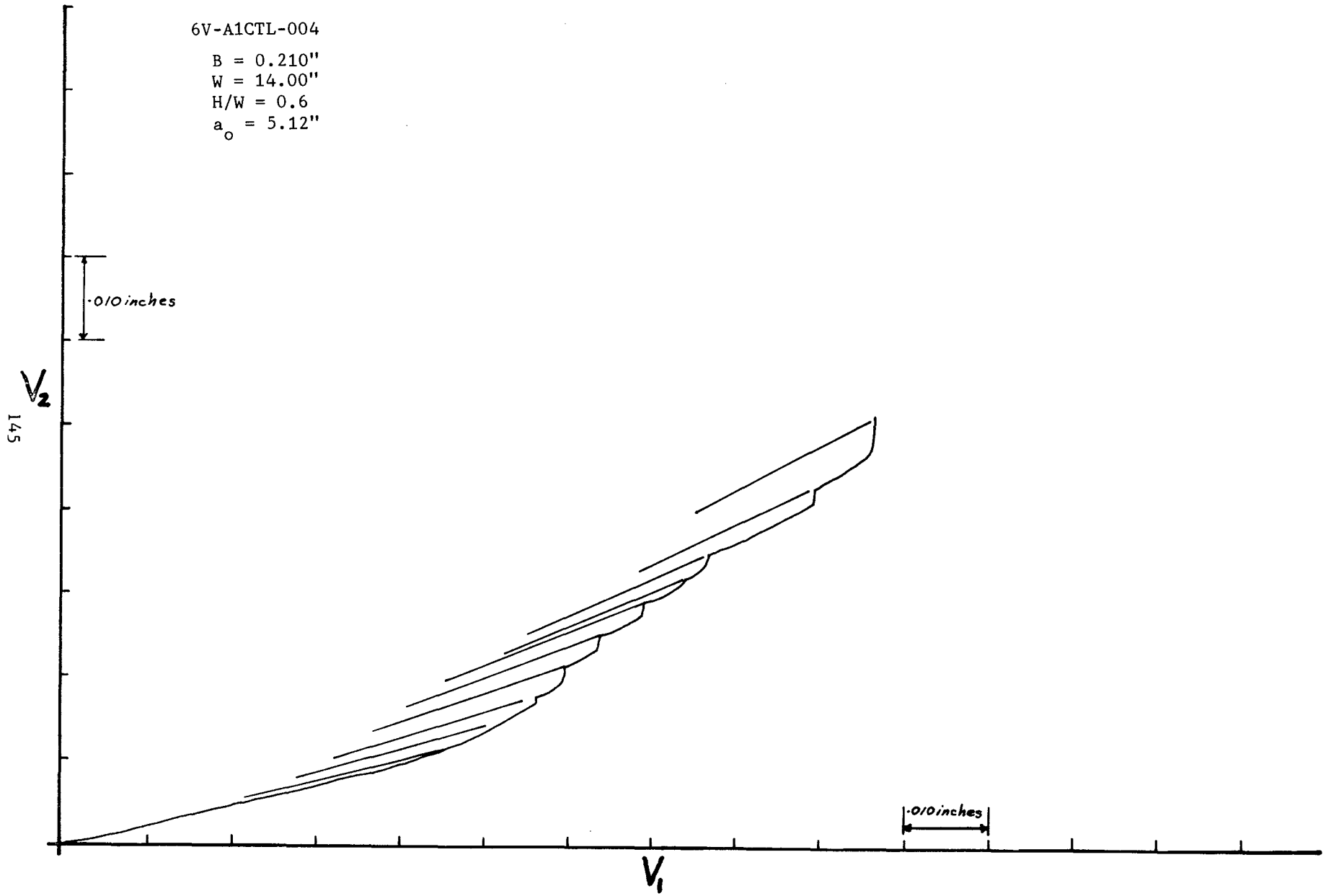

Figure 98. Deflection Curve - 0.210 Inch, Mill Annealed Ti-6Al-6V-2Sn (TL)

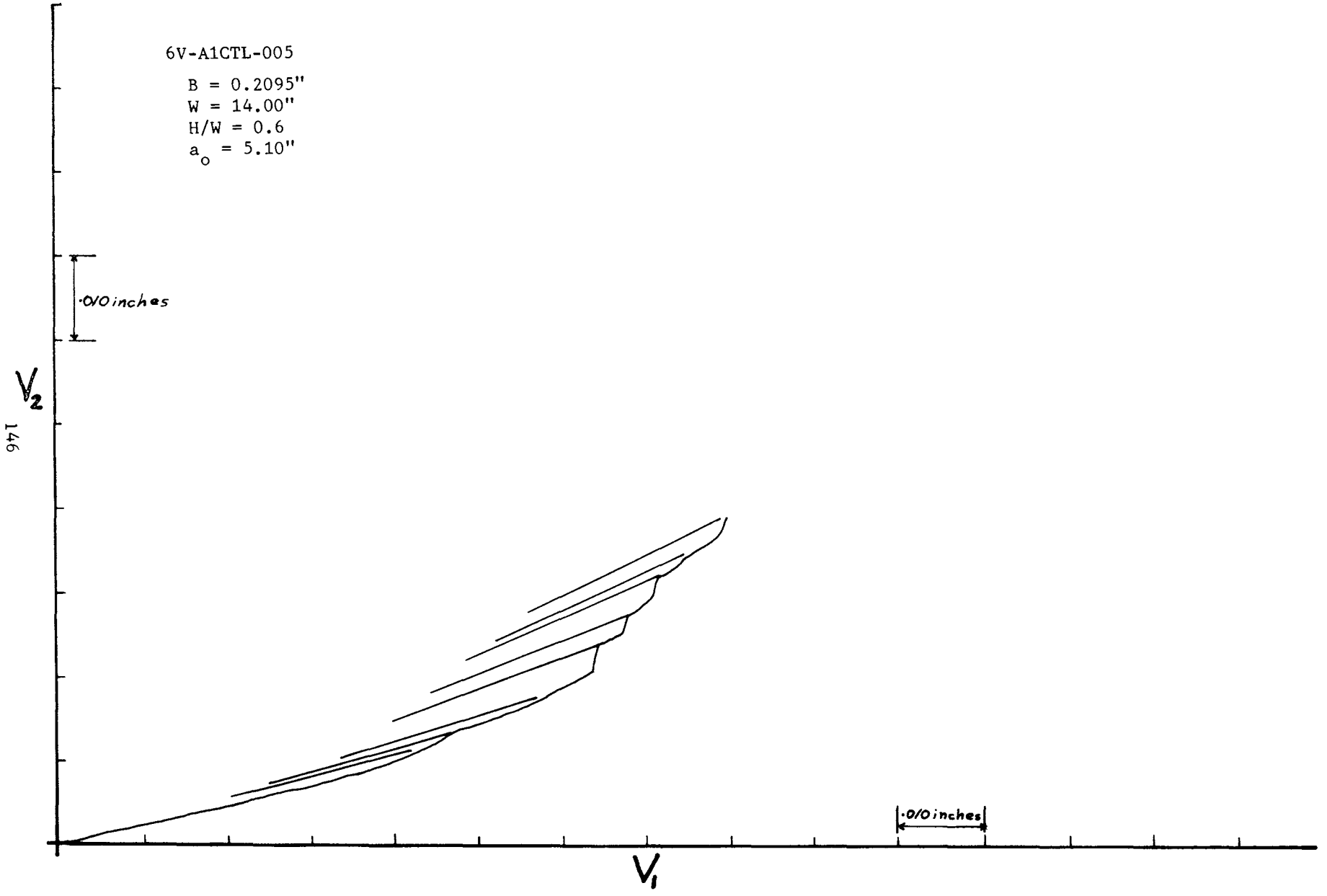

Figure 99. Deflection Curve - 0.2095 Inch, Mill Annealed Ti-6Aℓ-6V-2Sn (TL)

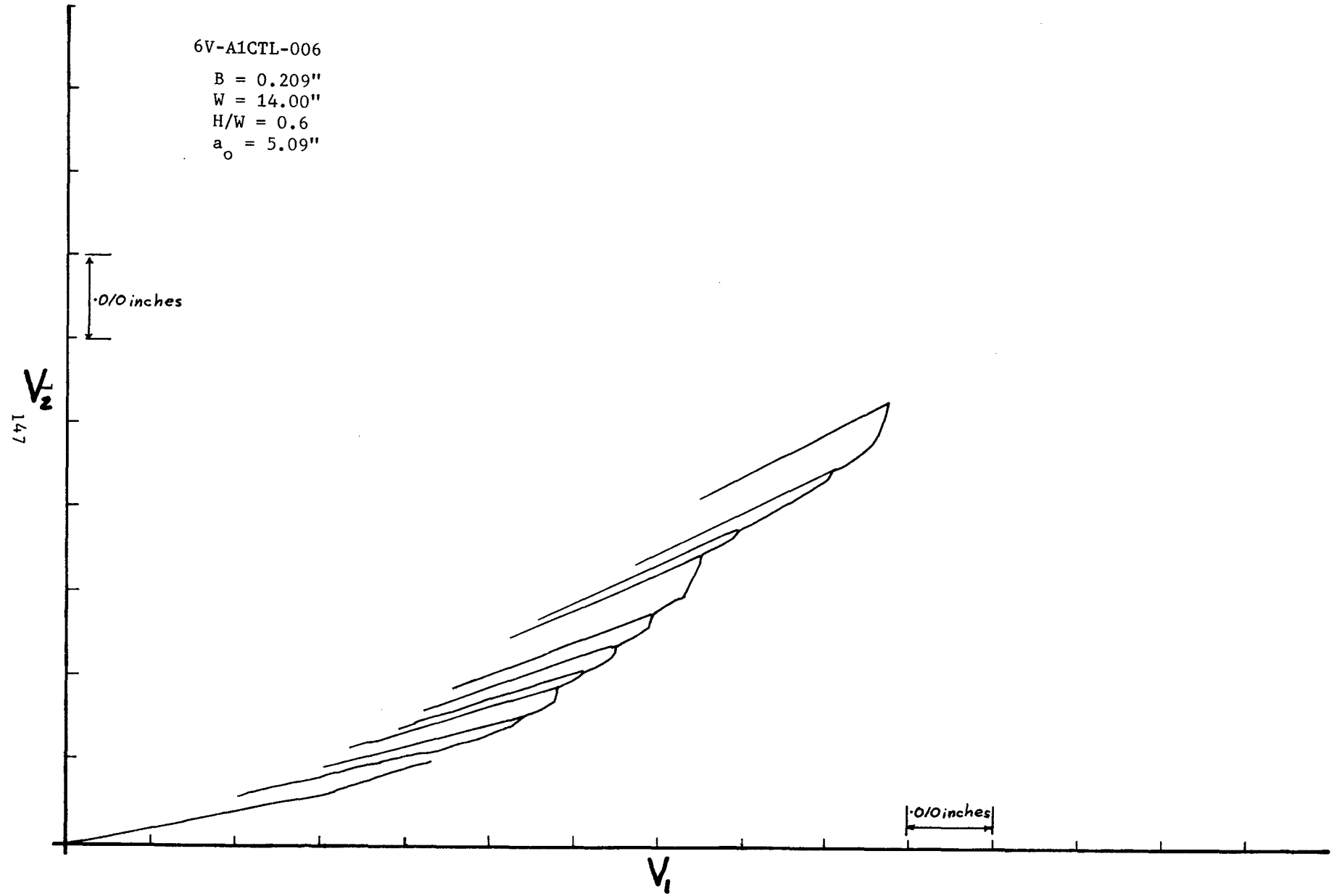

Figure 100. Deflection Curve - 0.209 Inch, Mill Annealed Ti-6Aℓ-6V-2Sn (TL)

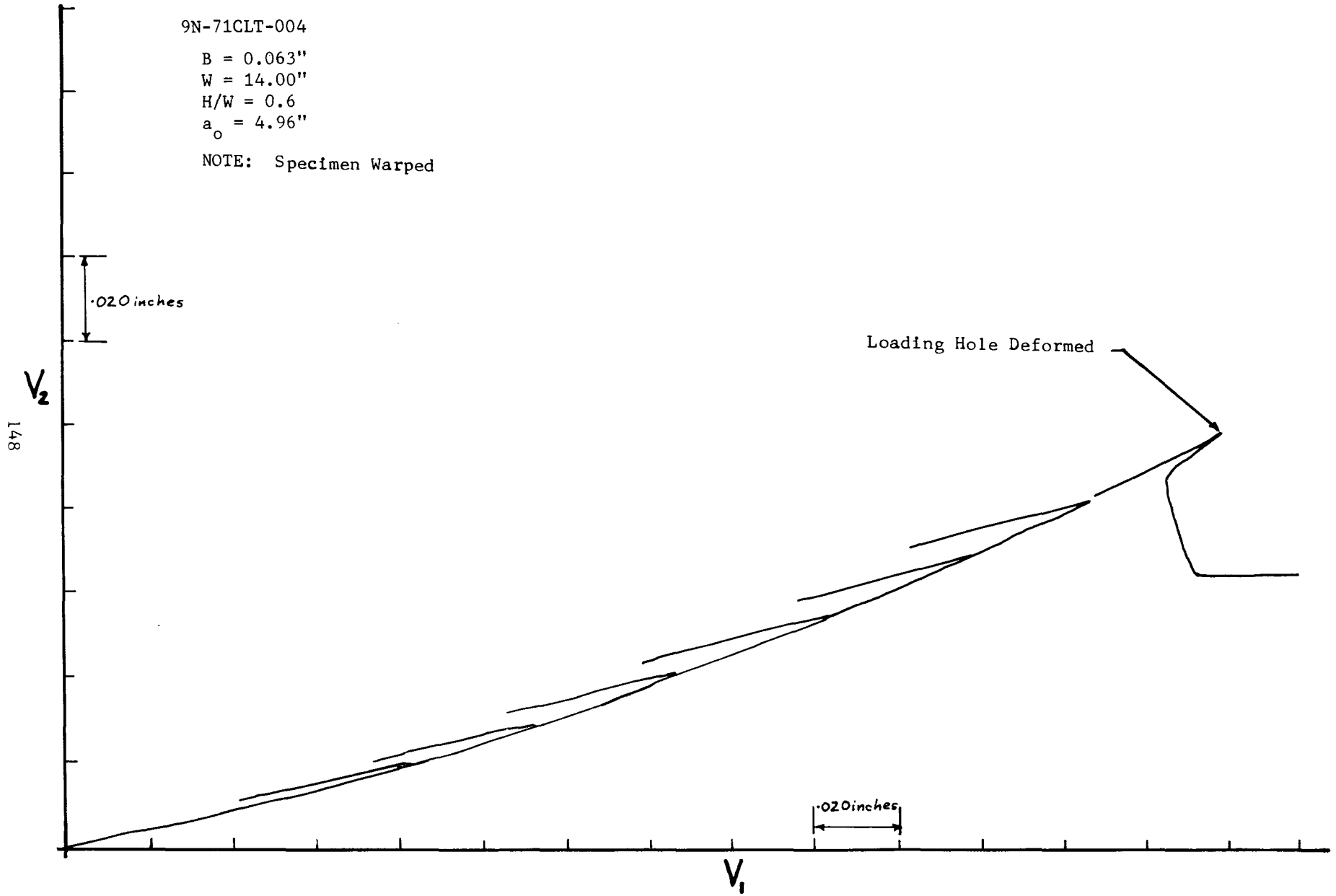

Figure 101. Deflection Curve - 0.063 Inch, 9Ni-4Co-.2C (LT)

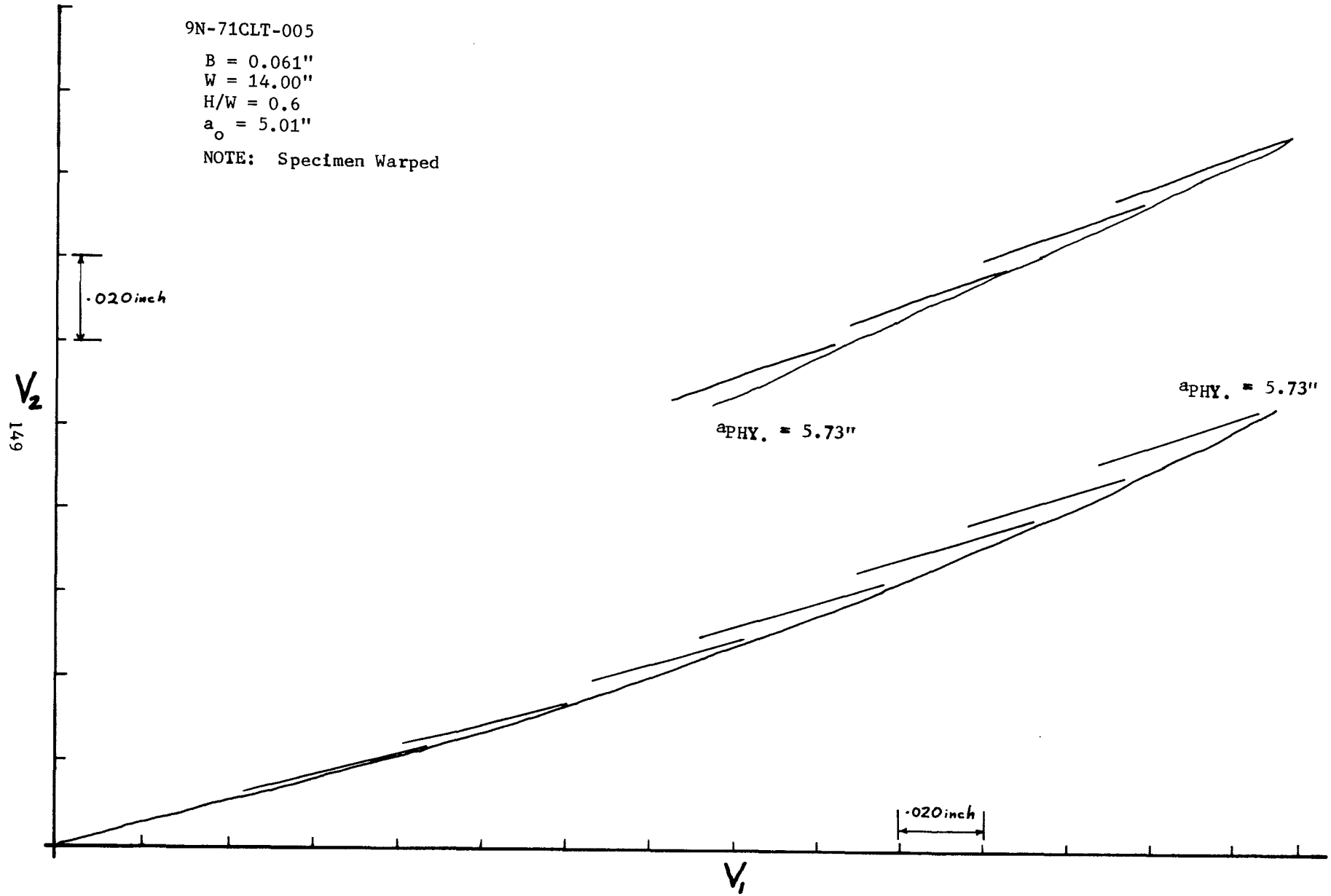

Figure 102. Deflection Curve - 0.061 Inch, 9Ni-4Co-.2C (LT)

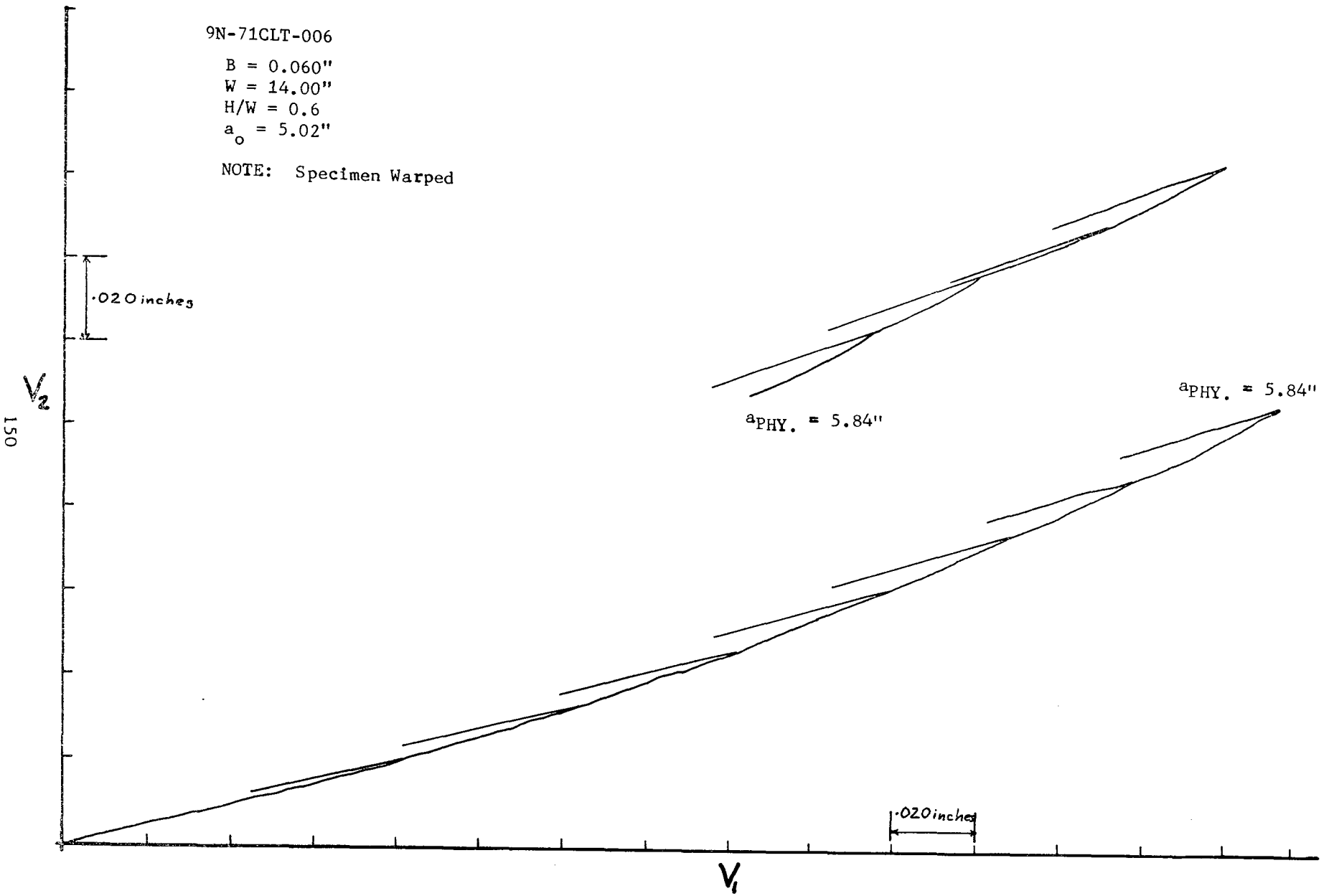

Figure 103. Deflection Curve - 0.060 Inch, 9Ni-4Co-.2C (LT)

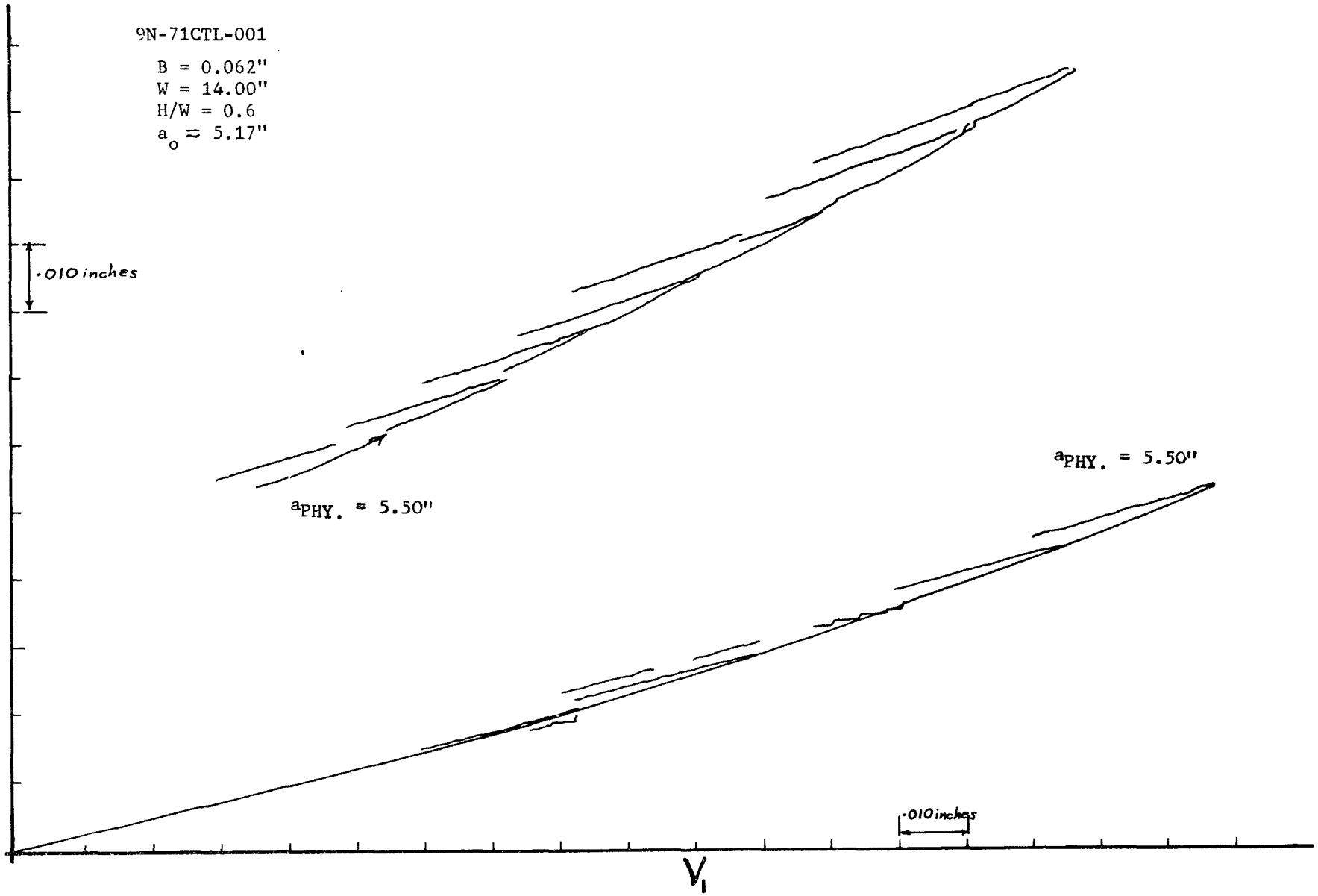

Figure 104. Deflection Curve - 0.062 Inch, 9Ni-4Co-.2C (TL)

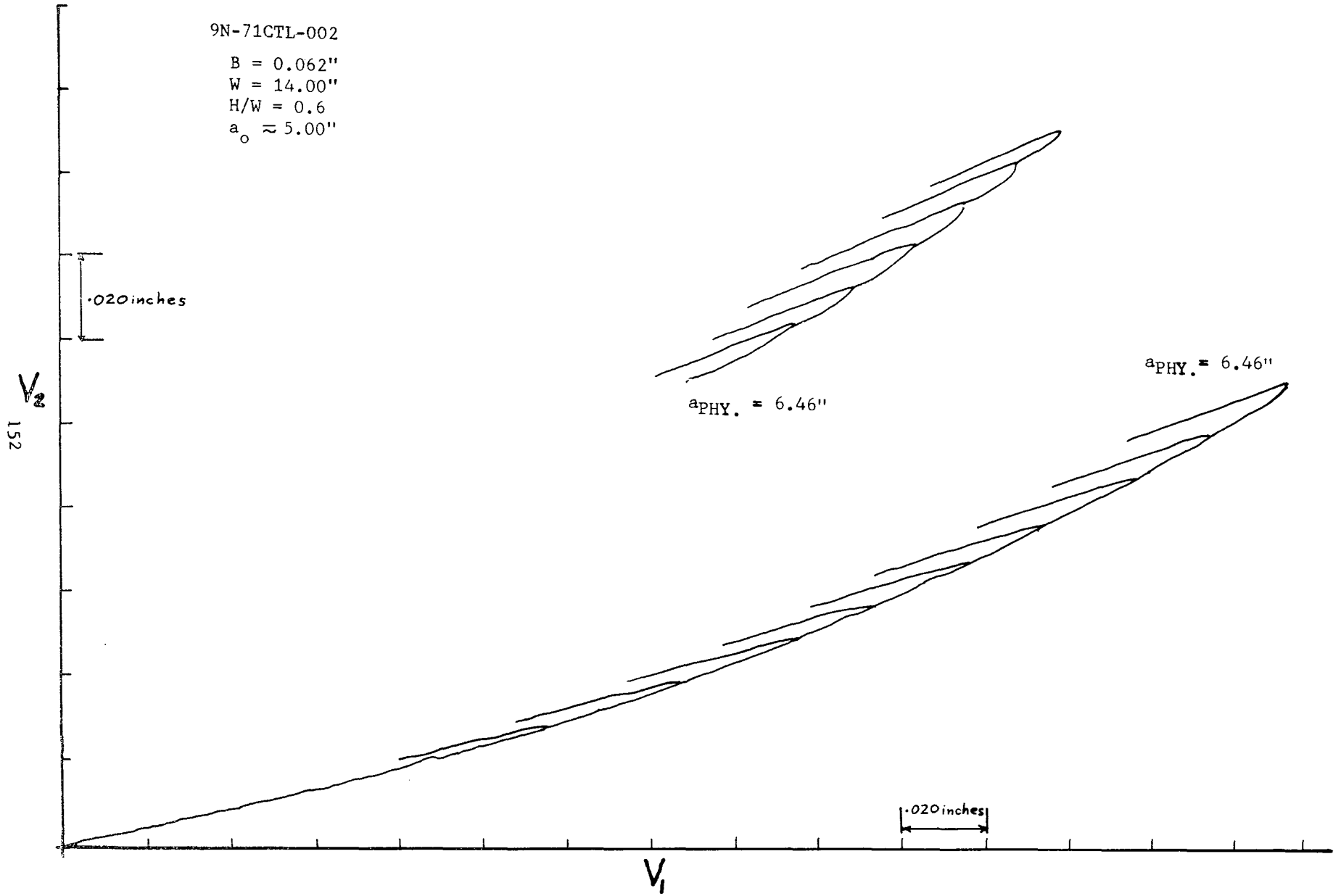

Figure 105. Deflection Curve - 0.062 Inch, 9Ni-4Co-.2C (TL)

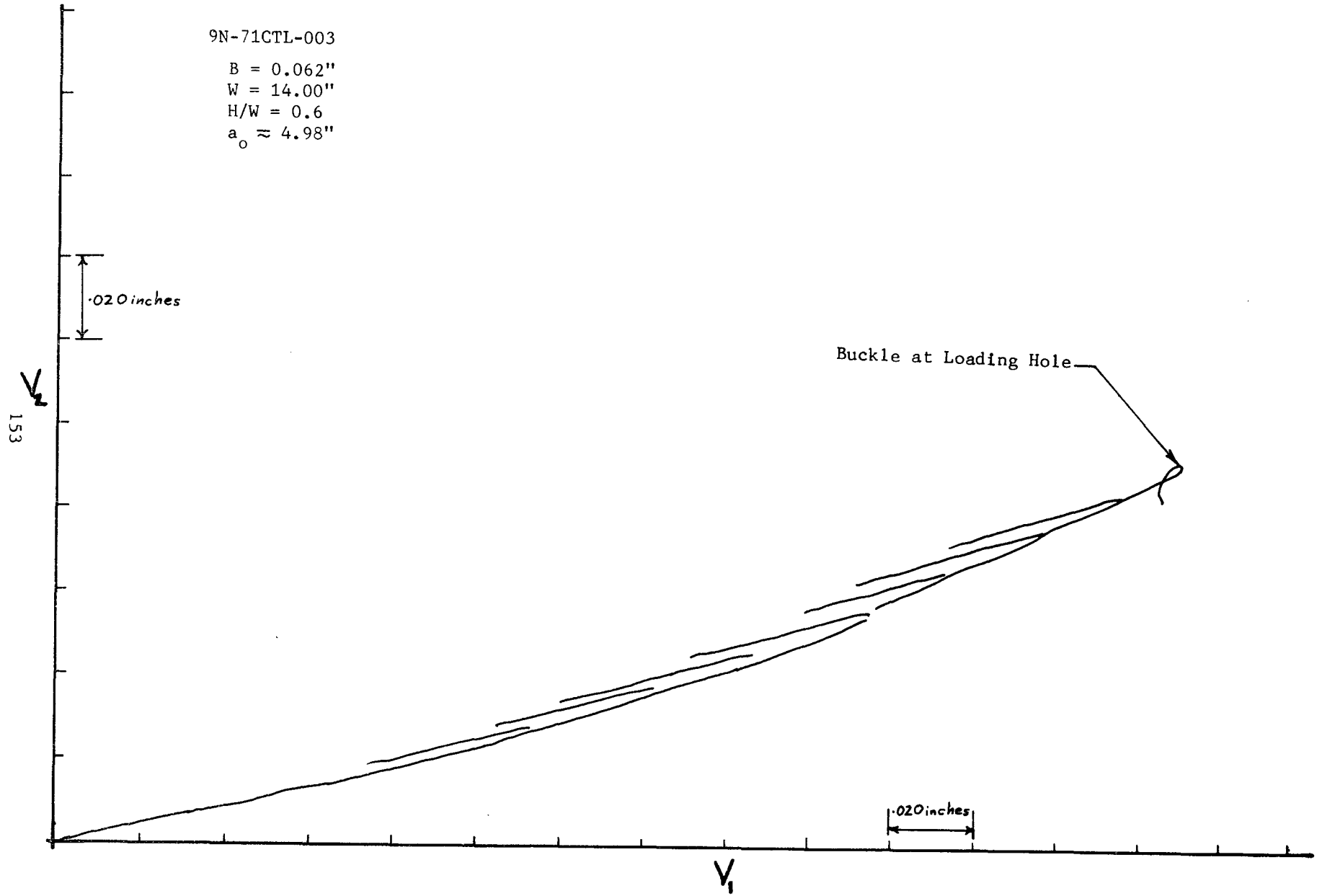

Figure 106. Deflection Curve - 0.062 Inch, 9Ni-4Co-.2C (TL)

VI CRACK GROWTH RESISTANCE DATA AND SPECIAL TEST SERIES

6.1 CALCULATION OF STRESS INTENSITY DATA FOR CRACK GROWTH RESISTANCE

The stress intensity equation employed for the CLWL specimen with semi-height (H) to width (W) ratio, H/W = 0.6 is from the following expression (see Reference 2):

$$K_R = \frac{P}{B\sqrt{W}}\left[29.6\left(\frac{a}{W}\right)^{1/2} - 185.5\left(\frac{a}{W}\right)^{3/2} + 655.7\left(\frac{a}{W}\right)^{5/2} - 1017.0\left(\frac{a}{W}\right)^{7/2} + 638.9\left(\frac{a}{W}\right)^{9/2}\right]. \quad (2$$

Here, K_R is the value of stress intensity (K) for crack growth resistance, a/W is the instantaneous value of crack length to specimen width ratio (either $\frac{a_{PHY.}}{W}$ or $\frac{a_{eff.}}{W}$ and P the corresponding value of maximum load at those selected values of a/W. The determination of a/W and P were explained previously in Section V and will not be repeated here.

As in the previous section, data will be presented by alloy class, fracture plane orientation and thickness. All data shown are based on physical crack extension, $\Delta a_{PHY.}$ and "effective" stress intensity. By "effective" stress intensity, it is meant the value of stress intensity associated with the maximum load (stress) and effective crack size which includes an artificial crack length or that increment which includes some result of crack tip plasticity. In other words, the value of K_R has been corrected for plasticity through use of the double compliance technique and is plotted as a function of physical (return slope determined) crack size. In all data, the value of a_o is the value of physical crack size (including fatigue precrack length) measured after specimen fracture.

6.1.1 K_R Data - Aluminum Alloys

Crack growth resistance data for 7075-T6 aluminum, .063 inch thick tested in the LT direction, are shown in Figure 107 and for the TL direction in Figure 108. Thicker 7075-T6 data are shown in Figures 109 and 110. It will be noted from Figures 107 and 108 that some experimentation was carried out on the configuration of the initial stress riser. It appeared that the scatter in the initial portion of the K_R curve could be attributed to the saw cut versus an electric discharge machined notch versus a natural fatigue starter crack. It was thus decided to fatigue precrack all subsequent CLWL specimens. In both the thin and thick LT specimen, it should be noted that deviation of the crack from a plane perpendicular to the loading axis precluded obtaining data beyond a $\Delta a_{PHY.}$ of approximately one inch (see Figures 107 and 109). However, even with this small amount of crack growth, a plateau level appears to have been reached which is approximately 20 to 30 percent higher than the TL test direction. As these data were some of the initial data obtained during the course of this phase of the program, the repeatability of the data of Figure 110 was quite encouraging.

Crack growth resistance data for 7075-T73 material (NOTE: This material is from the same lot as 7075-T6 and was batch-heat treated to the T73 condition) in the LT and TL direction for thin and thick gages are shown in Figures 111 - 114. As with the 7075-T6 material, change in crack direction (towards the rolling

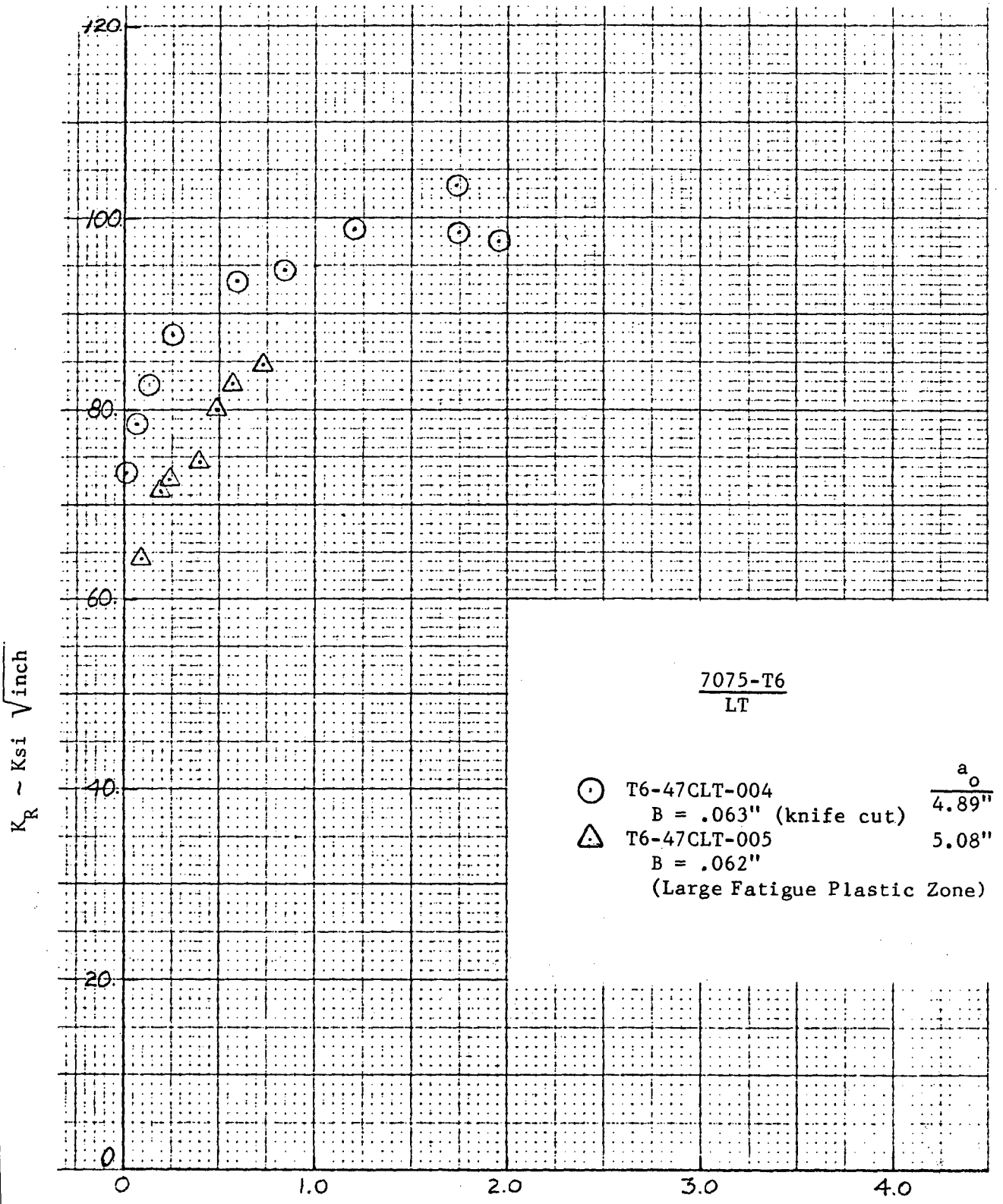

Figure 107. Crack Growth Resistance Data Based on Physical Crack Size - .063 Inch, 7075-T6 (LT)

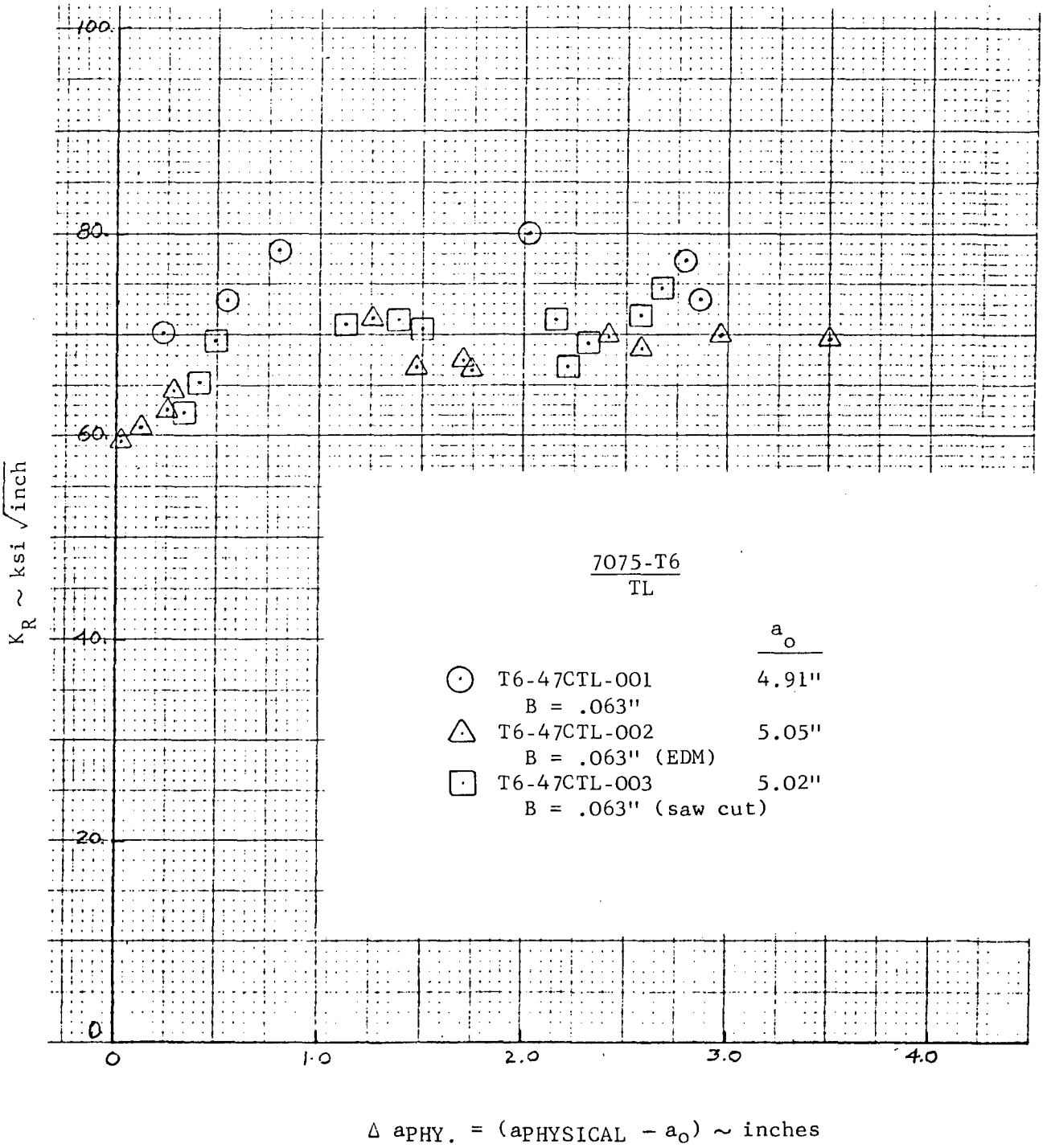

Figure 108. Crack Growth Resistance Data Based on Physical Crack Size - .063 Inch, 7075-T6 (TL)

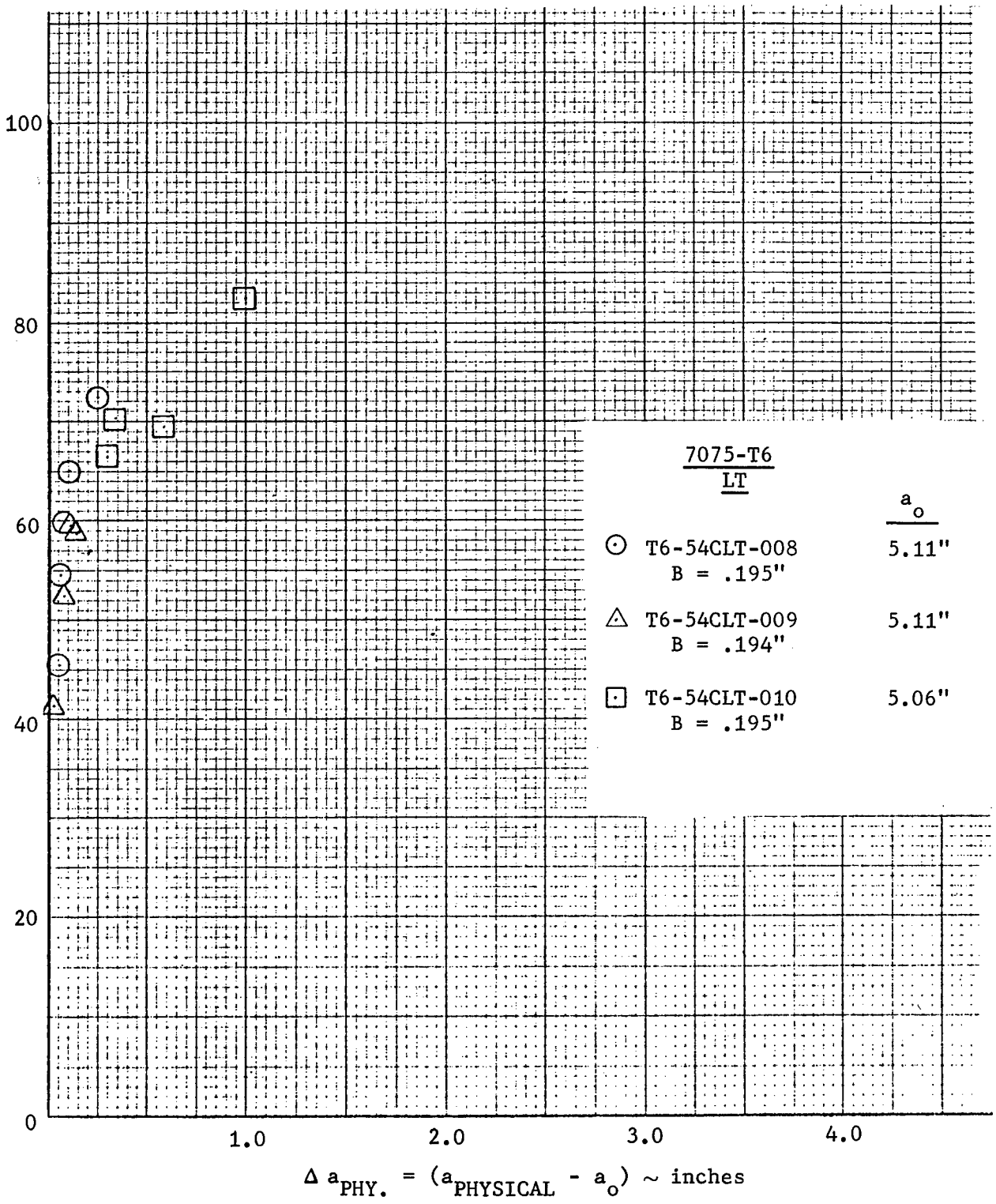

Figure 109. Crack Growth Resistance Based on Physical Crack Size - .195 Inch, 7075-T6 (LT)

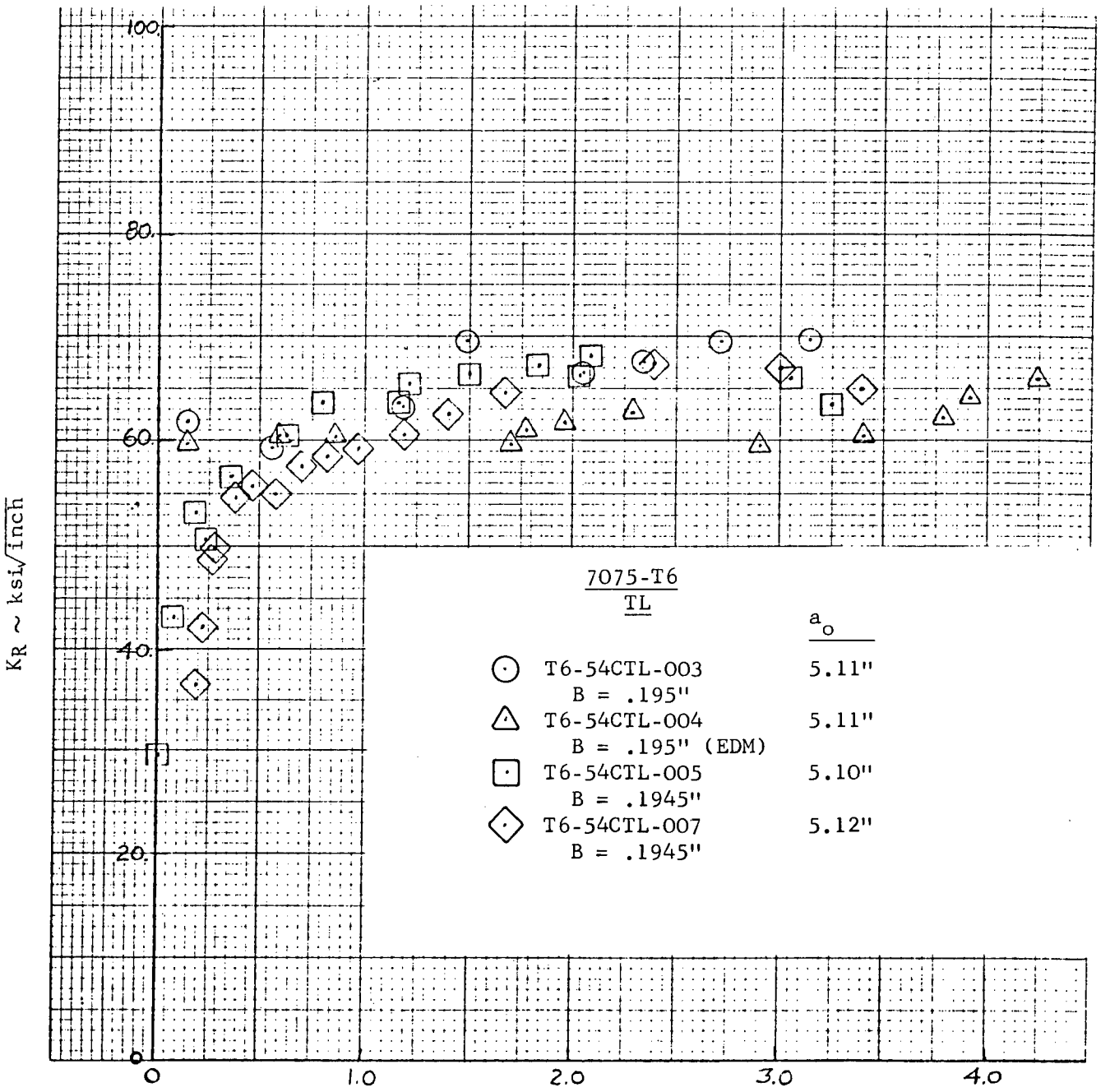

Figure 110. Crack Growth Resistance Data Based on Physical Crack Size - .195 Inch, 7075-T6 (TL)

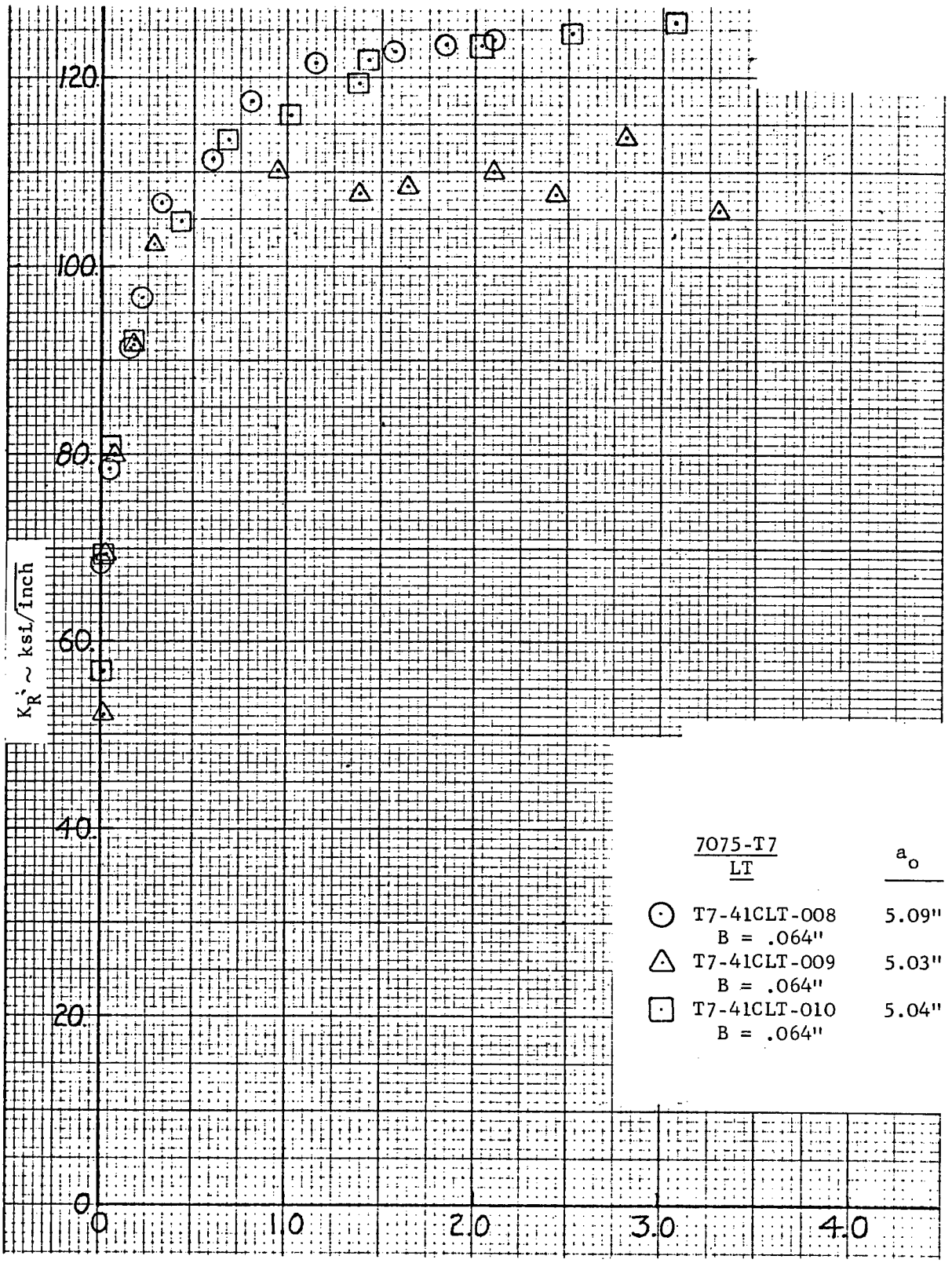

Figure 111. Crack Growth Resistance Data Based on Physical Crack Size - .064 Inch, 7075-T7 (LT)

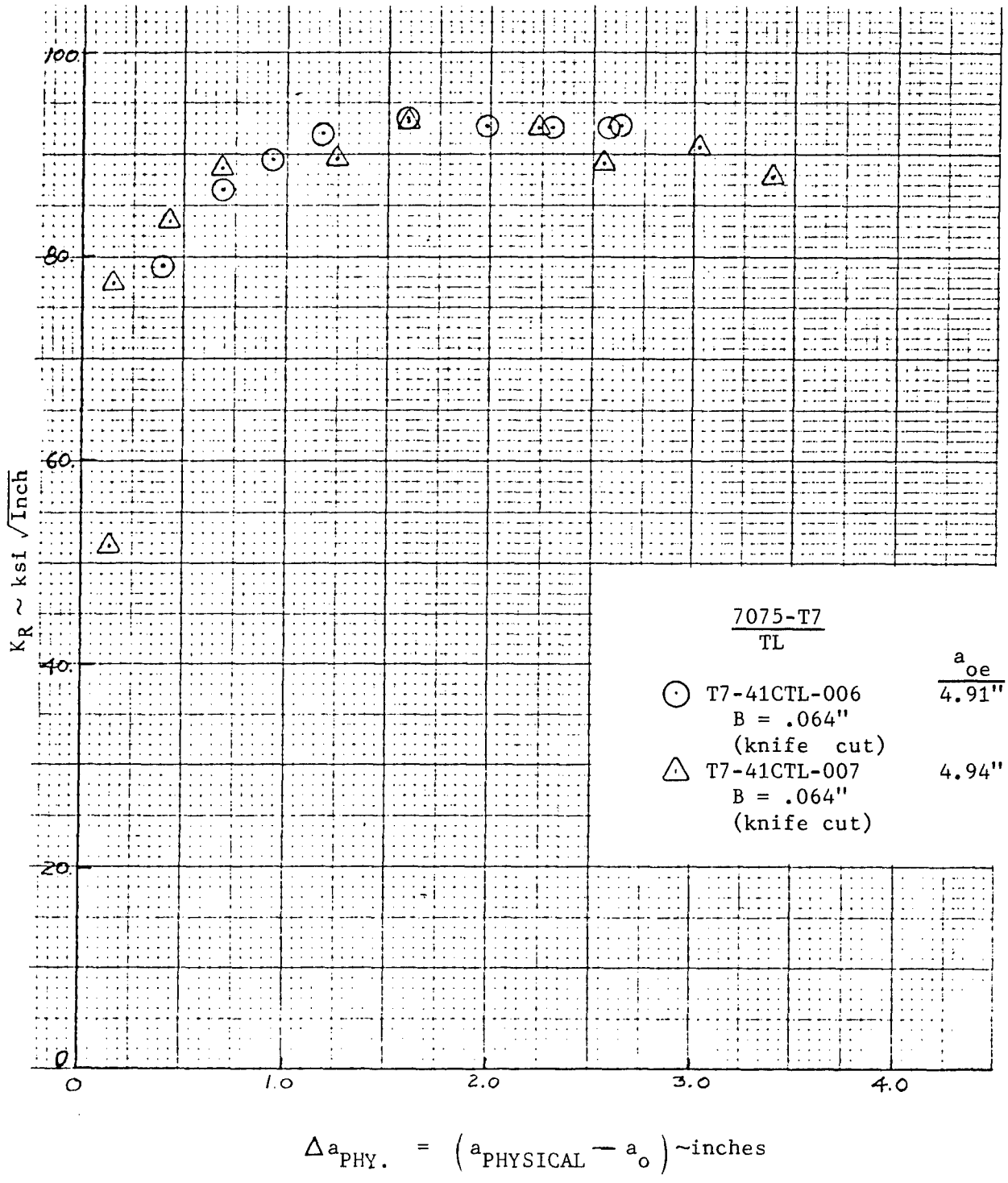

Figure 112. Crack Growth Resistance Data Based on Physical Crack Size - .064 Inch, 7075-T7 (TL)

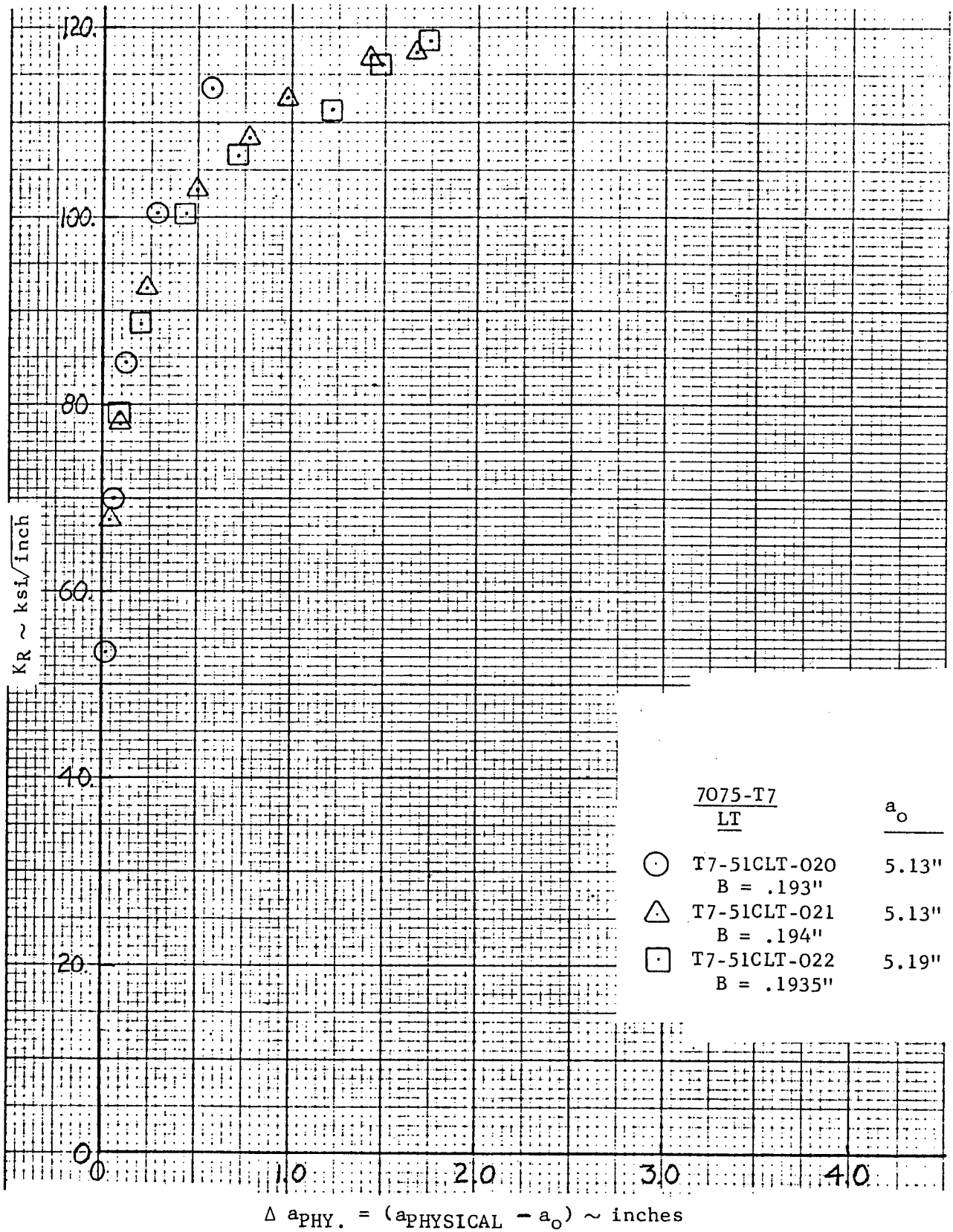

Figure 113. Crack Growth Resistance Data Based on Physical Crack Size - .195 Inch, 7075-T7 (LT)

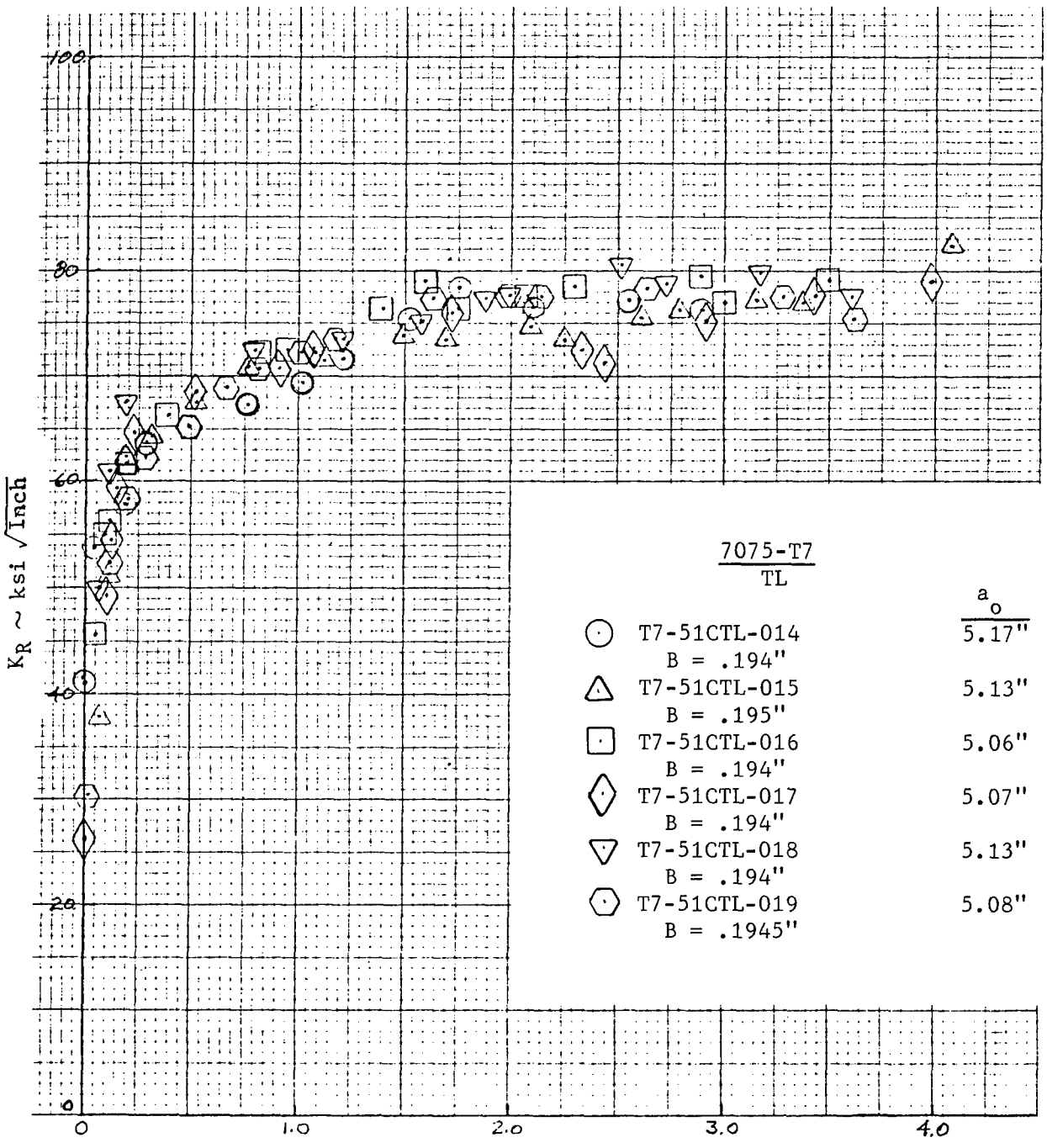

$$\Delta a_{PHY.} = \left(a_{PHYSICAL} - a_o\right) \sim \text{inches}$$

Figure 114. Crack Growth Resistance Data Based on Physical Crack Size - .195 Inch, 7075-T7 (TL)

direction) was noted for each thick specimen after 1 to 1½ inches of crack extension (see Figure 113). However, the deviation trend was less pronounced in this heat treatment (T7 versus T6) and took place over a longer crack length - eventually reaching a maximum of approximately 45 degrees to the original crack plane. Whereas the 7075-T6 material in the same thickness showed crack deviation of 90 degrees to the original fatigue crack direction after small amounts (0.75 inch) of crack extension.

As part of a separate study of preferred crack direction which will be explored deeper later in this section, the effect of side (or face) grooving was examined as a method of containing the crack in a plane normal to the loading axis. In addition, it was felt that the highly textured nature of the original material (7075-T6) was causing the crack to deviate when tested in the LT direction. To determine if this was a contributing factor, a specimen of 7075-T651 (B = 0.195 inch) was examined by x-ray diffraction which indicated the relative intensities of the (200) and (111) crystrallographic directions. These results indicated that the number of grains oriented in the (200) direction was higher than the (111) direction. For comparative purposes, a specimen of 2024-T351 was also examined in the same manner since crack deviation was not a problem in the LT direction for that material. These x-ray data indicated an opposite trend; i.e., more (111) than (200). It was thus concluded that texturing was the primary cause of the tendency for the crack to follow the rolling direction in the 7075 (0.195 inch) material. By going through the -T73 heat treatment, some of the texturing is reduced and the tendency for the crack to follow the rolling direction is still there, but to a lesser degree.

The 0.063 inch, 7075-T73 crack growth resistance data are shown in Figures 111 and 112. It will be noted that with the exception of specimen T7-41CLT-009 (Figure 111), there is little scatter in the data. Specimen T7-41CLT-009 had crack extension which angled after an initial extension of 0.8 inch of physical growth. This fact is reflected in the data of Figure 111, whereas the other two specimens (-008 and -010) did not show crack deviation until the crack aspect ratio, (a/W), was >0.5.

Figures 115-118 contain all of the K_R data from the 2024-T3 aluminum alloy sheet and plate. There was no tendency for the crack to deviate from its initial plane for the thicker specimens (Figure 117). The repeatability of data for both thicknesses is good and a plateau level of toughness of approximately 150-160 ksi inch is being reached for thin (0.063) material in the LT direction.

It will be noted that there is a spread in data at the longer crack extensions. Some slight angling of the crack ($< 15°$) did take place at a/W's greater than 0.5 for the thinner gage material. However, it is thought that a combination of back edge buckling caused by both specimen "hinging" and plastic zone-back edge interaction also contribute to this long crack length scatter. In fact, it is believed that these interactions are the principal cause of crack deviation, for the thinner gage 2024 material, due to the large plastic zones at the longer crack lengths.

The crack growth resistance data for the chem milled material are shown in Figure 119 for the LT direction and the TL direction in Figure 120. This

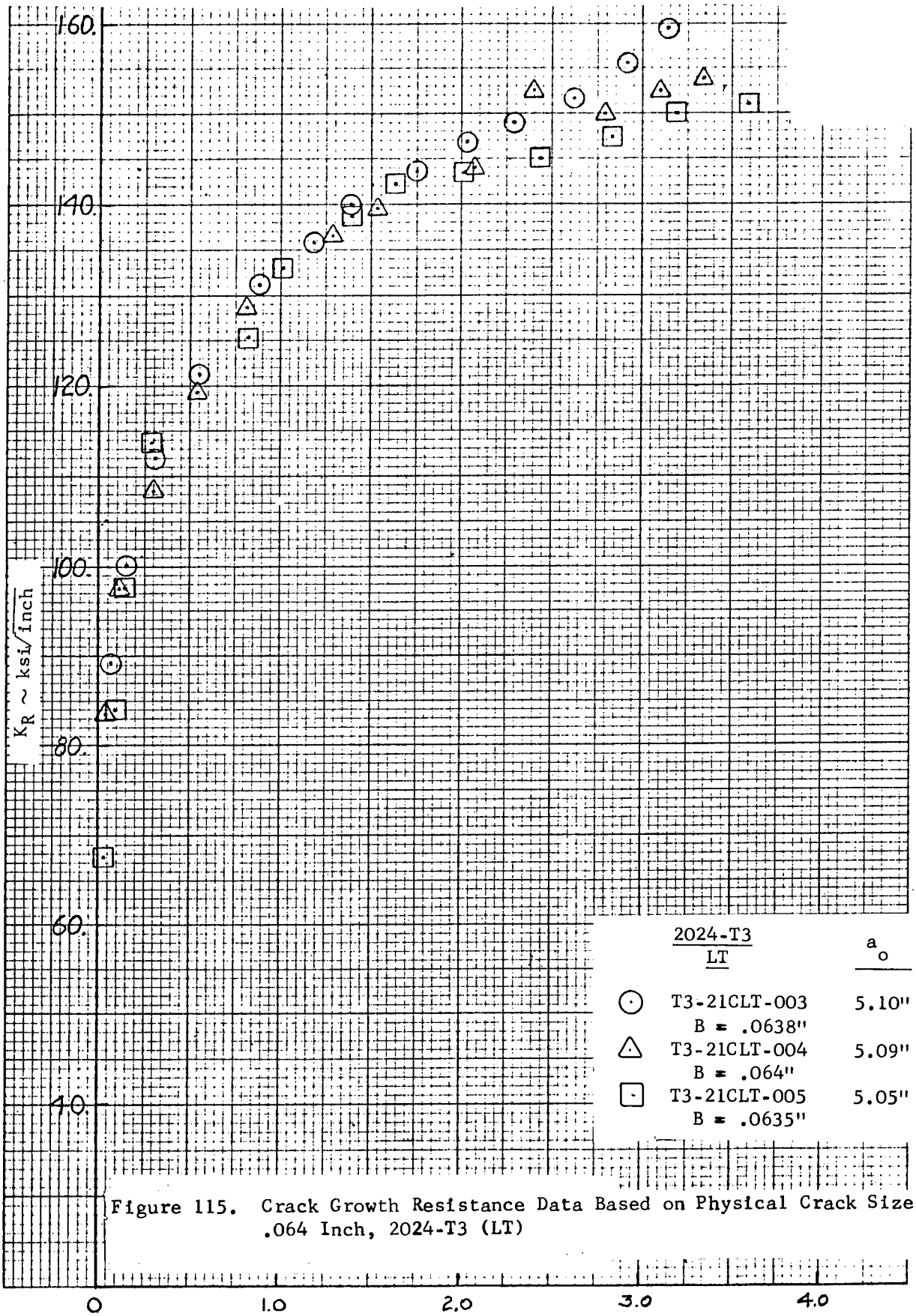

Figure 115. Crack Growth Resistance Data Based on Physical Crack Size - .064 Inch, 2024-T3 (LT)

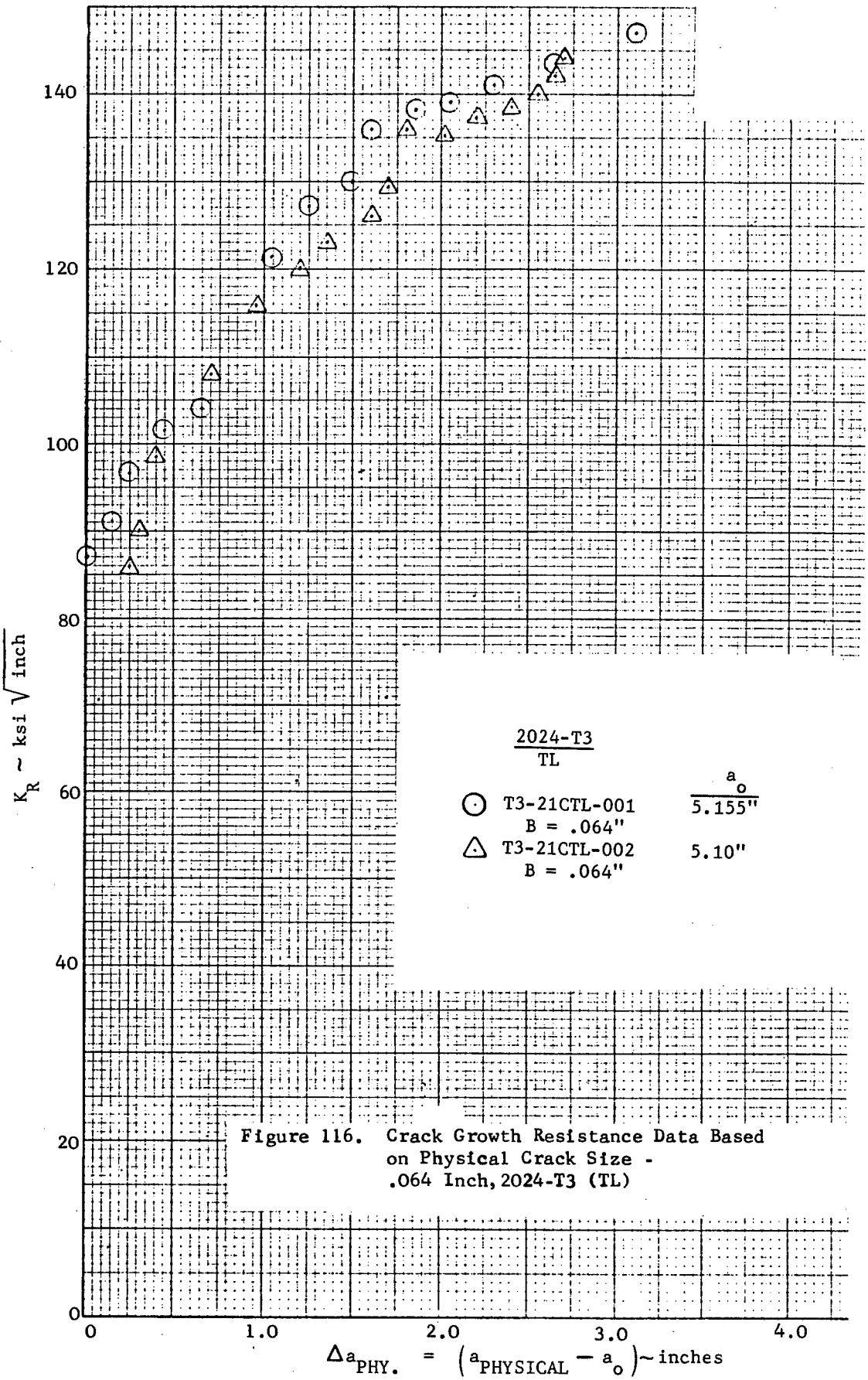

Figure 116. Crack Growth Resistance Data Based on Physical Crack Size - .064 Inch, 2024-T3 (TL)

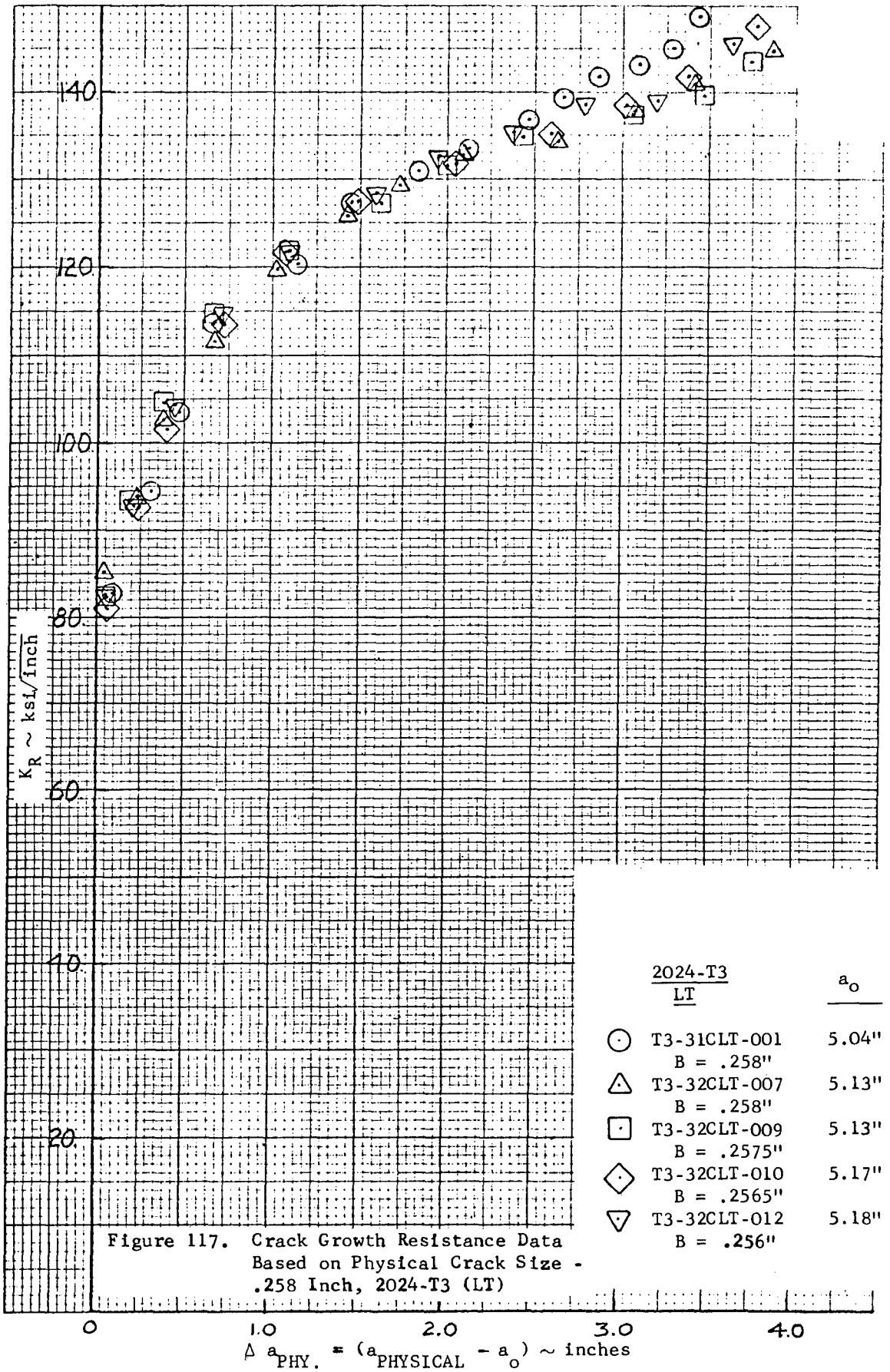

Figure 117. Crack Growth Resistance Data Based on Physical Crack Size - .258 Inch, 2024-T3 (LT)

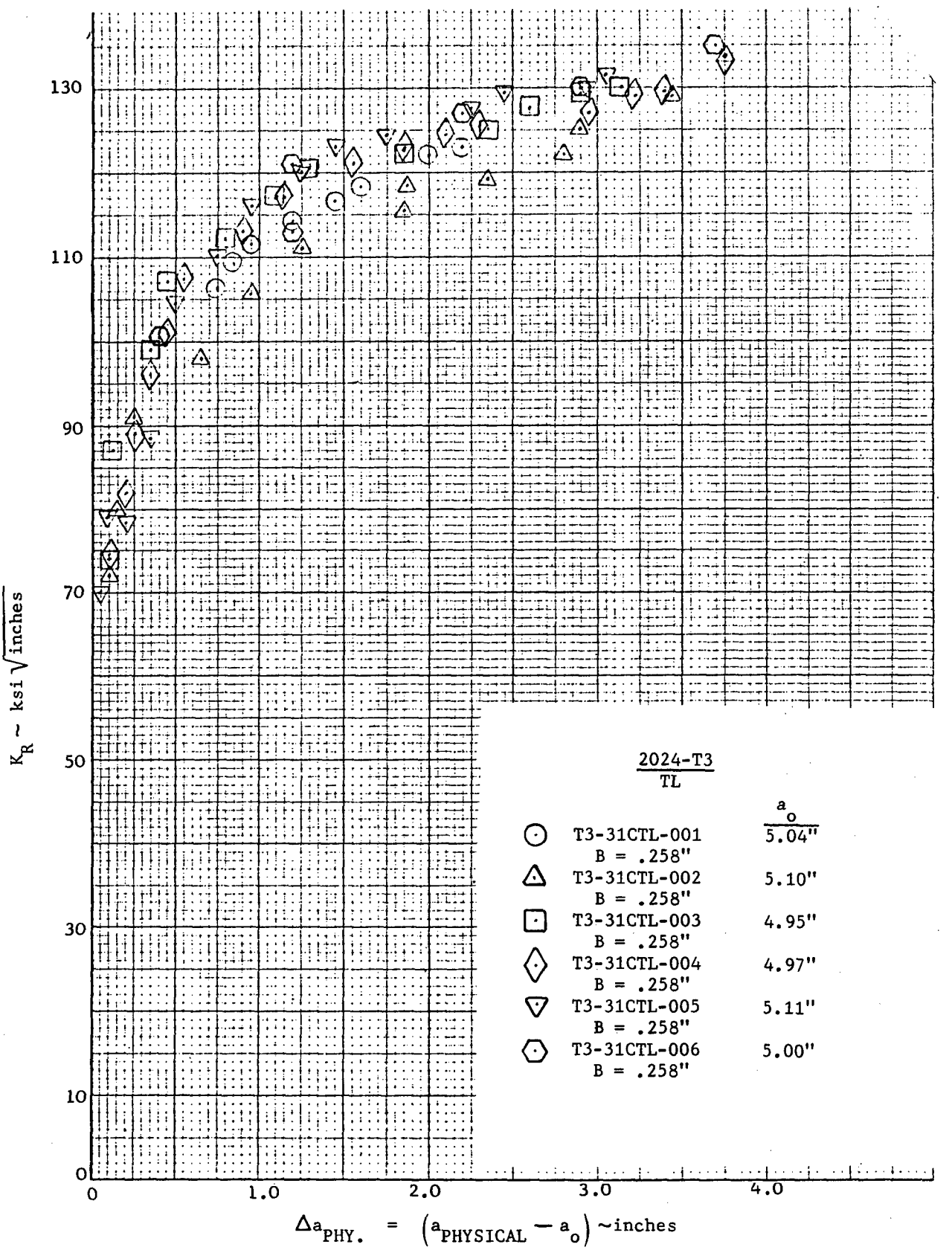

Figure 118. Crack Growth Resistance Data Based on Physical Crack Size - .258 Inch, 2024-T3 (TL)

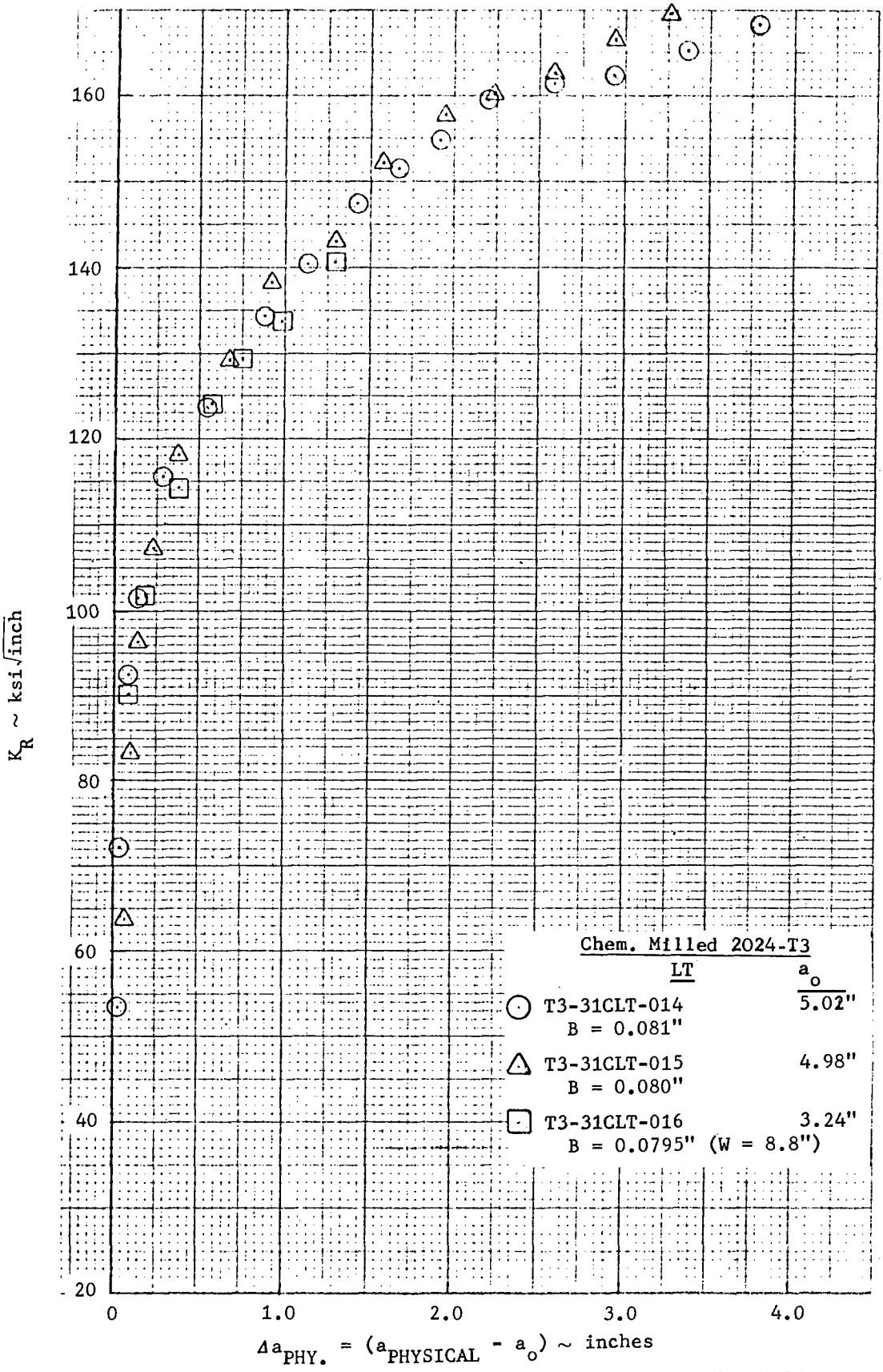

Figure 119. Crack Growth Resistance Data Based on Physical Crack Size - .08 Inch, Chem. Milled 2024-T3 (LT)

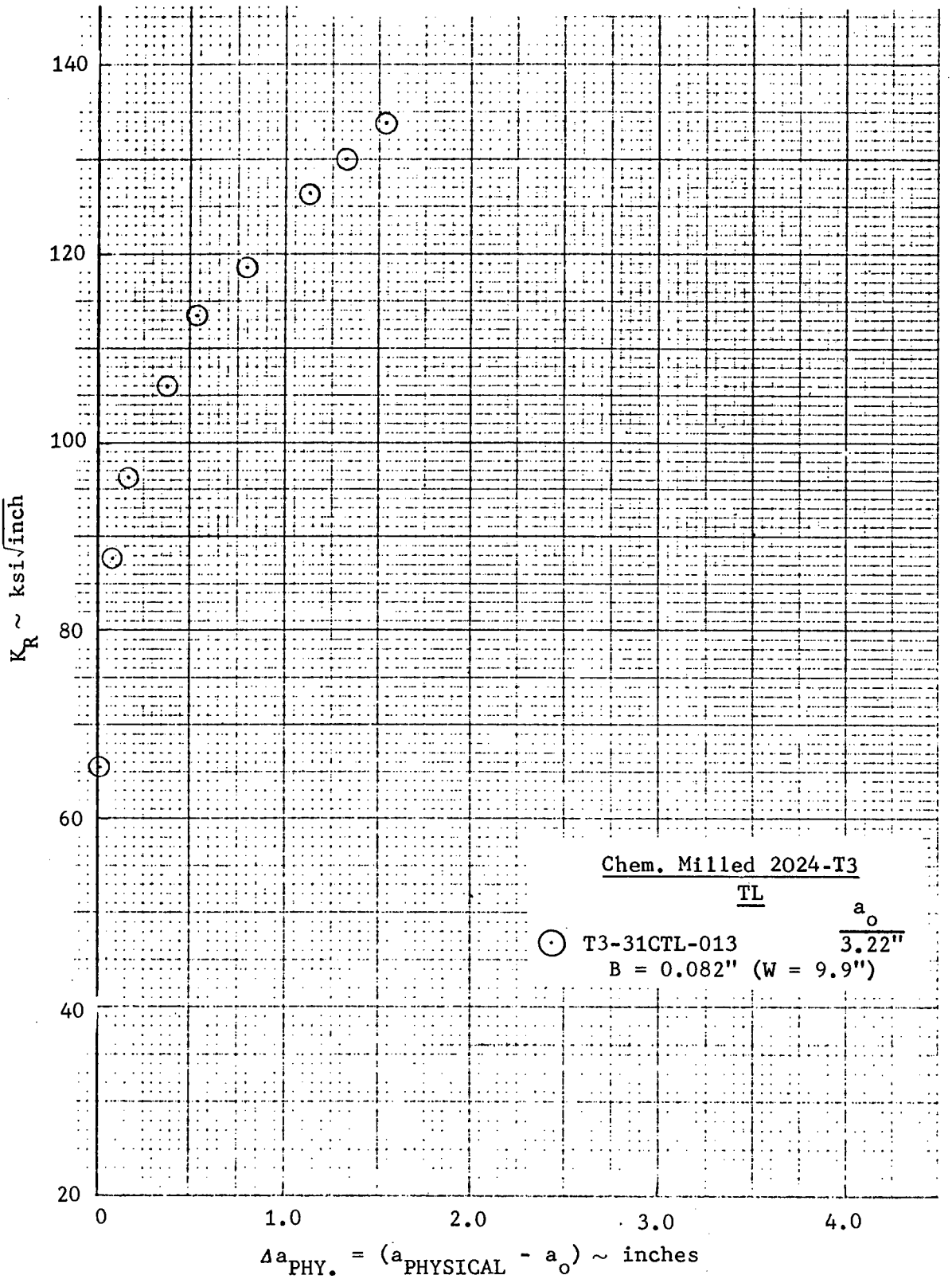

Figure 120. Crack Growth Resistance Data Based on Physical Crack Size - .08 Inch, Chem. Milled 2024-T3 (TL)

material was chem milled from the -31 piece (0.258 inches thick) by removing area from one face only. The data from Figure 119 was used as an integral part in analysis of the zee stiffened panels reported on in Volume I of this report.

6.1.2 K_R Data - Titanium Alloys

The beta mill annealed Ti-6Al-4V crack growth resistance data are shown in Figures 121-124.. The 0.053 inch gage material shows excellent repeatability for both the LT (Figure 121) and TL (Figure 122) directions. In Figure 123, it will be noted that specimen 4V-87CLT-012 does not follow the pattern of the other three specimens. A behavior typical of most of the more preferred directional materials of this study occurred; i.e., angling of the crack away from its original plane. These data have been included here to point out the differences in K_R data possible from a given plate of material. It can be seen, however, that the weak direction data (Figure 124) give consistent results where crack deviation was not a problem. It must also be pointed out that some of the thicker gage specimens (noteably 4V-87CLT-012, -014 and 4V-87CTL-008) were tested in a bowed condition where the bow was normally perpendicular to the crack.

Figures 125 and 126 show the CLWL, K_R data for the 0.062 inch thick Ti-6Al-6V-2Sn (mill annealed) material tested in the LT and TL direction. Extreme banding of the K_R data is noted for the LT direction data (see Figure 125). Specimens 6V-11CLT-007 and -009 had crack progression in a zig-zag fashion after approximately one half inch of crack extension. The crack deviated at 20 degree angles and could account for the scatter in the data. Specimen -008 (Figure 125) did not have a propensity for the crack to zig-zag and showed less than 10 degrees of angling and could explain the higher values of K_R for this specimen.

NOTE: The fact that physical crack size is determined from a return slope compliance relationship based on assumed straight line crack progression would lead to scatter for any data taken on any specimen where angling occurs. Projection of the crack back to the load line does not appear to alleviate the problem which is compounded by having a mixture of mode I and II crack progression when angling occurs. Further discussion of this problem and possible means of obtaining crack growth resistance data in materials and fracture plane orientations which show a propensity towards angling will be discussed later in this section.

It can be noted from the data of Figure 126 that the TL data does not appear to have the banding which occured in the LT data of Figure 125. Two specimens of this data set showed crack angling of approximately 20 degrees after 0.4 inches of crack extension, 6V-11-CTL-002 and -004. It can be noted that these specimen data are above and below the band of the other three specimens.

K_R data for the LT and TL direction for Ti-6Al-6V-2Sn, 0.20 thick, are given in Figures 127 and 128. One observation was made during the testing of the thicker specimens of Figure 128 which was unexpected. It was observed that after an a/W of .45 to .5 is reached, angling of the crack took place (approximately 20 degrees or less) from the plane normal to the loading direction. This is the

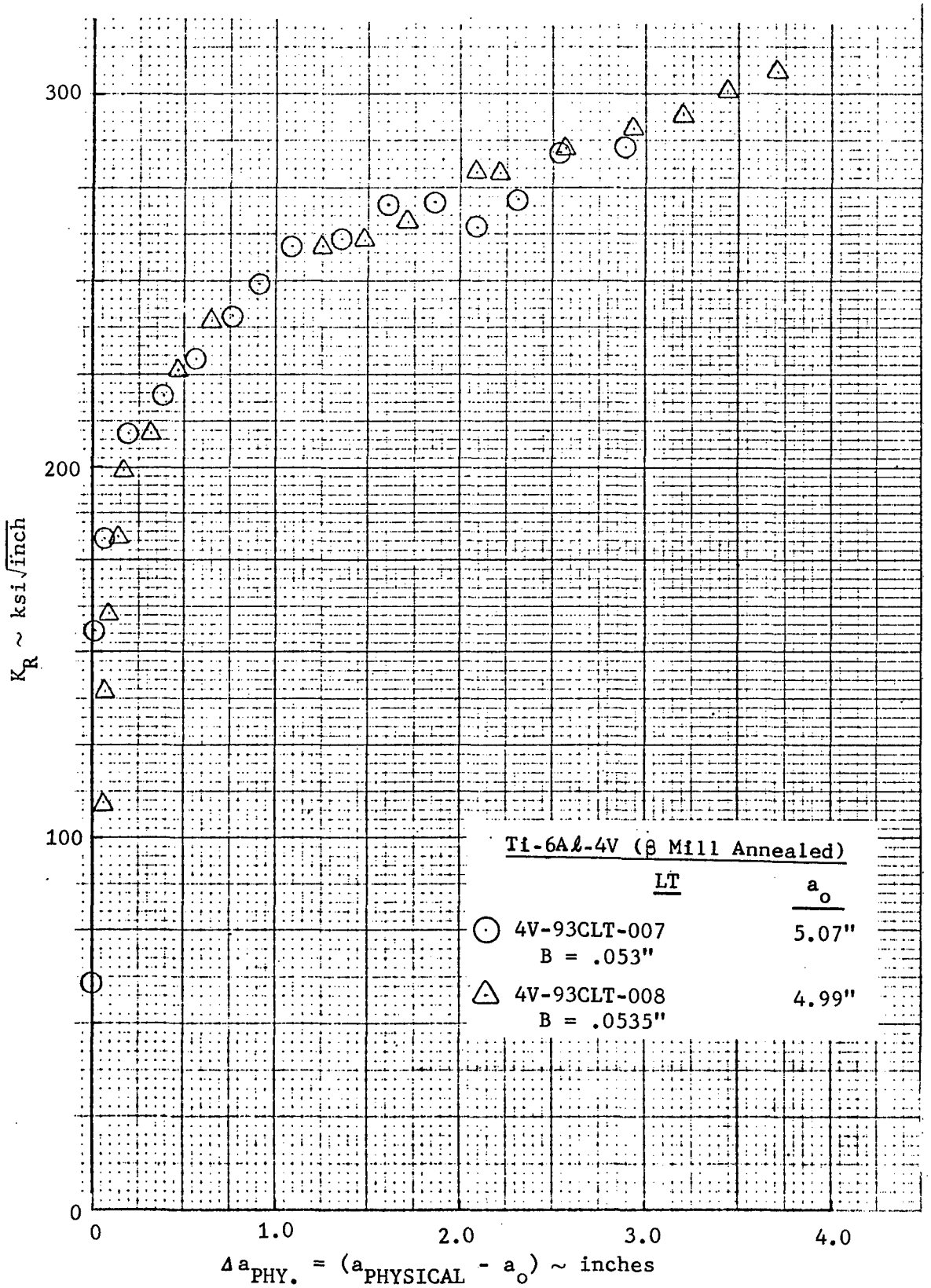

Figure 121. Crack Growth Resistance Data Based on Physical Crack Size - .053 Inch, Ti-6Aℓ-4V (β Mill Annealed) (LT)

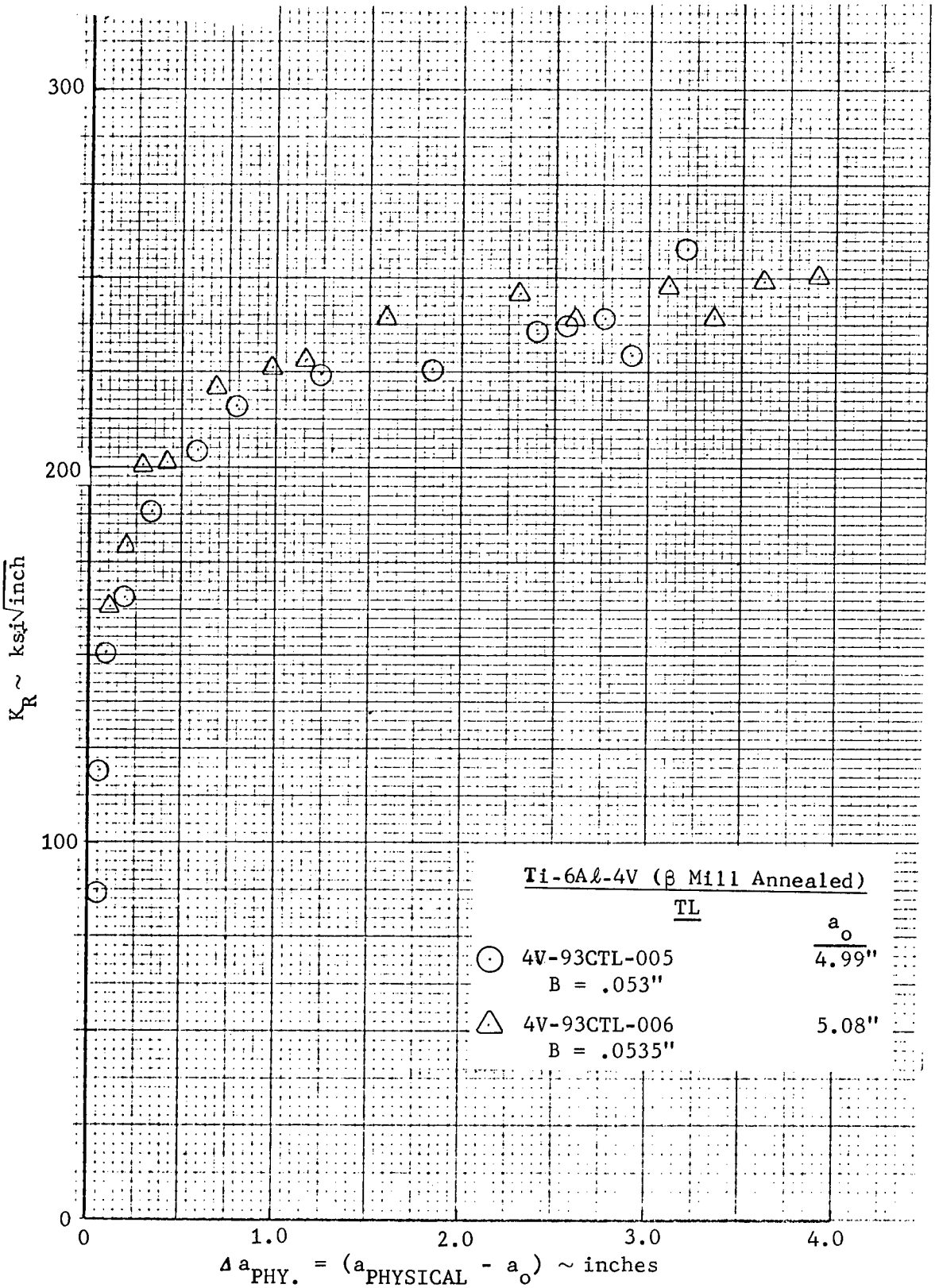

Figure 122. Crack Growth Resistance Data Based on Physical Crack Size - .053 Inch, Ti-6Aℓ-4V (β Mill Annealed) (TL)

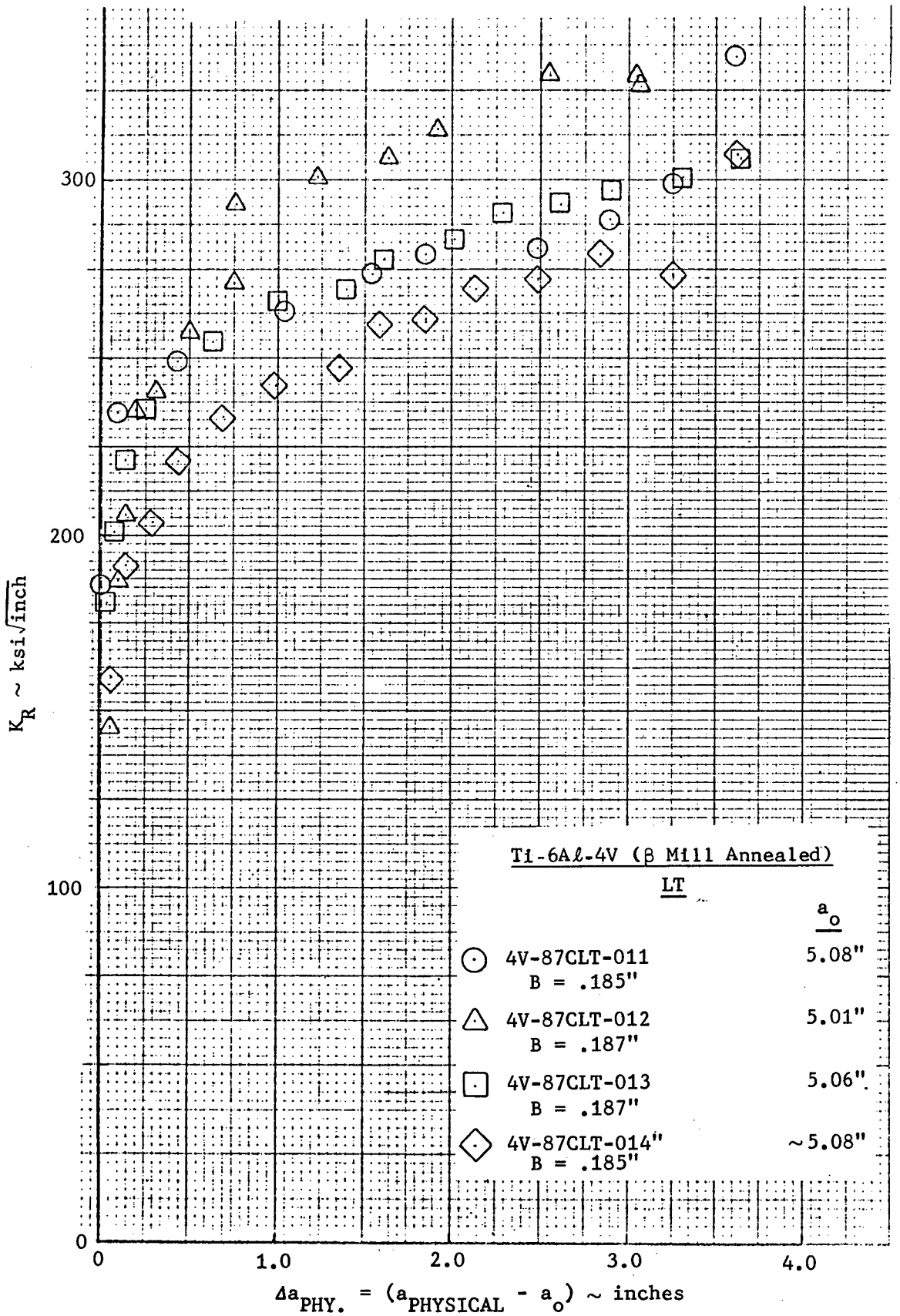

Figure 123. Crack Growth Resistance Data Based on Physical Crack Size - .185 Inch, Ti-6Aℓ-4V (β Mill Annealed) (LT)

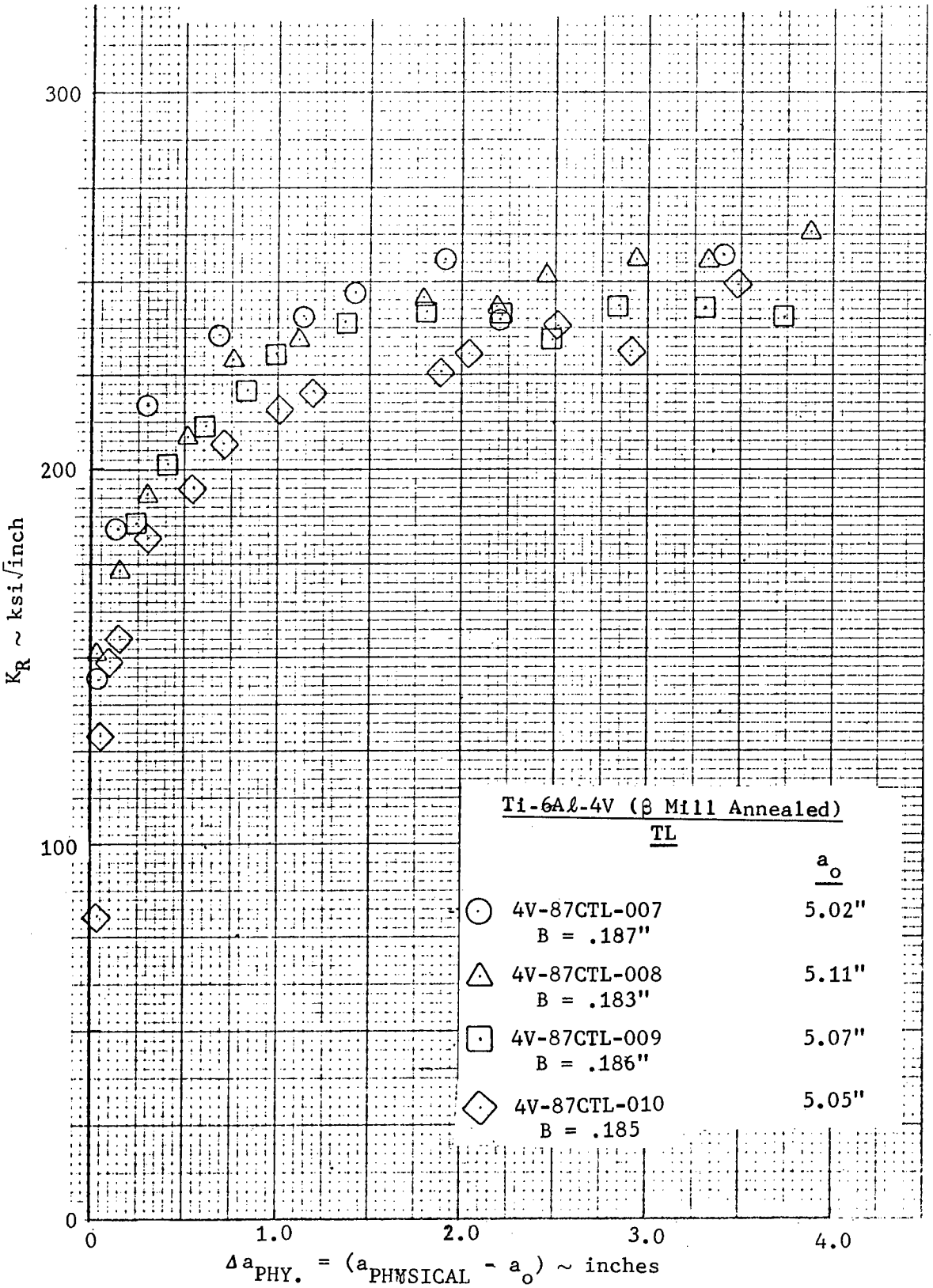

Figure 124. Crack Growth Resistance Data Based on Physical Crack Size - .185 Inch, Ti-6Aℓ-4V (β Mill Annealed) (TL)

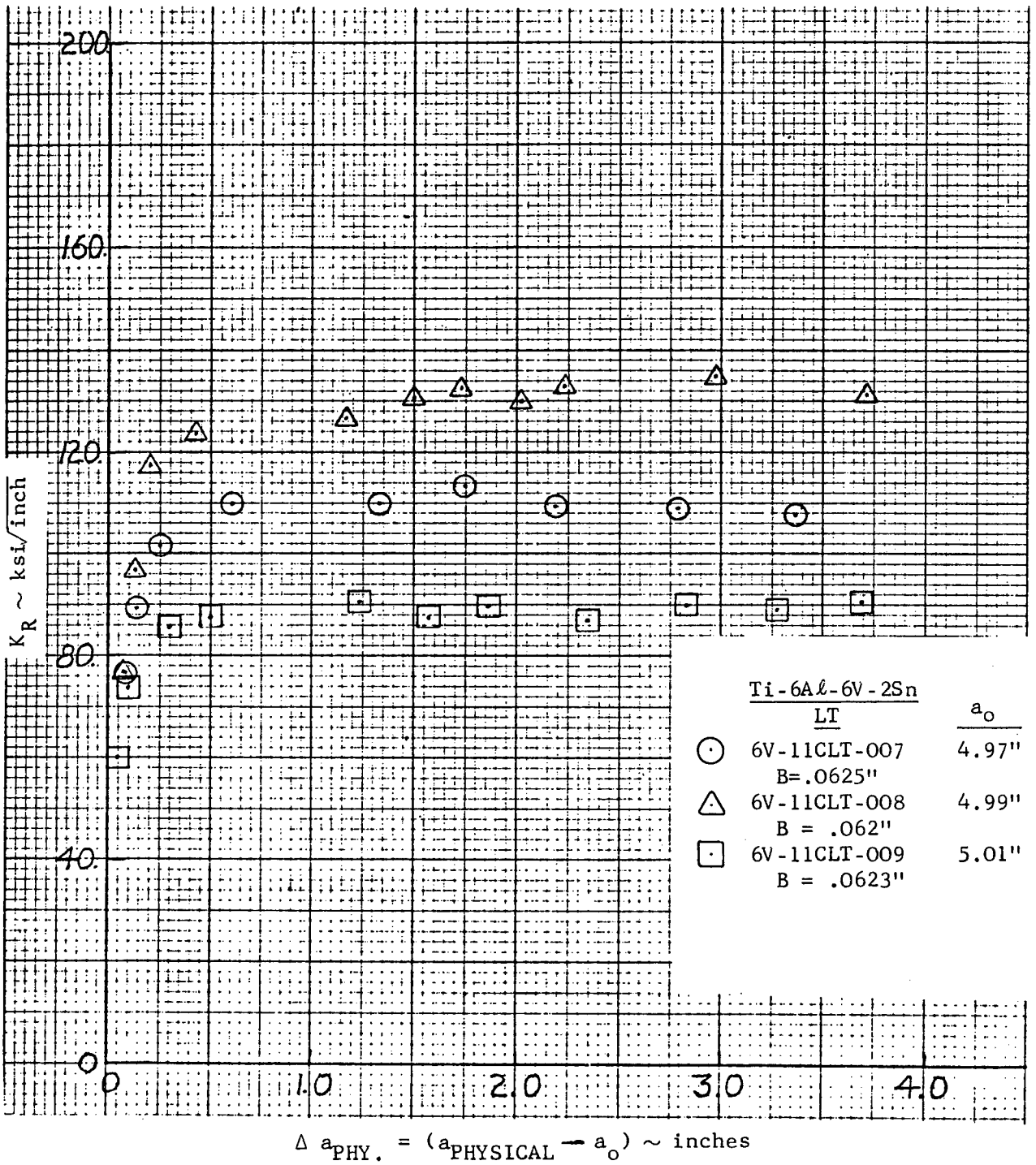

Figure 125. Crack Growth Resistance Data Based on Physical Crack Size - .062 Inch, Ti-6Aℓ-6V-2Sn (LT)

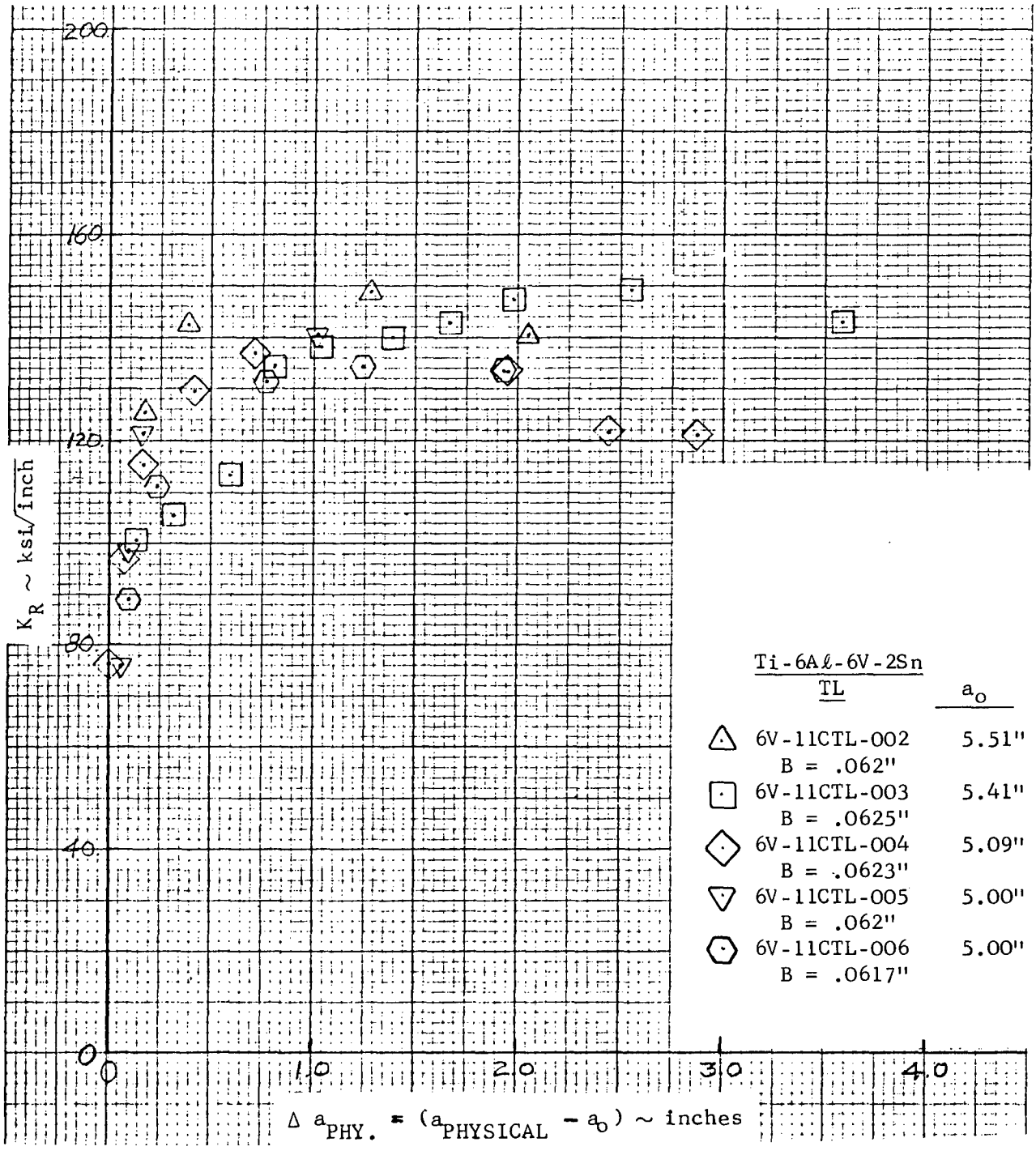

Figure 126. Crack Growth Resistance Data Based on Physical Crack Size - .062 Inch, Ti-6Aℓ-6V-2Sn (TL)

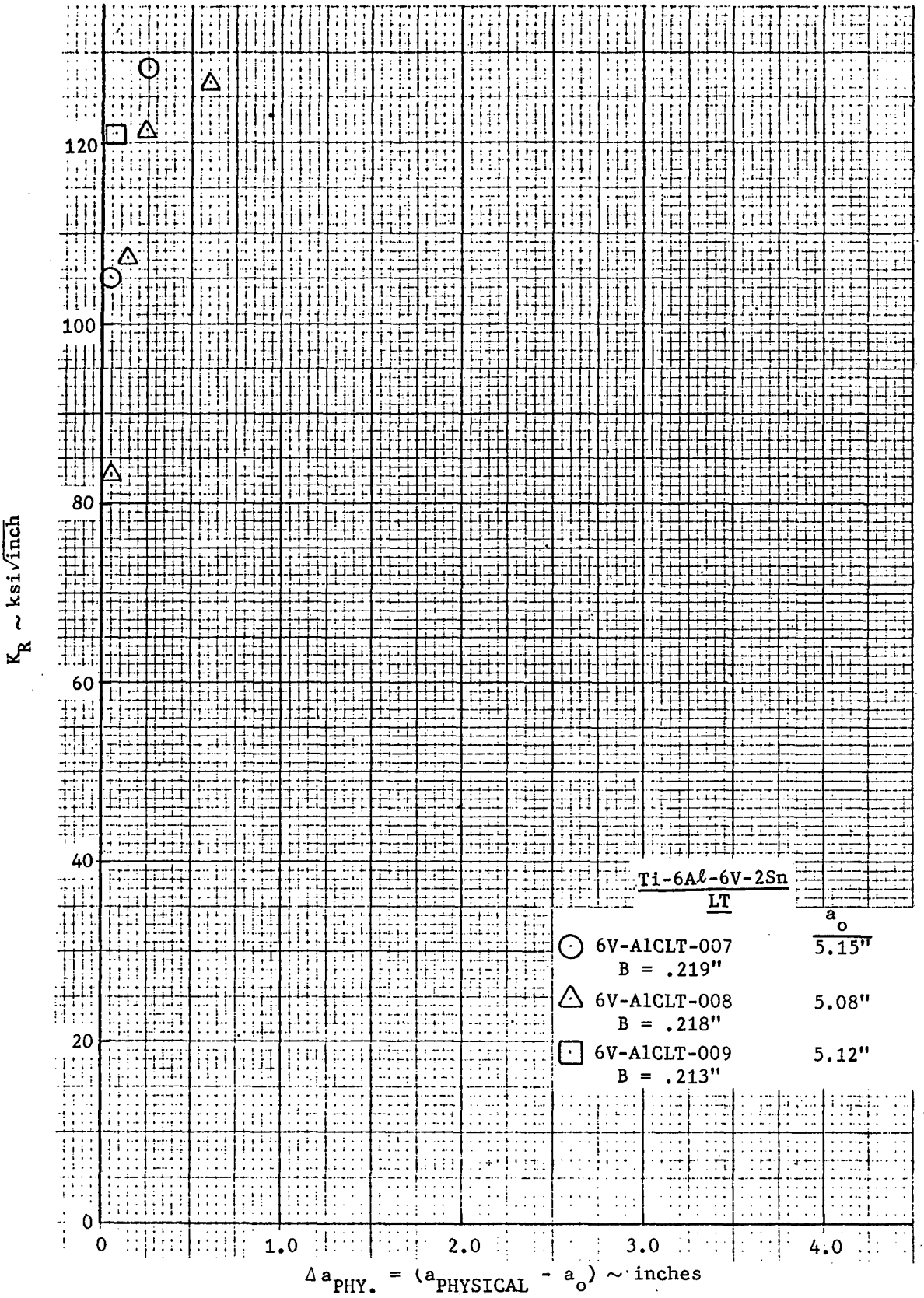

Figure 127. Crack Growth Resistance Data Based on Physical Crack Size - .21 Inch, Ti-6Aℓ-6V-2Sn (LT)

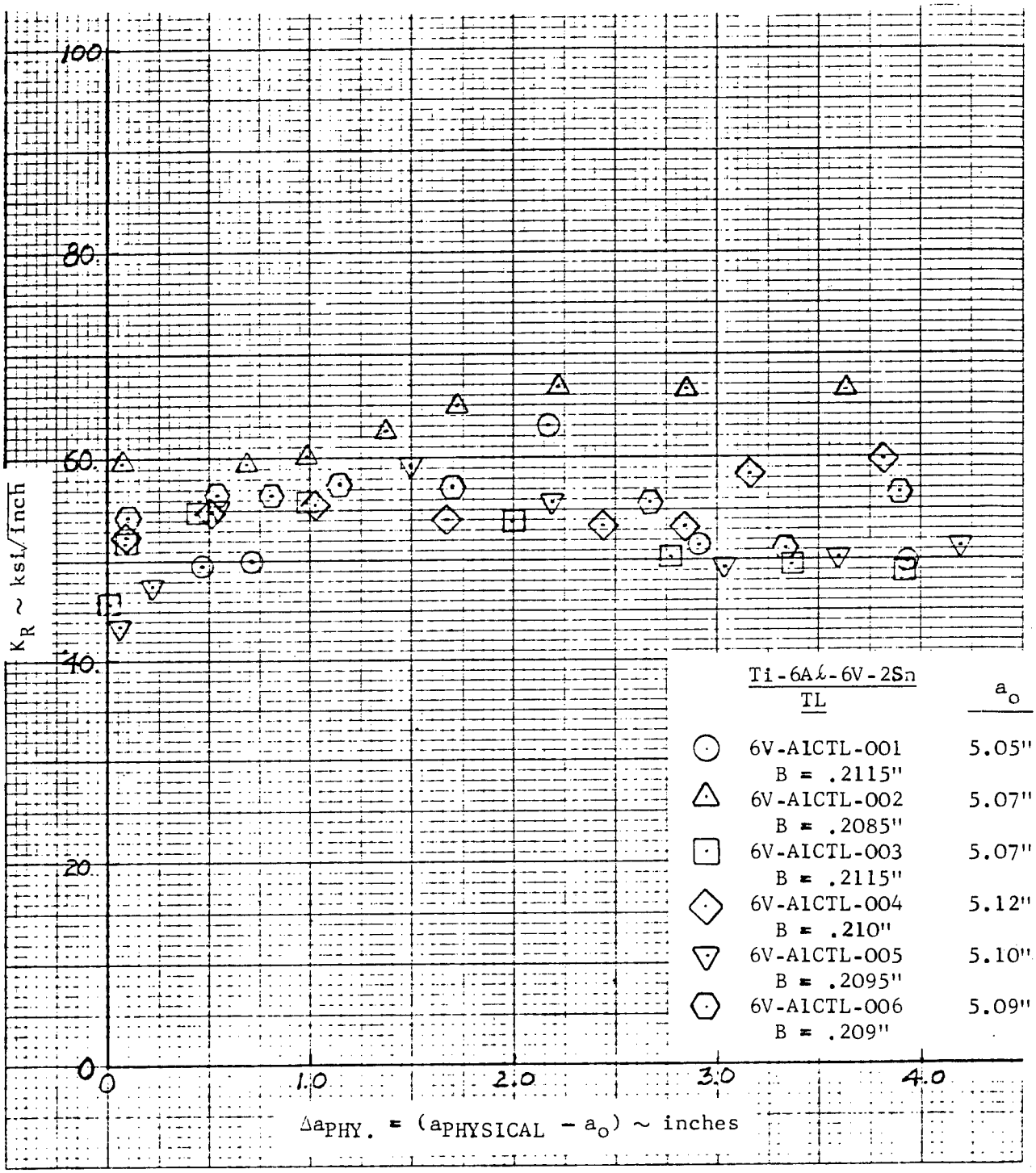

Figure 128. Crack Growth Resistance Data Based on Physical Crack Size - .200 Inch, Ti-6Aℓ-6V-2Sn (TL)

first instance of the crack deviating from a direction normal to the load for thicker specimens tested in the TL direction. Such behavior has been previously noticed for the LT orientation, in particular for 7075-T651 plate. There is a slight difference in average Young's Modulus 17.08 versus 16.66 x 10^6 psi (see Table IV) for the strong and weak direction which could explain this tendency toward crack deviation. An even greater difference in average Young's Modulus occurs for the 0.2 inch thick material (16.84 versus 14.58 x 10^6 psi) for the strong and weak directions. From the K_R data of Figure 127 it is obvious that the anisotropic nature of this material (as noted by Modulus) was evident where the crack deviated at 45 degree angles after minute crack extension. As a result the full K_R curve could not be obtained for this thickness material in the LT direction.

6.1.3 K_R Data - 9 Nickel Steel

Crack growth resistance data for the 0.063 inch gage, 9Ni-4Co-.2C steel are shown in Figures 129-131. Figure 129 shows the K_R data for this material in the LT direction. Extreme toughness is noted for this annealed material with no indication of a toughness plateau and values of toughness in excess of 600 ksi$\sqrt{\text{inch}}$. This material did experience back edge buckling at $a/W > 0.4$ indicating the extent of crack tip plasticity. The "as received" condition of this material was quite "rippled" and does cause considerable testing difficulties - particularly in keeping the specimen flat during unloading around the loading hole (e.g., twisting of the specimen).

Figure 130 shows K_R data for the TL test direction. More scatter is evident in this data; however, the problems associated with testing this material preclude making any definitive statements about the individual data.

A comparison of the 9 nickel steel TL and LT data is shown in Figure 131. A plateau of approximately 500 ksi$\sqrt{\text{inch}}$ appears for the material tested in the TL direction. No plateau is evident for the crack oriented in the LT direction.

6.1.4 Summary of K_R Data

In summary, K_R data have been obtained for all materials tested in this program but not without some difficulties for those materials which are anisotropic due to preferred rolling, banding, etc. In those cases, the complete K_R curve cannot be obtained from the CLWL geometry. Other specimen configurations must then be introduced to remedy this problem.

It is becoming apparent that the role of material rolling history on crack growth resistance becomes increasingly important in any fracture criteria. This will become evident from the aluminum side grooving and off angle tests to be reported on next. It is even more apparent in materials such as titanium where significant differences occur in the TL and LT mechanical properties.

6.2 SIDE OR FACE GROOVING OF THE CLWL SPECIMEN GEOMETRY

Initial tests on the 0.195 and 0.063 inch gage, 7075-T6 material in the LT (crack oriented normal to the rolling direction) direction for the CLWL specimen geometry indicated that some type of anisotropic material behavior was

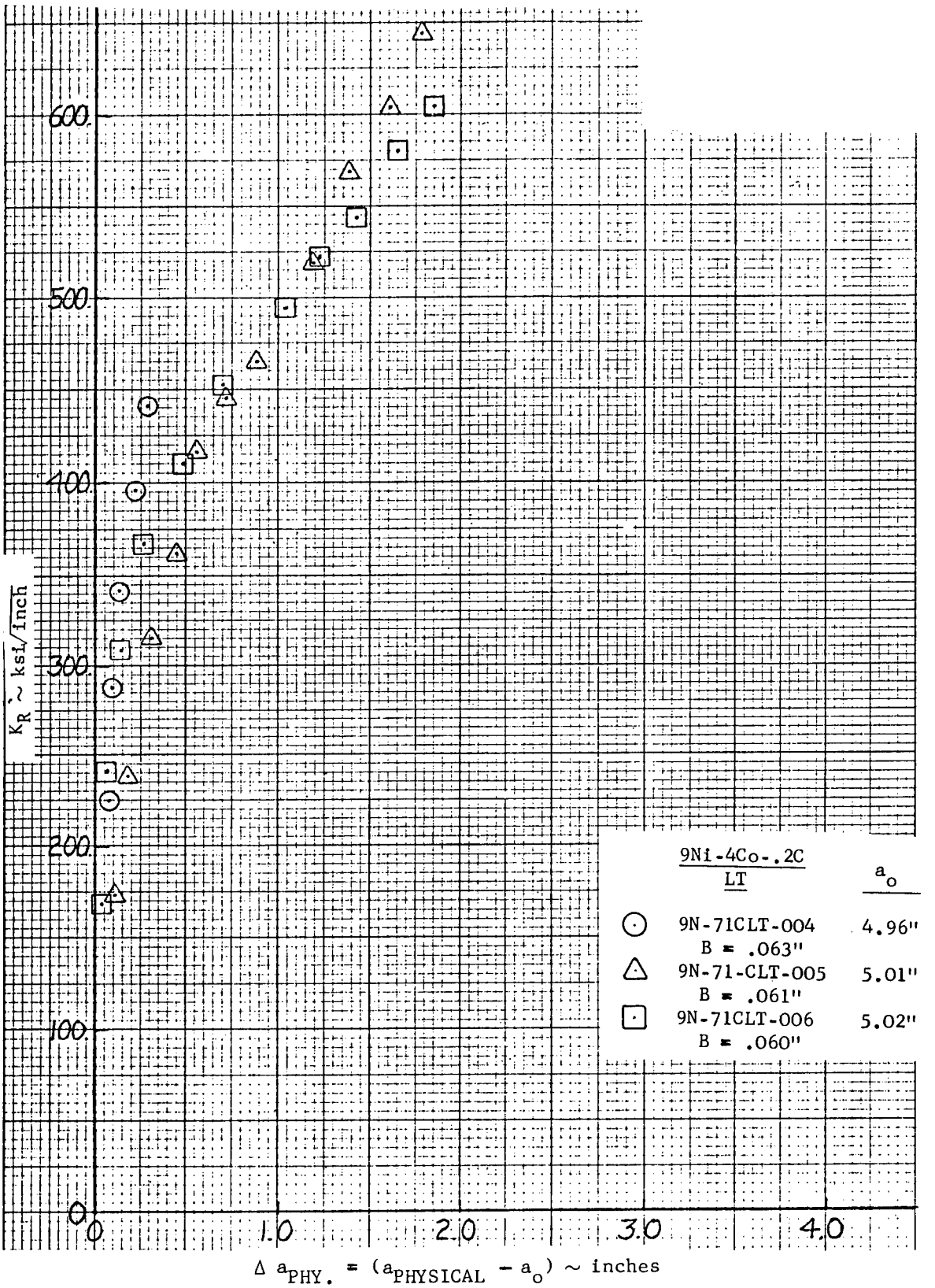

Figure 129. Crack Growth Resistance Data Based on Physical Crack Size - .062 Inch, 9Ni-4Co-.2C (LT)

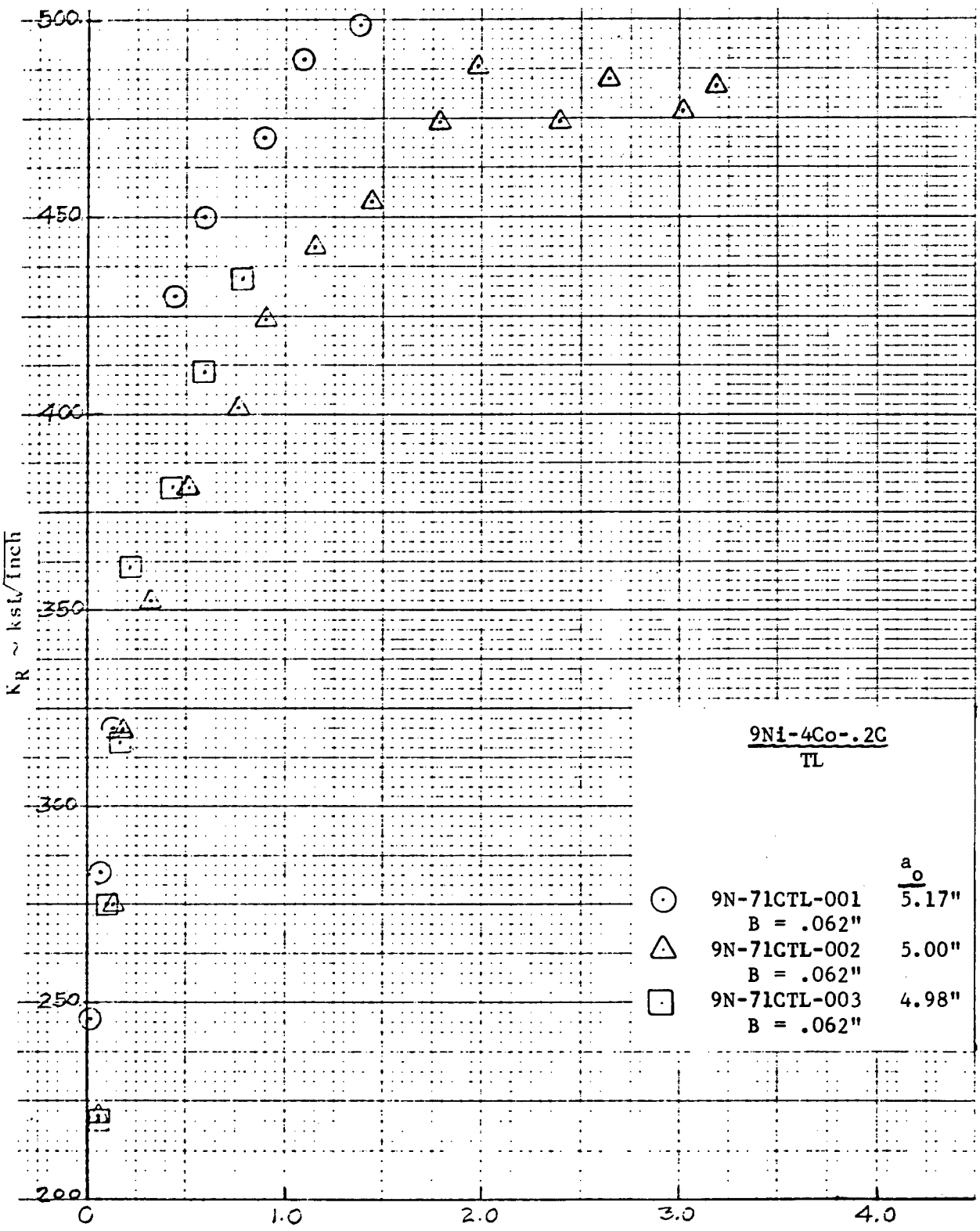

Figure 130. Crack Growth Resistance Data Based on Physical Crack Size - .062 Inch, 9Ni-4Co-.2C (TL)

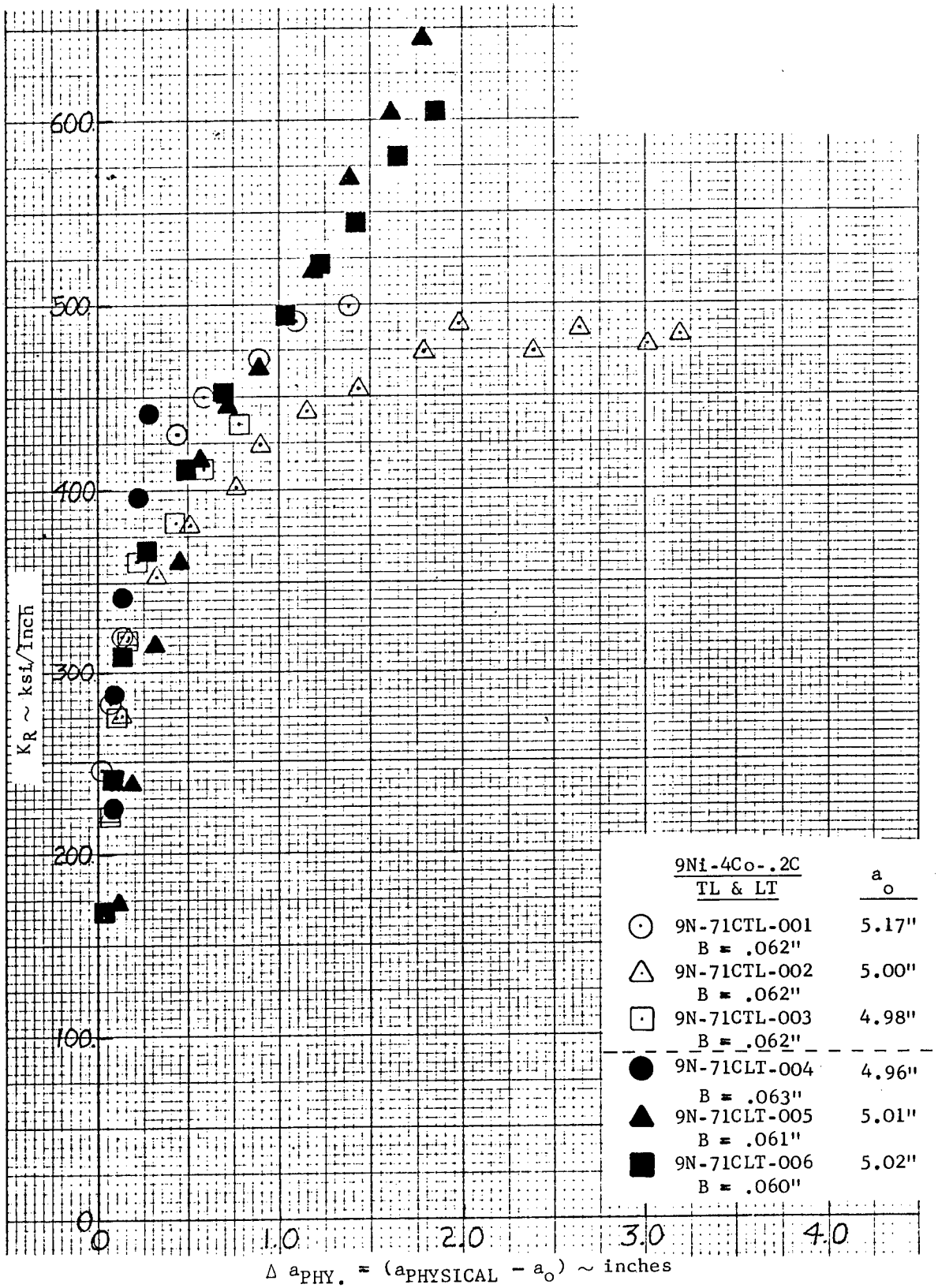

Figure 131. Crack Growth Resistance Data Based on Physical Crack Size - .062 Inch, 9Ni-4Co-.2C (TL and LT)

influencing crack extension. Cracks in all cases tended to deviate significantly from the plane normal to the rolling direction after small amounts (< 2.0 inches) of stable crack growth. Thus, the full resistance curve could not be developed for this crack orientation. Since in most aircraft applications, the path of crack extension can be in any of several directions, but principally in the TL and LT directions for through cracks, it was apparent that some means of controlling crack direction (principally normal to the loading axis) was mandatory if an effective residual strength analysis was to be developed which included a comprehensive fracture criterion. The criterion must include cracks which are oriented in this so-called "strong" orientation. Side grooving has been used in plane strain fracture toughness testing with some degree of success in suppressing the side boundary plastic zone formation but has been found to be influenced by groove geometry and material. A review of these complexities is given in Reference 3.

In our case, the groove would be serving as a guide to maintain the crack in the plane perpendicular to the rolling direction. This would, hopefully, be accomplished by minimum suppression of the surface plastic zone. Several CLWL specimens were prepared with side grooves as shown in Figure 132, in both the TL and LT directions from the 0.195 inch thick, 7075-T651 material. Control specimens without side grooving were also fabricated. In addition, specimens were also prepared from 0.258 inch thick 2024-T351 material to verify the observations from the 7075-T651 test series. In both cases, the depth of remaining material (after grooving), B_g, was kept as a constant percentage of the overall thickness, B, (nominally 85 percent to 90 percent) and the groove width, w_g, varied from 1 to 3 times the material nominal thickness. Using this procedure, the effect of surface plastic zone suppression, which was thought to be the most significant factor in effecting crack growth resistance, could be evaluated.

The 7075-T651 side grooving study will be discussed first, followed by the 2024-T351 results and the results of a special off-angled test series from both materials. At the conclusion of these discussions, recommendations as to the alternative specimens and disposition of LT (CLWL) specimens with strong material anisotropy will be presented.

6.2.1 7075-T6 Side Grooving Study

Figure 133 shows the data for side grooved, CLWL (TL) specimens. A control specimen is also indicated. It is obvious that decreasing the notch width (w_g) (i.e., decreasing notch radius) decreased the plateau level of the K_R curve. The initial one-half inch of physical crack extension does not appear to be influenced by the degree of side grooving. In all cases, the crack ran completely across the CLWL panel without deviation from the TL plane. However, the wider notch (larger w_g) did result in a crack advancement which ran from the bottom of the groove to the free surface and then back again as noted in Figure 133, specimen -00D. Cross sections of the control specimen (-00C) and -00D indicated typical 45 degrees shear (slant) crack progression typical of this thickness. On the other hand, when full plastic zone suppression takes place, as is the case when $w_g = B$ (-00A), crack progression occurred with little or no evidence of any shear development (i.e., flat cracking) across the entire specimen. This progression is shown in Figure 134 where crack growth resistance data from CLWL (LT) are presented. Specimens -00A and -00B are grooved such that the groove width w_g is equal to the thickness for maximum surface plastic zone

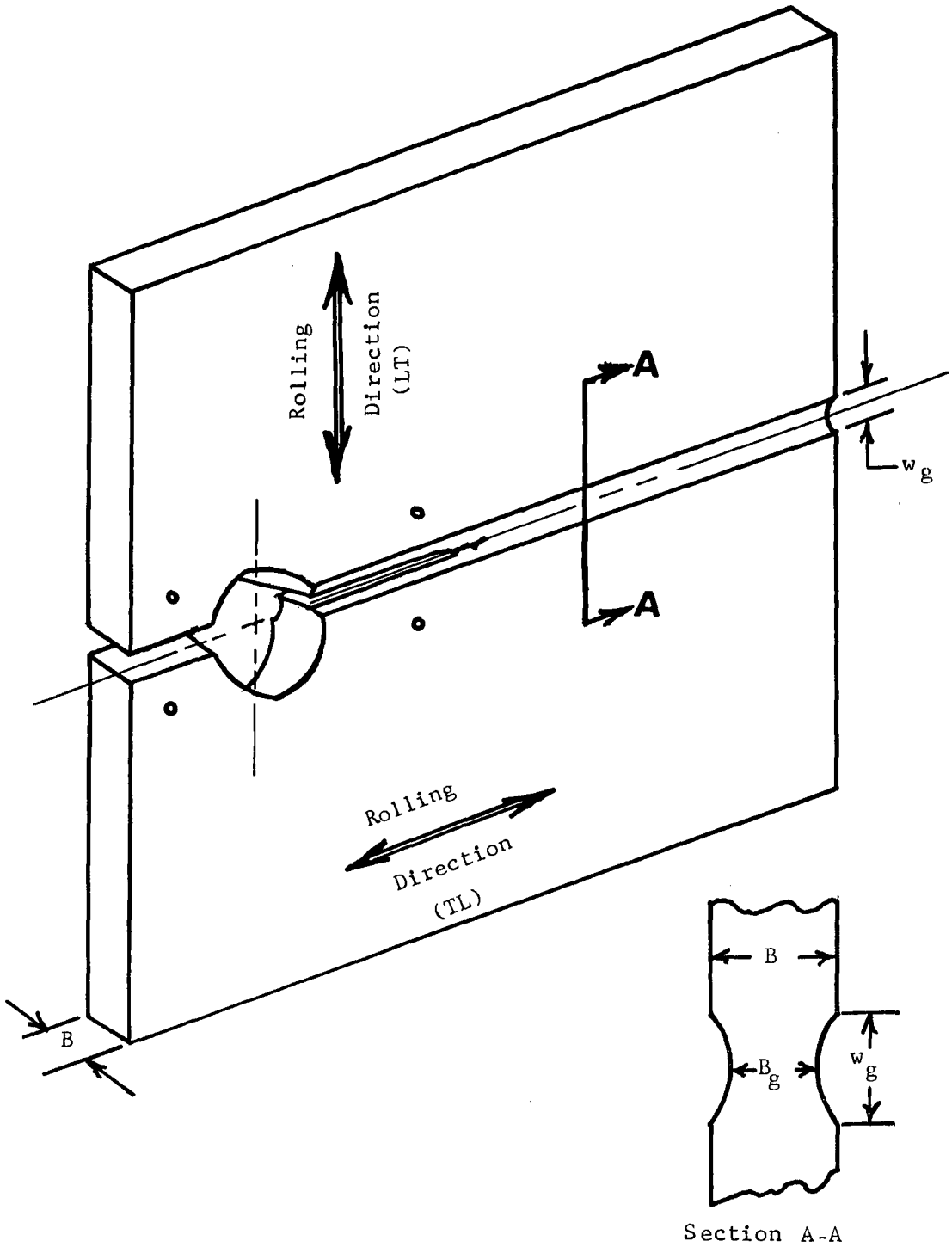

Figure 132. Geometry of Side Grooved, CLWL Specimen

T6-54CTL-00C

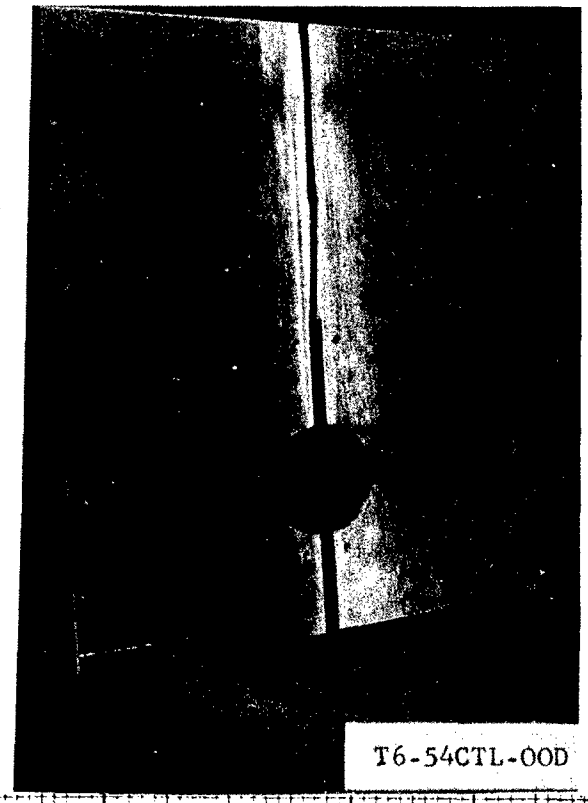

T6-54CTL-00D

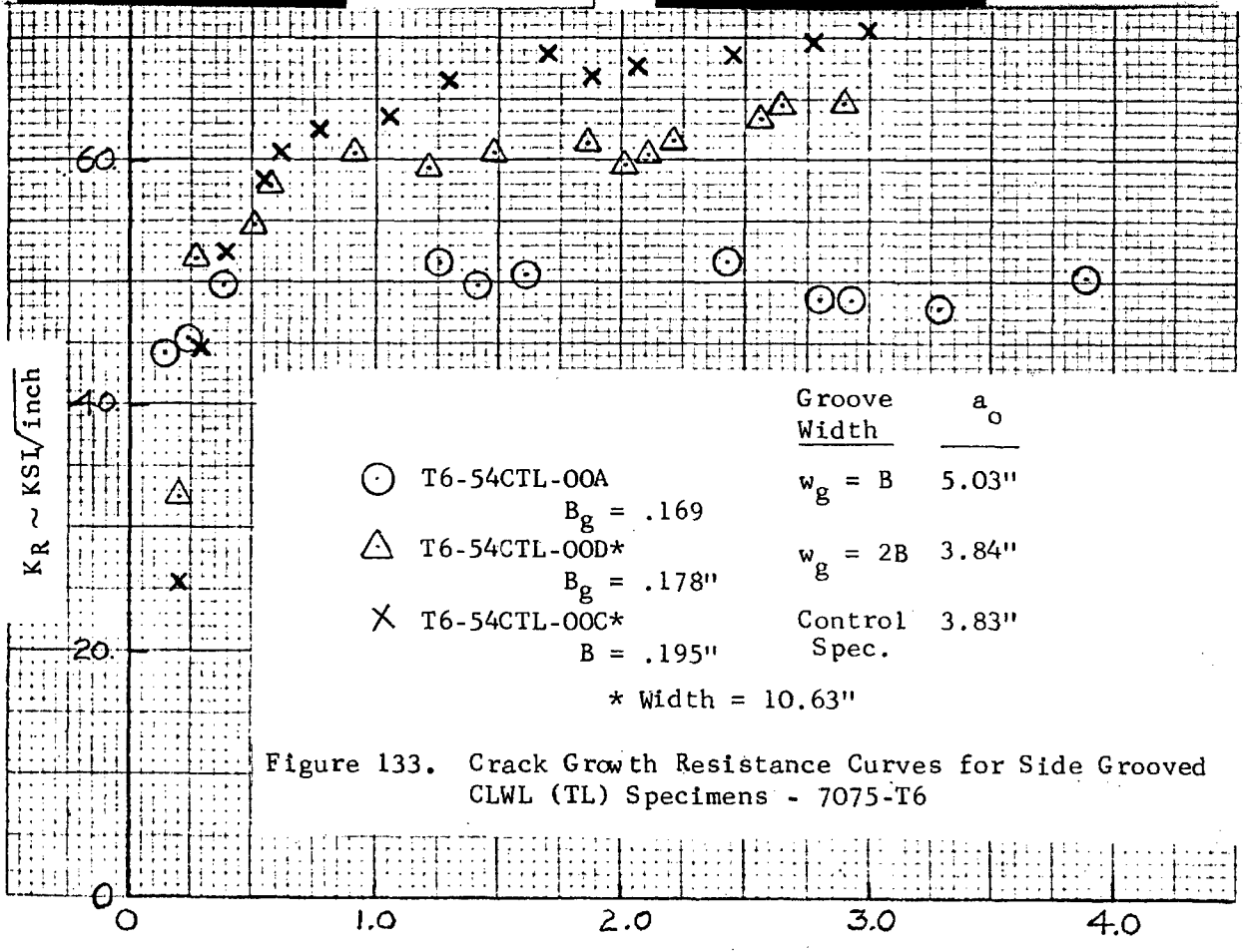

		Groove Width	a_o
⊙	T6-54CTL-00A B_g = .169	w_g = B	5.03"
△	T6-54CTL-00D* B_g = .178"	w_g = 2B	3.84"
X	T6-54CTL-00C* B = .195"	Control Spec.	3.83"

* Width = 10.63"

Figure 133. Crack Growth Resistance Curves for Side Grooved CLWL (TL) Specimens - 7075-T6

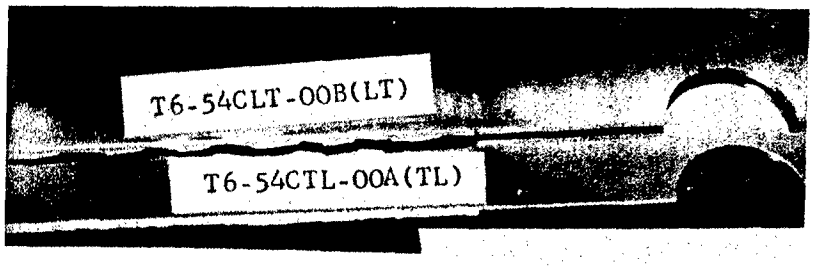

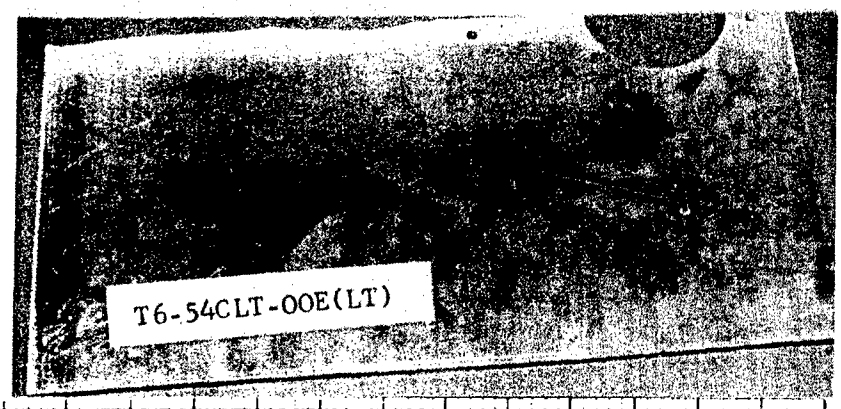

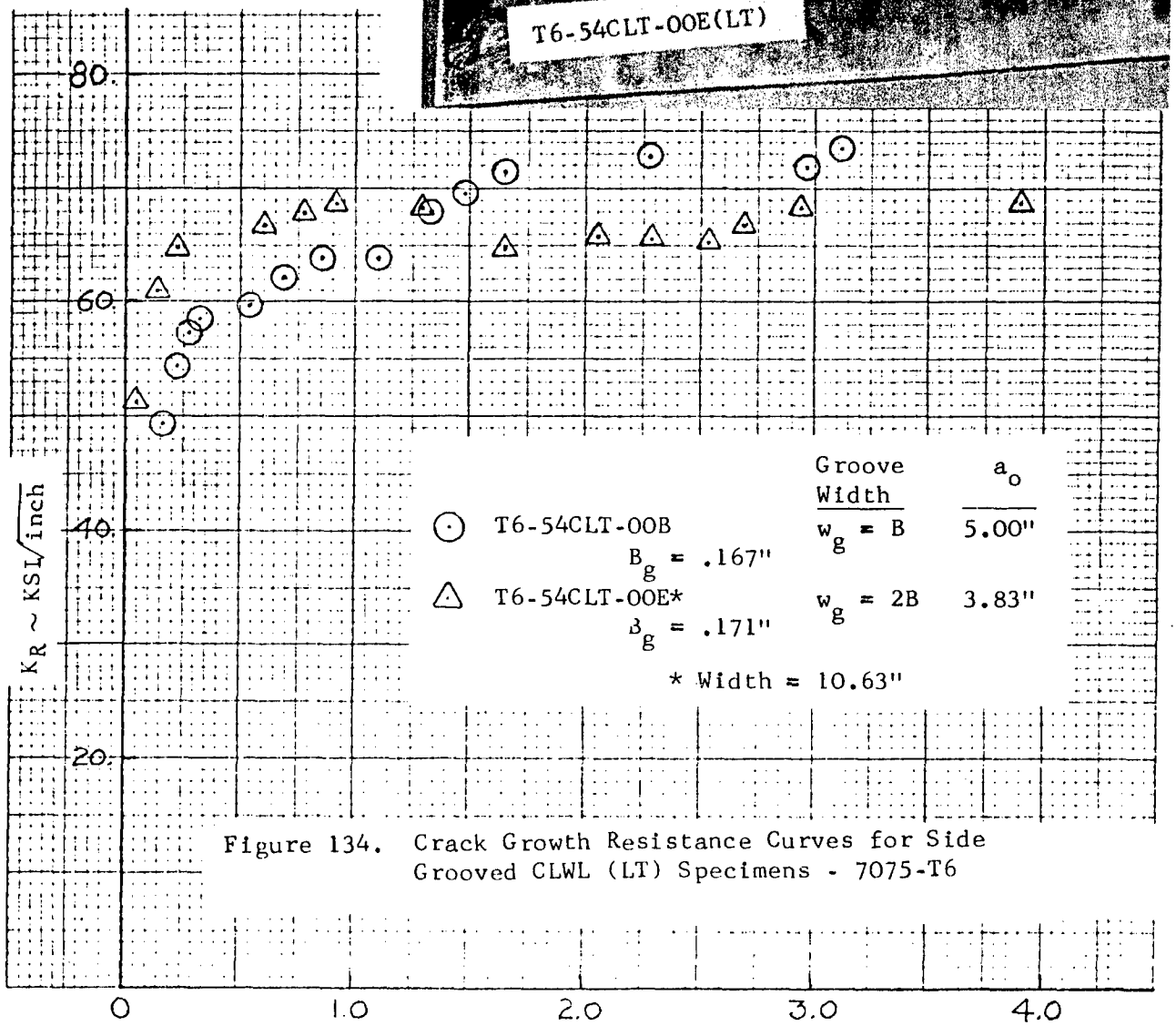

Figure 134. Crack Growth Resistance Curves for Side Grooved CLWL (LT) Specimens - 7075-T6

suppression. The -00A (TL) and -00B (LT) coupons are compared in the left hand photograph. The CLWL (LT) specimen has a "saw tooth" appearance (there was negligible shear development through the thickness) which indicated a strong tendency for the crack to turn toward the rolling direction even with full zone suppression. The data of Figure 134 also shows a difference in K_R curves with grooving over the full range of data with an unexplained cross over at approximately 1½ inches of physical crack extension.

6.2.2 2024-T3 Side Grooving Study

To further study the effect of side grooving on crack growth resistance and crack progression CLWL specimens of 0.258 inch thick 2024-T351 plate were side grooved with groove widths equal to two and three times the material thickness. The results of the TL specimen tests are shown in Figure 135 with accompanying fracture surfaces in Figure 136. The separation of data is similar to that obtained for the 7075 material (see Figure 133); however, the decrease in K_R for the specimen with full plastic zone suppression (-00B of Figure 135) is not as large as for the 7075 material. However, it must be noted that the K_R curve has barely reached a plateau value as with 7075 but the early stages of crack extension and subsequent trends are similar.

Figure 137 shows K_R data for CLWL specimens in the so-called strong direction, LT. Decreasing K_R with decreasing notch radii are once again evident. One factor of utmost importance is also indicated, that is the unnotched specimen (-001) showed no signs of crack deviation over the entire range of crack lengths. Thus a full range (for the 14 inch wide CLWL specimen) Δa versus K_R curve was readily obtained. This, of course, was also apparent from the data of Figure 117.

The fracture surfaces of all specimens showed no evidence of shear in either the grooved or ungrooved conditions for both the TL and LT direction. The fracture paths for the 2024-T351 (LT) specimens is shown in Figure 138.

In analyzing the data of Figure 137, one may conclude that the reduction in K_R with decreasing groove radii could also occur due to increasing initial starter fatigue crack length, a_o. However, the data of Figure 135 show similar trends for constant initial crack size. Indeed, the 7075-T651 data of Figure 133 for two specimen widths (14 and 10.63 inches) and dissimilar initial crack lengths (but same a_o/W's) definitely indicate the influence of surface plastic zone suppression on the K_R curve.

6.2.3 Off-Rolling Direction Specimens

To confirm the role of material anisotropy due to rolling for the change in fracture direction for the 7075-T651 material, two specimens were prepared from a 4 ft. x 8 ft. plate as indicated in Figure 139(a). The fracture direction for these 45 degree specimens is shown in Figure 139(b). The black triangle is a 45°/45°/90° triangle and indicates that almost immediately from the starter fatigue crack, the crack ran in the direction parallel to the rolling direction.

Similar tests were run on the 2024-T351 material and the results are shown in Figure 140. In this case, the crack slowly progressed to a 15-20 degree angle to the initial crack plane.

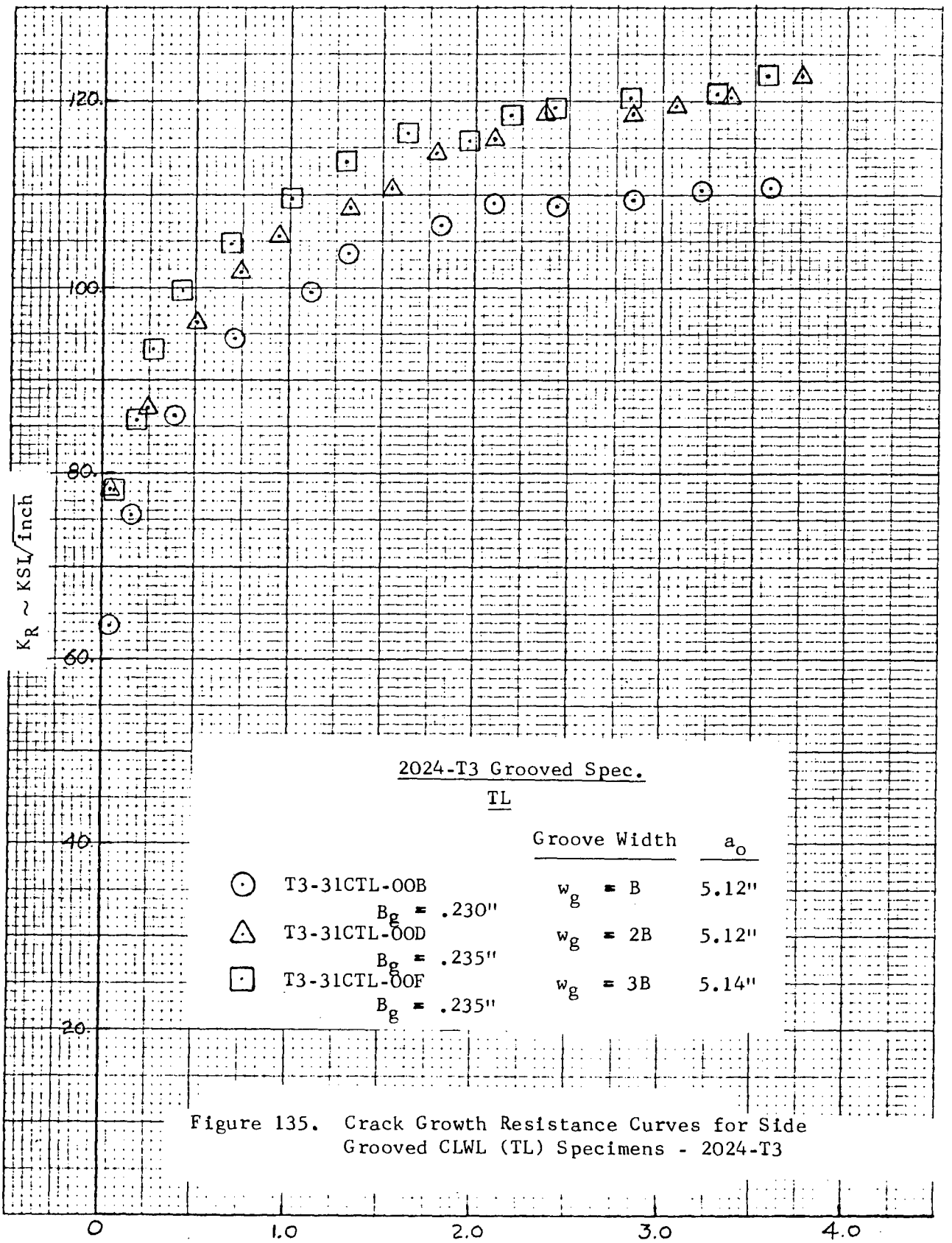

Figure 135. Crack Growth Resistance Curves for Side Grooved CLWL (TL) Specimens - 2024-T3

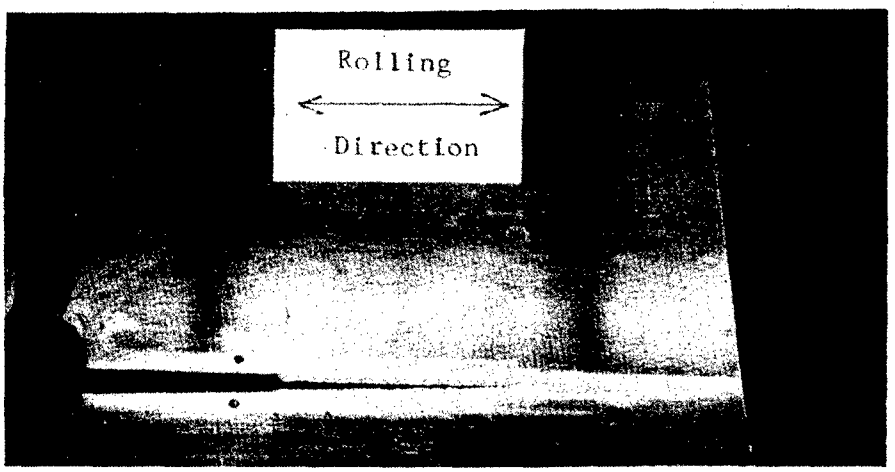

w_g = B

T3-31CTL-00B

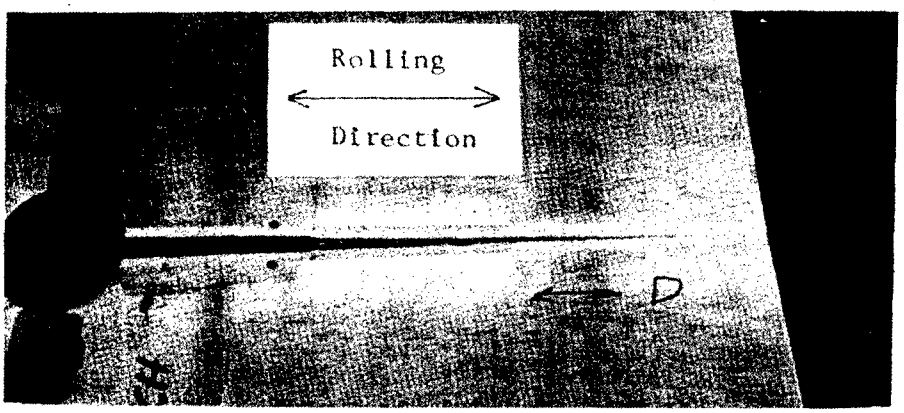

w_g = 2B

T3-31CTL-00D

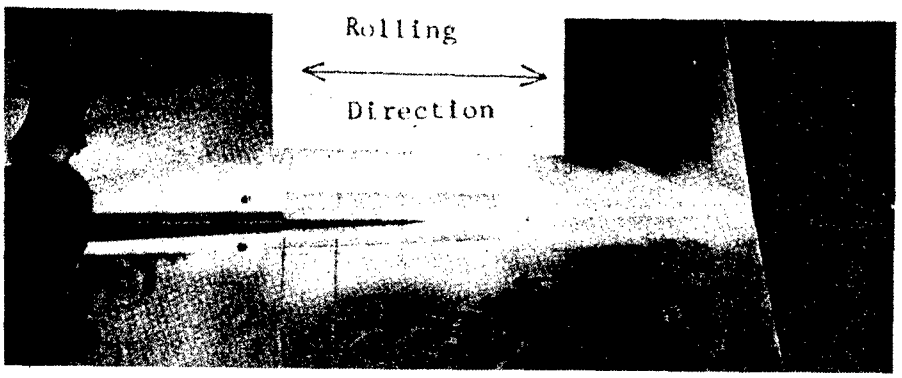

w_g = 3B

T3-31CTL-00F

Figure 136. Fracture Path for CLWL (TL) Specimens - 2024-T3

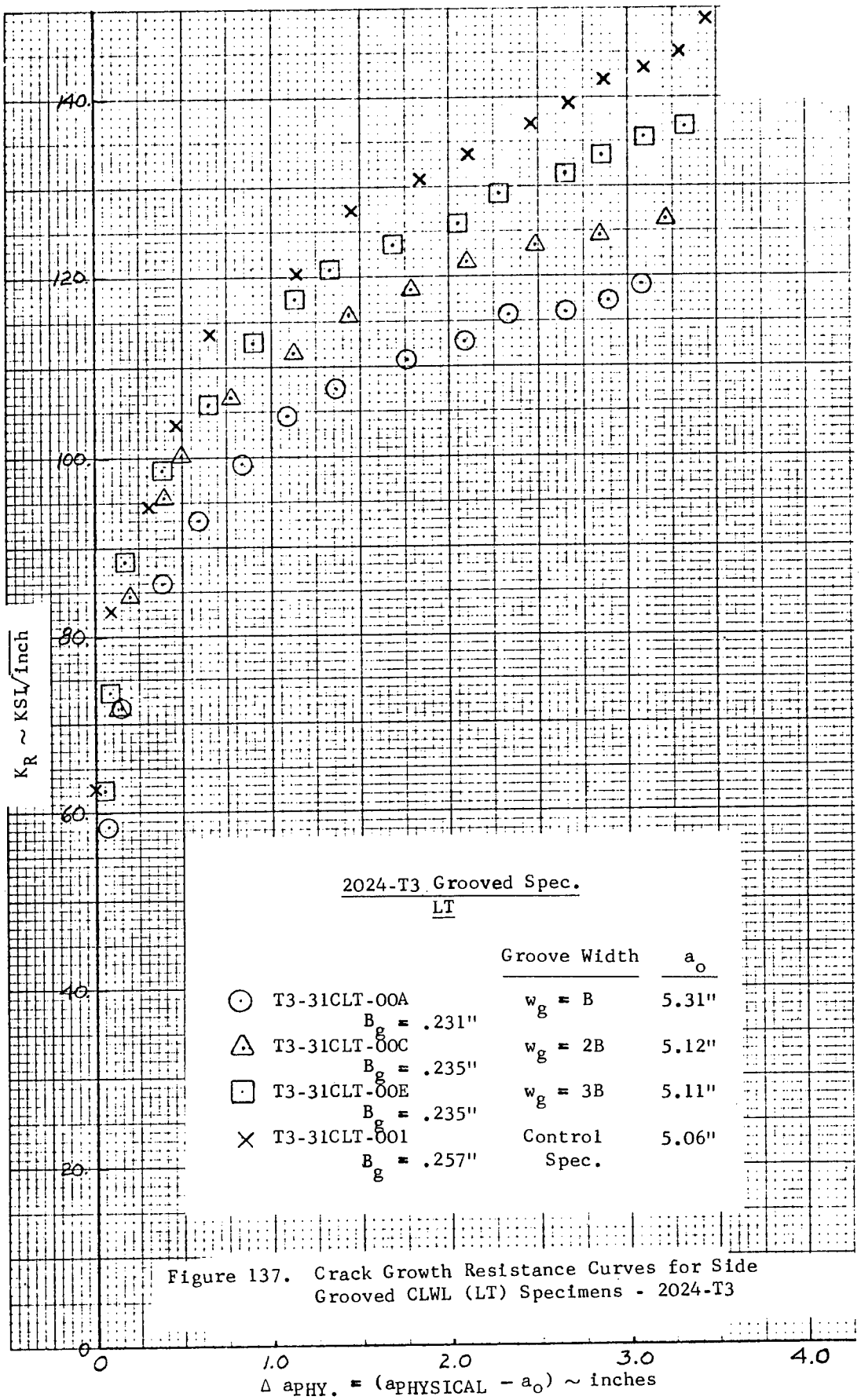

Figure 137. Crack Growth Resistance Curves for Side Grooved CLWL (LT) Specimens - 2024-T3

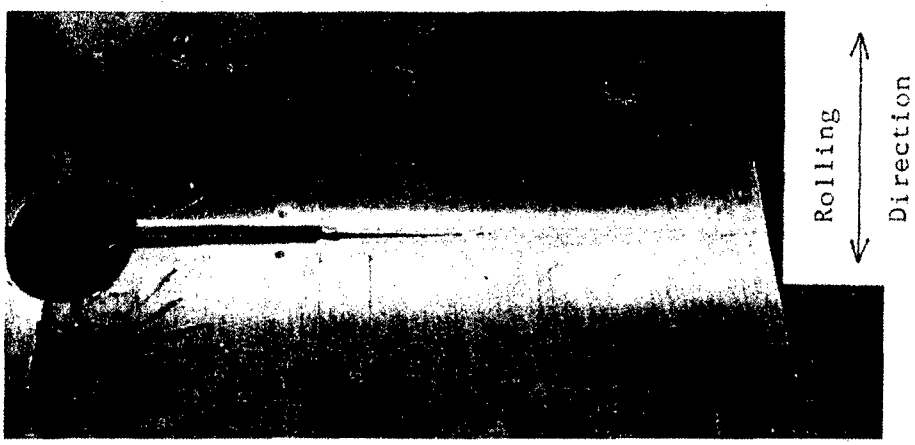

w_g = B

T3-31CLT-00A

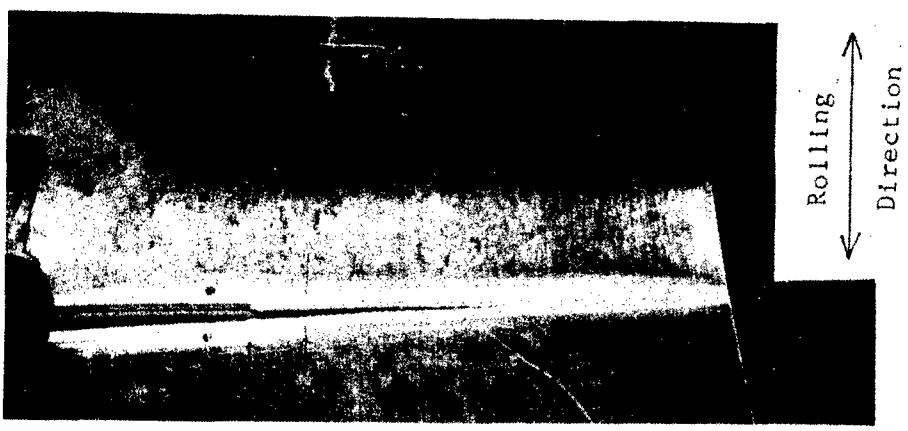

w_g = 2B

T3-31CLT-00C

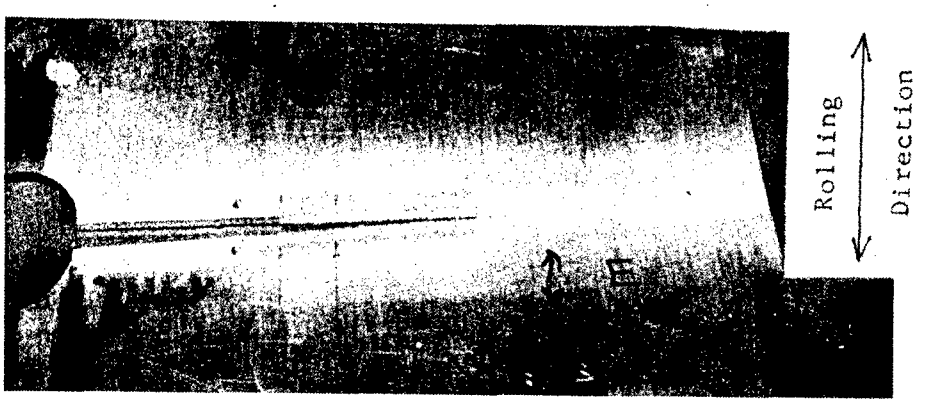

w_g = 3B

T3-31CLT-00E

Figure 138. Fracture Path for CLWL (LT) Specimens - 2024-T3

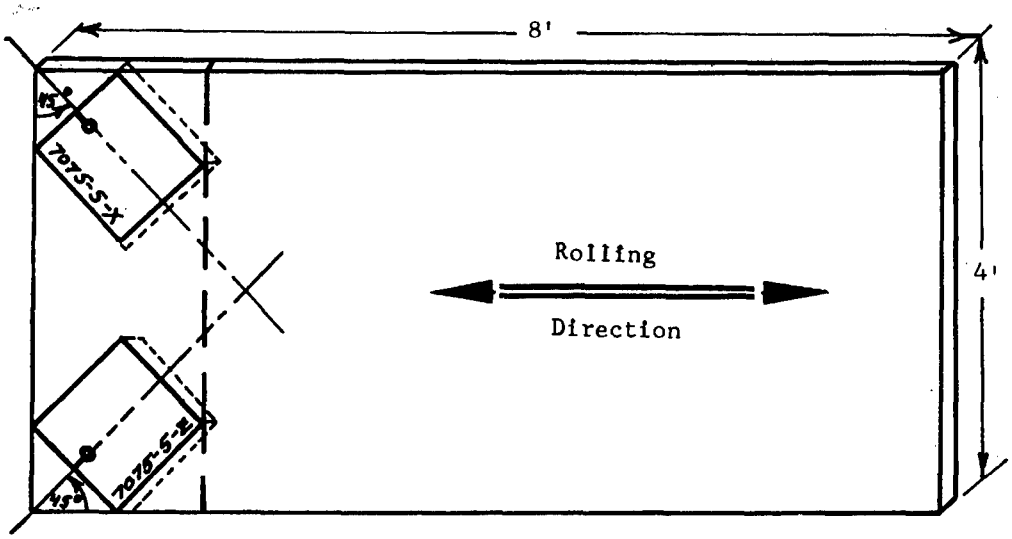

(a.)

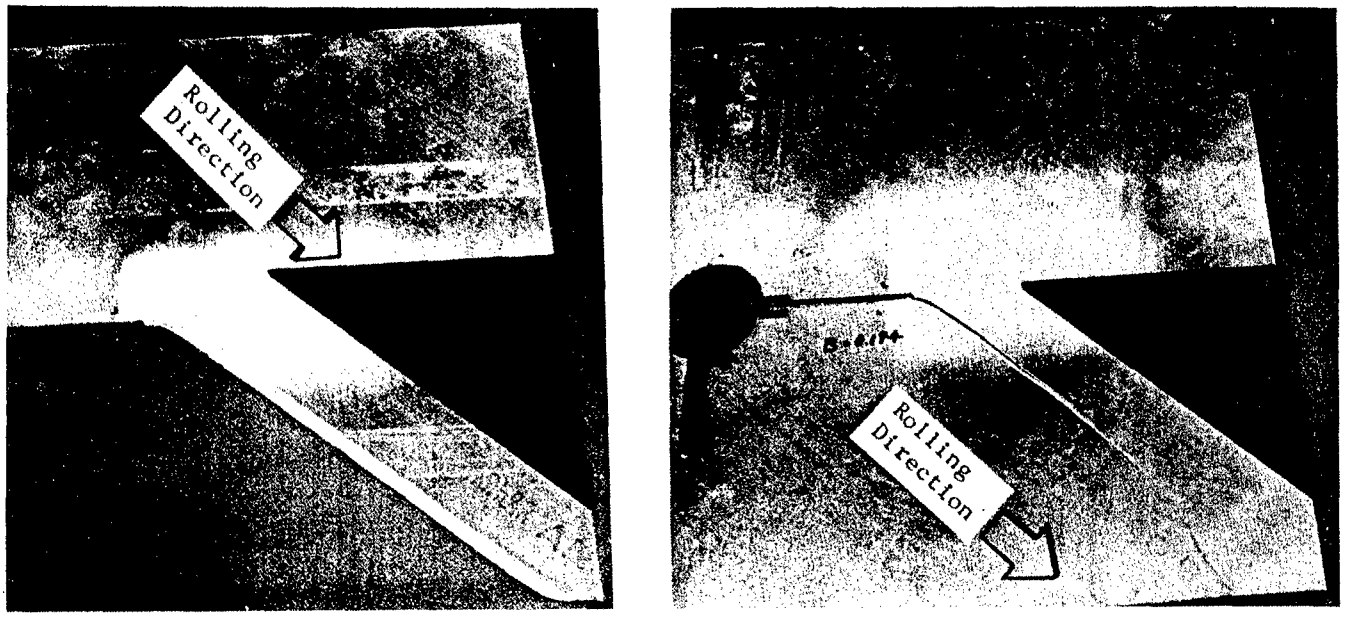

7075-5-5X

7075-5-5Z

(b.)

Figure 139. Specimen Layout and Subsequent Fracture Direction for Off-Rolling Direction Specimens - 7075-T651

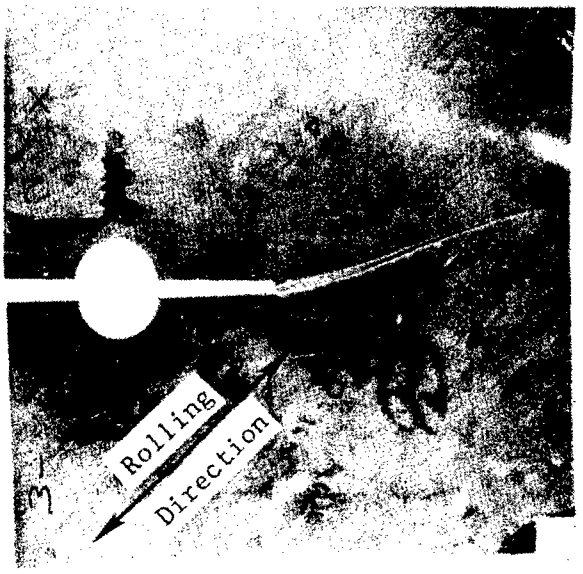

2024-3-2X

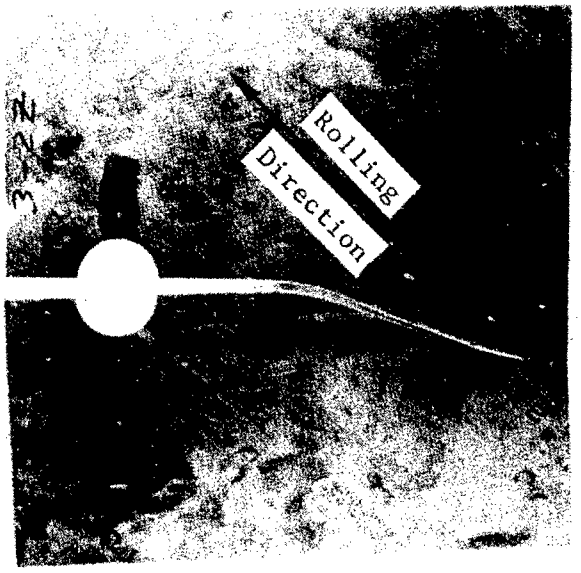

2024-3-2Z

Figure 140. Fracture Direction for Off-Rolling Direction Specimens - 2024-T351

6.2.4 Conclusions and Recommendations Based on Side Grooving Studies

Based on the results of the previous sub-studies, the following comments apply:

The use of crack growth resistance as a fracture criterion would have definite limitations if CLWL curves cannot be developed in the LT direction for materials with strong directional properties. This may be partially overcome by testing the center cracked tension geometry (CCT) with corresponding increased cost and effort.

Side grooving should be used as a last resort to obtain a K_R curve for the following reasons:

(i) Extrapolation to the base (ungrooved) geometry would currently be a matter of judgment based on limited data obtained thus far.

(ii) The early life (small crack extension) portion of the curve indicates small changes in K_R with groove radii for the highly directional 7075-T651 material. Since the rising portion of the resistance curve is of prime concern in application to structural failure, this portion can be obtained (at least for 7075-T651) quite readily from ungrooved specimens.

(iii) The plateau level is definitely affected by side grooving and use of crack growth resistance curves for material evaluation purposes would require additional study, particularly for the CLWL specimen geometry.

Perhaps the unexpected crack extension of the ungrooved 2024-T351 (LT) specimen compared to the strongly directional behavior of the 7075-T651 (LT specimens can be explained by examining the respective TL and LT resistance curves. In comparing data from the LT direction with similar data for the TL direction (data presented earlier in this report), it is shown that there is little difference in the K_R curves for 2024-T351 for the two crack orientations; e.g., Figures 117 and 118. (The LT direction is approximately two to five ksi $\sqrt{\text{inch}}$ higher than the TL.) By comparison, the 7075-T651 material data (see Figures 109 and 110), indicate that differences in K_R of 10 to 15 ksi $\sqrt{\text{inch}}$ between the TL and LT direction are evident.

6.3 SUMMARY

This report contains all of the essential materials test data obtained from Phase II of the program. Only those data deemed necessary to the development of the failure criterion were explored. These data are presented here so that a wider understanding of the problems and difficulties associated with crack growth resistance type tests and the resultant data may be objectively examined and evaluated.

The intent has been to obtain only those data necessary to the method proposed in Volume I of this report so that more accurate and reliable predictions can be made of the residual strength of thin section structures.

REFERENCES

1. Heyer, R. H. and McCabe, D. E., "Crack Growth Resistance Testing in Plane-Stress Fracture Testing," Engineering Fracture Mechanics, 1972, Vol. 4, pp. 413-430.

2. Proposed Recommended Practice for R-Curve Determination, 1974 Annual Book of ASTM Standards, Part 10 (Published as information only, November 1974).

3. Brown, Jr., W. F. and Srawley, J. E., "Plane Strain Crack Toughness Testing of High Strength Metallic Materials," American Society for Testing and Materials Publication 410, 1967.

☆U.S.Government Printing Office: 1977 — 757-001/98